UNIVERSITÀ DEGLI STUDI DI TRIESTE

XXXIII CICLO DEL DOTTORATO DI RICERCA IN INGEGNERIA INDUSTRIALE E DELL'INFORMAZIONE

METODOLOGIE E STRUMENTI PER IL PROGETTO DI SISTEMI ELETTRICI NAVALI E MARINI

Settore scientifico-disciplinare: **ING-IND/33**

DOTTORANDO
DOTT. ANDREA COLAVITTO

COORDINATORE
PROF. FULVIO BABICH

SUPERVISORE DI TESI
PROF. GIORGIO SULLIGOI

CO-SUPERVISORE DI TESI
DOTT. RIC. ANDREA VICENZUTTI

CO-SUPERVISORE DI TESI
CV GENNARO LIPARDI

ANNO ACCADEMICO 2019/2020

"There is a powerful agent, obedient, rapid, easy, which conforms to every use, and reigns supreme onboard my vessel. Everything is done by means of it. It lights, warms it, and is the soul of my mechanical apparatus. This agent is electricity."

Twenty Thousand Leagues Under the Seas - Jules Verne

Abstract

Sommario

Lo scopo di questa tesi è quello di presentare metodologie e strumenti innovativi, applicabili ai sistemi elettrici navali, in grado di affrontare le problematiche date sia dal processo di progettazione convenzionale che dalla volontà di installare a bordo nuovi sottosistemi, dati i requisiti crescenti degli armatori e viste le stringenti normative sull'inquinamento. Le metodologie e strumenti analizzati in questo lavoro di tesi possono migliorare la conoscenza del sistema già nelle prime fasi di progettazione. L'obiettivo finale è definire tutte le scelte progettuali possibili prima della fase contrattuale. Infatti, gli imprevisti legati all'utilizzo di soluzioni innovative possono portare a conseguenze dannose per il sistema nave. Tali metodologie e strumenti forniscono dati coerenti su cui basare le decisioni di progettazione, valutando diverse configurazioni e riducendo inoltre i tempi e i costi di progettazione. Riducendo l'impegno richiesto per ottenere le stesse informazioni, ovvero a parità di tempo e risorse investite prima di siglare il contratto, si possono proporre soluzioni realizzabili e di cui si può stimare con più accuratezza il prezzo. Inoltre, nuovi sottosistemi possono essere integrati evitando un aumento incontrollato dei costi.

In questa tesi viene effettuata un'ampia rassegna dello stato dell'arte, per consentire la comprensione del contesto, del perché tecniche innovative possono essere utilizzate come un aiuto nella progettazione. Ogni punto è discusso concentrandosi sullo scopo di questa tesi, presentando così argomenti, bibliografia, e considerazioni volte ad indirizzare il lettore a comprendere l'impatto dei nuovi strumenti per la progettazione di impianti elettrici navali.

In particolare, dopo un primo capitolo dedicato all'introduzione delle navi a propulsione elettrica, in cui viene descritto come tali navi si siano evolute. Nel secondo capitolo, vengono presentati sistemi di distribuzione innovativi e nuovi requisiti soprattutto per navi da crociera e militari. Dato il significativo impatto di tali innovazioni, un excursus su questi due temi è fatto con riferimento alla bibliografia più recente.

Nel terzo capitolo, invece, si effettua una discussione ragionata sul processo di progettazione convenzionale delle navi. In aggiunta a questo viene effettuata un'analisi approfondita del processo di progettazione dei sistemi elettrici, per spiegare il contesto in cui un approccio innovativo alla deve essere integrato.

Il quarto capitolo è dedicato alle nuove tecniche di progettazione e di come questi strumenti, assieme all'utilizzo di software specifici, possano essere utili per migliorare la progettazione dell'intera nave. In questo contesto, viene introdotto il concetto di uno spazio

riservato dedicato al sistema elettrico, il cui impatto sul sistema nave può essere valutato sin dalle fasi iniziali del progetto.

Nel quinto capitolo viene presentato il caso di studio di questa tesi. Successivamente, la nave di riferimento viene riprogettata con due diversi sistemi di distribuzione in corrente continua. Entrambe le soluzioni sono confrontate in termini di volumi e pesi verificando così la loro fattibilità nonché la validità del metodo di redesign proposto.

Le soluzioni innovative proposte possono però impattare negativamente sulle prestazioni del sistema elettrico. Per questo motivo, nel capitolo sei, si è analizzato il loro impatto sull'impianto elettrico al fine di prevenire problemi di integrazione. Nello specifico si sono analizzati gli effetti che la propagazione dei disturbi ad alta frequenza, causati dai convertitori elettronici, può avere su cavi di distribuzione e trasformatori, validando sperimentalmente il modello di quest'ultimo.

Nel settimo capitolo, infine, servendosi dei dati precedentemente ricavati, si è utilizzato un software modulare per la simulazione del sistema elettrico della nave di riferimento al fine di valutare l'accuratezza e il carico computazionale di diversi modelli proposti.

Summary

The aim of this thesis is to present an innovative methods and tools, applicable to the shipboard integrated power system, able to address the issues given by both the conventional design process and the desire to install on board new subsystems, giving both the ever-increasing ship-owners' requirements and pollution regulations. Methods and tools analyzed throughout this thesis work can enhance the knowledge of the system already in the early stage design phases. The final goal is to define the feasible design choices before the contract phase. Indeed, such commitments can lead to harmful consequences since the project may not be feasible at the end due to unforeseen issues related to the exploitation of innovative power system solutions. Such methods and tools are a mean to provide consistent data on which base innovative design decisions exploring different design choices and thus lowering the design times and costs. By reducing the effort required to obtain the same information, or with the same amount of time and resources invested before signing the contract, feasible solutions can be proposed and the price of which can be estimated more accurately. Furthermore, innovative subsystems can be integrated avoiding an uncontrolled cost increase.

In this thesis, a wide review of the state of the art is done, to allow understanding the context, why such innovative techniques can be used as an aid in design. Each point is discussed focusing on the aim of this thesis, thus presenting arguments, bibliography, and considerations tailored to direct the reader to comprehend the impact of new tools in the ship power systems design.

In particular, after a first chapter dedicated to the introduction of electric propelled ships, in which are described how such ships have evolved. In the second chapter, innovative distribution systems and new requirements are presented, especially for cruise and military ships. Given the significant impact of these innovations, an excursus of both these two topics is given, referring to recent literature and research activities.

In the third chapter, however, a reasoned discussion on the conventional ship design process is depicted. In addition, an in-depth analysis of the onboard ship systems design process is carried out to explain the context in which the innovative design approach has to be integrated.

The fourth chapter is dedicated to new design methods and tools, together with the use of specific software, and how they can be useful for improving the entire ship design. In this scenario, the new concept of space reserved on board is proposed to accommodate the power

system. The space reservation impact on the overall ship design can be evaluated from the early stage design phase.

In the fifth chapter the case study of this thesis is presented. Subsequently, the reference ship is redesigned with two different dc distribution systems. Both the solutions are compared in terms of volumes and weights, thus verifying their feasibility and the validity of the proposed redesign method.

However, the innovative solutions proposed can have a negative impact on the performance of the power system. For this reason, in chapter six, their impact on the onboard power system has been analyzed in order to prevent integration issues. Specifically, the high frequency disturbances propagation has been assessed both in power cables and transformers, experimentally validating the latter model.

Finally, in the seventh chapter, using the data previously obtained, a modular software was used to simulate the reference ship power system in order to evaluate the accuracy and computational load of the various models proposed.

Contents

List of Figures

List of Tables

Introduction

Nowadays, the marine power systems' sector is undergoing significant changes, due to both the ever-increasing ship-owners' efficiency requirements and pollution regulations. For the latter, increasingly stricter limits have been enforced in April 2018, when the International Maritime Organization (IMO) mandate that by 2050 the maritime industry must cut its carbon footprint to half the 2008 level of emissions. Thus, the introduction of power electronics apparatuses is increasingly used as a mean to improve system efficiency. The recent enhancements in power electronics technologies are making it possible to design new electrical systems, by taking advantage of the new devices capabilities. The power electronics exploitation allows building power systems in which the power flow, the faults response, and the loads can be controlled by the converters through suitable algorithms, rather than being an effect of physic laws that must be coped with during system design and operation. Such capabilities are even more critical for naval applications, where the introduction of electrically powered innovative sensors and weapons require an improvement in ship's power and energy system capabilities.

Designing such complex systems is difficult, due to two main issues: the classic ship design process has been conceived when ships were simpler, thus it is becoming inadequate to address the design of modern complex ships; and the proposal of new distribution systems and components imply designing the power system having no previous knowledge on which to base. Moreover, it should be noticed that the existing shipboard power system solutions may evolve in the future resulting in the need of a completely different devices or components. Consequently, the system integrator must be aware to evaluate new and different design choices regardless of the technology or component utilized.

Due to that, the aim of this thesis is to present innovative methods and tools, applicable to the shipboard integrated power system. Such methods and tools address the issues given by both the conventional design process and the desire to install on board new subsystems, whatever the components are. Methods and tools analyzed throughout this thesis work can increase the knowledge of the system already in the early stage design phases. The final goal is to define the feasible design choices before the contract phase. Indeed, such commitments can lead to harmful consequences since the project may not be feasible at the end due to unforeseen issues related to the exploitation of innovative power system solutions. Such methods and tools are a mean to provide consistent data on which base innovative design decisions and explore different design choices. Thus, the design costs can be lowered, as well as the involved industrial risk. New solutions are required due to both the ever-increasing ship-owners' requirements and pollution regulations.

The research work, developed during the PhD activity, has been performed at the Digital Energy Transformation & Electrification Facility (D-ETEF) within the University of Trieste (Italy) and at the School of Electrical and Electronic Engineering within the University College Dublin (Ireland). The development of the research has been made throughout several research projects and activities, which have contributed to achieve the necessary theoretical and practical bases to develop the innovative design methods and tools presented in this thesis work.

In this thesis, a wide review of the state of the art is done, to allow understanding the context, why such innovative techniques can be used as an aid in design. Each point is discussed focusing on the aim of this thesis, thus presenting arguments, bibliography, and considerations tailored to direct the reader to comprehend the design process impact of the proposed innovative ship power systems.

The first chapter is aimed at giving an overview on the innovation in the ship power system throughout the years. At first, the evolution in ship power systems that have led to electric powered ships birth is presented, followed by a concise state of the art of different type of integrated shipboard power systems. The last section of the chapter analyze the current research trajectories. Indeed, four main research paths have been identified along with their specific goals: reduction of volumes/weights leading to a payload maximization efficiency improvement, enabling of new electric pulsed loads/sensors/systems, and cost reduction.

Goal of the second chapter is to present some innovative distribution systems and new requirements. Indeed, onboard systems are evolving from conventional radial ac distributions to new systems, on which no previous design experience is available (such as Medium Voltage dc distribution, Mixed ac/dc distribution systems, etc.). Moreover, new requirements from owners (such as pulsed loads supply or feeding land systems from the ship) are creating new issues never faced before. The design of a ship power system endowed with these new characteristics is difficult to face with common design process, pushing towards the need of a new methods and tools. Due to that, the chapter depicts concisely the characteristics of these innovative distribution systems and possible new impacting requirements, thus allowing the comprehension of the problems the power system designers are facing nowadays.

The conventional ship design process is illustrated in the third chapter along with a discussion on the shipboard power systems design. Firstly, some definitions are given to better comprehend this process and the entities that are involved in it. Then, the ship design process is presented depicting the conventional ship design methodology. Therefore, the main shipboard power system design choices are identified in the overall ship design process.

Innovative methods and tools to design the shipboard power system are described in the fourth chapter. Firstly, the concurrent engineering approach is explained and compared to the methodology described in the previous chapter, emphasizing the advantages of this innovative design method. Then, the focus moves to the innovative distribution system design process highlighting the need to anticipate all the possible information in order to better evaluate the innovative power systems performance. In this context, some examples are depicted to better comprehend such new approach. Moreover, the new space reservation concept is presented evaluating its impact from the early stage design phase.

A reference surface combatant ship has been chosen as case study in the fifth chapter. Thereby, a consistent comparison is carried out between the actual ship power system and other two innovative dc power system architectures. Both the solutions are compared in terms of volumes and weights, thus verifying their feasibility and the validity of the proposed redesign method.

However, the innovative solutions proposed can have a negative impact on the performance of the power system. For this reason, in chapter six, their impact on the onboard power system is analyzed in order to prevent integration issues. Specifically, the high frequency disturbances propagation is assessed both in power cables and transformers though the development of suitable frequency dependent models. In addition, the model for foil-type transformers is validated through experimental results emphasizing the need of a new approach to correct integrate shipboard power system equipment. Then, the cable bundles equivalent parameters are assessed in the last sub-section of this chapter, providing both a reliable inductance matrix reduction method and a Python code capable of obtaining the same results of finite element software.

In the seventh chapter, a modular software endowed with the previously calculated parameters has been used to simulate the reference ship power system. Detailed data about the cables length and their equivalent parameters have been assessed thanks to the combined approach proposed in this thesis work. Moreover, the power system simulations have been evaluated in terms of their accuracy and the computational load required by the different models proposed.

1 Ships Power System Evolution

1.1 Abstract

Goal of this chapter is to give an overview on ship power system evolution. At first, a brief history of the ship power system is presented from its birth to the present. Thus, an overview on the different type of ships is given with the aim of better understanding their peculiarities and their operation. Finally, the current research trajectories have been presented along with their specific goals to allow comprehending the changes that are happening. This to the aim of both introducing the ship power system challenges and explaining why this thesis work has been focused on the design of such systems.

1.2 Ship's innovation

Towards the end of the 30s of the nineteenth century the Prussian inventor Moritz Hermann von Jacobi studied the galvanic phenomena and the practical applications of electric power. Therefore, he built a rudimentary DC electric motor which he used as a propulsion system for small boats along the Neva River in St. Petersburg. In his latest experiment the boat reached the speed of 4 km/h thanks to his motor (1 kW rated power fed by 69 Grove cells[1]). However, this DC motor was soon forgotten and it never found practical application [1] due to the many imperfections and its primitive design. During the early 1870s commercially available shipboard power systems first appeared on marine vessels in the form of gun firing circuits powered by battery cells [2]. Electric call bells appeared on same time in luxury passenger cruise ships. The timeline with the historical highlights of the marine shipboard IPES development is depicted in Figure 1. In those same years, the public lighting spread in big cities (e.g., Los Angeles, Paris, London) thanks to the development of the first arc lamps[2]. Moreover, those lamps were also used onboard to light

[1] The Grove cell was an early electric primary cell named for its inventor (1839) and first investigator, the English physicist William Robert Grove. The cell was made up of a zinc (Zn) anode in dilute sulfuric acid (H_2SO_4) and a platinum (Pt) cathode in concentrated nitric acid (HNO_3), the two separated by a porous ceramic pot.

[2] The arc lamp produces light by an electric arc (also called a voltaic arc). The carbon arc light, which consists of an arc between carbon electrodes in air, invented by Humphry Davy in the first decade of the 1800s, was the first practical electric light.

other ships and to blind any looters. The shipboard arc lamps could reach up to 11000 candlepower and they were powered by steam generators.

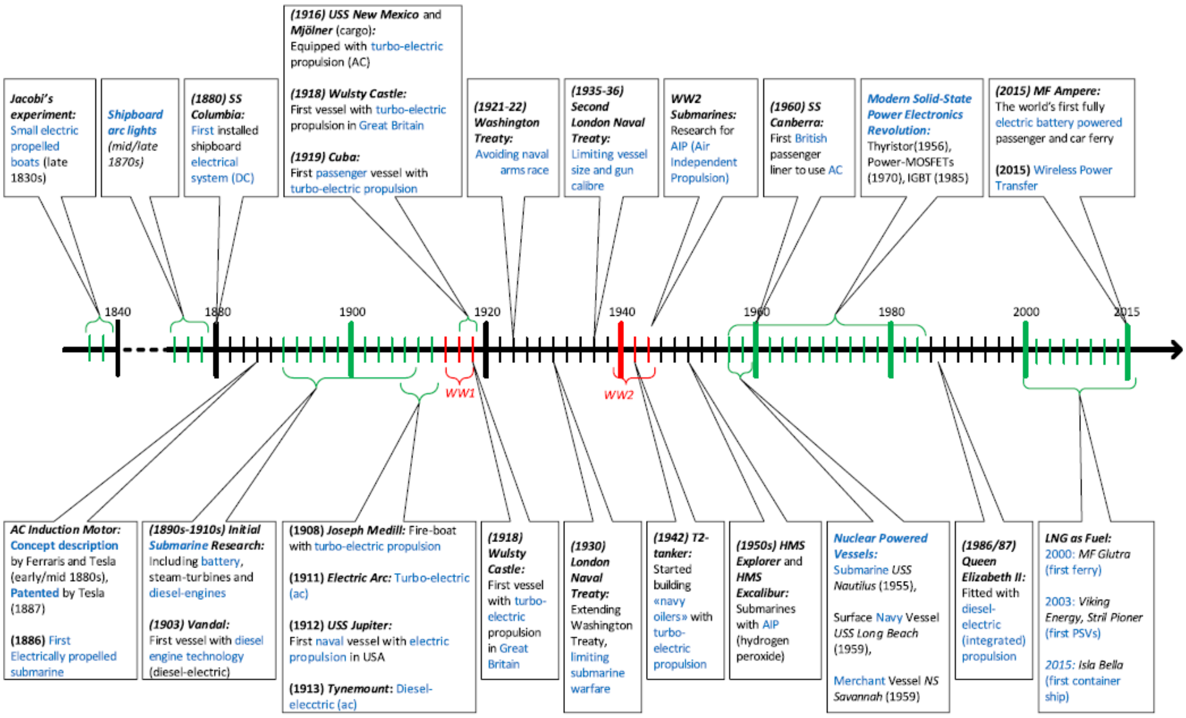

Figure 1 - Timeline with the historical highlights of the marine shipboard IPES development [1]

Then Thomas Edison devised the incandescent electric light bulb in the 1878. Nevertheless, at that time there was no commercial power system for generating and distributing electricity to end users. Thus, an electrical distribution system was needed in order to achieve profitable business. The idea was to develop a direct current electrical distribution network that through a single point of generation and a system of cables would be able to reach multiple end users at the same time. Therefore, the following year he organized a practical demonstration, on his property in Menlo Park, NJ, USA, to prove that it was possible to light some houses and streets through a dynamo placed in his laboratory [3]. Among the potential investors and company heads was Henry Villard, president of the Oregon Railway and Navigation Company. He commissioned to Edison the implementation of the on board lighting system for the SS Columbia. Indeed, his company's new ship was under construction in Chester, PA, USA. Therefore, the ship was equipped with a direct current lighting system powered by four 6 kW dynamos with belt drive. The dynamos were connected to the steam engine driving the propeller through a mechanical shaft. The lighting system consisted of 120 incandescent lights and each DC generator could supply up to 60 lamps (rated 16 candlepower[3] apiece). Since there was no control system, an operator was entrusted to perform the voltage regulation assessing the brightness of the bulbs in the engine room. Indeed, one of the generators was operated at reduced voltage to control the excitation of the other three generators field magnets [1]. Simplified diagram of the propulsion and lighting system installed on the SS Columbia is depicted in Figure 2.

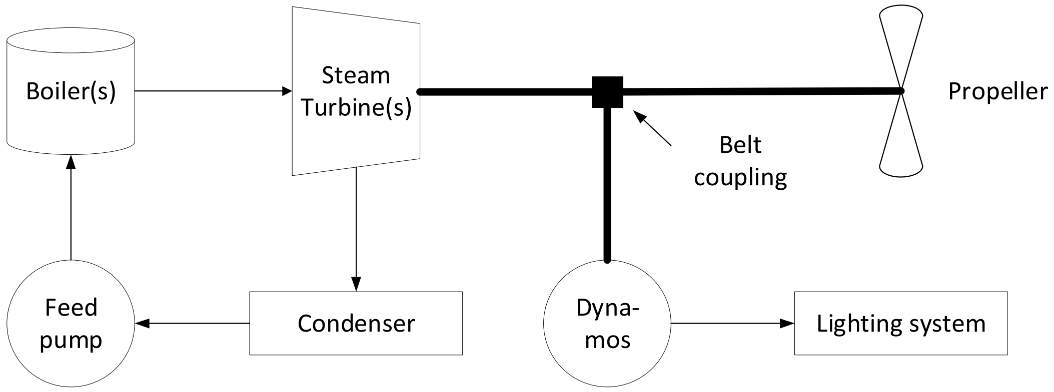

Figure 2 - Simplified drawing of the propulsion and lighting system installed on the SS Columbia

Then, the US Navy USS Trenton was the first vessel equipped with a lighting system installed onboard in 1883, given the SS Columbia successful result. Within a few years, the lighting system became a standard on both commercial and military ships. The low voltage direct current system (110 V) developed by Edison was the only one designed for incandescent lamps at the beginning. Nevertheless, the competition soon became numerous and this period can be considered as the birth of the shipboard power systems.

In the late 1880s, various inventors including Galileo Ferraris (Italy), Nikola Tesla (United States), who worked for Edison until 1885, and Michael Osipowitch von Dilvio-Dobrowolsky (Germany) had successfully exploited the alternate current. Indeed, they independently discovered that three conductors with 120° phase difference (or two with 90° phase difference) could be used to rotate a magnetic field. Thus, this marked the birth of the induction motor, patented by Tesla in 1887. The invention of the AC motor led to the beginning of the so-called "war of currents" with Edison's company and George Westinghouse's Westinghouse Electric Co. as main rivals.

[3] Candlepower (abbreviated as cp or CP) is an obsolete unit of measurement for luminous intensity. It expresses levels of light intensity relative to the light emitted by a candle of specific size and constituents.

The main drawback of the Edison power system was the power losses along the dc transmission lines. Indeed, the higher the line voltage, the lower the line current and thus the Joule power losses should be lower. Nevertheless, rotating machines were the only path to level up or down the dc voltage at that time, resulting in higher costs and losses for the Edison's solution. Instead, the ac power system voltage could be easily leveled up or down through transformers. Thus, the power transmission over long distances was possible and cost optimized (the first 4 kV ac transmission line was almost 20 km long and was built by Westinghouse in 1890). However, the early ac power systems had a power factor lower than 0,8 due to high reactive power flows to support the rotating machines and transformers magnetic field with consequent poor exploitation of the transmission lines capabilities [4].

Regarding the shipboard applications, the early twentieth century dc motors still had better variable loads control compared to the ac ones. Nonetheless, the 1930s ac rotating machines were much easier to build and less expensive than the dc ones. Moreover, the ac control system were less bulky and less heavy. The coal mine USS Jupiter[4] was the very first turbo-electric powered military vessel in 1912 [5]. Thus, the USS New Mexico was equipped with electric propulsion despite being originally designed with steam propulsion, given the success of the USS Jupiter experiment. The battleship power system had two 11.5 MW ac turbo-electric generators (with dual voltage 3000/4242 V) feeding four asynchronous motors. The installed power allowed the ship to reach speeds of 21 kn. Moreover, there were also six auxiliary turbo generators (300 kW each) to feed the lighting system and other loads. Figure 3 schematically illustrates the simplified drawing of the shipboard power system installed on the USS New Mexico. Nevertheless, it should be emphasized that in those years the power electronics had not yet been developed and therefore the speed of the ship was controlled through a complex combination of frequency (speed) and voltage variations of the generators and by changing the configuration of the magnetic poles of the motor.

The advantages brought by the turbo-electric propulsion systems were numerous:

- On-board transmission shaft length reduction and therefore of the hull. The generators and the engines were connected through power cables.
- Fuel consumption optimization.

[4] It was refitted into the very first US Navy aircraft carrier and named USS Langley between 1920-1922.

- Increased reversal speed, given by the higher response speed of an electromagnetic system, compared to a mechanical one.

All those benefits, however, came at the cost of weight, since the electric motors and generators weighed much more than the drive shaft they replaced [1].

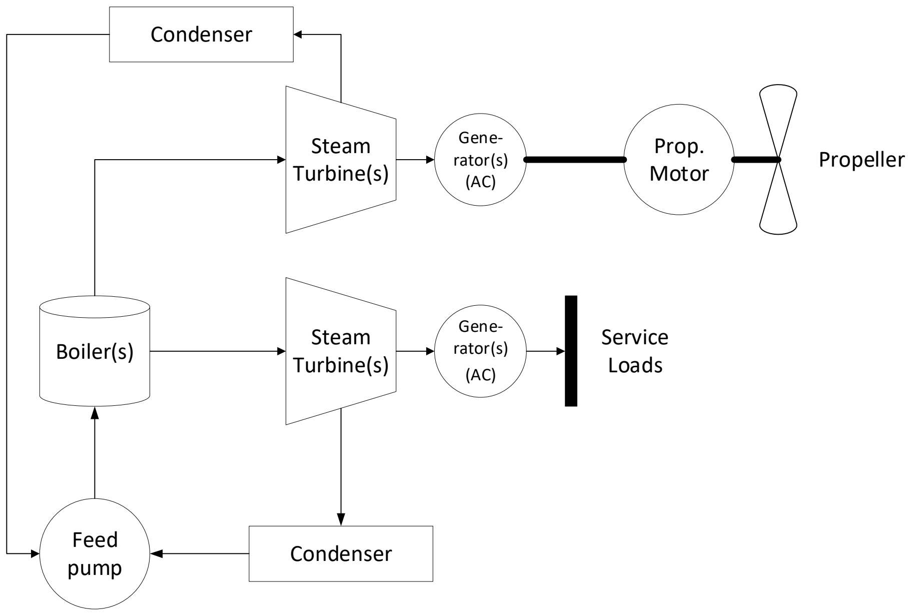

Figure 3 - Simplified drawing of the shipboard power system installed on the USS New Mexico

Another invention from a few decades earlier, however, was bound to slow the development of turbo-electric propulsion systems. In 1892 the German mechanical engineer Rudolf Diesel patented the engine that bears his name (a technology destined to radically change even land-based propulsion systems) and granted the Swedish Emanuel Nobel an exclusive license to build his engine in Sweden and Russia [6]. Thus, the river tanker Vandal was launched in 1903 to transport oil from the lower Volga to St. Petersburg and Finland. The Vandal had three diesel engines coupled with an electric controlled transmission capable of varying the speed from 30 to 300 rpm. This was the first working example of a diesel-electric transmission and it was not employed on military vessels until the First World War.

Regarding the submarines, they first appeared during the First World War and they were initially designed as surface ships that could dive only for a limited period of time depending on the cruising speed (from about one hour to two days [7]). The propulsion was entrusted directly to the Diesel engines during the surface navigation as depicted in Figure 4, while the electric motors recharged the batteries and fed the ship's loads. Conversely, the entire power system was supported by the batteries in diving operations and thus the underwater time was significantly limited: this limit was later solved thanks to the nuclear power exploitation[5].

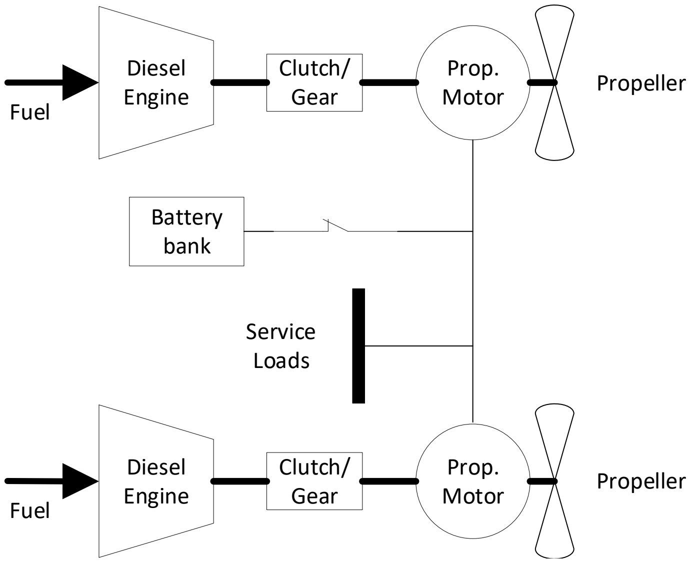

Figure 4 - Simplified drawing of a submarine propulsion system

In the early decades of the twentieth century, however, the turbo-electric power system ensured higher propulsion power than the Diesel engine. Nevertheless, the entire turbo-electric propulsion system had an overall efficiency close to 10% (from fuel to propeller). Therefore, the continuous Diesel engines technology improvements made them the main onboard power propulsion source together with the parallel increase in their rated power. Moreover, the Diesel engine efficiency can reach the 40% (in fixed speed applications) and that is the reason why electric power propulsion hadn't been use for years until the early 1980s [8], [9].

Indeed, in the early 1980s, the development of semiconductors devices allowed to fully control the speed and the torque of the electric machines with ever-higher power outputs. Firstly, a thyristor rectifier controlled a dc motor by varying the supply voltage. Secondly, the speed of an ac motor was controlled through supply frequency variation. Thus, the

[5] The USS Nautilus (SSN-571) was the first nuclear-powered military submarine launched in the world in 1954. The submarine can now be visited at the Submarine Force Museum in Groton (Connecticut).

possibility of having a propeller speed adjustment independent of the internal combustion engine speed has paved the way for new ways of exploiting electric propulsion.

Nowadays, a ship usually provides multiple Diesel generators (or gas turbine generators) that can maintain the power system nominal voltage and its frequency values. The shipboard power system act as a land based microgrid in island operation with short distances between producer and consumer and thus makes the power system management and control even more tough. Thanks to the power electronics it was possible to use controlled electric motors for propulsion at low speeds with an efficiency of about 95% in a range between 5% and 100% of the rated power. Conversely, the traditional combustion engines have an optimal efficiency around 85%-90% of the rated power but very low in other configurations. Making an extensive comparison to all possible operating conditions of a ship, the electrical losses of the former are negligible since the operations at maximum speed, and therefore at maximum power are limited to very short time periods. Such concept can be illustrated through Figure 5, in which the total efficiency of the power system (diesel to propeller) is shown in respect to the engine Maximum Continuous Rating (MCR) percentage, for both mechanical and electric propulsion.

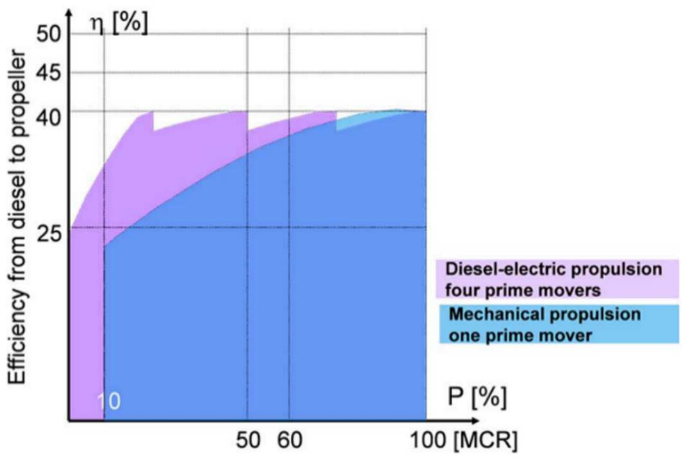

Figure 5 - Electrical propulsion versus mechanical propulsion efficiency in shipboard power systems [1]

The British transatlantic cruise ship Queen Elizabeth 2 (QE2) was equipped with a diesel-electric propulsion system (Figure 6) in this regard. The ship was initially built for the Cunard Line[6] in 1968 with steam propulsion. However, the owner decided to retrofit the

[6] The Cunard Line (also known as the Cunard White Star Line) is the most prestigious British shipping company. The company was founded by Samuel Cunard in 1838.

QE2 with a total installed power of about 100 MW given the serious technical problems it suffered: a boiler failure in 1983 and a blackout due to a fire in 1984. This was a record among electric-powered ships, recently overcome by the British aircraft carrier QE2 with a total of 112 MW. Such a ship is example of the worldwide Navies interest in the AES concept together with some lesser tonnage units. The QE2 cruise ship system consisted of nine Diesel generation groups capable to fully powering the vessel. The cruising speed of 28.5 kn was reached with only 7 groups in operation and with a fuel saving of 35% compared to the previous engine [7].

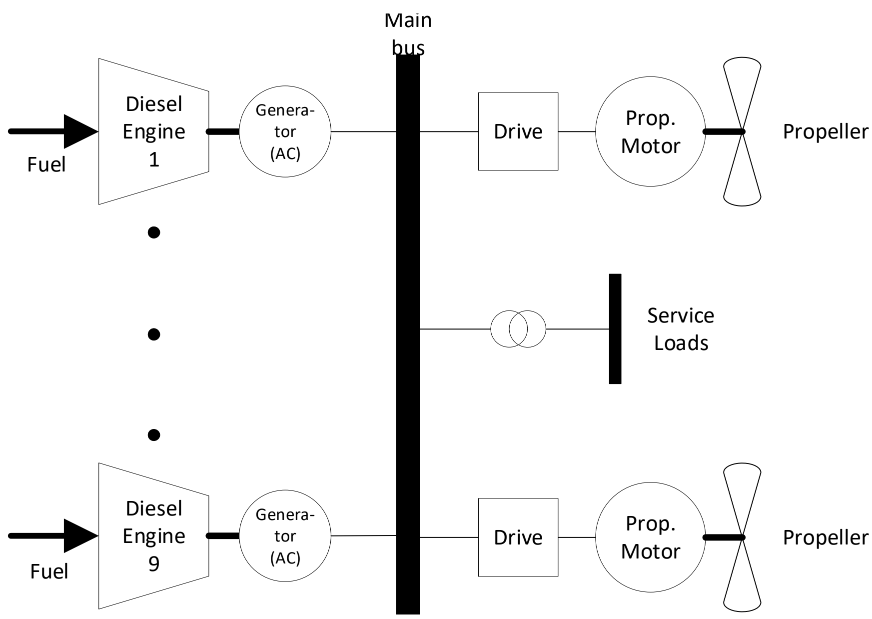

Figure 6 - Simplified drawing of the Queen Elizabeth 2 integrated power system

The shipowners were highly responsive to the huge fuel savings provided by the electric propulsion. Thus, this solution was soon applied not only in many other cruise liners but also in the icebreakers due to the need for maximum torque with stuck propellers, for instance. As aforementioned, the electric propulsion allowed to keep the global efficiency at a high level also for low loads, given the chance to start the generators (thus their prime movers) only when needed. However, this reasoning is true not only for the propulsion but also for the other onboard loads. In fact, the total installed power can be lowered if both are supplied by the same power system. As an example, cruise ships sails mostly by night, when passengers sleep. Therefore, the electric load required by the hotel section of the ship drops, whereas the power required for propulsion increases in the nighttime. Conversely, the ship is usually moored in port in the daytime and, thus, the propulsion load is absent;

however, at the same time all the passengers are awake and use ship's commodities, increasing the hotel load. Indeed, the concept of electric propelled ship evolved until the definition of the so-called All Electric Ships (AESs). The AES can be defined as a vessel endowed with a single power system supplying both the propulsion and all the other onboard loads [9]. Despite the various improvements in the shipboard power system design and capabilities, its enhancements has not stopped [10]. In fact, the power system can be now equipped with Energy Storage Systems (ESS) demanding innovative dc power system sections, for instance. Moreover, the today regulatory framework increasingly requires more environmentally friendly (or even zero emission) shipboard power systems to meet the Emission Controlled Areas (ECAs) restrictions. Both the dc power systems and the today regulatory framework will be later treated in detail (see sections 2.2 and 2.3 respectively). However, zero emission navigation is currently not possible in huge size ships (e.g., cruise ship) due to the required battery pack dimension to meet the operational profile consumption. Therefore, the ESS would cause a considerable bulk and weight increase, along with the costs. Nevertheless, the first zero emission ferry was the MF Ampere launched in Norway in January 2015 [1].

Finally, the Hybrid Electric Drive (HED) System deserves to be mentioned especially as regards the naval combatants [11]. The HED system is endowed with both mechanical and electrical propulsion as depicted in Figure 7. The shaft generator can act as motor in the so-called Power Take In/Power Take Off (PTI/PTO) mode. Such a configuration allows the power distribution system to propel the ship in a low speed condition (PTI) and therefore when the mechanical propulsion is less efficient (see also Figure 5). Conversely, the mechanical propulsion feed the propeller at medium/high cruising speed and thus the shaft generator can act in the PTO mode in order to maximize the internal combustion engine (or gas turbine) consumption.

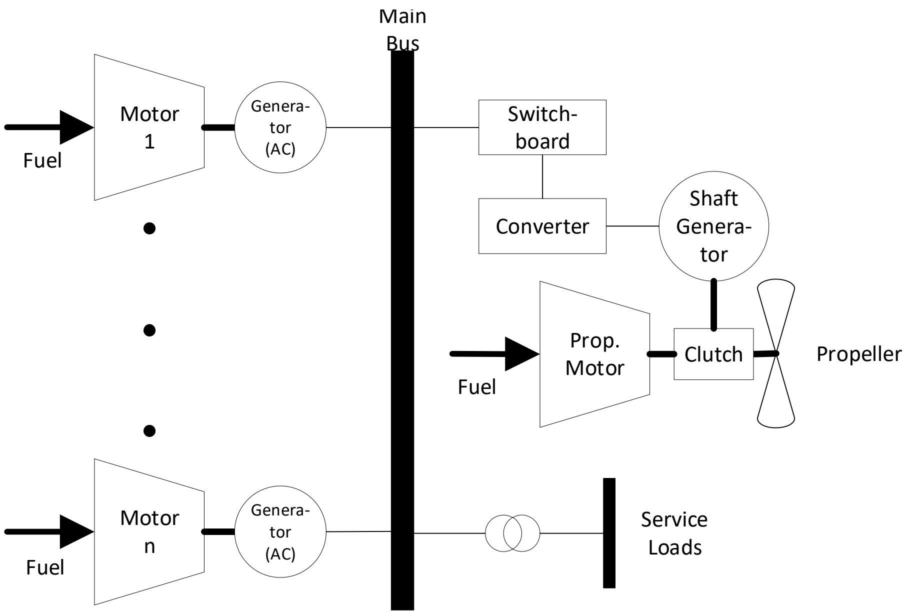

Figure 7 - Simplified drawing of a hybrid-electric power system

1.3 Ship power system application

Nowadays almost the totality of newly built ships are endowed the Integrated Power System, at least as far as large vessels. The benefits brought by the integrated power system are considerable and mainly due to the electric propulsion exploitation [12]. The main benefits can be summarized as follow:

- The electric propulsion has a better dynamic response compared to the mechanical propulsion. Moreover, the acceleration and maneuvering operations are enhanced with the electric propulsion system control.
- Higher freedom in the power system layout design. Indeed, the electric generators and the propulsion motors are connected through power cables (no long shafts) and thus they can be placed in different areas resulting in better space and weight management. Moreover, the ship survivability is increased since the generators are not located in one engine room.
- The availability of podded-drive solution can enhance even further the ship maneuverability due to the rudders and shafts removal.
- Higher overall efficiency as depicted in Figure 5, for instance.
- Reduction of onboard noise and vibration resulting in improved comfort and in lower vessel acoustic footprint.
- Enhanced maintainability and operating life due to lower prime mover stress and less mechanical components.

- The integrated power system enables new automation features resulting in crew reduction.

Nevertheless, the shipboard power distribution system can be arranged in different solutions, which are the result of different vessels requirements and duties. Common power system architectures can be identified despite the strong application dependency. In [7], [8], [13] the shipboard integrated power systems are thoroughly depicted. Generally, the shipbuilding industry is still little responsive in adopting new power system architectures or in leveraging new technologies. Indeed, only when a new solution proves to be reliable enough is then exploited onboard. Hence arises the need to develop new methods and tools for the design of naval and marine power systems aiming at boosting the electric ship innovation.

Nowadays, the majority of the existing cruise ships and commercial vessels are endowed with an ac radial distribution system, as shown in Figure 8. Such a structure is the result of regulations and technical improvement that have occurred over the years. Concerning the regulations, the SOLAS (Safety of Life at Sea) Convention [14] in its successive forms is generally regarded as the most important of all international treaties regarding the merchant ships safety. Indeed, the first version was adopted in response to the Titanic disaster in 1914. Furthermore, the SRtP - Safe Return to Port regulation, part of requirements published by the SOLAS, had a huge impact in the power system design [15] and it entered into force on July 1st, 2010. The regulation requires passenger vessels with a length of 120 meters or more or with three or more main vertical zones to be designed with the goal to achieve the required ship survivability. A ship Main Vertical Zone (MVZ) has been defined by the SOLAS as the section into which the hull, superstructure, and deckhouses are divided by “A” class divisions, the mean length of which on any deck does not in general exceed 40 m. An “A” class division is a bulkhead or part of a deck constructed of steel or other 'equivalent material' and capable of preventing the passage of smoke and flame for a period not less than 60 minutes. This means that, in the event of fire emergency of a flood, passengers and crew can stay safely on board as the ship proceeds to port under its own power. It defines a threshold where the ship’s crew should be able to return to port without requiring passengers to evacuate. The scale of the SRtP compliance sets great challenges for ship design [15]. Many systems need to be doubled or their operation in a damage situation needs to be secured in other ways. The SRtP safety regulations involve an innovative approach, modern tools, and the application of best practices. Moreover, the required redundancy should be reached at the lowest possible cost.

The radial power system architecture usually involves one up to three main generators for each main busbar, connected through tie-breakers, feeding all the onboard loads through a Medium Voltage ac (MVac) distribution system (Figure 8). The tie-breakers are always closed in the normal ship operation and, therefore, resulting in a single power system. This is the so called closed bus condition. Thus, the aforementioned efficiency goals can be achieved, and the two main switchboards can still be separated by the tie-breakers opening in case of faults. In the so called open bus operation the two main switchboards can operate as two separate power systems.

Three-phase distribution is always applied due to the high power level required by the integrated power system, while some low voltage end-circuits can be single-phase. Concerning the voltage levels, MVac primary distribution is required in such ships ranging from 4.4. to 11 kV, while secondary Low Voltage ac (LVac) distribution can range from 127 to 690 V. Those values depend on the total installed power, the shipowner requirements, and ship's area of operation. As an example, the cruise liner power system depicted in Figure 8 has a primary 11 kV distribution with 230, 440 and 690 V secondary LVac distribution sections. Standard voltage levels are identified in [16], [17] and other applicable standards. In such an architecture, the main generators frequency is strictly connected to the power system frequency (50 or 60 Hz). Note, that the choice between these two values is mainly due to owner requirement and the ship's area of operation. Indeed, it can be stated in general terms that the ship's that will operate in Europe are built with 50 Hz, while other use 60 Hz.

Finally, there are some loads directly connected to the MVac through transformers and power electronics converters (e.g., the thrusters and the electrical propulsion motors), usually one per main busbar as depicted in Figure 8. The secondary LVac switchboards supply all other ship loads and they are fed by the MVac distribution system through MVac/LVac transformers.

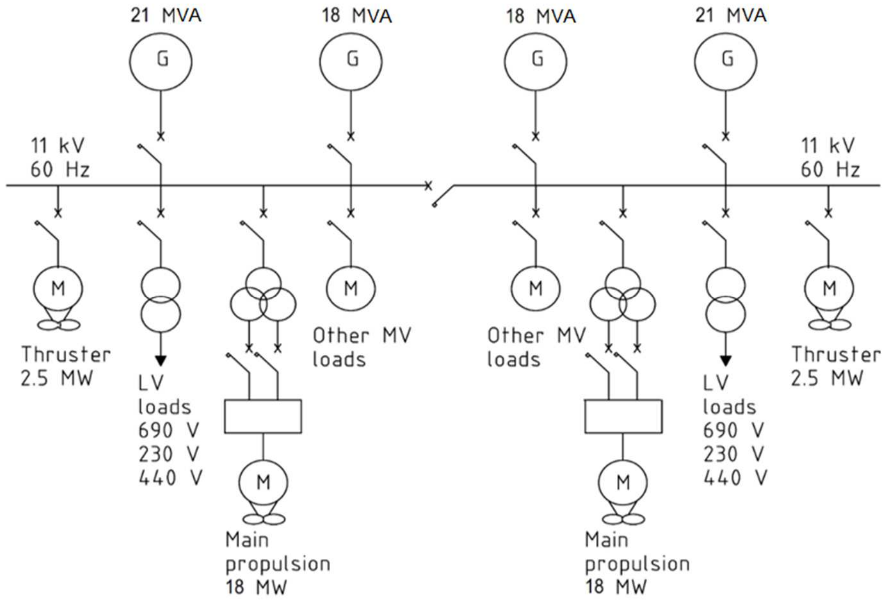

Figure 8 - Typical cruise ship integrated power system layout [9]

Other ships can have different power system layouts, such as the one depicted in Figure 9, used in offshore drillships [18]. A drillship is a merchant vessel designed for use in exploratory offshore drilling of new oil and gas wells or for scientific purposes. In such a vessel, the strict Dynamic Positioning (DP) requirements result in a complex power system design. Indeed, the ship operating capability must be ensured in the event of faults avoiding environment or people damage. Such a ship requires a fast acting power system capable to meet the propulsion system's load profile to keep the vessel at the desired coordinates. In addition to DP systems, the vessel maneuverability is enhanced by different thruster designs, such as bow and azimuth thrusters. The management of all these different equipments is tricky due to their fast changing load profiles. Thus, also the fuel consumption optimization is tough making the offshore drillships power system design challenging.

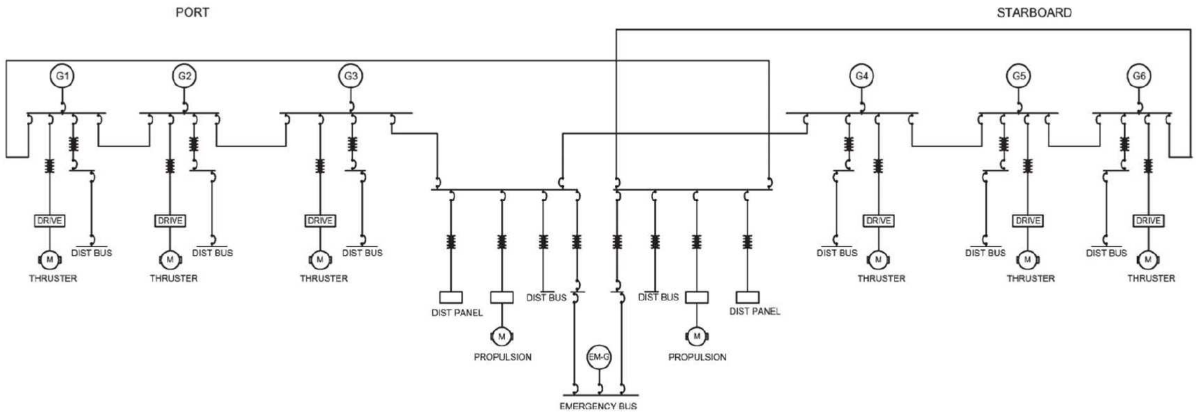

Figure 9 - Typical offshore drillship integrated power system layout [18]

The IT Navy aircraft carrier “Nave Cavour” has another different power system layout as illustrated in Figure 10. The integrated power system has a ring structure in order to maximize the ship’s survivability. Indeed, the generators are distributed onboard the ship hull with the aim to limit the power system damage in case of external threats [19], [20]. Moreover, other frequencies can be used in such a power system. The 400 Hz distribution is dedicated to aircraft supply in aircraft carriers, for instance, and other peculiar frequencies can be exploited for military grade electronic warfare equipment. However, those sections are small and limited to end-circuits.

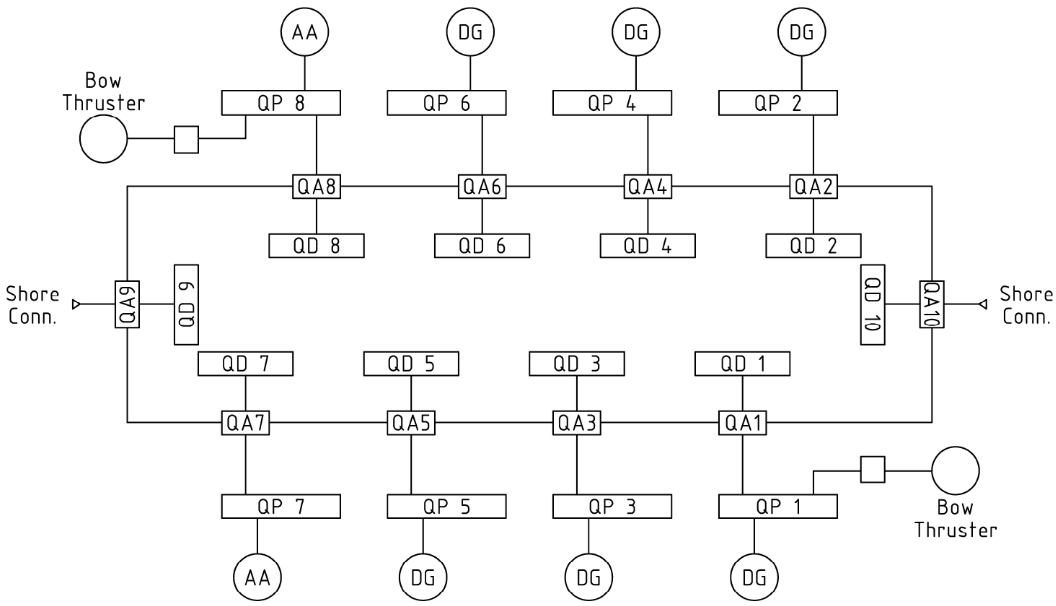

Figure 10 - IT Navy "Nave Cavour" aircraft carrier integrated ring power system one-line diagram [19]

As stated in the section 1.2, the ESS technologies improvement result in the MF Ampere which is the first zero emission passenger and car ferry [1]. The vessel is 80 m long and its simplified one-line diagram is depicted in Figure 11. The ferry can accommodate 360 passengers and can carry 120 cars during its 30 minutes trip between Oppedal and Lavik, near Bergen, Norway. The vessel, which was certified by DNV-GL, is powered by two Corvus Energy battery packs approximately 500 kW each feeding, of course, two separated main switchboards. Thus, the SRtP requirements are still met in the MF Ampere power system. The ship batteries are charged on each side of the route using the land based power grid. Nevertheless, the villages' power grid is too weak to provide the required ferry energy in the limited charging time. And therefore, as illustrated in Figure 11, two more ESSs are provided to smooth the grid power peak demand.

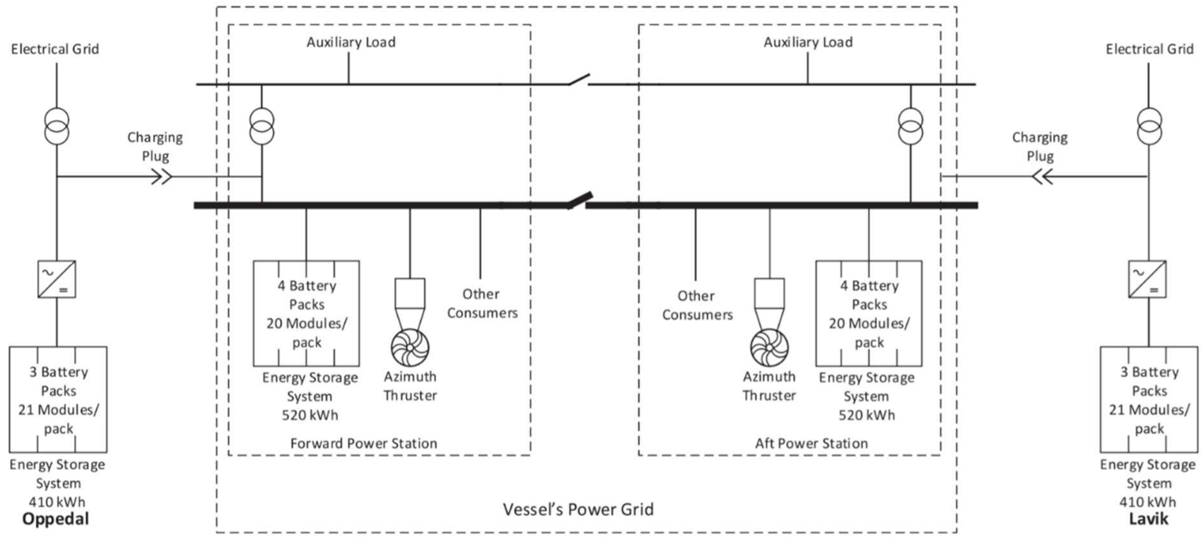

Figure 11 - Simplified one-line diagram of MF Ampere all electric battery ferry [1]

Despite the high variety of ship power systems duties and requirements, the main electrical loads are common to all types of ships presented so far. The loads can be then summarized in a few categories:

- Main propulsion loads. Usually the highest power loads onboard, the main propulsion system is used to propel the vessel forward and backward. Nowadays a cruise ship can reach tens of MW for each propulsion axis, as seen in Figure 8 (18 MW), while other ships can reach even higher power levels [21]. The variable speed electric motor is directly connected to the fixed pitch propeller fed by power electronic converters. Nonetheless, variable pitch propeller can be exploited to meet high performance requirements. Both PWM converters controlling induction machines and cycloconverters (or synchroconverters) coupled with synchronous machines are used as a motor onboard: the formers are increasingly being employed and the latter can be found in older power systems.

- Maneuvering propulsion (thrusters, azipods); The ship maneuvering capabilities can be enhanced both during navigation and in docking operation through auxiliary propellers. As depicted in Figure 8, the thrusters are a Direct On Line (DOL) induction motor coupled with a variable pitch propeller. In the foreseeable future also the PWM supplied motors coupled with fixed pitch propellers could reach the same hydrodynamic performance of the DOL motors.
- Heating, Ventilation and Air Conditioning (HVAC) loads. Set of subsystems needed to keep the ship indoor environmental comfort in terms of thermal comfort and acceptable indoor air quality. Heating and ventilation subsystems are electrically powered and distributed onboard, while air-cooling is usually attained through a cold-water closed loop system. Thus, the main switchboard directly supplies the heat exchangers and electrical compressors to provide the required cold-water.
- Hotel loads. All the electric loads needed to ensure the ship habitability like lighting, kitchens, waste treatment, entertainment, and so forth. In cruise vessels the hotel load can be compared to the ship propulsion in terms of required power, while it can be a small percentage of the total load in merchant and naval vessels, for instance.
- Navigation system loads. A set of subsystems that are used to keep the right route avoiding harmful collisions such as radio systems, satellite, GPS, radar systems. These loads are supplied by dedicated power converters due to high power quality they need.
- Other loads not mentioned in the above classification are here grouped (e.g., firefighting pumps, fuel management, etc.)

The integrated power system is a rather complex system and thus proper control systems have to be designed and installed onboard. Moreover, it should also bear in mind that the onboard power system acts as an islanded grid without the aid of a slack bus as commonly happens in land power systems [22]. Therefore, the power system voltage and frequency, which are the main system variables, need to be kept within an acceptable range. The voltage and frequency limits are imposed by the regulatory bodies on both static and transient voltage and frequency deviations. In Table 1 the ship power system voltage and frequency limits are shown, taken from Lloyd's Register of Shipping [23]. To be compliant with these limits is not an easy task, despite they appears fairly broad when compared to the land power system ones. Indeed, some loads can have a size comparable to the power system generators in shipboard power systems and thus their connection/disconnection leads to significant transients. Nevertheless, the limited number of running generators (and thus the low system inertia) and the power system reduced extension amplifies the perturbation. Therefore, the Automatic Voltage Regulators (AVRs) and the Speed Governors (SGs) are the most important control system to ensure the compliance with the limits in Table 1. The former acts on the generators' excitation mainly to control the power system voltage, while the latter adjusts the prime mover power output mainly to meet the power system frequency limits. In addition the Power Management System (PMS) can be installed onboard to coordinate all the subsystems' control system [24], [25].

Table 1 – Ship power system voltage and frequency limits [23]

Voltage	Steady state tolerance	+6%, -10%
	Transient tolerance	±20%
	Transient recovery time	1.5 s
Frequen	Steady state tolerance	±5%
	Transient tolerance	±10%
	Transient recovery time	5 s

Not only technical limits should be ensured, but also the safety requirements imposed by the regulatory bodies (e.g., the SRtP regulation for merchant ships). Moreover, the rules greatly differ according to the different types of ship and therefore defining methods and tools that are suitable for each purpose is not easy. Thus, a deeper focus on the ship power system evolution and design will be presented in the next section.

1.4 Ship power system revolution

In the section 1.2 the ship power system history has been illustrated discussing the main technological milestones. Moreover, the mayor one-line diagram changes have been depicted accordingly. The shipboard power system has not only complex electrical design and requirements, but it also must cope with the available onboard space and the weight constrains. Indeed, the transition from steam plants and mechanical propulsion to Diesel generators and electric propulsion has revolutionized the onboard space allocation in the cruise ships, for instance. The spaces previously dedicated to the engine room were thus exploited as a consequence to increase the ship payload. In Figure 12 such a scenario is shown in three separated periods for different type of ships: merchant ship, cruise ship, and military vessels. The main changes in shipboard power system can be graphically displayed and therefore the resulting ship layout arrangements. It must be highlighted that what is labeled in Figure 12 as possible future scenario is the present one for full electric ferries like the MF Ampere, as stated in the previous section. This has been called the second electronic revolution [26]: just as the first electronic revolution changed the concept of shipboard power system, the second electronic revolution is redefining its control. What stands out most is how the ships' funnels have gradually disappeared over the years or substantially reduced. Therefore, more efforts are needed to proof the successful integration of new electric technologies in the ship design process not only in terms of higher power system capabilities but also taking into account their space allocation.

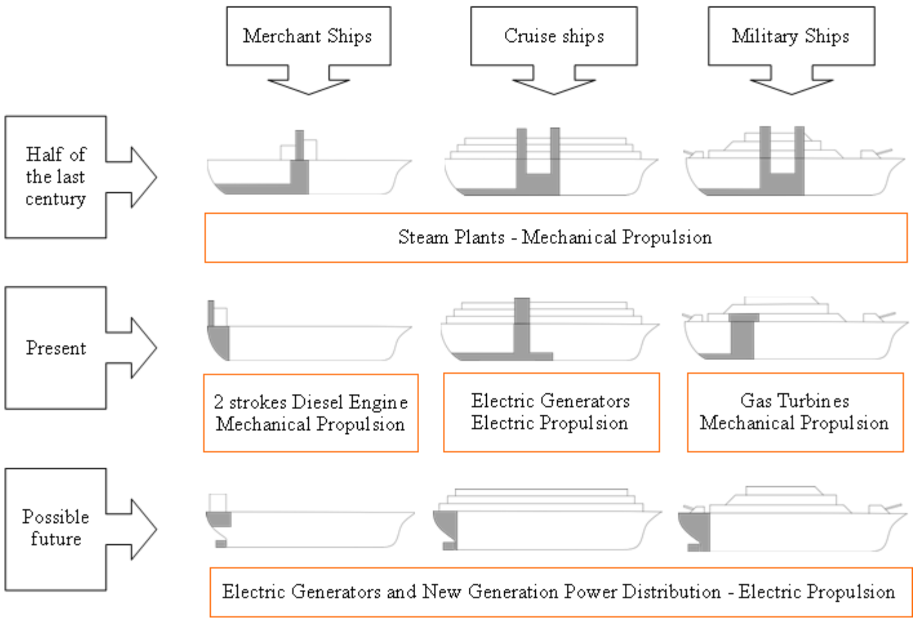

Figure 12 - Different ship layout arrangement due to power system evolution over the years [27]

Since the goal of this thesis is to provide new methods and tools capable to enhance the future shipboard power system design, the current research trajectories should be taken into account with the aim of better understanding the changes that are happening. In this scenario, four main research paths can be identified along with their specific goals:

- Reduction of power system volumes and weights in order to maximize the ship payload. As seen in Figure 12, the transition from the present ship layout arrangement to the possible future one could bring a significant power system volume reduction. Indeed, many papers have compared the benefit of onboard technical volume reduction exploiting new equipment [28]–[30] or different voltage levels [31]–[33]. Moreover, high-speed prime movers and generators can also enable weight reduction [34]. The decrease in the volume reserved to the power system can thus enable improvements in the volumes devoted to the ship payload in quality or in quantity. Finally, innovative sky-line and innovative hull-forms may be designed as a consequence, bringing further advantages [35].

- Efficiency improvement and different power system layouts enhance the ship capability, reliability, and functional safety [36]–[38]. New integrated power system layouts are attractive with particular emphasis to shipboard MVdc distribution (see section 2.2.1), in this regard. MVdc distribution systems can enable the high-speed prime movers/generators exploitation decoupling the loads' frequency from the generators' one. Moreover, the dc distribution can easily integrate innovative storage systems for different on-board users [27], [39]–[41]. Those new solutions must be compliant with the SRtP rules of course and can improve the ship reliability [42], functional safety [43].
- In navy application, the integration of new sensors and weapon systems is easier, given the availability of a dc power supply [44], [45]. Indeed, new electric pulsed loads are becoming trustworthy and thus they are already installed onboard as in the innovative US Navy destroyer "U.S.S. Zumwalt" (class DDG1000) [46]. Those systems such as Solid State Lasers (SSLs) [47], new solid state radars [46], railgun [44], Electromagnetic Aircraft Launch System (EMALS) [48] results in the need to improve ship power and energy system capabilities along with its design [49].
- Cost reduction can be achieved through new methods and design tools. The ship MVZs can be designed in order to reduce the interferences between each other (e.g. lower number of power cables passing through "A" class division bulkheads [33]) resulting in shipbuilding time and cost reduction. Moreover, different modular vertical zones can be realized during shipbuilding in parallel instead of in time consequence. In this regard, the payload zones can be designed on-demand with more flexibility and with less interferences with zones devoted to propulsion or power generation, for instance. Thus, the shipbuilder has better margins to negotiate with shipowner thanks to those new design methods and tools.

As an example, considering that volume and weight imposes hard constraints in shipboard application, the cumbersome and heavy low frequency transformers can be replaced by lighter power electronics devices. Nevertheless, power electronics equipment should be adopted not only for its volume and weight reduction, but also reliability and safety constraints should be considered. Therefore, research on new design tools and methods is needed to integrate onboard innovative technologies. In such a scenario the cross-fertilization from other technical areas (i.e., smart grids, aero-space, etc.) can be useful to achieve the goal. The impact of these technologies on ship design drivers should be evaluated in order to properly select the vessel design in advance, in the so-called early stage design phase (see chapter 3).

This thesis work does not propose a comprehensive method to redefine all the ship design process since there are too many and too complex aspects to consider but tries to give a methodology to improve system design. This work will give a general overview on those issues focusing on some particular aspects that will be dealt with in the following chapters.

2 Innovative distribution systems and new requirements

2.1 Abstract

Goal of this chapter is to present some innovative distribution systems and new requirements. Indeed, onboard systems are evolving from conventional radial ac distributions to new ones, on which no previous design experience is available. Moreover, new requirements from owners are creating new issues in ship design never faced before. The design of a shipboard power system endowed with these new characteristics is difficult to face with common design process, pushing towards the need of a new methodology able to address the design of such an innovative system.

In the following, these innovative distribution systems and possible new impacting requirements will be described, to allow comprehending the problems the designers are facing nowadays.

2.2 Innovative distribution systems

Regarding innovative shipboard distribution systems, the naval application can be considered the most demanding in terms of both capability and reliability. In this scenario the U.S. Navy is certainly the most advanced navy and thus its research trajectories are paramount. Indeed, the Naval Power and Energy System Technology Development Roadmap [50] aligns electric power and energy system development with increasing warfighter power needs. Development of the roadmap was spearheaded by NavSEA's Electric Ships Office (PMS 320) and represents the Navy's vision for the future of electric power and energy systems. As illustrated in Figure 13, the MVdc distribution will have an ever-growing impact in the next generation of ship power systems. Nevertheless, also mixed ac/dc distribution will play an important role in the transition to MVdc distribution and thus should be taken into account.

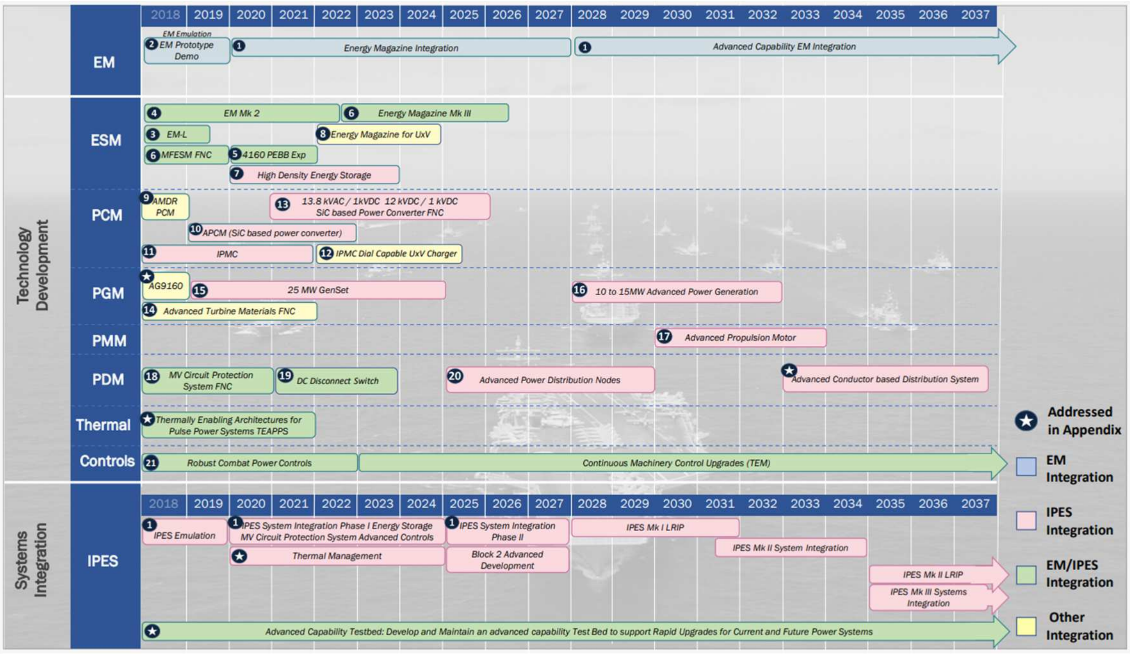

Figure 13 – U.S. Navy's vision for the future of electric power and energy systems [50]

2.2.1 MVdc distribution

In recent times, the new navies' vessels are exploiting the AES concept through the installation of MVac power systems. In this context, the know-how gained in the merchant field allowed navy designers to successfully design such ships. Giving a well-known design base, the goal was to enhance the mission capabilities along with high reliability levels. The most recent vessels built using AES concept are, for instance, the U.S. Navy DDG1000, the abovementioned aircraft carrier HMS Queen Elizabeth by the U.K. Navy, and the French/Italian multi mission frigates. In addition, the IT Navy has planned the acquisition of hybrid-propelled ships for all its new ships exploiting the interest of navies in AES concept. Nonetheless, the adoption of MVac based AES concept is not an ending point for navies. In fact, the research effort is going towards new power system concept as stated in Figure 13. In the last years, the U.S. Navy research has been focused on the exploitation of new MVdc distribution power systems [39], [51]–[53]. Despite the advantages brought by the dc distribution system, some major issues are still present, whose solving require both industrial and academic research effort.

The most important advantages of the dc power distribution over ac can be listed as follows:

- There is no need for phase angle synchronization, thus the generators connection procedure is simplified.
- After faults, reconfiguration is enabled by the use of power electronics devices.
- Shipboard generators are no more strictly coupled with the power system frequency (50 or 60 Hz) and therefore high-speed generators can be used for reducing power system weight and volume.
- Prime movers can operate in variable speed mode and thus the fuel consumption can be reduced and optimized.
- Energy storage can be directly connected to the MVdc bus thereby enhancing power availability and overall system efficiency. Moreover, energy storage enables peak shaving and therefore generators and prime movers can be sized no more for the load peak resulting in reduced fuel consumptions too.
- In navy application, the availability of a dc power supply enables an easier integration of weapon systems and new sensors.
- Finally, the power flow control is improved, particularly in emergency and transient conditions.

Power electronics conversion systems are needed to exploit the above listed advantages. Indeed, dc distribution requires conversion systems to operate properly: power electronics devices are the only mean available to change the voltage level in dc power systems, for instance. Nevertheless, MVdc power systems have some critical issues that must be addressed before a full onboard adoption. These issues can be listed as follows:

- The absence of voltage or current zero crossing makes it difficult to extinguish the dc arcs and thus the build of suitable dc breakers is a complex task [54].
- The dc grounding strategies are a sensitive issue since the common mode currents should be limited [55]–[58] to ensure the crew electrical safety.
- Nowadays the MVdc power systems are not as successful as the MVac ones and thus there is a lack of a well-established industrial base [59].

The last point is the main obstacle in the exploitation of MVdc power systems. Indeed, there is a lack of industrial partners, although the research efforts, which can provide reliable dc components. Thus, the MVdc solution has been ignored by ship designers discouraging suppliers' investments in the MVdc components. Luckily, the ESS technologies development has pushed the main power components supplier to develop new reliable devices that are no longer mere prototypes nor reduced scale demonstrators. Main power system companies have found new business opportunities in this sector, such as ABB, Siemens, Danfoss, Yaskawa, and so on.

A functional block diagram of the MVdc power system is illustrated in Figure 14 [51] to better understand how MVdc distribution works. Therefore, the functional blocks can be defined as follows:

- Shore power interface: a connection interface that allows the MVdc shipboard power system to be fed by the utility system on shore usually through a transformer coupled with an ac/dc interface converter.
- Power generation: a power source that use prime energy (marine diesel oil, hydrogen, natural gas, etc.) to generate electric energy. This block is usually composed by a prime mover coupled with an electric generator (or fuel cell using hydrogen) and then the power is adapted to the desired MVdc level through an ac/dc interface converter.
- Energy storage: a system which can store energy for use at a later time to reduce imbalances between energy demand and energy production (e.g., batteries, supercapacitor, flywheel). Such a system can improve the overall system power quality if exploited, for example, in peak shaving configuration.
- Pulsed load: high performance demanding loads generally used in military sector. Such a loads require high power in little amount of time (e.g., EMALS, railgun, and laser).
- Propulsion: a load center that provides the required propulsion power to the propellers. The electric motors are supplied from the dc grid through variable speed drive dc/ac converters.
- Ship service: a load center that power the ship service systems, such as the hotel load.
- Dedicated High Power Load: a load center feeding other high power demanding loads (1 MW or more of power in steady-state operation), such as military radar, large thruster, and compressor.
- Ship-wide power and energy management control: the PMS optimize the power flows throughout the ship maximizing the continuity of service of vital loads in case of threats or faults.
- System Protection: dc system protection is achieved through different layers. Such protection layers are composed by the converter control, dc circuit breakers (e.g., solid-state dc breakers), and high speed fuses.

- MVDC bus: the mean to connect and deliver power from and to all the functional blocks above listed.

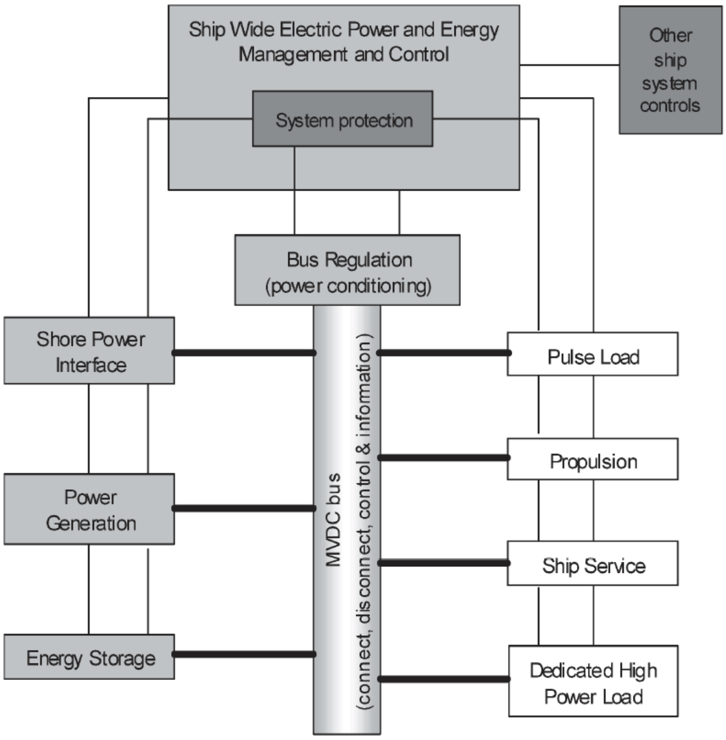

Figure 14 - Functional block diagram of MVdc power system [51]

As stated before, the power electronics converters are key enablers for the MVdc distribution systems [60]. In fact, power electronics converters are widely use in the notional shipboard power system with MVdc radial distribution shown in Figure 16. The converter becomes a key component of the power system. In addition, the converter can be endowed with advanced features capable to enhance the overall reliability, such as integrated short circuit protection or fast reconfiguration. These new converter features are described in the IEEE Std. 1676 [61] and in [42] for a comprehensive approach. Moreover, they are briefly reported in Figure 15 to highlight their complex implementation.

Therefore, new tools are required in order correctly design innovative power systems. Moreover, the absence of prior knowledge can be an issue giving the installation of never used components in shipboard power systems. The goal is to provide appropriate methods and tools to help designers understand the impact of these new devices on the overall system. In this regard, the next chapters of this thesis work can help designers to better understand how to tackle these new issues.

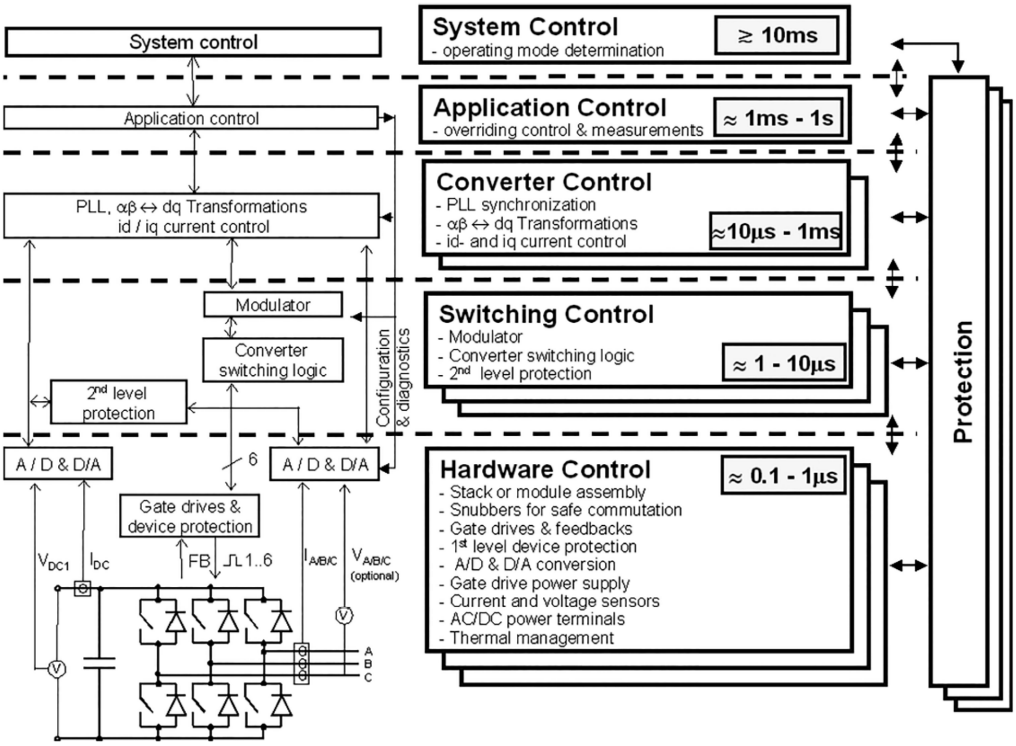

Figure 15 - Hierarchical control architecture in power electronics converters [61]

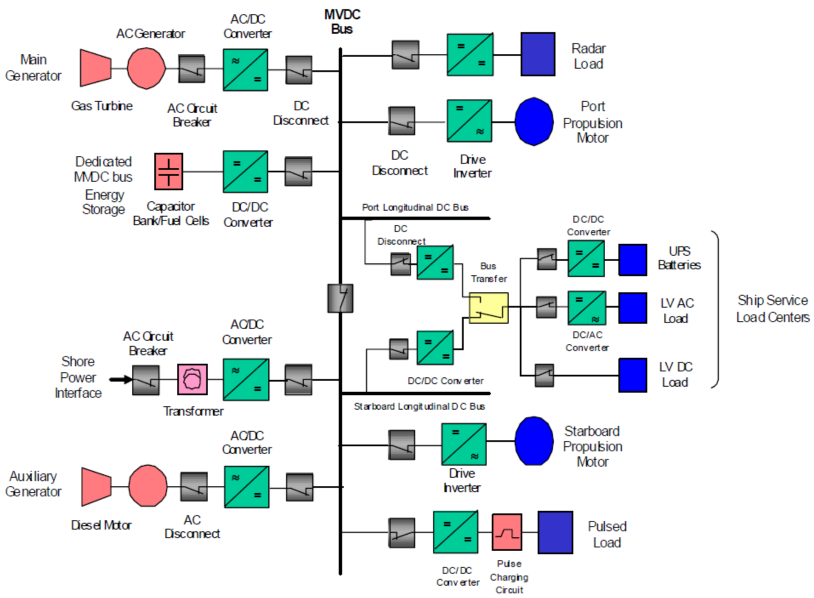

Figure 16 – Shipboard power system with MVdc radial distribution [51]

2.2.2 Zonal distribution

Radial distribution system is a standard de facto in the shipboard applications, as stated in the section 1.4. Also, the ring distribution system (Figure 10) can be a suitable solution, but it is scarcely used onboard ships. Among this ship power system distribution topologies, the zonal distribution layout has been recently proposed. The Zonal Electrical Distribution Systems (ZEDS) are considered a next technological evolution, as they provide optimal power sharing (and energy storage) along with high reliability. Indeed, at least two independent power supply inputs for loads should be available in shipboard zonal distribution and thus maximizing the continuity of service. In Figure 17 the notional diagram of a zonal power system is depicted, while Figure 18 the concepts of ZEDS and zone are illustrated [62]. The IEEE Std. 1826 defines the standard practice for power electronics open system interfaces in ZEDS rated above 100 kW and it is the reference standard for the design of such systems. In Figure 18 the main blocks of a zone are shown and can be below summarized:

- External-to-bus conversion: this block has several functions listed as follows
  - Faults within the zone should not be propagated to other zones or power systems and the zone should similarly not be affected by external faults.
  - The block converts the power from and to other external power system or zone into the required type needed for the in-zone distribution bus or the external power sources, respectively.

    Multiple external-to-bus conversion interfaces can be installed in a single zone in order to connect more zones or external power systems.
- In-zone distribution bus: The in-zone distribution bus may be subdivided into multiple buses and it interconnects all the in-zone blocks. Thus, the bus can be either distributed throughout the zone or fully enclosed in one cabinet.
- In-zone energy storage: this element can store energy for use at a later time to reduce imbalances between energy demand and energy production (e.g., batteries, supercapacitor, flywheel). Such a system can improve the zone power quality if exploited, for example, in peak shaving configuration. This block is an optional element of the ZEDS.
- In-zone generation: this block represents a power source that use prime energy (marine diesel oil, hydrogen, natural gas, etc.) to generate electric energy. This block is usually composed by a prime mover coupled with an electric generator (or fuel cell using hydrogen). This block is an optional element of the ZEDS.
- Bus-to-internal conversion: this block interfaces the in-zone distribution bus to either the distributions panels or the end-use devices. Bus-to-internal conversion shall

protect the in-zone distribution bus from faults occurring in either the distributions panels or the end-use devices.

- Distribution panel: this block interfaces the end-use device to the bus-to-internal conversion and it shall protect the latter from faults occurring in end-use devices.
- End-use device: this block is not directly connected to the in-zone distribution bus and it can be either a load or a source. It can be connected to a distribution panel or a bus-to-internal conversion device.

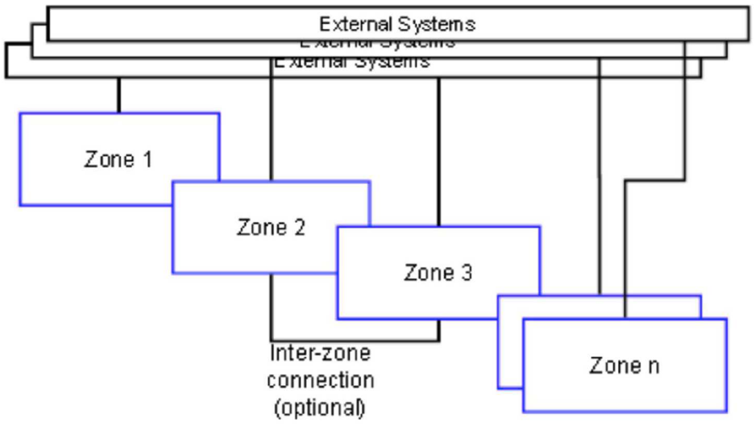

Figure 17 - Notional diagram of a zonal power system [62]

Figure 10

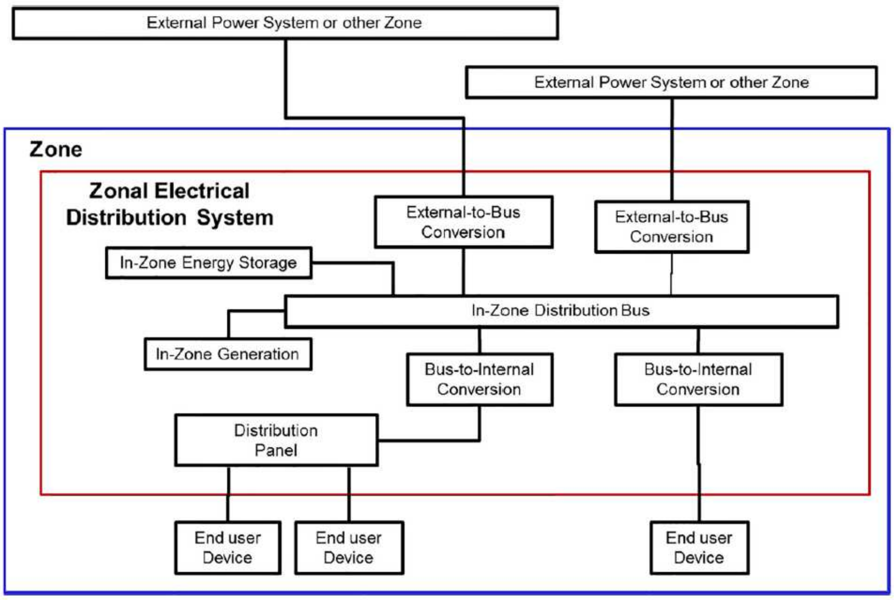

Figure 18 - Concepts of ZEDS and Zone [62]

The zonal distribution system can easily integrate different power sources, energy storage systems, and external power supply paths and this is both its main pro and con. In fact, the degree of freedom given by such a configuration results in its complex control system design. For example, in Figure 19 the ZEDS hierarchical control system architecture is given. Such a control scheme requires a high level of automation capable to continuously monitor and manage the system to reach the desired point of work.

ZEDS are a promising solution for the future shipboard power systems due to its high modularity and both power quality and continuity of service standard. Nevertheless, the technical issue in ensuring a reliable zonal power system configuration is the main obstacle in the spread of such a solution. Indeed, hidden interrelations among the high number of active devices paves the way to unforeseen issues. Finally, the zonal version of the notional MVdc shipboard power system is given in Figure 20 [51]. The ZEDS concept is merged in the zone load center block and thus providing an overview of the entire chipboard power system.

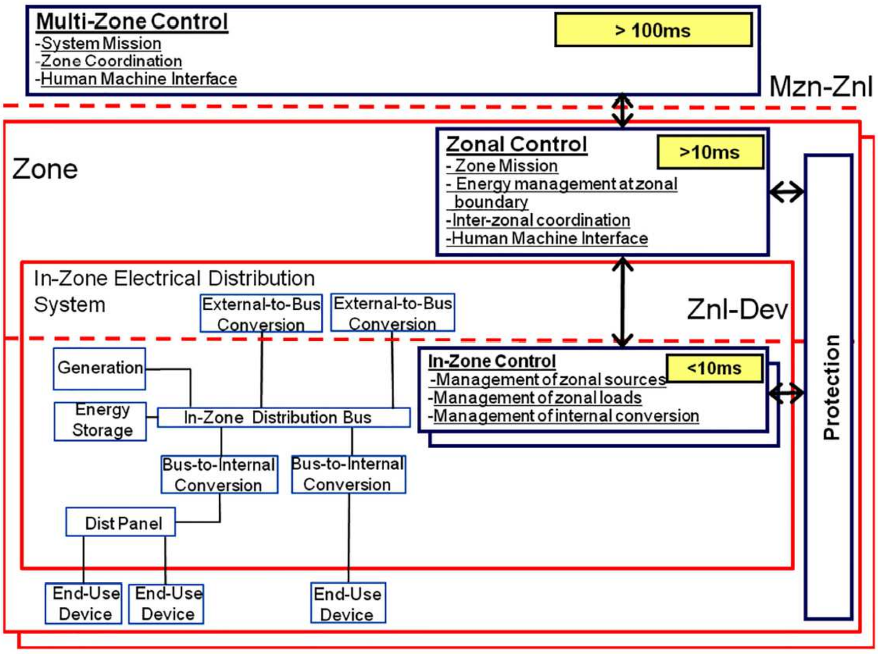

Figure 19 - ZEDS hierarchical control architecture [42]

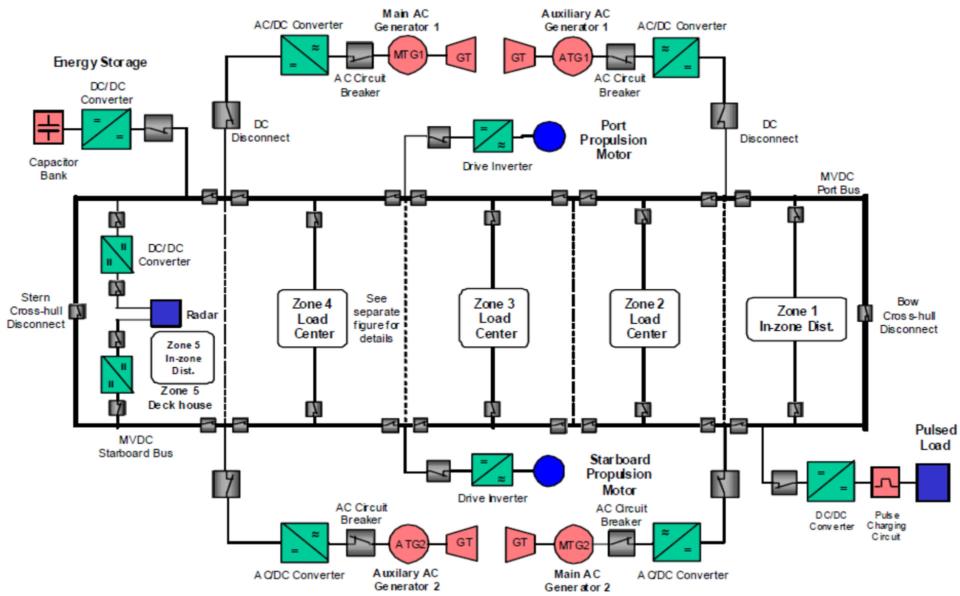

Figure 20 - Shipboard power system with MVdc zonal distribution [51]

2.2.3 Mixed ac/dc distribution

The innovative MVdc shipboard power system has been previously described in section 2.2.1. But for the time being, there are no existing application of such a system onboard despite several land based demonstrator aiming at de-risking the MVdc technology. Nevertheless, the conventional MVac distribution system can be coupled with a Low Voltage direct current (LVdc) secondary distribution. The concepts of zonal distribution system can be endowed in the LVdc network achieving some of the pro of the MVdc power distribution. In Figure 21 a notional mixed MVac/LVdc integrated power system is depicted. The LVdc zonal distribution is interconnected with the main MVac distribution through power converter interfaces. Thus, the zonal distribution network can achieve most of the dc advantages previously described: power flow active control, easy integration of ESS, high power quality, and fast reconfiguration actions. The ship essential loads (e.g., electronic warfare systems and radars for naval vessels, navigation and communication subsystems for merchant ships) will benefit of the dc grid pros. Moreover, LVdc components are nowadays market available and thus allowing to design such a system in a reliable way. The best example of mixed ac/dc grid is the U.S. Navy guided missile destroyer USS Zumwalt (DDG1000) [63], reported in Figure 22. The U.S. Navy initially planned the construction of thirty-two vessels but then the number falls to three due to the issues encountered during the ship design and construction. Indeed, the cost of the ship dramatically increased due to the design and technical problems of such a new solution. At the same time, the IT Navy is financing the Naval Smart Grid research project [32], [64] on the same topic. The aim of the research project is to define guidelines for the new design of IT Navy vessels endowed with innovative power system distribution. In particular, the possible exploitation of mixed ac/dc distribution systems can enhance the ship power system capabilities and thus supplying innovative loads. The guidelines aiming at the integration of the best present technologies with the future ones. The project goals can be summarized as follows:

- Analyze the actual technologies state of art and identify the ones suitable to enhance the power system capabilities.
- Integrate the best present technologies by leveraging the research activities results.
- Define new operative requirements.
- Design electric propelled vessels endowed with improved power system capabilities.

The lack of MVdc market available components can be overcome through the exploitation of mixed ac/dc power systems. Nonetheless, unforeseen issues can arise even with an architecture with a lower design impact than the MVdc, as learnt by the US designer with the Zumwalt class destroyers. Thus, new design methods and tools can avoid such issues or at least reduce them.

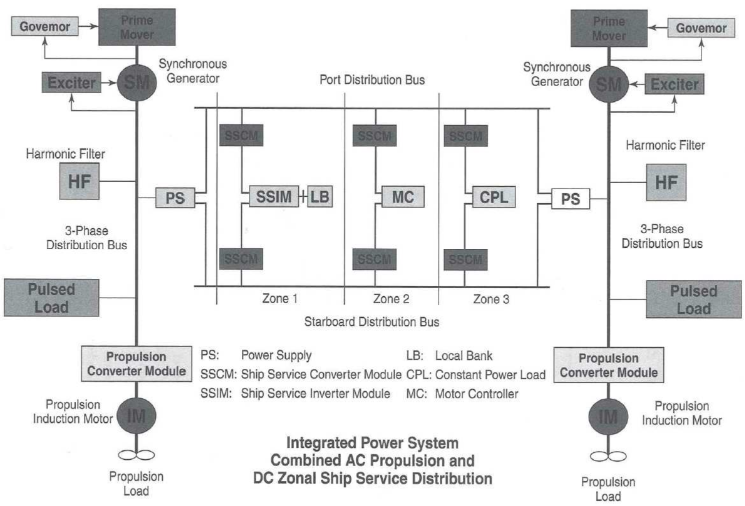

Figure 21 - Notional mixed MVac/LVdc integrated power system [65]

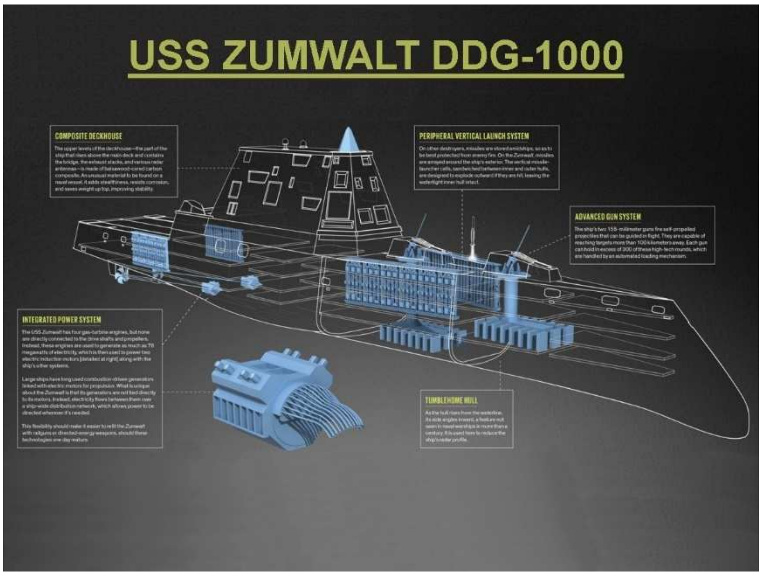

Figure 22 - USS Zumwalt (DDG1000) most innovative characteristics [63]

2.3 New requirements

In the military sector, the U.S. Navy is known to be one of the navies that invest most in the research and development of new weapon systems and new ships. Therefore, the U.S. Navy is currently the reference for the new requirements of the ship power system, at least for the western geographical regions (America and Europe). Obviously, the Navies of the individual States have specificities that are reflected in the issuance of their own requirements, alternative or additional to those found in the development lines of the U.S. Navy. The Italian Navy – Marina Militare Italiana (MMI) is no exception in this defining some specific requirements (New weapons, new sensors, shore-to-ship connection) for its naval units that impact on the onboard power system. The distinction between combat system and platform is becoming increasingly blurred. Indeed, this section aims to provide an overview of the causes of such phenomena given that naval units are becoming more and more electric. This will be done in order to motivate the innovative approach to the design of modern naval units, proposed in the next chapters.

In the merchant sector, there is obviously no need to power such new systems. Indeed, the merchant ships new requirements are due to the adoption of stricter rules on pollution, requiring shore-to-ship connection and zero emission navigation in some areas.

2.3.1 Military innovative requirements

The U.S. Navy research and development guidelines are periodically published by Naval Sea Systems Command (NavSEA) in a report entitled “Naval Power and Energy Systems Technology Development Roadmap” [50]. This document presents the operational context and the short-term, medium-term, and long-term requirements regarding the evolution of onboard power system technologies for surface combatant ships. This document clearly identifies the technological challenges and priorities to be faced in order to achieve the development goals set by the U.S. Navy. A quick analysis of the document shows how most of the research and development priorities defined by NavSEA. The electrical technologies are considered an enabling element for almost all the objectives to be achieved in terms of mission capacity, environmental impact, sustainability (including economic), and safety.

The most technologically advanced expression (result of the activities defined by this roadmap) is the DDG1000 (Zumwalt Class), which already meets some of the new electrical requirements defined for combat ships: there are impulsive loads, a new flat face radar, innovative weapon systems, multifunction converters and related necessary functional ESS. Nonetheless, the DDG1000 represents a result obtained with current technology, and capable of responding only partially to the challenges defined by the NavSEA document. Therefore, the DDG1000 can be considered as already outdated in a research and development context.

A rough distinction can be made between short-term and long-term Research and Development (R&D) requirements. For the former, solutions that make it possible to meet these requirements are already available, with a Technology Readiness Level (TRL) that can reach level 5 or 6 (see Figure 23). For the latter, significant research and development is required to raise their TRL and make them available for integration onboard ship in the near future. All this cannot go beyond the operational context in which a specific naval unit is designed and built.

Phase	TRL	Hardware	Software
Research	1	Basic principles	
	2	Concept and application formulation	
	3	Concept validation	
Development	4	Experimental pilot	
	5	Demonstration pilot	
	6	Industrial pilot	
Deployment	7	First implementation	Industrialization detailed scope
	8	A few records of implementation	Release version
	9	Extensive implementation	

Figure 23 - Technology Readiness Level (TRL) scale

As already stated, the electrical technologies are a key enabler for the achievement of the objectives set by NavSEA. The new weapon systems currently under development (for example the LASERs, the Railguns, EMALS – see Figure 24) are all electrically powered, and they are a key element for maintaining an operational advantage over competitors. In addition, the incremental improvement of existing sensors and weapon systems (such as radars) is itself the cause of an increase in electrical requirements with the aim to), to add new functions and/or increase performance. An example of the power level required by these new systems is shown in Table 2 [66].

Table 2 - Hypothetical specification of innovative high power weapon systems

Equipment	**Required Power [MW]**	**Weight [t]**	**Square Footage [m²]**
Railgun	60	152	110
Laser (Medium Power)	2	21	12
Laser (High Power)	60	65	297
Multi-Function Phased-Array Radar	4	70	137

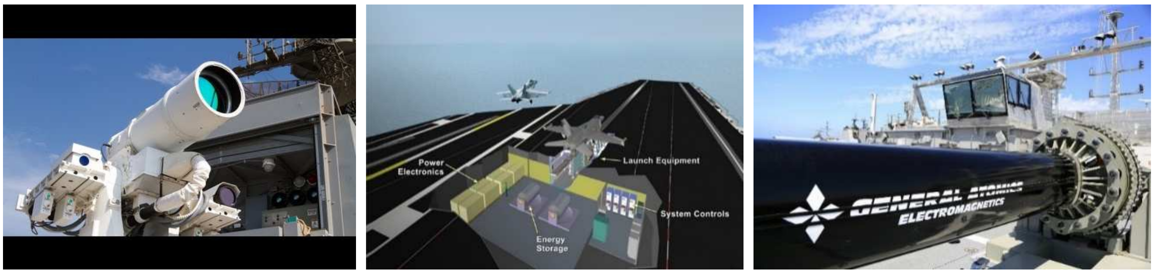

Figure 24 - Example of pulsed power loads: Solid State Medium Power Laser (on the left), EMALS (center), Railgun (on the right)

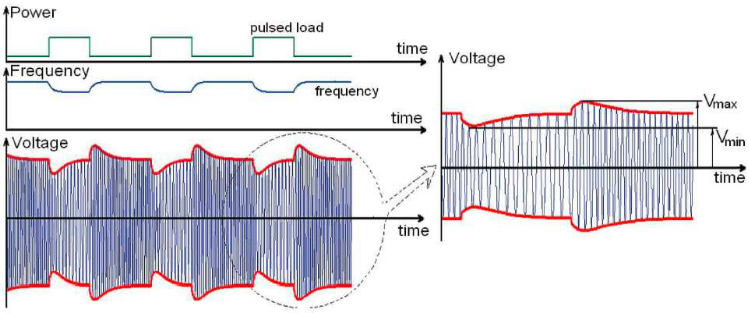

Figure 25 - Impact of a generic pulsed power load on an ac power system [67]

These systems, in addition to the high power required have another feature that distinguishes them from common loads: they are pulsed loads. This means that the continuous power absorption of such systems is relatively reduced but at regular intervals (for sensors) or when fired (for weapons). Their absorption peak (see Table 2) lasts for a very short time (from a few milliseconds up to values in the order of seconds). Due to the peculiarities of shipboard power systems, this behavior stresses the integrated power system in such a way to impair the Power Quality down to levels below the requirements. Such an issue can be clearly seen in Figure 25, where it is shown the effect of the operation of a pulsed load on a conventional ac power system. Therefore, the pulsed loads require special considerations in order to be fed without affecting the overall system operation, despite being characterized by an amount of energy manageable without problems from the power system. Indeed, a high power absorption but in a short time of application means low power system required energy.

As previously stated, the pulsed loads can heavily affect the power system performance. Thus, the pulsed load impact on the overall power system power quality should be reduced. In this scenario, the ESS can be used as a power buffer interposed between the power system and the pulsed load. Indeed, the ESS can supply the pulsed load absorption peak while acting as a not pulsed power load for the grid: constant power load in recharging scenario.

By doing so, the proper power system power quality can be achieved despite the presence of pulsed loads decoupling these loads from the rest of the power system. This solution has been considered by many researchers [45], [47], [68], [69] but this topic is not the subject of this thesis work.

As it is clear from the values shown in the Table 2, the impact of these electrical loads on the ship power system becomes significant, even not considering the Railgun or the High Power Laser. The power required by combat system loads (up to a few MW) can no longer be tackled with a separate project, in which platforms and weapon systems are developed separately and integrated together only at the end.

The introduction of electric propulsion on board the ship (albeit of limited power given the frequent adoption of hybrid configurations) already forced the power system designers to consider the onboard power system and the propulsion system as a whole. Thus, the introduction of these loads brings the level of complexity to grow further and blurs the distinction between platform and combat system. In fact, the operation of these systems requires the design of an electrical system with sufficient generation capacity, flexibility (in terms of transient management and power quality), reconfigurability, and possibly the presence of ESS, leading the NavSEA to coin the new term “Power and Energy System”.

Nonetheless, it should be highlighted that these new combat systems are powered at 1 kV in direct current. This choice is evident in [66], but is also demonstrated by the adoption in the DDG1000 of a 1 kV dc zonal distribution. In addition, the DDG1000 radar will be installed on board the DDG51 Flight III, equipped with appropriate static converters for its power supply at 1 kV dc (ref. Figure 26). In addition to the installation of these converters, the installation of more powerful generators and the adoption of a medium voltage ac distribution system (4160 V) is envisaged to cope with the increase in the platform required power. This is the first time that a U.S. Navy unit of this type has adopted a medium voltage distribution, which is significant especially considering that DDG51 type ships were purely mechanical propulsion units. Of course, a profound revision of the ship project is needed to accommodate the new system components in the existing project. The thermal load related to this new radar is also not negligible, which requires additional cooling systems (also electric), spaces on board, and further increases the complexity of its onboard integration. It is therefore clear that future weapon systems will have an ever greater impact not only on the onboard power system, but also on the entire ship project. given the increasing power requirements to be installed on board and the close relationship between the mission capability of the unit and the effectiveness of the on-board electrical system. Given this scenario, the 1 kV LVdc distribution is the new de facto standard for powering the sensors and weapon systems of the future.

Physical Characteristics

	X-Band SPY-3 Array
Height	107 in.
Width	82 in.
Depth	25 in.
Weight	5,500 lbs.
Total Weight Below Decks	45,025 lbs.
Total DBR Power Consumption	2,000 KW
Total DBR Chilled Water Consumption	900 gpm@11°C
Total DBR Heat Load	1,350 KW

Figure 26 - Characteristics of Raytheon's DBR radar installed on board the DDG1000, and its integration on board the DDG51 - Flight III

As stated earlier, the navies of the various countries define specific requirements, based on their operational concept and their typical missions. A specific requirement of the MMI is the adoption of mechanical-electric hybrid propulsion (in various configurations depending on the unit) for all new naval units. This choice makes it possible to exploit the advantages of electric propulsion at low speeds (see 1.2): low noise and vibrations, high efficiency at partial loads, possibility of using the shaft-generator function, low operating costs. At the same time, the mechanical propulsive part allows to obtain high operating speeds with smaller dimensions and weight for the same installed power compared to an all-electric solution. The integration of a hybrid type propulsion onboard is an impactful operation, which requires a design approach that considers its presence from the early stages of the project.

Moreover, the possibility of supplying shore-side electricity grids in emergency conditions is another specific requirement of the MMI (“ship-to-shore” functionality, in Figure 27). This functionality is enabled by the significant level of electrical power that can be generated on board the ship, resulting from the increase in electrical loads on board and the adoption of hybrid propulsion as already described above. From the design point of view, this means having to manage a bidirectional shore-connection system, with more complex protections and equipment than the classic dock connection systems already present [70], [71]. In addition, it requires the deployment of a part of electrical equipment dedicated to the interconnection of the ship with the electrical system present on site. This equipment can be transported on board the ship itself, or transported by other units, with consequent impacts on the ship project and the performance of the mission.

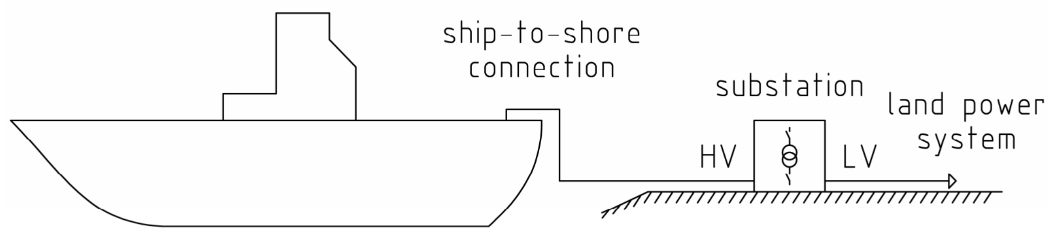

Figure 27 - Ship-to-shore connection [71]

2.3.2 Merchant ships innovative requirements

The today regulatory framework increasingly requires more environmentally friendly (or even zero emission) shipboard power systems to meet the Emission Controlled Areas (ECAs) restrictions. Indeed, the IMO ship pollution rules are given by the “International Convention on the Prevention of Pollution from Ships”, known as MARPOL 73/78. Just like SOLAS, which regulates the shipping industry to follow minimum standards to safeguard life at sea, MARPOL is another important convention which safeguards the marine environment against ship pollution. On September 1997, the MARPOL Convention has been amended by the “1997 Protocol”, which includes Annex VI titled “Regulations for the Prevention of Air Pollution from Ships”. MARPOL Annex VI sets limits on NOx and SOx emissions from ship exhausts and prohibits deliberate emissions of ozone depleting substances from ships of 400 gross tonnage and above engaged in voyages to ports or offshore terminals under the jurisdiction of states that have ratified Annex VI.

The IMO emission standards are commonly referred to as Tier I, Tier II, and Tier III standards. The Tier I standards were defined in the 1997 version of Annex VI, while the Tier II/III standards were introduced by Annex VI amendments adopted in 2008, as follows:

- 1997 Protocol (Tier I)—The “1997 Protocol” to MARPOL, which includes Annex VI, becomes effective 12 months after being accepted by 15 States with not less than 50% of world merchant shipping tonnage. On 18 May 2004, Samoa deposited its ratification as the 15th State (joining Bahamas, Bangladesh, Barbados, Denmark, Germany, Greece, Liberia, Marshal Islands, Norway, Panama, Singapore, Spain, Sweden, and Vanuatu). At that date, Annex VI was ratified by States with 54.57% of world merchant shipping tonnage. Accordingly, Annex VI entered into force on 19 May 2005. It applies retroactively to new engines greater than 130 kW installed on vessels constructed on or after January 1, 2000, or which undergo a major conversion after that date. The regulation also applies to fixed and floating rigs and to drilling platforms (except for emissions associated directly with exploration and/or handling of sea-bed minerals). In anticipation of the Annex VI ratification, most marine engine manufacturers have been building engines compliant with the above standards since 2000.
- 2008 Amendments (Tier II/III)—Annex VI amendments adopted in October 2008 introduced (1) new fuel quality requirements beginning from July 2010, (2) Tier II and III NOx emission standards for new engines, and (3) Tier I NOx requirements for existing pre-2000 engines. The revised Annex VI entered into force on 1 July 2010. By October 2008, Annex VI was ratified by 53 countries (including the Unites States), representing 81.88% of tonnage.

Moreover, two sets of emission and fuel quality requirements are defined by Annex VI: global requirements, and more stringent requirements applicable to ships in ECAs. An ECA can be designated for sulfur oxides (SOx) and Particulate Matter (PM), or nitrogen oxides (NOx), or all three types of emissions from ships, subject to a proposal from a Party to Annex VI. In addition, 2011 Amendments to MARPOL Annex VI introduced mandatory measures to reduce emissions of greenhouse gases. The Amendments added a new Chapter 4 to Annex VI on “Regulations on energy efficiency for ships”. In particular, a roadmap has been delivered by IMO in order to reduce environmental footprint of ships as summarized in Figure 28.

Regulations enter into force for over 94% of wolrd fleet	EEDI requires new ships to meet agreed efficiency targets	New ships must improve efficiency 10%	New ships must improve efficiency up to 20%	New ships must improve efficiency 30%		
Ship Energy Efficiency Management Plan (SEEMP): mandatory implementation for all ships		20% CO_2 reduction per t/km (industry goal)				50% CO_2 reduction per t/km (industry goal)
2013	2015	2020	2025	2030		2050

Figure 28 - IMO MARPOL Annex VI roadmap for the reduction of ships' environmental footprint [72]

The NOx emission limits of Regulation 13 of MARPOL Annex VI apply to each marine diesel engine with a power output of more than 130 kW installed on a ship. The NOx emission limits are set for diesel engines depending on the engine maximum operating speed (n, rpm), as presented graphically in Figure 29. The Tier I and Tier II limits are global, while the Tier III standards apply only in NOx ECAs. Tier II standards are expected to be met by combustion process optimization. The parameters examined by engine manufacturers include fuel injection timing, pressure, and rate (rate shaping), fuel nozzle flow area, exhaust valve timing, and cylinder compression volume. Finally, Tier III standards are expected to require dedicated NOx emission control technologies such as various forms of water induction into the combustion process (with fuel, scavenging air, or in-cylinder), exhaust gas recirculation, or selective catalytic reduction.

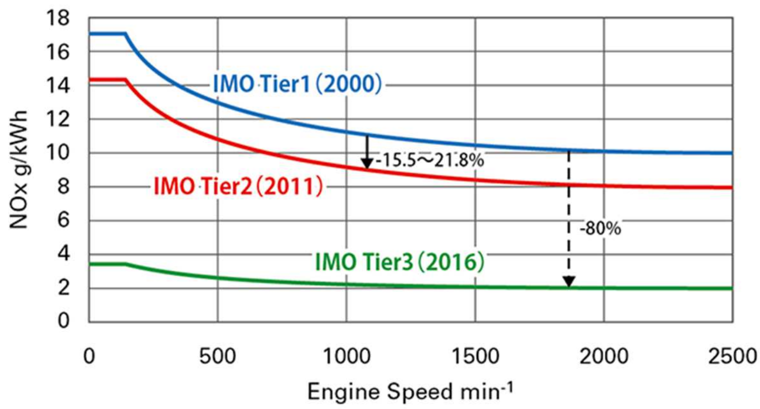

Figure 29 - MARPOL Annex VI NOx emission limits

Annex VI regulations include caps on sulfur content of fuel oil as a measure to control SOx emissions and, indirectly, PM emissions (there are no explicit PM emission limits).

Special fuel quality provisions exist for SOx Emission Control Areas (SOx ECA or SECA). The sulfur limits and implementation dates are illustrated in Figure 30. As an example, heavy fuel oil (HFO) is allowed provided it meets the applicable sulfur limit (i.e., there is no mandate to use distillate fuels). Alternative measures are also allowed (in the SOx ECAs and globally) to reduce sulfur emissions, such as through the use exhaust gas cleaning systems (EGCS), aka scrubbers. For example, in lieu of using the 0.5% S fuel (2020), ships can fit an exhaust gas cleaning system or use any other technological method to limit SOx emissions to ≤ 6 g/kWh.

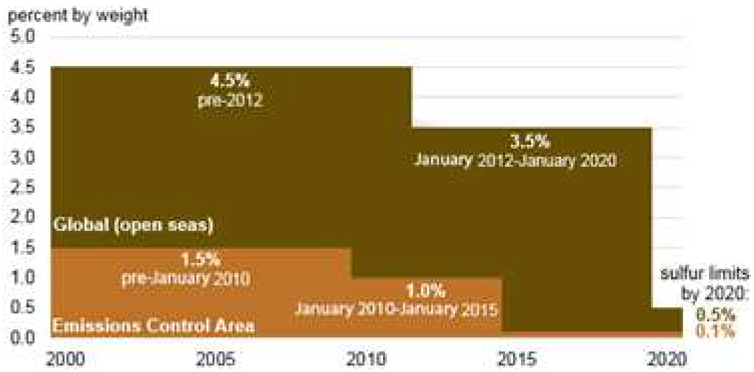

Figure 30 - MARPOL Annex VI fuel sulfur limits

However, ships generate emissions also while docked in port. In fact, the ship power system is still fed by running the ship main (or auxiliary) engines. In ports with heavy ship traffic, this practice creates emissions and negative health and environmental impact to the local surrounding communities. As global trade steadily expands, ship emissions represent an ever-increasing environmental concern. Sustainability is today a key area of focus in the shipping industry, where strong measures are being taken on several fronts to dramatically reduce ship emissions [73]. One such measure is shore-to-ship electric power supply, which eliminates pollution problems such as SOx, NOx, CO_2, and particle discharge as well as noise and vibration from ships in port.

In this regard, an important milestone that will contribute to the growth of shore power is the new global standard High Voltage Shore Connection (HVSC) by IEC, ISO and IEEE [74] to avoid keep running onboard generators during port operations [71], [75], [76]. Shore power is especially applicable to ships operating on dedicated routes and vessels that consume large amounts of power and emit high levels of air pollutants when berthed. Typical vessel types include ferries, cruise ships, LNG carriers, tankers, and container ships.

With shore-to-ship power, ships can shut down their engines while berthed and plug into an onshore power source. The ship´s power load is seamlessly transferred to the shoreside power supply without disruption to onboard services, eliminating emissions to the local environment.

Nevertheless, the electrical safety should be also taken into account for both the shipboard distribution system and the supplying land distribution system. Thus, the safety of all the users involved must be ensured through proper evaluations about grounding for both ship and land system. Despite being conceptually simple, the possible adoption of a shore-to-ship connection imposes to assess design and safety items, requiring case study analysis. Ship and land power systems grounding, selectivity, and equipment design must be properly assessed. However, the integration of such a functionality into the ship power system must be carefully designed to achieve correct operation of the power system, crew electric safety, and suppling land system safety.

2.3.3 Standardization of innovative power systems

Some of the applicable standards are already given in this thesis work, when relevant. Nevertheless, the lack of standardization is one of the main issues related to such innovative systems. While the standard and regulations applied to the conventional shipboard power systems are widely accepted, innovative systems may have components not covered by the regulatory bodies requirements (or only partially covered). In fact, the lack of a standard practice to follow lead to absence of legal definition of which are the requirements needed to correctly design and built the ship and its parts. Moreover, there is no indication on how correctly integrate innovative technologies limiting their application. The research activities so far discussed need a parallel standardization work to be correctly exploited onboard. Commonly, industrial practice or industrial research results can lead to new standards. Indeed, proper research activity can origin new standards or contribute to the modification of already present ones, especially when coupled with wide experimental validation. An example of such a practice is the IEEE Std. 1709 [51] concerning recommended practice for MVdc shipboard power systems. Such a standard address most of the issues of designing MVdc power systems, but also highlights some points that needs to be studied further. As previously stated, the 1 kV LVdc distribution system arises as a standard de facto for the innovative ship power systems, for instance.

Also, maritime classification society are deeply involved in defining ship design guidelines and requirements. A ship classification society (see section 3.2.1) establishes and maintains technical standards for the construction and operation of ships and offshore structures. The worldwide most important societies are Lloyd's Register (LR), Bureau Veritas (BV), Registro Italiano Navale (RINA), American Bureau of Shipping (ABS), and Det Norske Veritas (DNV-GL). The ABS gives, for example, the guide for the “direct current power distribution systems for marine and offshore applications” [77]. As reported in Table 3, the guide states that electric dc battery powered systems shall be designed and installed so that the voltage variations on the main distribution board are maintained within the voltage tolerance limits set therein. Moreover, a dc distribution system shall be designed and installed so that the stationary voltage variation in supply to individual consumers does not exceed ±10% of system nominal voltage, measured from the battery distribution to the consumer terminals. All the main ship classification societies give the same limits regarding dc powered systems. In addition, the LR “Rules for Direct Current Distribution Systems – July 2019” [78] asserts that distribution systems supplying consumers through semi-conductor converting equipment have to ensure galvanic isolation and ground separation.

Table 3 - Voltage variations for shipboard dc distribution systems [78]

Voltage Variations for DC Distribution Systems (such as systems supplied by DC generators or rectifiers)	
Parameters	*Variations*
Voltage Tolerance (continuous)	±10%
Voltage cyclic variation deviation	5%
Voltage ripple (AC r.m.s over steady DC voltage)	10%

Voltage Variations for Battery Systems	
Type of System	*Variations*
Components connected to the battery during charging (see note)	+30%, -25%
Components not connected to the battery during charging	+20%, -25%

Note: Different voltage variations as determined by the charging/discharging characteristics, including the ripple voltage from the charging device, may be considered.

Other guides are given also for the ship power systems endowed with fuel cells. As an example, the RINA guide “Rules for Fuel Cells Installation in Ships” [79] gives rules about the Fuel Cells (FC) electrical safety. Nevertheless, such requirements are not enough to correctly design an innovative power system avoiding all the issues above mentioned. Thus, more research activity is needed to properly standardize such innovative systems.

In conclusion, in this chapter has been provided several examples of new sensors and weapon systems, new electrical technologies, and more generally new requirements and future development trends. What has been said so far will have a significant impact on the onboard power system, and consequently on the whole ship. In general, all these new requirements translate into an increase in the demand for electrical power, with a consequent increase in the size of the onboard power plant.

2.4 Conclusions

In this chapter some innovative distribution systems and new requirements have been presented. Indeed, onboard systems are evolving from conventional radial ac distributions to new ones, on which no previous design experience is available. Moreover, new requirements from owners are creating new issues in ship design never faced before. The design of a shipboard power system endowed with these new characteristics is difficult to face with common design process, pushing towards the need of a new methodology able to address the design of such an innovative system.

These innovative distribution systems and possible new impacting requirements have been described, to allow comprehending the problems the designers are facing nowadays.

3 Conventional design process

3.1 Abstract

The conventional ship design process will be illustrated in this chapter along with a discussion on the shipboard power systems design. Firstly, some definitions will be given to better comprehend this process and the entities that are involved in it. Then the ship design process will be presented depicting the conventional ship design methodology. Therefore, the focus will be moved to the ship power systems, together with the identification of the main shipboard power system design choices in the overall ship design process. Nevertheless, the ship design is a complex process, involving different branches of engineering, teams of several designers, and relevant time and financial resources. Due to that, a complete treatment cannot be provided in this thesis work. However, a good source is the book "Ship Design and Construction" [80] if more information about ship design are wanted.

3.2 Conventional ship design process

3.2.1 Relevant definitions in the ship design process

The ship design is a very complex process greatly depending on the type of project to be developed. Therefore, some definitions are needed to understand this process and the entities that are involved in it. First and foremost, the ship design requires some input data (e.g., mission profile, field of use, autonomy, route, etc.) in order to properly size the ship to perform the required task specifying all its systems, and the information necessary to build and assemble it. However, the ship design process is not unique, and it strictly depend on the peculiar application. Indeed, four different type of projects can be identified each having different design and building complexity:

- The routine design is that design which substantially differs slightly from similar ships of the same class previously built. The design process is the less complex since the owner may require only different changes in the ship equipment/requirements.
- When new impacting requirements or equipment are required by the owner, for instance, the project of a previous ship of the same class should be overhauled and thus leading to a new creative project. Nevertheless, indications on the feasible solution can be obtained from common designs, despite the redesign of relevant ship systems.

- Innovative projects require a complex activity to identify the feasible design. Indeed, the differences are considerable comparing similar ships of the same class previously built due to the new challenging requirements.
- Refitting projects consist in the modification of an existing ship due to improvements in subsystems, change in the classification societies requirements, or change in the ship duty. Obviously, the design process is highly affected by the refitting extension that can span from the subsystem's substitution to even the addition of new hull pieces. Example of the integrated power system refitting can be found in [81], [82].

Moreover, many entities are involved in shipbuilding process each with different tasks and duties as described below. These entities are the ship owner, the ship designer, the ship builder, the classification society, the national authorities.

- The ship owner is obviously the owner of a ship. It may develop the concept design of the ship. It contracts the basic design with the shipbuilder. It detains the property of the ship after it is built, although it is not necessarily the entity that operates it.
- The designer is the entity which is responsible of the development of the basic design of the ship, and which prepares the related technical documents. It can be either an independent design office or a department of a shipyard. It can sub-contract the development of some parts of the design to other designers.
- The ship builder is the yard building the ship. It is responsible towards the ship owner for the compliancy to all the contract clauses and to the ship design given by the designer. It develops detailed design accordingly with its facilities and equipment/capacities. It can sub-contract other entities for both the development of some parts of the detailed design and building of some parts/sections of the ship.
- The classification society is an organization that establishes and applies technical standards for the design, manufacture, and maintenance of installations in marine field (regulatory body). Technical standards are developed by classification society, on the base of other relevant standards if applicable, and published in the form of Rules and Regulations (see section 2.3.3). It has also a verification and classification function. Indeed, a ship built in compliance with the rules of a classification societies can obtain from it a class certificate. The classification societies gives such a certificate only after the approval of the design and a set of inspections during construction to check the design and building compliance. classification societies are important in marine industry because their approval is related to the liabilities that arise in case of accident. Indeed, if a classified ship has an accident related with its

design, the responsibility is lifted from the designer because it was compliant with rules and regulations (a similar condition happens in land power systems with IEC regulations).

- National Authorities: State Authority that has the responsibility of conceding the Building License and of verifying the compliancy with international conventions (IMO, ILO, etc.) and relevant national standards, issuing the related Certificates. It can delegate in other recognized institutions (namely the classification societies) the competence to issue the certificates of conformity with the IMO conventions.

3.2.2 The ship design process

The ship owner (or Navy) need results in the start of the ship design process. Indeed, the business opportunities (or military needs) encourage the ship owners to buy new vessels. The decision, of course, is made after benchmark and business analysis in order to generate profit (for merchant ships) or enhance the existing fleet capabilities (for military vessels). The result of such analysis lead to five different decision described as follows:

- Relocation of a ship from the existing owner fleet.
- Freight of a ship.
- Acquisition of an existing ship (2nd hand).
- Existing ship refitting.
- Building of a new ship.

The design process can start when the ship owner decide to build a new ship. The general ship design process is depicted in Figure 31 to better comprehend the process flow [33]. Indeed, to build a ship is a difficult and complex task, be it a cruise liner or a Navy vessel. Normally building a ship takes many years to complete the entire design and construction process. As an example, the building takes at least two years, after the signing the contract, for a 330 meters long all-electric cruise liner that can accommodate a maximum of 5600 persons onboard. Instead, the construction of a military vessel requires even more time. To give for instance an idea of the complexity of an all-electric cruise ship of this size, the ship power system of the above mentioned example is supplied by two main power plants with 39 MVA of installed power for each. Moreover, the total aggregated power cable length installed onboard is more than 4000 km running in 65 km of cableways. The design and the building of an all-electric ship is a demanding task given the huge amount of power to be installed in such a limited space (330 meters). Thus, the ship design complexity needs to be addressed with trustworthy design methods. Indeed, the general ship design process (depicted in Figure 31) is composed by two main phases: the former is the basic design, and the latter is the product engineering. And beyond that, there are six steps representing the ship design completion level defined as follows:

- The first step is the concept design where the shipowner’s requirements are translated into practical ship design solutions after technical feasibility analysis.
- The preliminary design is the second step where more in-depth analysis are carried out (i.e., trade-off analysis, technical and economic feasibility analysis, risk analyses). Moreover, the overall configuration and the ship size are decided in this stage as well as the major ship components.
- In the third stage the ship general arrangement is defined, and the contract is signed between the shipowner and the shipbuilder. Thus, in this phase the production plan is developed together with the ship explanatory drawings.
- In the functional design (the fourth step) the design calculations are performed, and the purchase technical specifications are issued. Thereby, the functional design is the last phase of the basic design process.
- The so called “transition” is the fifth phase of the design completion level. Indeed, in this step all the information developed during the basic design process are translated in the yard plans and shipbuilding process can start.
- Finally, in the last step all the manufacturing and fitting work instructions are carried out till the ship is completed.

For each design phase are also highlighted the results of the activities done into it, to explicit the flow of information developed in each phase and the consequent data transferred to the following one.

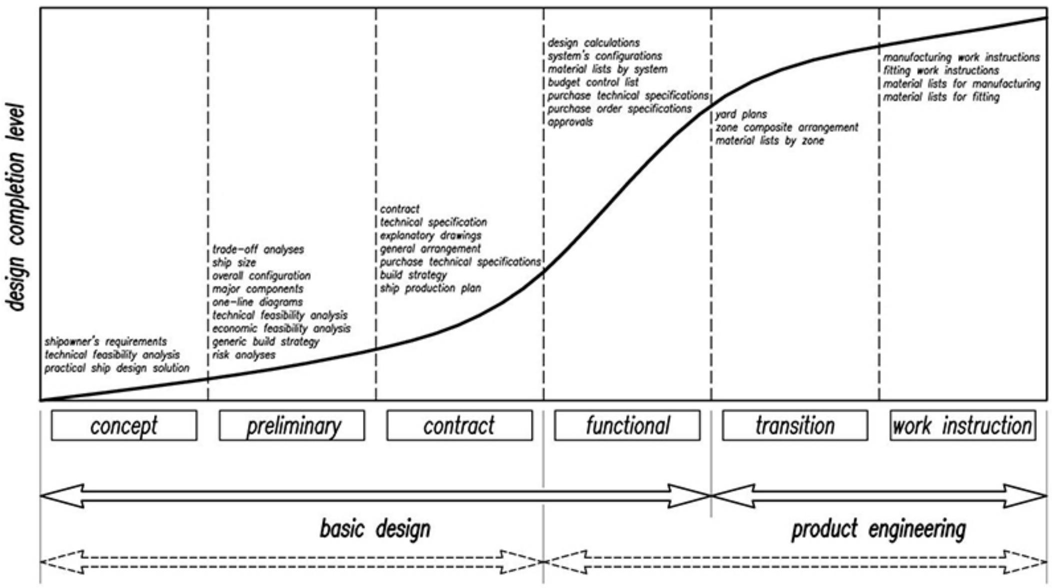

Figure 31 - Ship design process [33]

The ship design process of a military vessel follows the similar design process, although the very different ship capabilities requirement and thus different concept design. However, there are no significative differences in the step following the concept design phase between merchant and military area. An exhaustive definition of the military vessel design process is given in [83] and in [35] for electric propelled ships.

Once the owner has decided to build a new ship and the concept design is completed, a ship designer has to be chosen. The designer is responsible for estimating the main ship data and thus developing the ship preliminary design. This phase is of paramount importance since it allows to evaluate the ship building and exploitation costs. These data can therefore be used to request quotations from different yards. Nevertheless, the quotation is only a parameter in the selection of a particular yard rather than another. Indeed, the shipyard reputation, existing commercial agreements, specific circumstances, and so on can determine the choice of the shipyard. As an example, the U.S. Navy vessels are mandatory built in USA yards.

During the contractual phase, the preliminary design data are exploited by the designers to define the contract design. Indeed, in this stage the ship explanatory drawings are defined along with the ship production plan. Thus, the ship general arrangement is decided, and the contract is signed between the shipowner and the shipbuilder. The classification societies play in important role in this stage assessing if the contract design complies with regulatory bodies' requirements.

Once the contract is signed, the shipyard is responsible for the remaining parts of the ship design process. Therefore, the aim of the functional design phase is to provide all the documents and drawings required to effectively start the shipbuilding process. In this stage relevant calculation about the ship subsystems are performed in order to define the equipment configuration in detail. Then the hull building starts within the acquisition of all the components to be installed onboard. This is the last phase dedicated to the design since the remain two phases are mainly devoted to the ship construction process.

In functional stage all the information developed during the basic design process are thereafter translated in the yard plans dividing the ship into zones. Each zone requires its own material lists, workshop drawings, and arrangements with all the related documentation. Such subdivision allows the shipbuilder to start the shipbuilding process and to define the work instruction for the shipyard. In the last phase all the components, purchased or built, are available to be assembled onboard. Nevertheless, during this last phase some issue can arise due to either errors in design or discrepancies between real and documental data. Indeed, as-built documentation is also provided due to the possible modification made during the construction process. When all the ship is assembled, sea trials are performed in order to verify the ship compliance with the contractual requirements. Finally, at the end of ship building process the ship is delivered to the ship owner.

The design process presented in Figure 31 is generally applicable to either cruise ships or aircraft carrier, for instance. Moreover, not only the requirements defined in the contract, but also the skills and knowledge of the ship designers impact the final ship layout. In fact, different designers can exploit different design tools based on their knowledge and thus leading to other final ship layouts. Given this scenario, the exploitation of innovative design methods and tools can help the designers to boost the innovation in the ship design process. As depicted in Figure 32, the concept design stage is the one that influence most the overall design process. The limited amount of information available at this stage affects more than half of design choices, despite the preliminary data have a high uncertainty. Furthermore, the concept design stage requires less than 5% of the total project time being responsible for only 2-3% of the ship total costs. On the other hand, the cost increase is noteworthy when changes are introduced in the last phases of the ship design process (Figure 32). The decisions taken in the concept design phase affect the overall performance of the ship, determining up to 80% of the costs of the entire operational life of the ship (Capital expenditure and Operating expenditure) [84], [85]. Therefore, Figure 32 highlights the importance of spending more time and resources on the concept design phase in order to avoid additional costs as much as possible.

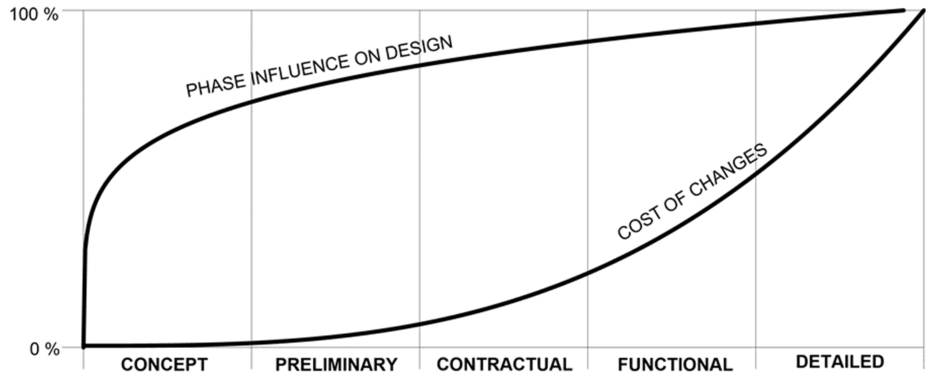

Figure 32 - Single phase influence and cost of changes in the ship building process [83]

This issue is pushing towards new design concepts, conceived with the aim of including tools capable of assessing the future impact of design decisions in the ship early stage design phase. These tools will be explored in the next chapter. However, this evolution has not yet reached the designers, whose distrust of new tools and technologies is commonly high. Similar behavior is common in the industry, being the main obstacle to possible improvements.

Nonetheless, some companies are leading the way for these innovations dragging the rest of the industry with them. The U.S. Navy, for instance, has focused on integrated and optimized design for its ships [36], [39], [49], [83]. This behavior is leading to an increase in research in the area and a subsequent modernization of the involved shipyards, which are obliged to adopt innovative tools if they want to continue working with the Navy.

3.2.3 The conventional ship design methodology

The design of a modern ship cannot obviously be done by a single person due to the high complexity reached by this process. Indeed, the work need to be split into more affordable sub-designs, each related to a single subsystem or aspect. Moreover, the specific sub-design requires a dedicated designers' team. Then the teams work together in order to complete the ship design process. Given this scenario, the solution that can be optimal for one team is not necessarily compatible with another team one, and therefore the right compromise must be found between each other. In fact, there would be no need for compromises only if the sub-designs were not linked together, and thus allowing the choose for the optimal solution for each sub-design. Since this solution is not possible, the division of the design into sub-designs has to be aimed to limit the interrelations among them and at the same time limiting the number of sub-processes to be done [86]. The most common subdivision criterion that is applied in ship design is the division by functions: hull structure, propulsion plant, electric plant, auxiliary systems, and so on. Thereby, a design methodology has to be exploited in order to proper define the overall design.

The conventional ship design methodology is represented by a spiral, as depicted in Figure 33. This design methodology consists in a sequential process that leads to the definition of a solution after a number of consecutive iterations, each round with a higher detail level than the previous. This approach is based on a series of activities that lead to a solution through a meaningful review of information throughout the design process [83]. In the spiral vessel design, the design can be addressed in a sequential manner, with increasing detail as one proceeds in the spiral or, equivalently, in the solution of the process. The process is iterated until all the design constraints are solved and thus resulting in the final solution. The design stages are highlighted in Figure 34 to better understand the process previously described. Nevertheless, the spiral design is not perfectly representative of how the ship design work, despite is useful to explain this ship design methodology. Indeed, the sub-design activities previously described are not all linked together, and thus some activities can proceed in a parallel way until information from other sub-processes is needed. An example of the conventional ship design flow chart is given in Figure 35. The parallel processes occurring are depicted in the figure, starting from the concept design (Marketing block in figure) to the validation and verification block [87]. Obviously, some iterations are needed and only one round of the spiral is depicted to ease the figure comprehension.

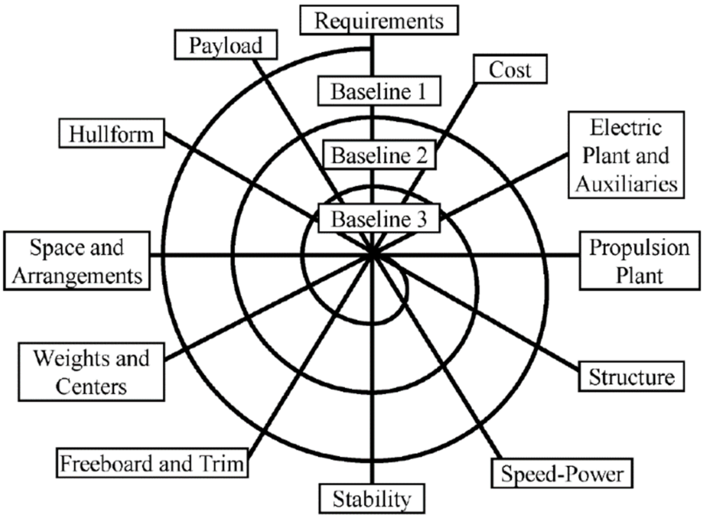

Figure 33 - Spiral vessel design process [83]

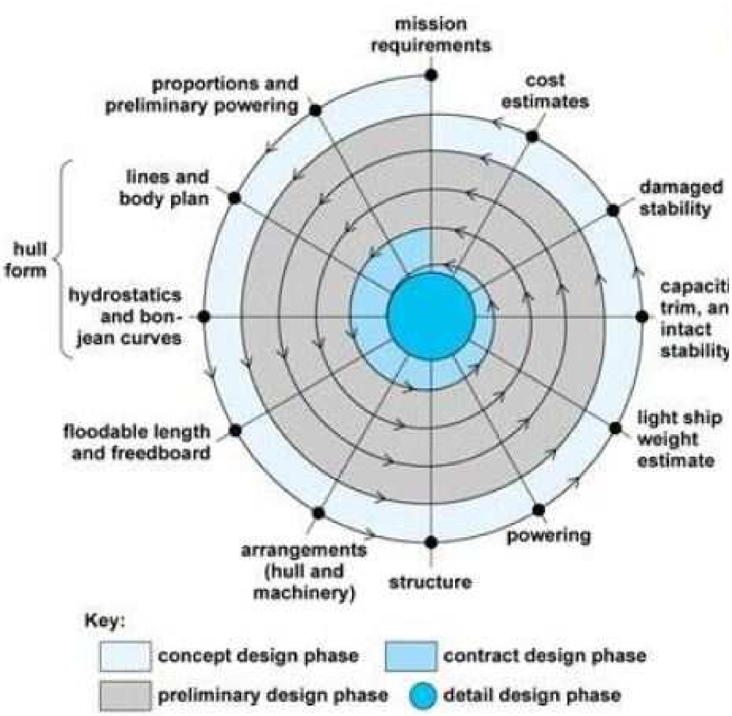

Figure 34 - Spiral vessel design process with the design phase highlighted [83]

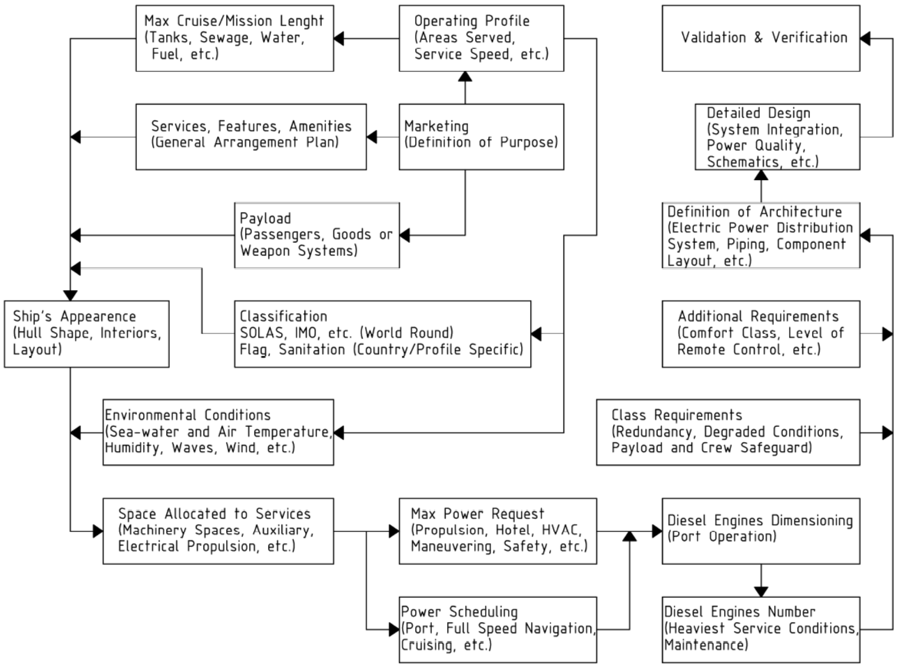

Figure 35 - Conventional ship design flow chart [87]

However, this design methodology can be classified as point-based design because it defines only one point in the design space (i.e., the only possible solution among many). Once a design space has been defined with dimensions equal to the constraints imposed on the system, the solution will constitute only a portion of the space defined by the possible solutions. On the other hand, the set-based design explores the solution's space with the awareness that there is no single solution as a response to the various stages of the design process. Therefore, the set-based design tries to identify a set of optimal solutions, the selection of which can then be made with appropriate criteria. The point-based design, furthermore, leads to the definition of a single solution without assessing the optimal one. The essential difference between set-based design and point-based design are graphically given in Figure 36.

A single acceptable solution is provided by the spiral methodology process which respects all the shipowner's constraints and requests, but not the best possible solution and thus resulting in its main disadvantage. The design space is defined by dependent and independent variables. For instance, the definition of hull, an independent variable, is essential to perform stability calculations, forecast of the required propeller power, and seakeeping analysis. All those variables are dependent on the geometry of the hull. These inter-dependencies are the most important constraints during the ship design process [86].

Therefore, new design approaches are needed in order to pursue the shipboard power system innovation.

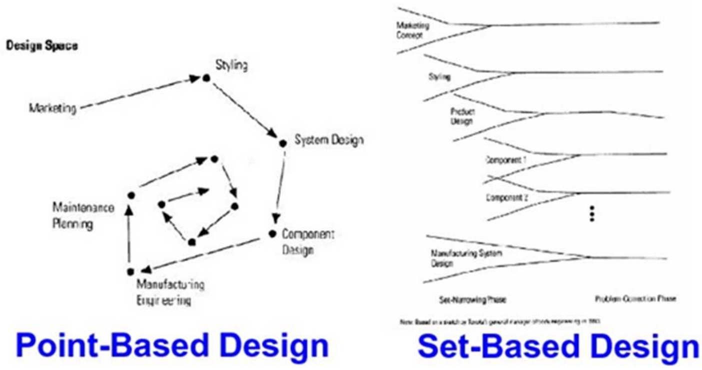

Figure 36 - Graphic comparison between point-based design and set-based design [88]

3.3 Conventional ship power system design process

The design process given in the previous sections is general and valid for all kind of ships. Nowadays, the transition from steam plants and mechanical propulsion to Diesel generators and electric propulsion has revolutionized the onboard space allocation. The ship power system plays a key role in the overall ship design, and thus its design process must be studied carefully in order to provide useful methods and tools enhancing it. Two significant design steps have been already highlighted in Figure 33: “Propulsion Plant” and “Electric Plant and Auxiliaries”. Given an electric propulsion scenario, these two sub-processes are the core of all the integrated shipboard power system along with its subsystems (propulsion, generation, power distribution, etc.). The shipboard power system spiral design process is illustrated in Figure 37.

The first step in the ship power system design process is the evaluation of the power required by all the electric loads to be installed onboard. The so-called “preliminary electric loads balance” comprehends a list of all the electric loads in different operating condition and environmental conditions. The output of such evaluation is a matrix where the expected shipboard power plant size is assessed for each possible ship’s operative condition and environmental condition. Therefore, the preliminary electric loads balance allows to define rating and number of generators to be installed onboard considering other design requirements such as the SRtP compliance. Moreover, the generators choice (number and rating) should achieve the maximum efficiency in all the operative conditions of the ship, limit the installation costs, and, mostly, comply with the onboard space availability.

Once the power plant size is defined, the main bus voltage is selected consequently, while frequency is usually defined by the ship's area of operation. Here the two main constraints are the voltage level and the associated fault current levels. The former is desirable as low as possible to limit electric machines costs and volumes depending on the electric insulation level; the latter must be kept within acceptable limits fulfilled by commercially available protection devices.

The choice of the power plant configuration is the following step as result of the technical constraints, regulations guidelines, and owner requirements. Since the installation of never used components in shipboard power systems can be an issue, the integrated power system architecture is generally chosen between some configurations already exploited, and thus decreasing the design effort. Of course, the configuration chosen depends on the ship duty and some examples have been already illustrated in the first two chapters.

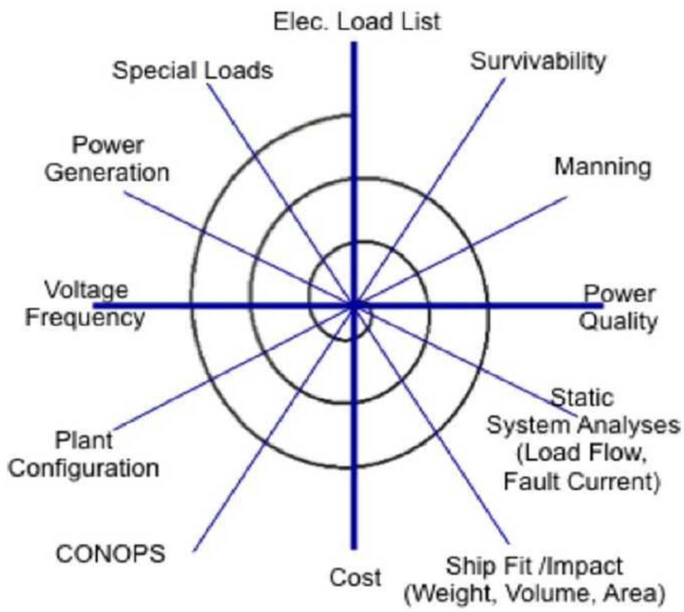

Figure 37 - Shipboard power system spiral design process

After the design of the power system other evaluations are carried out, such as cost assessment and space allocation evaluation. If the result of the power system design process does not meet the other ship constraints, a redesign activity is needed in order to fulfil with the vessel requirements. The power system design process has ended when an acceptable compromise is achieved.

Nevertheless, this design process may be suitable for conventional power systems, but it can hardly lead to the adoption of innovative solutions. The absence of innovative power system proof of concept is a limiting factor along with the lack of available data on such new systems. Therefore, more efforts are needed to proof the successful integration of new electric technologies in the ship design process not only in terms of higher power system capabilities but also taking into account their space allocation.

3.3.1 Identification of the main shipboard power system design choices in the overall ship design process

Going deeper in the more electric ship power system design process, it is useful to understand where the main decision about the shipboard integrated power system design are taken within the framework of the general ship design process in Figure 31. Such evaluation has been carried out analyzing the ship design process of ships built by the Italian shipyard Fincantieri. This activity, developed within the first PhD year, allows to comprehend which data can be anticipated in the shipboard power system design process in order to lead the innovation through innovative power systems. Indeed, the limited amount of information available at the concept design stage affects more than half of design choices, as highlighted in Figure 32 (see section 3.2.2).

The conventional power system design process steps analyzed in the previous section have been melded together with Figure 31. Therefore, these steps are shown in Figure 38 highlighting their collocation in the ship design completion level, as follows:

- In the concept design stage, the ship cruising speed, and its overall dimensions (A), the type of ship (marine vessels, cruise ship, drill ship, etc.) (B), and the shipowner requirements (C) defines the main characteristic and features to be fulfilled by the shipboard power system.
- Then in the preliminary design fundamental choices are made regarding the definition of the onboard power system. The following data project are defined in order: the required propulsion power (D), the power required by the main electrical devices (E), and then the power plant size (F) is specified through a preliminary electrical load balance analysis. Thus, the size evaluation of transformers and

switchboards (G) is carried out as well as the one-line diagram for the integrated power system (H). Finally, in this stage there is a preliminary assessment of the equipment volume (I) together with the equipment arrangement (L). It should be noticed that the equipment volume assessment and arrangement is not a not trivial in, for instance, an all-electric 330 meters long ship with a 78 MVA power plant.

- In the contract design phase, all the power plant characteristics (M) are defined, and the contract is signed between the shipowner and the shipbuilder. From this point on the changes in the power system design will lead to a huge increase in the overall chip design costs.
- Last but not least, in the functional design the purchase technical specification (N) is issued for all the power system components. Moreover, the cables length assessment (O) is fulfilled together with the short-circuit calculation (P) and the switchgears specification (Q).

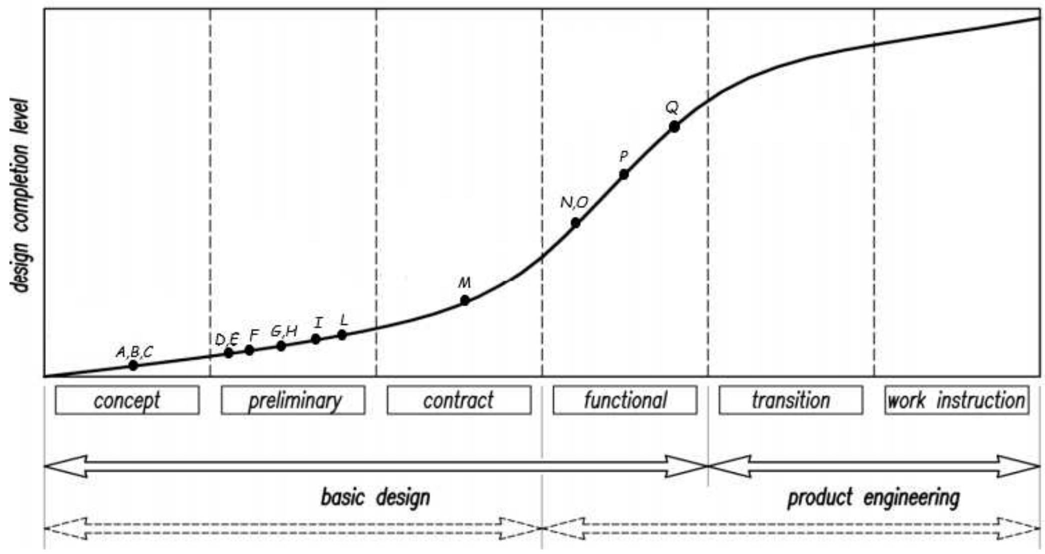

Figure 38 – Ship power system design process highlighting the main steps in the ship design completion level [33]

In this complex design scenario, the designers may be prompted by new market available devices to exploit new design solutions and thus modifying the power system design process (Figure 38). In fact, new components are a key enabler to develop new power system architectures with improved features as seen in the previous chapter (see section 2.2).

The Solid-State Transformer (SST) for instance (Figure 39 on the right side) is a new equipment that can be use in place of the traditional MV/LV transformers [28], [89]–[91] (Figure 39 on the left side). The SST is a fully controllable power electronics-based device with a high frequency transformer ensuring galvanic insulation between the MV and the LV side. And besides, it may make available a low voltage dc section at its secondary side enabling the LVdc power distribution network described in the section 2.2.3. The SST is a suitable device for shipboard application since it is lighter and less cumbersome compared with the traditional 60 Hz frequency transformer [92]. The onboard required power furthermore is rapidly increasing likewise the space needed to arrange the components of the shipboard power system and their subsystems. Moreover, the required power increase leads to several issues mostly related to the rise in number and size of electronics devices. Several new constraints have to be taken into account such as the correct disposal of the heat load generated by the electric devices, the reliability and controllability of the power system, the electrical safety, the power quality problems, and the arising harmonic pollution assessment brought by these new components [93].

Given this premises, it is pretty obvious that it is possible to evaluate all the above mentioned issues only after the functional design stage thus once the ship power system is fully defined. However, in the functional stage design is no more possible to provide substantial changes to the integrated power system without significantly affect the ship cost (see Figure 32). Thus, there is a need to anticipate all the possible information regarding the power system design in previous stages in order to better evaluate the power system behavior in the new scenario pervaded by power electronic devices.

Therefore, these new devices cannot be integrated as a mere refitting in the existing power systems but shall be integrated in a better and rational manner. Indeed, this is the reason which led to the drafting of this thesis. Thus, new methods and tools are required to lead the innovation brought by these new devices as well as the proof of concept for their onboard application.

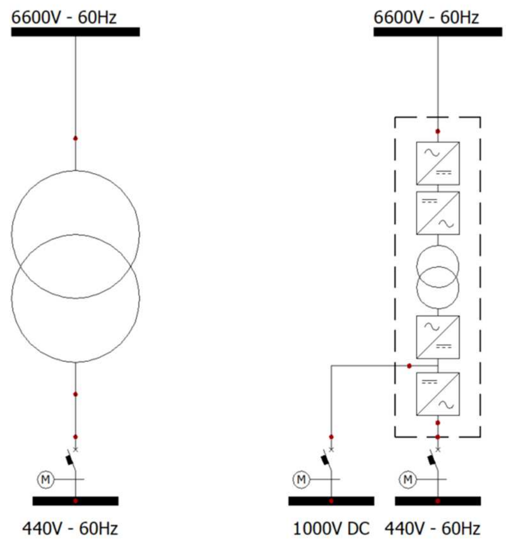

Figure 39 - A traditional 60 Hz MV/LV transformer (on the left) and a Solid-State Transformer (on the right)

3.4 Conclusions

The conventional ship design process has been illustrated in this chapter along with a discussion on the shipboard power systems design. Firstly, some definitions have been given to better comprehend this process and the entities that are involved in it. Then the ship design process has been presented depicting the conventional ship design methodology. Therefore, the focus has been moved to the ship power systems, together with the identification of the main shipboard power system design choices in the overall ship design process. Nevertheless, the ship design is a complex process, involving different branches of engineering, teams of several designers, and relevant time and financial resources.

In this scenario, new power electronics devices cannot be integrated as a mere refitting in the existing power systems but shall be integrated in a better and rational manner. Indeed, this is the reason which led to the drafting of this thesis. Thus, new methods and tools are required to lead the innovation brought by these new devices as well as the proof of concept for their onboard application.

4 Innovative design methods and tools

4.1 Abstract

Innovative methods and tools to design the shipboard power system will be illustrated in this chapter. Firstly, the concurrent engineering approach will be explained and compared to the methodology described in the previous chapter emphasizing the advantages of this innovative design method. Therefore, the focus will be moved to the innovative distribution system design process. The need to anticipate all the possible information regarding the power system design in previous stages will be highlighted in order to better evaluate the innovative power systems performance.

In this scenario, new tools and software play an important role in assessing the power system behavior since the early stage design phase. Indeed, modern complex ships can be designed relying on Computer System Integration software, thus allowing to produce three-dimensional parametric models. The parametric 3D ship model contains mainly detailed data about the ship power system equipment including cables layout and their onboard paths. Given these data availability, an integrated approach in the definition of innovative ship power system will be presented aiming at anticipating useful information. Such information are not only useful in the term of a weight and volume comparison but also allows to perform studies that would otherwise be done in the functional stage design.

Finally, some examples will be depicted to better comprehend such new approach. Then, the new concept of space reserved on board is proposed as a mean to accommodate the future power system in a modular manner and thus resulting in several advantages. Moreover, the space reservation impact on the overall ship design can be evaluated from the early stage design phase.

4.2 Innovative ship design methodologies

In the previous chapter (see 3.2.3), the spiral design methodology has been classified as point-based design process uncapable to assess the optimal design solution. Therefore, the set-based design process (see Figure 36) is preferred in order to explore all the solution's space applying appropriate selection criteria. In fact, the design of a modern electric powered ship requires new methodologies. Being a tough process, the ship design complexity tends to increase along with the number and required power of loads installed on board. This trend is shown, for instance, in Figure 40, where an important load increase is foreseen for the mission system (weapons, surveillance, etc.) and the various services of the U.S. Navy fleet [66], [94]. Thus, the designer can no longer rely on his experience for the design of modern and complex ships. Appropriate methods and tools are needed capable to provide useful information to support the designer in making rational decisions right from the first design stages [94].

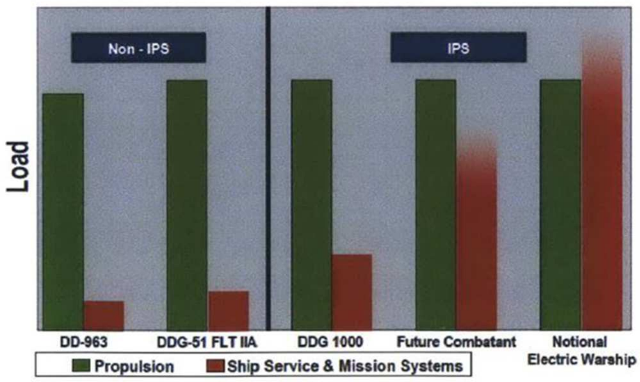

Figure 40 – U.S. Navy forecast for their ship total electric installed power [95]

Nowadays, the various steps that characterize the ship design process can be speeded up through the use of tools based on the increased computing power given by modern computers, increasingly connected and integrated [96]. The today computer technology offers more detailed analysis in less time, decisively increasing the efficiency of the entire process and therefore enhancing the competitiveness of the yard on the global market. Indeed, it must be remembered that the designer's goal is to achieve the requirements imposed by the owner at minimum costs. Costs include the cost of the entire life cycle of the ship (project, construction, operating costs).

4.2.1 Computer engineering

Nowadays, the use of efficient and coordinated computer-based tools in the project and construction of the ship represents an important aspect to be evaluated when defining the shipyard's commercial competitiveness.

In fact, faster and safer estimations can be provided by means of these tools, following the owner's requests and obtaining more accurate results. Changes to the project can be implemented with more flexibility, while ensuring a high level of consistency. Moreover, the improvement in the cost control process allows rational and timely purchases of materials. A common database, continuously updated, is a necessary mean to exploit these functionalities in order to ensure the constant presence of reliable information. The functions of this assisted approach concern initial modeling, design (CAD), engineering (CAE), production (CAM), product model, integrated production and integration of the sub-systems [94].

The modern project design, and thus the shipbuilding process, is essentially based on the following approaches:

- Computer-Aided Synthesis Modeling: starting point to define a baseline on which the preliminary design of the ship will then be developed. In this context, the project data are processed taking into account the shipyard's database or sister ships or similar. The project output data can be exploited to perform a preliminary cost analysis.
- Computer-Aided Design (CAD): it represents the natural evolution of digitalization in the production of drawings in the world of naval engineering. Although most of the drawings are designed with computers, the outputs are still printed on paper. The trend of modern CAD is oriented towards the definition of 3D models of the project in order to give a real scale perception as it is built.
- Computer-Aided Engineering (CAE): software that contain statements about all the calculations foreseen in the design phase. These software are dedicated to specific tasks (e.g., stability and hydrostatic calculations, weight distribution, power/speed calculations, structural calculations, pipeline sizing, electrical load analysis, seakeeping, radiated noise, and so on). Some CAEs have been designed to interoperate between the different tasks (obviously to speed up and optimize the naval project), giving quick responses to any shipowner's requests. The common goal is to develop a specific database endowed with parametric data in order to enhance the preliminary stage design capabilities.
- Computer-Aided Manufacturing (CAM): software that are the connection point between the design and the ship construction. Indeed, all the functional design stage outputs are translated in work instructions (welding, cutting, painting, etc.).

An alternative approach to the traditional tools seen above is represented by the so-called Product Model Programs (PMPs), (i.e., software endowed with both CAD and CAE, and in some cases even CAM capabilities). Through these software users can work with a 3D model from the earliest design stages. This approach contrasts with the traditional one, which envisages working in 2 dimensions in the preliminary stages while the third dimension is added only in the last stages. The PMPs also exploit a common multi-user database. In this way it is easy to check the interior spaces, paying attention to clutter and any interference between hull structure and sub-systems. Despite these advantages, the different tasks can only be tackled with dedicated sub-modules of the same PMP. Thus, there is no integration among different PMPs modules. Figure 41 depicts the above mentioned processes through a block diagram.

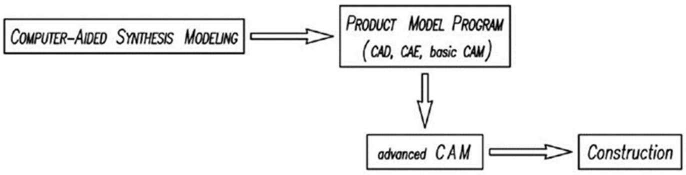

Figure 41 – Ship design process based on Product Model Program

A further step is marked by leveraging Computer Integrated Manufacturing Programs (CIMs), a PMPs improvement especially for the production phase. CIMs are able to coordinate independent modules interfaced to a single common database. Obviously, these independent programs managed by the CIM must be customized to correctly operate with both yard technologies and standards. In the CIM environment, the information management is fundamental since both the technical and administrative division exploits the same database. Another fundamental characteristic is represented by the possibility of managing the data in possession based on the decision-making parameters of the construction site. The block diagram in Figure 42 illustrates the CIMs task subdivision.

Nowadays, the main challenge for the shipbuilding industry is represented by the use of Computer System Integrations software (CSIs) [83], [92], [97]. Indeed, the complete integration is achieved only connecting all different organizations involved in the same shipbuilding process. While the CIM manages all the tasks of a specific shipyard, the CSI involves various important entities (shipyard, shipowner, suppliers, classification societies, regulatory bodies). Obviously, the common database should be shared (Figure 44) between the various entities in such a way as to allow everyone to work with reliable and consistent data. The block diagram in Figure 43Figure 42 depicts the ship design process based on CSI approach.

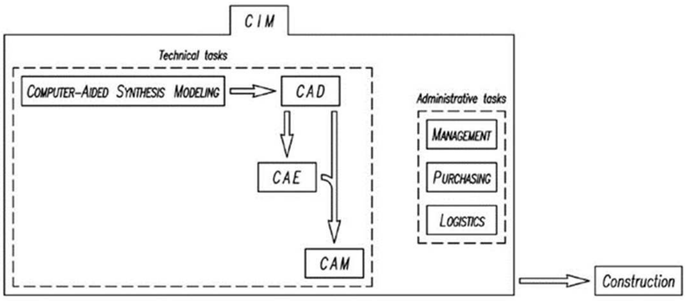

Figure 42 - Ship design process based on Computer Integrated Manufacturing Program

The shipyard commercial competitiveness can be assessed through the use or not of computer-assisted tools in the various shipbuilding and design stages. In fact, faster answers can be given to shipowners' requirement changes through these tools, also with the related cost assessments. In addition, the results accuracy is enhanced as well as the possibility to develop different project solutions. In this context of high digitalization of industrial processes, the development of these new technological tools implies a multidisciplinary knowledge. Therefore, the ship design process is the set of a team effort, where collaboration and data sharing is fundamental. An appropriate paradigm for this new approach is the so-called Concurrent Engineering (CE) parallel design outlined in the next section.

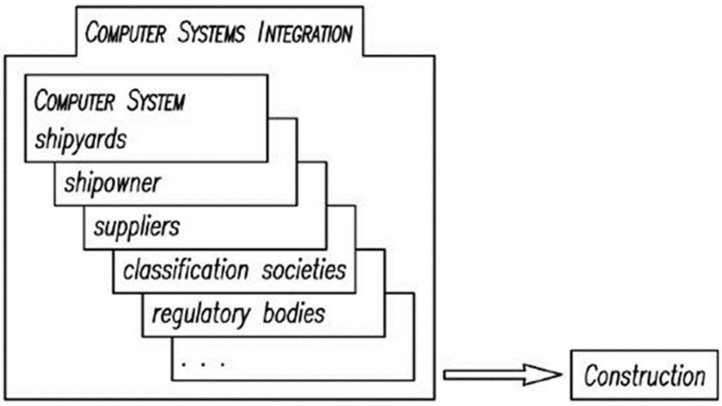

Figure 43 - Ship design process based on Computer System Integration

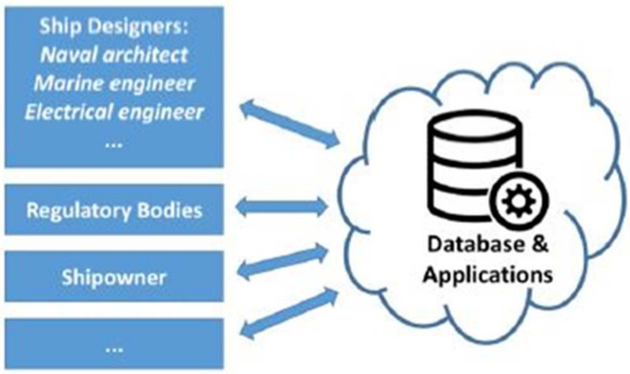

Figure 44 - Database shared with the main entities involved in the shipbuilding process [97]

4.2.2 Concurrent engineering

The main goal of parallel design is to reduce the delivery times of an industrial product by minimizing costs and maximizing quality. Figure 45schematically shows the CE approach, where all the most important activities are carried out through a bidirectional integration. A parallel rather than sequential process is used for the different functional parts of the project.

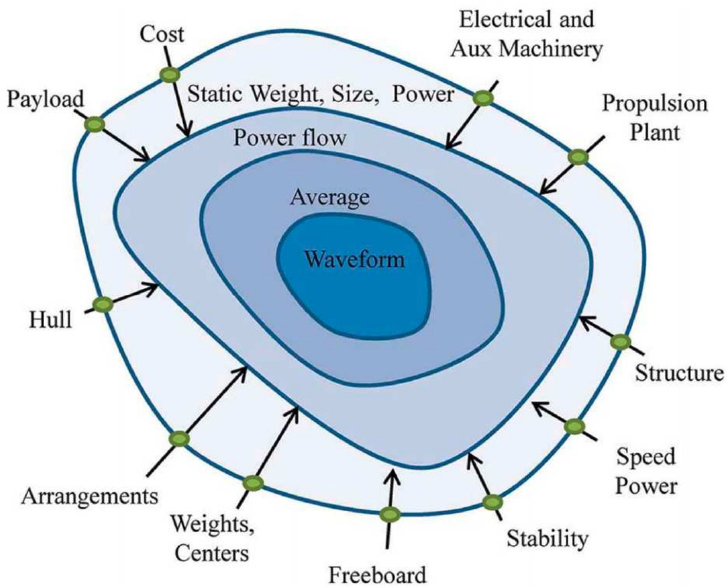

Figure 45 - Collaborative, concurrent design

The concept of CE gained significant attention during the 1980s when the US automotive companies needed to shorten design times by speeding up production to compete with the Japanese industry. The CE has been widely accepted as an effective engineering practice to decrease project development time, increase quality and decrease production costs. Since the CE takes into account all elements of the product life cycle from the beginning, the process complexity is consequently increased.

In the past, there has been a widespread emphasis on the task specialization resulting in a structured stovepipe organization. Indeed, the information flow ins such an organization inhibits the data sharing between the teams. To prevent this trend, CE aims at the total integration of the design and construction process using cooperating and multidisciplinary teams. Given this scenario, the CE is more a philosophical problem approach than an engineering discipline. Thus, all the elements of the product life cycle are integrated in a single feedback-guided design phase.

In this context, the design activity is defined by a multi-disciplinary approach relied on functional requirements, production, quality assurance and economic feasibility of the product. Thus, the designer works no longer only with his team but with the entire design team, gaining in terms of experience and knowledge. Following this path, the design process must also guide the entire production process. A team exploiting the CE principles should include experts in requirements analysis, cost analysis (acquisition and operational), production engineering, marketing, and so on.

In fact, the CE distinctive elements are:

- This approach relies on a multidisciplinary team that optimizes the design, the production, and the service activities of a given product.
- The CE exploits the computer-based approach through the sharing of models and databases.

The design team is generally located in the same building, but the use of an ad hoc network can connect offices in various parts of the world. The team's ability to communicate and share design choices is a major factor in the design process. Indeed, the CE aims to eliminate the high level of the project redesign peculiar of the spiral design process. Conversely, the project downstream constraints are tackled as soon as possible by this approach. Thus, the designers are forced to be more aware of all the design aspects of the process [94]. The early stage design phase is particularly meaningful since the most effective decisions are taken in this stage, and thus they have a remarkable impact on the final design.

It has been assessed that the changes made in the early stage design phase led to a high quality of the project with a significant reduction in development time. Otherwise, the costs associated with any change increase dramatically since the design freedom level is heavily limited in the functional and detail design phase. Figure 46 highlights the comparison between the traditional approach and the CE one. The costs increase exponentially if changes are made during the production phase.

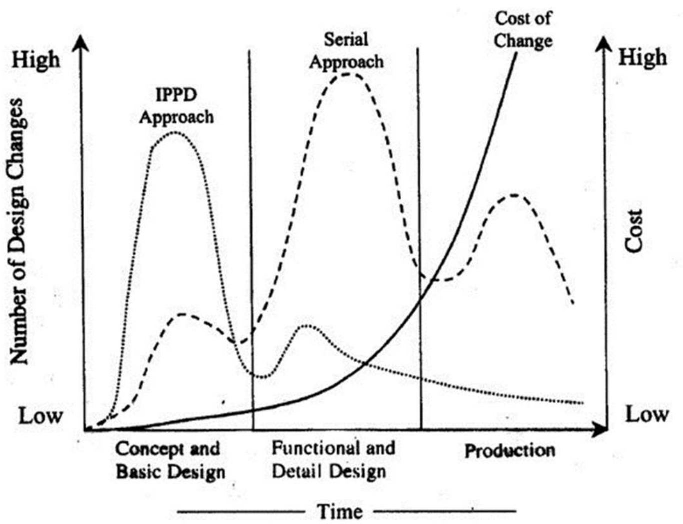

Figure 46 - Costs evaluation vs number of design changes – comparison between IPPD and serial approach

Thanks to the exploitation of the so-called Integrated Product Process Development (IPPD), the designers are able to make rational decisions based on the anticipation of the significant project data. In this scenario, the more the design process moves forward (and the decisions are taken), the more the freedom to apply changes decreases, and thus the level of information on the product increases. Thereby, the CE can anticipate the information curve and consequently increase the ratio between hard/soft information. Therefore, the concept and preliminary design are increasingly important in order to enhance the overall project quality. The decisions taken in these phases play a critical role in the design process and have a meaningful impact on the final design. Moreover, the identification of the shipowner's requests, the application of attributes of interest, and the selection of proper analysis tools (mathematical models) are relevant.

4.3 Integrated ship power system design process

Focusing on the innovative distribution systems, there is a need to anticipate all the possible information regarding the power system design in previous stages in order to better evaluate the innovative power system performance. For instance, the cable length assessment (point O in Figure 38) is one of the most important information in order to perform harmonic pollution analyses [33], [93], [98]. Indeed, higher the signal's frequency higher the impact of the cable length on the possible arise of undesired resonances in the power cables according to the travelling waves model (see section 6.3). Therefore, these new devices cannot be integrated as a mere refitting in the existing ship power systems but shall be integrated in a better and rational manner. To evaluate new technologies' impact in terms of the grid power quality through simulations is not enough if there is no proof of concept of the correct onboard installation. Nonetheless, software simulations are paramount in assessing detailed issue related to the integration of single components and sub-systems (see section 4.6). Luckily, modern complex ships can be designed relying on CSI software, thus allowing to produce three-dimensional parametric models (Figure 47). The parametric 3D ship model contains mainly detailed data about the ship power system equipment including cables layout and their onboard paths. Thus, the idea is to apply the parametric capabilities offered by the new CSI software to evaluate different system's solutions in terms of weights, volumes, cable lengths, and so on. The benefits in the design process enabled by the integrated design approach are even more important when innovative ship power systems are assessed.

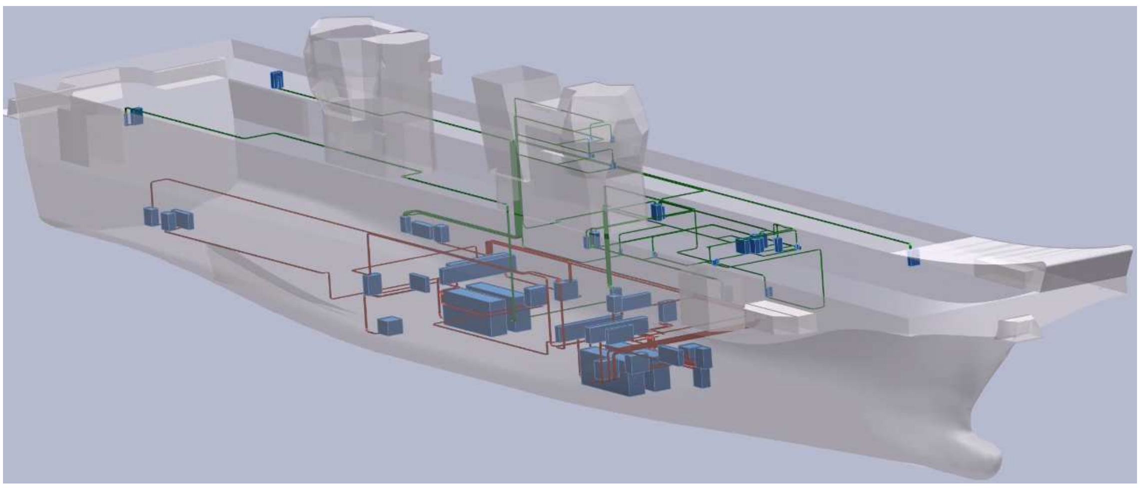

Figure 47 - 3D parametric model of military vessel highlighting the power system with its distribution system cableways [33]

Nowadays, different CSI software packages are available on the market: for example, AVEVA, Dassault Systemes, Foran v.80 and Intergraph Smart 3D are representative of the current state-of-the-art [92]. The software integrators are tools capable of interfacing with numerous applications commonly used both in naval and electrical engineering. Most importantly, CSI software advances the ship design process into a multi-user environment, while providing a full-ship 3D-based database. Moreover, the database is accessible by all interested entities with constantly updated and consistent information on the overall ship's project. Detailed information on the project and the list of materials can be checked by all involved teams at any time. Furthermore, CSI software dynamically faces design changes: for instance, a hull-form change can trigger an automatic update of the involved structures/systems, upon the requested permission from the project manager.

The architecture of these software is modular and thus ready to integrate new tasks including automatic calculation of interest indices, project optimization algorithms, and so on. The CSIs provide a significant improvement in the product engineering phase since the project data compatible with the yard's standards. The comparison between different design solutions (and their relative performance indices) is easier, highlighting in a short time the pros and cons with less effort. Since CSI software shares the data with other software task, the influence of the new design choice can be evaluated over other areas of design interest. For example, a CSI software can be used already at the beginning of the design phase to define the position of the onboard power generation system based on different empty spaces, also optimizing the distribution of the weight-volumes involved. Thus, the impact of a sub-system on the others can be assessed, estimating the ship's capabilities with respect to any possible performance index (efficiency, consumption, seakeeping).

The CSI applications remove the data conversion barriers from one standard to another when different software are used. Therefore, the design time can be optimized eliminating the risk of data loss. Indeed, the integrated ship design methodology is enhanced, and all designers work with the same set of information at the same time, dynamically modifying their sub-project in case of need.

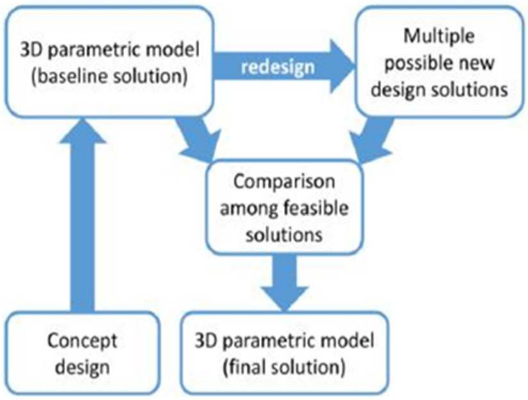

Figure 48 - Computer System Integration design flow chart [97]

For example, a change in the definition of an electric load can trigger, with the permission of the project manager, an automatic update of the electric equipment involved (e.g., power cables, circuit breaker). The use of this type of software can be adapted to different applications, from the optimization of the project to the theoretical verification of some new technologies. Thanks to the CSI software exploitation, the impact related to the introduction of a new power system technology can be analyzed, such as MVdc distribution as well as to optimize the refitting of existing ships with advanced technology [81]. In fact, the CSI software can be used to test the integration of systems, comparing different possible project solutions, evaluating their feasibility, and possibly finding the most appropriate solution in order to overcome the project constraints. The CSI design flow chart is given in Figure 48.

Finally, it is possible to give fast and consistent answers to the shipowner's questions during the entire design process. In addition, the CSI applications reduce the difficulties caused by the introduction of new regulations and rules that deeply affect the ship's structures, accommodation and operations (for example SRtP [15]).

4.4 Software simulations

Nevertheless, the proof of concept of the correct onboard installation is not enough if not supported by power system simulation evaluating new technologies' impact in terms of the grid power quality [45], [99], the system reliability [64], protections coordination [43], [100], and so on.

Nowadays, power systems are composed by many components interconnected to supply the correct service to the end-users with the required power quality. Mathematical representations are available for each component or can be obtained if not. As an example, the synchronous generator's Heffron-Phillips model [101] is a two order one exploited in electromechanical oscillations analysis. On the other hand, the highest detailed model of a synchronous generator has order eight [102]. Thus, the entire mathematical model of the power system can be obtained merging each component model. The model complexity depends upon the output data to be calculated depending on the desired approximation with real system results. For instance, the shipboard power system can be modeled as in [99] to evaluate the power system transient caused by a load disconnection and reconnection.

In general. software simulations can support the power system design already during the early stage design phase. Analyzing results available both in literature and developed during the PhD activity, it is clear that the exploitation of software simulation can aid in the definition of the power system components and in their integration in the system. Hard/soft information can be assessed in advance through this approach and thus leading to the product success on the market. Indeed, the design choices can be evaluated (e.g., the high frequency disturbances caused by power electronic devices) and the system dynamic response can be assessed before building the real system.

Examples of the advantages of such approach are listed below:

- The design flexibility is enhanced being able to evaluate different power system layouts at the same time.
- Testing different control methods or algorithms.
- Evaluating the correct protection coordination.
- The crew can be trained through a power system simulator.

Nevertheless, software simulator are not representative of the real system behavior in all the operative conditions. Indeed, a simulation aiming to assess the power system electromechanical oscillations cannot be used in electric transient studies. The detail model level required by the two phenomena are significantly different: the former requires a low detail model, while the latter need a high detail model. Moreover, the model complexity must be the same in all the power system components. For this reason, the scope of a software simulation has to be previously defined allowing the use of correct components' models. In fact, the mathematical models have well-defined validity areas and cannot correctly represent the system outside their validity limits.

In literature many examples can be found exploiting simulation software to assess power system behaviors. In [99] simulations are used to evaluate the effect of the introduction of a static converter interfaced generator on the system's power quality.. A set of simulations has been performed to assess the effect of the grid-side converter regulators parametric variations on the system's voltage and frequency regulation performance. As an example, the system frequency transient is shown in Figure 49 because of the disconnection (at t = 50 s) and reconnection (at t = 60 s) of a perturbing load. Moreover, different regulator parameters have been used for the grid side converter to evaluate system frequency regulation sensitivity (Figure 50).

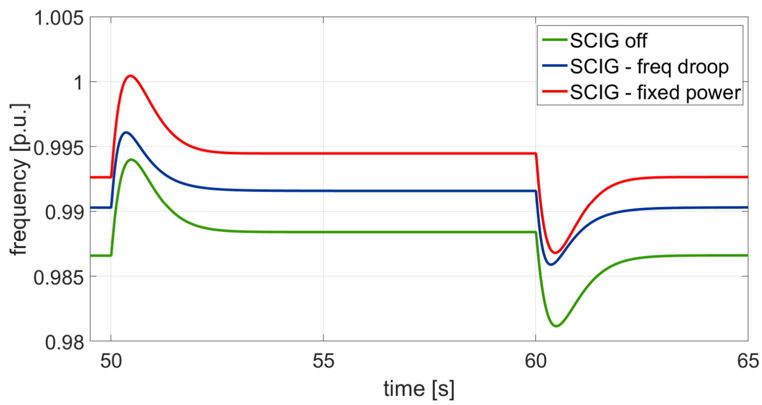

Figure 49 – Integrated power system frequency transient, effect of the static converter interfaced generator presence [99]

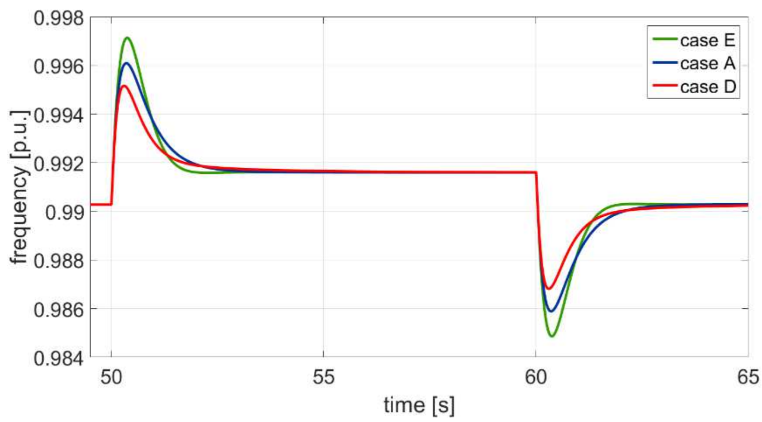

Figure 50 - Integrated power system frequency transient, effect of different PI converter parameters [99]

However, it should be remembered that system components are usually not clearly defined in the early stage phase, because their parameters can be fixed only in a later design stage. Indeed, during system design the supplier has not been chosen yet. Indeed, precise component parameters can be evaluated only after component building, through the so-called Factory Acceptance Test (FAT). Nevertheless, such parameters can be estimated in advance with a high level of confidence relying on experience and common component data. Despite the simulation results may differ from the real system, trends and criticalities can be highlighted easily, helping in the definition of the system layout and control. Then, the simulator can be later tuned during the shipbuilding construction exploiting the components real data. This approach allows to test the power system emergency procedure, for instance, avoiding damaging the real system.

4.5 Combined approach in the definition of innovative ship power system

Given the new data available from the CSI software exploitation and the capabilities of both finite element simulations (FEM) and software tool for power system analysis, a combined approach in the definition of innovative ship power system is presented. The information obtained from CSI software are not only useful in the term of a weight and volume comparison but also allows to perform studies that would otherwise be done in the functional stage design. Indeed, the weight and volume assessment is fundamental in the definition of the ship general arrangement plan and in seakeeping analysis. Nevertheless, the shipboard power system endowed with innovative distribution system and equipment can lead to unexpected issue.

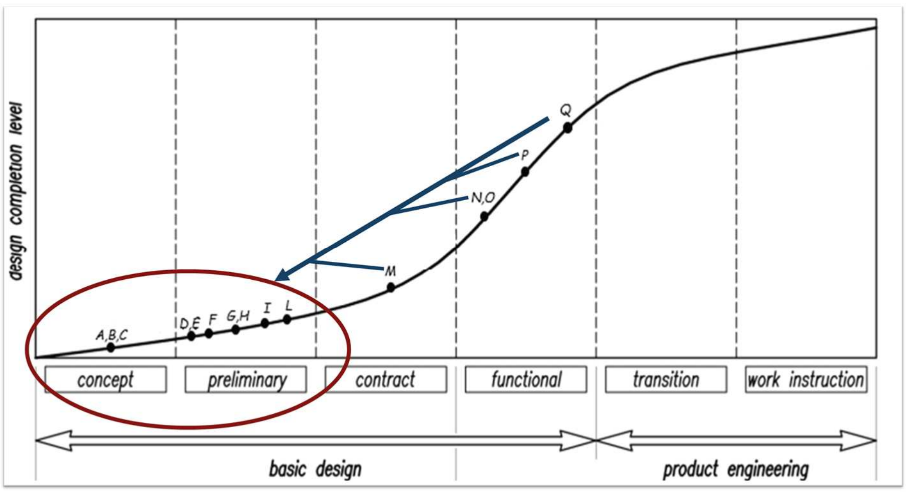

Figure 51 – Anticipation of the ship power system design data

Indeed, in an integrated power and energy system it is now possible to have high frequency disturbances injection with a significant energy level, thus leading to possibly harmful consequences for the system. This highlights the presence of a damaging phenomenon related to high frequency disturbances propagation in power systems, currently not sufficiently addressed by actual power system design. Thus, Figure 51 shows that all the information regarding the ship power (as presented in the section 3.3.1) can be anticipated thanks to this combined approach allowing high fidelity power system simulations.

Thus, specific system weaknesses can be identified through the development of a reliable modelling approach exploiting both frequency-dependent mathematical models and CSI software capabilities. For instance, the cable path and lengths must be known with a good accuracy in order to correctly assess the impact of high frequency disturbances propagation as will be depicted in chapter 6. In addition, the performed power system analysis can lead to further benefits in the correct integration of the new devices. The block diagram of the proposed innovative approach is given Figure 52. The power system software simulation can be performed in the early stage design phase enabled by the CSI software capabilities. Moreover, those simulations can be no more performed only in the functional stage design and thus can enhanced the ship power system design process even modifying the ship general arrangement the output electrical data, as depicted in the next section.

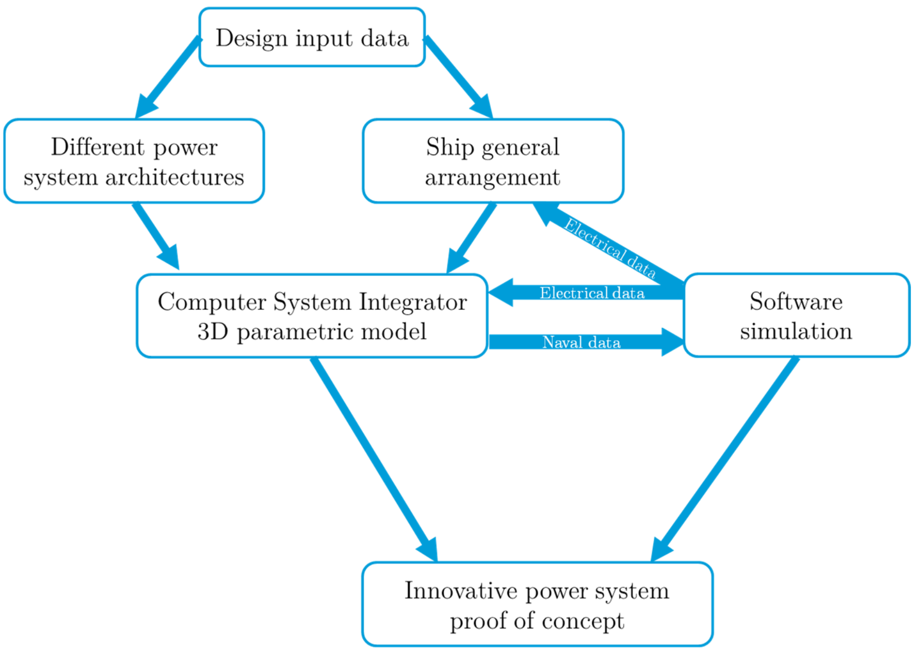

Figure 52 – Block diagram of the proposed innovative approach

4.6 The modular integrated power and energy corridor concept

Both CSI and simulation software can provide huge improvements in the ship power system design helping to overcome further design issues in innovative shipboard power system projects. As a result of what has been said so far, the modular Integrated Power and Energy Corridor (IPEC) is the perfect example of such a new methodological approach. Recently, Massachusetts Institute of Technology (MIT) Sea Grant has been focusing on developing new concepts for power distribution on an all-electric surface combatant ship, introducing the concepts of the power corridor [103] and reserved space [104]. The MIT is part of the Electric Ship Research and Development Consortium (ESRDC) supported through a grant from the United States Office of Naval Research. The IPEC (Figure 53) combines the distribution, conversion, isolation, and storage of main bus power throughout the ship into one entity, which creates advantages in cost, survivability, and arrangement. Because the modular IPEC combines the majority of the power for the all-electric ship into a small space, and it is based on static power conversion technology (source of current harmonics), the thermal conditions of the corridor are of great interest.

Indeed in [105] the effect of the current harmonics on the Joule losses and the resulting temperature field are quantified in a 3D model of a MVdc multi-cable conduit, simulating two different geometries (four 1000A cables and sixteen 250A cables) at three different air flow conditions each, under representative current loading. Such a study is representative of the CE approach illustrated in section 4.2.2. Indeed, this work exploits multidisciplinary knowledge to tackle the same issue leading to an early stage assessment of the new MVdc distribution concept. Electrical engineers, mechanical engineers, and naval architects cooperate together at the same time sharing experience and knowledge. More specifically, the onboard reserved space concept is more related to the naval architecture field, while the conduit temperature evaluation is up to both electrical and mechanical engineers since it is caused by power electronic devices.

Therefore, the goal is to evaluate the Joule power losses in multiple MVdc cable pairs supplying a set of power converters through taps, and then quantify the temperature field in a 3D model of a cable conduit. The evaluation of the power losses is achieved by simulating the cables and taps under full load conditions, in presence of harmonic pollution. Then the thermal analysis is performed, aimed at: verify that the cables insulation does not exceed its allowable temperature; define the air temperature in the cable conduit that allows safe operating conditions; and evaluate the temperature of the cable conduit top, to understand how much cooling the above power electronics will need.

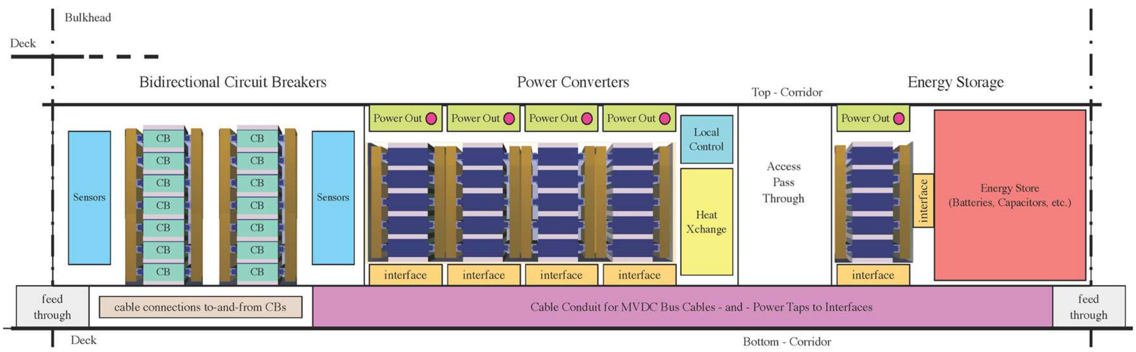

Figure 53 - Side view of sample power corridor [103]. In pink the cable conduit for MVdc bus cables and power taps to interfaces [103]

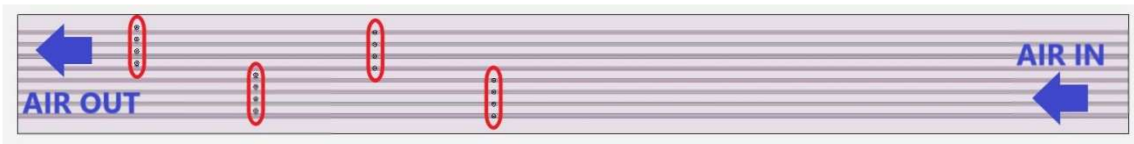

Figure 54 - Top view of the cable conduit for MVdc bus cables and power taps to interfaces. Tap connections circled in red [105]

The studied conduit is assumed as an enclosed box with solid metal sides, bottom, and top. The ends of the conduit are open, thus allowing either forced or natural convection. A top view of the cable conduit is shown in Figure 54. Given the possibility to achieve the same power delivery with different power cable layouts, it is significant to understand how the latter affect the temperature trend throughout the cable conduit. The conduit is designed to carry 24 MW, with a 20% installed margin already included, at +/- 6 kV dc. The cables are arranged in pairs, alternating polarity both horizontally and vertically to system preserve symmetry. Tap cables leading to and from power converters are sized at 125 A. Two different configurations have been considered with different number and type of cables:

- Case A: the IPEC cables have an ampacity of 1000 A. There are two pairs of cables, each supplying four taps (Figure 55 – left side). In this case each cable has four taps, one at each location for the taps, as represented by the numbers adjacent to each cable.

- Case B: the IPEC cables have an ampacity of 250 A. There are eight pairs of cables, each feeding a single tap, as depicted in Figure 55 on the right side. In this case, its number determines the single tap location along the cable.

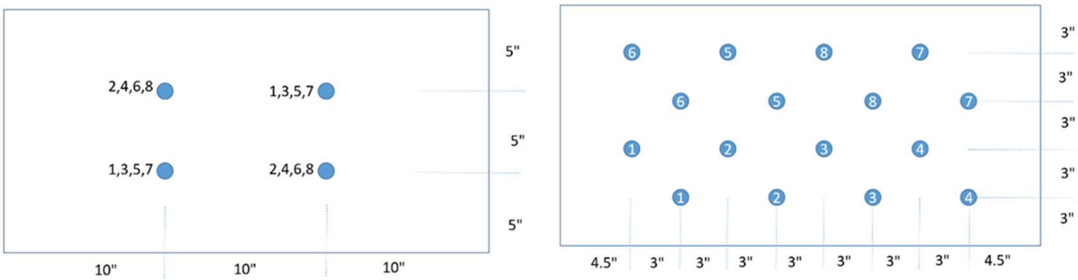

Figure 55 -Case A with four 1000 A cables (two pairs, on the left) and Case B - sixteen 250 A cables (eight pairs, on the right), frontal view [105]

All the cables consist of a copper conductor, with 10 millimeters thick cross-linked polyethylene (XLPE) insulation layer (inner layer detail is not shown in the figures). The geometry specifications for each case are reported in Table 5. The cable sizes have been selected to keep the same current density (i.e., 3.76 A/mm^2) in all of them. Therefore, the Joule power losses in each configuration should be constant, with the exception of skin effects. The latter effect is expected to be significant, thus it will be evaluated in the following. Despite fixing the same current density, temperature differences among the cables are still expected due to the differences in the cable surface area to cross-sectional area ratio.

To simulate the effect of the power electronics operation, a given harmonic content has been added to the steady state dc current (Table 4). The amplitude is represented as a percentage of the total dc component. Despite a total of 12% harmonic content is a high value not compliant with the current classification societies requirements, such assumption takes into account a worst case scenario as a precautionary measure. Of course, real power converters data can be used later on the design stage and thus improving the results obtained.

Table 4 - Harmonic content used in the power corridor simulations

Frequency [kHz]	0.5	2	2.5	4	10	10, $\pi/4$ phase shift
Amplitude %	4	2	2	1.5	1.5	1

Table 5 - Geometry specifications for the power corridor cables

	Cable Ampacity [A]	Conductor Diameter [mm]	Outer Diameter [mm]
Case A	1000	18.4	38.4
Case B	250	9.2	29.2
Tap	125	6.5	26.5

4.6.1 Model implementation

In this section, the electrical and thermal studies that have been performed are briefly described, to specify how the results have been reached using dedicated software tools.

First, the effect of the current harmonic content on the cables' Joule losses has been evaluated for each case considered. COMSOL Multiphysics 5.2 (finite element software) has been used to develop 2D models of the cables (cross sections) and a complete 3D model of the junction. The latter allowed analyzing the tee junction behavior, whose structure is more complex than the cable. Thus, the Table 5 cases have been applied, to define the amount of power that is lost as heat in the cables, along all the IPEC. The finite element software allowed evaluating the increase in Joule losses due to the skin effect without relying on empirical analytical equations.

Then, by using the Joule power losses data coming from the electrical analysis, it has been possible to determine the temperature field in the cable conduit using ANSYS AIM Fluid-Solid Heat Transfer, a Computational Fluid Dynamics (CFD) solver. For each geometry, three thermal simulations have been run:

- no air flow.
- ambient-temperature air flow.
- chilled air flow.

To perform the thermal simulations, proper boundary conditions have been set (Table 6). The air inlet is at the opposite side of the taps, as shown in Figure 54. In the no-air-flow cases, an additional boundary condition was required to fully define the model, so the outlet temperature was set to 33°C (same as the ambient temperature).

Table 6 - ANSYS 3D model boundary conditions

	No air flow	Ambient air flow	Chilled air flow
Air Inlet velocity [m/s]	0	1	1
Air Inlet Temperature [°C]	33	33	12
Air Outlet Gauge Pressure [Pa]	0	0	0
Air Outlet Temperature [°C]	33	Not required	Not required
Cable Temperature at Conduit Ends [°C]	65	65	65
Power Corridor Wall Conditions	Convection, Film coefficient: 4 W/m^2K, Ambient temperature: 33°C		

4.6.2 Electrical simulations

The simulations have been performed assuming the maximum power flow through the conduit, as well as the maximum power demand from the converters. Thus, the power flowing in the corridor at its input (left side of Figure 54) is 24 MW at +/- 6kV. At each of the four operational power taps, 1 MW is diverted to the power converters installed on top of the conduit, yielding a load current of 83.333 A in each tap cable. The remaining 20 MW exits the conduit at the far end of the conduit, on the right side in Figure 54.

At first, a 3D simplified model of the tee junction has been analyzed, to evaluate the skin effect in its geometry. The results are shown in Figure 56 and Figure 57. The former figure shows the current density on the surface of the tee connector and related cables, for the first tap of Case A. The simulation has been performed with a single fixed frequency current (i.e., 10 kHz), to evaluate the worst case for the skin effect. The deep red sections present a higher current density at the surface in respect to the dark blue ones while the magnitude and direction of the current flow is determined by the red arrows. The latter figure depicts the current density in the rectangular section of the connector. It is noticeable that the current density at a given frequency in the junction is appreciably lower than the density in both the main and tap cables. This is mainly due to two factors: the junction cross section is higher than the cables one (due to mechanical reasons); the rectangular shape of the connector limits the skin effect. As can be seen from Figure 56, the current in the connector presents very little skin effect and nearly negligible localized density increases. Therefore, the losses increase due to the current harmonic content in the tap junctions has been considered as negligible. Moreover, the Joule losses of the tee connector have been neglected due to the low current density in the junction in respect to the cables. Consequently, a computational time saving is achieved when performing the thermal analyses. However, a real tap connector 3D model can be exploited in such a simulation if provided by its constructor resulting in an overall more realistic model. Thus, the shared database approach, as depicted in Figure 44, can lead to more realistic simulations as proven by this simple evaluation.

As a second step, the conductors' cross sections have been simulated by means of 2D models, to obtain their power losses. In this case, a time dependent simulation (200 ms length) has been run, with the purpose of calculating the power losses RMS value. To highlight the skin effect in the dc cables, in Figure 58 a snap of the Case A current densities at 100 ms in three different cable sections is given. The shown cable sections are: prior to first tap (left); after fourth tap (center); tap cable (right). The current density scale range is the same for all sections. The losses resulting from the analyses for the two configurations are depicted in Table 7.

In Case A, being more than one tap connected to the same cable, different cable sections have been considered. Concerning the tap cables, they present the same power losses in both cases (being the current flowing in them the same). Clearly, the cables' losses reduce after each tap, due to the reduction of the flowing current (diverted into the tap cables).

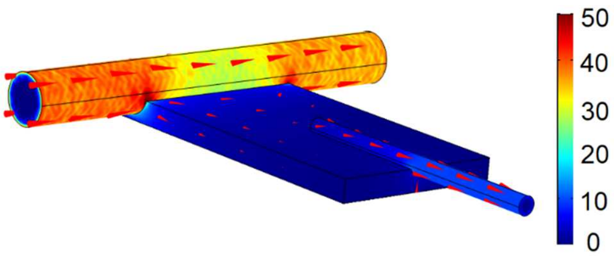

Figure 56 - Current density (A/mm²) in a tee junction at 10 kHz - side view

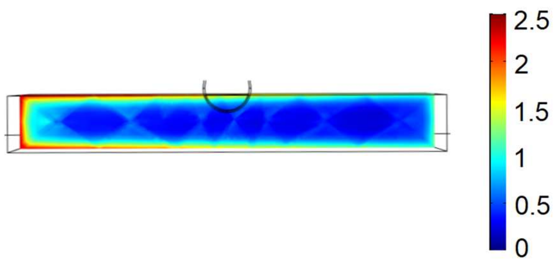

Figure 57 - Current density (A/mm²) in a slice of the tee junction at 10 kHz – magnified front view

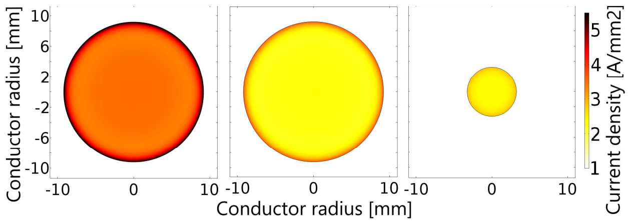

Figure 58 - Case A current density in cables cross section: prior to first tap (left), after fourth taps (center), tap cable (right)

Table 7 - Resulting power losses in the analyzed cables

Case	Cable section	Power losses [W/m]
A	Prior to first tap	78.10256144
	Between first and second tap	65.64823993
	Between second and third tap	54.23031342
	Between third and fourth tap	43.9138765
	After fourth tap	34.72861953
B	Prior to tap	17.52710963
	After tap	7.789829618
Both	Tap cable	3.768483094

4.6.3 Thermal analysis

After having evaluated the Joule power losses in each cable section, it is possible to analyze the thermal behavior of the cable conduit. Thus, three thermal data are of paramount importance: the internal cable temperature field; the air temperature field; and the cable conduit top wall temperature field.

To condense the results, the maximum temperatures found for each of these locations is depicted in Table 8. However, since in some cases the maximum temperature is not the most relevant value, a second temperature with an asterisk (*) before it is included, to indicate a more relevant value. This issue happens when a boundary condition directly causes the maximum temperature. In one case, a carat (^) indicates the approximate temperature of the cable near the tap, because the maximum temperature of the cable was caused by the boundary condition.

As can be seen in Table 8, Case A shows much higher temperatures for all locations and air flow conditions. This is caused by the higher power traveling through each cable. Additionally, there is less total cable surface area in Case A than in Case B. Indeed, the smaller the surface area, the less heat transfer can occur through convection (the primary form of heat transfer in these designs), and the higher the resultant temperature. Finally, it is relevant to notice that the temperatures for Case A, in all the performed simulations, may be so high to impair the cable life expectancy.

Figure 59 shows top views of the cable conduit in *Case A*, for each possible air flow configuration. Note that in the figures, the color scale is determined by the maximum and minimum temperature in each simulation and is not set to a fixed value. This improves visualization of the change in temperature within each figure at the price of losing the possibility of directly compare the figures. In the no-flow case (Figure 59, left) the maximum top wall temperature is 72.369°C. Since this maximum is a localized temperature spike, adjacent to a tap cable that penetrates the top surface of the conduit, it is not representative of the temperature of the overall top wall.

Table 8 - Maximum temperature value for the IPEC in the simulated cases

		No air flow [°C]	**Ambient-temperature air flow [°C]**	**Chilled air flow [°C]**
Case A - 1000A	**Cable**	175.68	150.84	127.06
	Air	149.85	127.01	102.89
	Wall	72.369 *57	58.835 *42	56.153 *29
Case B - 250A	**Cable**	98.154	72.213	65.00 ^50
	Air	90.741	65.873	60.008
	Wall	62.074 *54	53.377 *36	53.508 *26

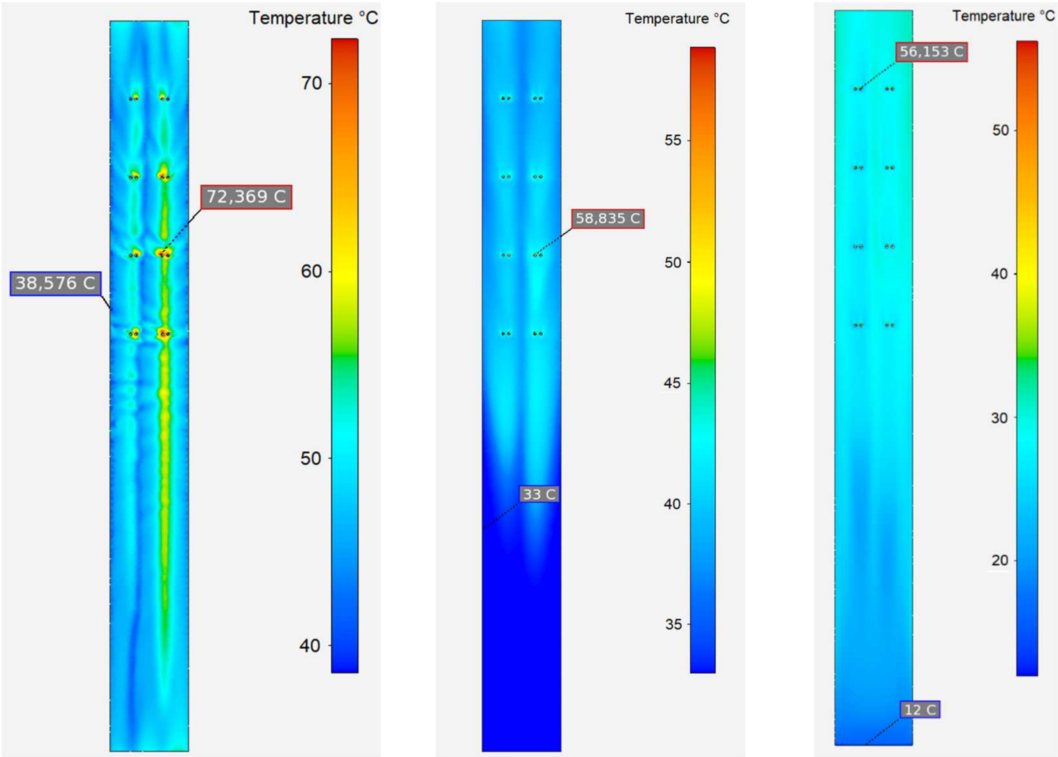

Figure 59 - Top view of Case A cable conduit for three air flow configurations: no air flow (left), ambient-temperature air flow (center) and chilled air flow (right). Air inlet at the bottom, outlet at the top [105]

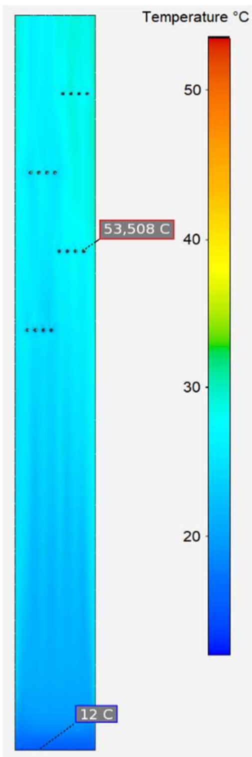

Figure 60 - Top view of Case B, chilled air flow. Air inlet at the bottom, outlet at the top [105]

In fact, most of the top wall is at a lower temperature, around 57°C, which is the one depicted in Table 8 with an asterisk. In the ambient-temperature air flow case (Figure 59, center) the maximum top wall temperature is 58.835°C, while most of the wall is at a lower temperature (circa 42°C). In the chilled-air case (Figure 59, right) the maximum wall temperature is 56.153°C, while most of the wall is at 29°C. For what concerns Case B, in Figure 60 the top wall temperature results are depicted, in the chilled air flow condition. The figure can be directly compared with the right-hand image in Figure 59, showing that all the temperatures in Case B are lower than those in Case A.

Finally, Figure 61 shows the temperature distribution at the outlet of Case B, chilled air flow. The maximum temperature in the cable in this simulation (65°C, occurring at the boundary) is caused by the boundary condition. Bulk air temperature increases in the vertical direction, even with chilled air flow. This effect is more apparent in the simulation with no air flow due to natural convection. The taps presence makes the surrounding air a little warmer, at the same time slowing the air flow because of their obstruction. In the no-flow cases, the taps create a pocket of hot air surrounding them, due to the natural convection effect. However, further detail on the IPEC thermal analysis can be found in [105].

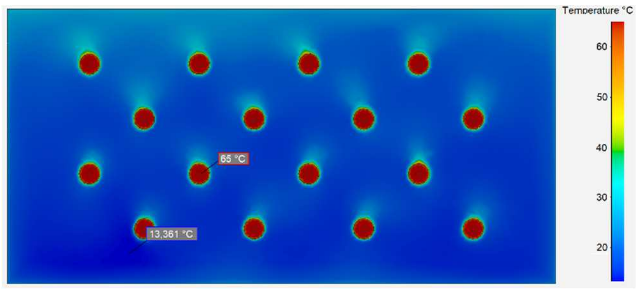

Figure 61 - Temperature distribution at Case B outlet, chilled air flow [105]

4.6.4 Final considerations on the IPEC concept

In this section 4.6, physics-based simulations of multiple cables located in a cable conduit have been performed in a configuration representative of the one required for the modular IPEC. The simulated cases here evaluated included harmonic pollution data (worst case scenario). The latter is representative of operational conditions for MVdc main bus cables in a power distribution system using significant amounts of power electronics. Through these simulations, it has been possible to assess the increase in the Joule losses caused by the harmonic pollution in the dc currents, as well as evaluate the thermal behavior of some significant system configurations [93].

The results show that configurations exist for which active thermal management is not required to maintain acceptable temperatures in the cables, insulation, surrounding air space, and conduit walls. However, it has been found that the design of the cable configuration for the system must include thermal considerations. This is demonstrated by the existence of configurations in which the temperatures of cables and air is so high to possibly impair the system life expectancy.

In particular, Case A (using two pairs of 1000 A cables) is very hot even with cooled air flow, making it a non-feasible configuration for the power corridor. Instead, Case B (using sixteen pairs of 250 A cables) has a very reasonable temperature with ambient temperature air flow, making the additional chilled air cooling not necessary. However, Case B with no air flow also has an acceptable temperature.

Based on the above results (Table 8), the best design for the cable conduit is 250 A cables with no air flow. Air flow provides an added complexity to the design of the ship that should be avoided if it can, as in Case B. The temperature of the cables is low enough that the insulation does not exceed its allowable temperature. While the maximum air temperature is quite warm, the average air temperature should be cool enough to provide workable conditions. Additionally, the top of the cable conduit is at a temperature sufficiently low to make it possible to keep the power electronics modules placed above it at reasonable temperatures if some cooling is provided within them. However, it has to be noticed that the effect of support structures, needed to hold the cables in position, on the heat dissipation has been neglected.

Despite further simulations should be done in more detail to shed more light on the issue, such a study is representative of the CE approach where different multidisciplinary designers tackle the same issue together. The modular IPEC concept is being investigated with a huge research effort by the ESRDC. More specifically, the research activity aim is to develop an early-stage design tool to model the MVdc distribution system of an all-electric ship in line with what has been described in the section 1.4. Existing design tool needs to be enhanced in order to address the increasingly integrated, powerful and heat-producing nature of future payloads (in military applications) [106].

As an example of the current ESRDC state of art, detailed algorithms and processes [107] have been assessed to model the electrical distribution system of an all-electric warship, using the IPEC concept. Using these algorithms, it is possible to design a balanced network of connections to deliver full power between the generators and the loads using N-1 corridors. Thus, the power system reliability is improved against faults, cybersecurity attacks [108], and threats. Finally, the IPEC is embedded in a 3D notional warship model in Figure 62.

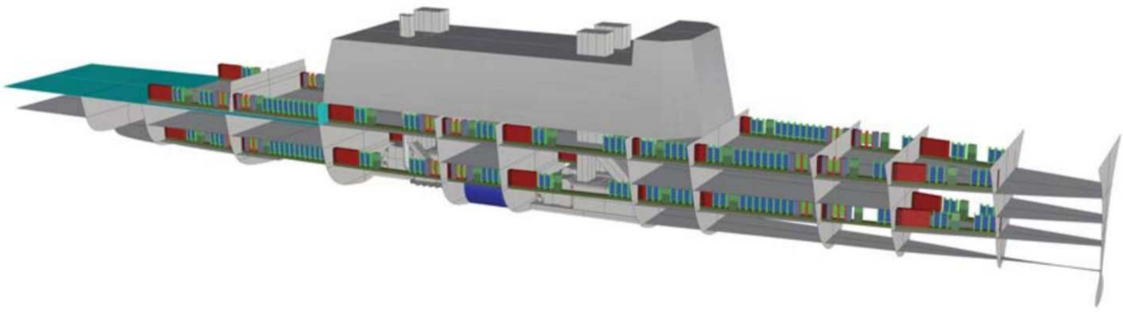

Figure 62 - General view of the IPEC in the ESRDC notional ship [107]

4.7 Conclusions

Innovative methods and tools to design the shipboard power system have been illustrated in this chapter. Firstly, the concurrent engineering approach have been explained and compared to the methodology described in the previous chapter emphasizing the advantages of this innovative design method. Therefore, the focus has been moved to the innovative distribution system design process. The need to anticipate all the possible information regarding the power system design in previous stages has been highlighted in order to better evaluate the innovative power systems performance.

In this scenario, new tools and software play an important role in assessing the power system behavior since the early stage design phase. Indeed, modern complex ships can be designed relying on Computer System Integration software, thus allowing to produce three-dimensional parametric models. The parametric 3D ship model contains mainly detailed data about the ship power system equipment including cables layout and their onboard paths. Given these data availability, an integrated approach in the definition of innovative ship power system has been presented aiming at anticipating useful information. Such information are not only useful in the term of a weight and volume comparison but also allows to perform studies that would otherwise be done in the functional stage design.

Finally, the IPEC concept has been depicted to better comprehend such new approach. Indeed, the new concept of space reserved on board is proposed as a mean to accommodate the future power system in a modular manner and thus resulting in several advantages. Moreover, the space reservation impact on the overall ship design can be evaluated from the early stage design phase.

5 Reference surface combatant ship power system redesign

5.1 Abstract

In chapter 3, more specifically in the section 3.2.1, the ship design process has been defined as not unique, strictly depending on the peculiar application. Moreover, four different type of projects have been identified each having different design and building complexity. In this scenario, an innovative project will be depicted in this chapter outlining the complex activity to identify the feasible design. In such a project, the differences are considerable comparing similar ships of the same class previously built due to the new challenging requirements.

Thus, the main goal is to anticipate all the possible information regarding the power system since the early stage design phase in order to better evaluate the power system behavior in the new scenario pervaded by power electronic devices. Therefore, the entire ship 3D model will be endowed with parametric (and shared among the designers) data in order to enhance the early stage design capabilities. Referring to the proposed innovative approach in Figure 52, such step is needed to ensure reliable information for the software simulations presented in the chapter 6.

5.2 Case study

To this aim, a reference surface combatant ship has been chosen as case study. All the vessel relevant data are available and thus it is worth assessing how to redesign such a reference ship with an innovative distribution system. Thereby, a consistent comparison can be carried out between the actual ship power system and the other two solutions further unfolded. In order to have a comparison as reliable as possible, the power distribution system was not analyzed in its entirety. Indeed, the ship power system have been analyzed from the main power plants to the low voltage secondary distribution panels. All the load connections below the secondary distribution panels, with the exception of the LV/LV transformers, have not been taken into account as they remain unchanged among different power system configurations.

The case study presented in this chapter will also be used for the research activities depicted in the chapters 6 and 7. Thus, the design of innovative power system can be addressed on a variety of levels requiring different methods and tools. The ship power system in analysis is constituted by four main Diesel Generators (DG) rated 2.65 MVA each. These conventional generating systems supply two MVac (6.6 kV – 60 Hz) main switchboards, as shown in Figure 63. The MVac switchboards (QP/1 and QP/2) feed all the ship's electric loads through a radial distribution system, by using different voltage levels. The most relevant loads are directly connected to the main switchboards (DOL azimuth thruster – 1 MW) or through a transformer plus a converter, such as the two Electric Propulsion Motors (EPM) rated 2.15 MW each. Moreover, a HV shore panel is connected to the QP/1 main switchboard enabling shore-to-ship connection and vice versa. Therefore, the two primary distribution switchboards (QD/1 and QD/2) are supplied by the main distribution switchboards through MV/LV transformers (3.4 MVA each) at 440 V – 60 Hz. Moreover, a LV shore panel is connected to the QD/2 primary switchboard with the same task of the previous shore panel. Both main and primary switchboards have a tie connector between each of them compatible with the voltage levels. Finally, each of the primary distribution panels directly fed the secondary distribution panels (SWB) at 440 V – 60 Hz supplying all the ship lower power loads. In Figure 63, also the LV/LV transformers providing 400 V, 240 V or 115 V power supply are highlighted, despite being below the secondary power distribution panels.

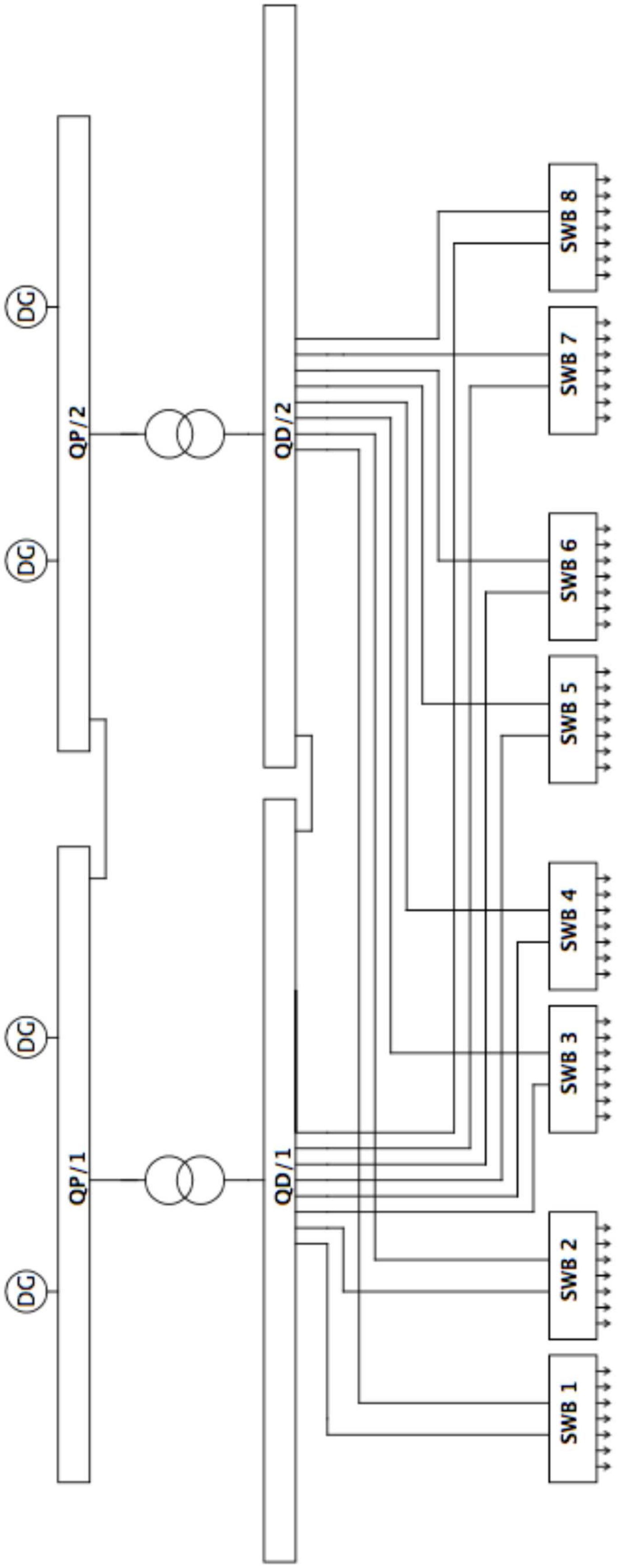

Figure 63 – Reference combatant ship with ac radial power system

Starting from the conventional radial MVac power system layout, two new one line diagrams are provided: the former redesign is endowed with a radial LVdc power system (Figure 66), the latter comes with a zonal LVdc distribution system (Figure 69). Moreover, a structure as similar as possible to the reference radial ac power system has been maintained for the former case. Conversely, the only constrain is the loads and power plants location for the latter case and thus enhancing the designers' freedom in the definition of new innovative proposals. In addition, the integration of a new pulsed load has been evaluated in the zonal LVdc distribution system aiming to replace the one previously installed. The goal is, therefore, to evaluate the impact of the proposed solutions from the point of view of total weights and volumes.

In addition, not only a total weights and volumes assessment has been carried out, but also the proof of concept of the onboard placement has been evaluated for both the proposed innovative solutions. Thus, the power cables length has been estimated with higher precision once the electric equipments have been placed onboard. Referring to Figure 38, the cable length assessment usually comes in the functional design stage (point O). Such analysis enables to foresee the cable length in an early stage design phase enhancing the overall project quality. In addition, the power cables data can be taken from the common database and thus allowing to also perform power system analysis in the early stage design phase (e.g., short circuit assessment, voltage drop analysis, harmonic pollution analysis, and so on). Figure 64 briefly shows the workflow followed in the redesign process.

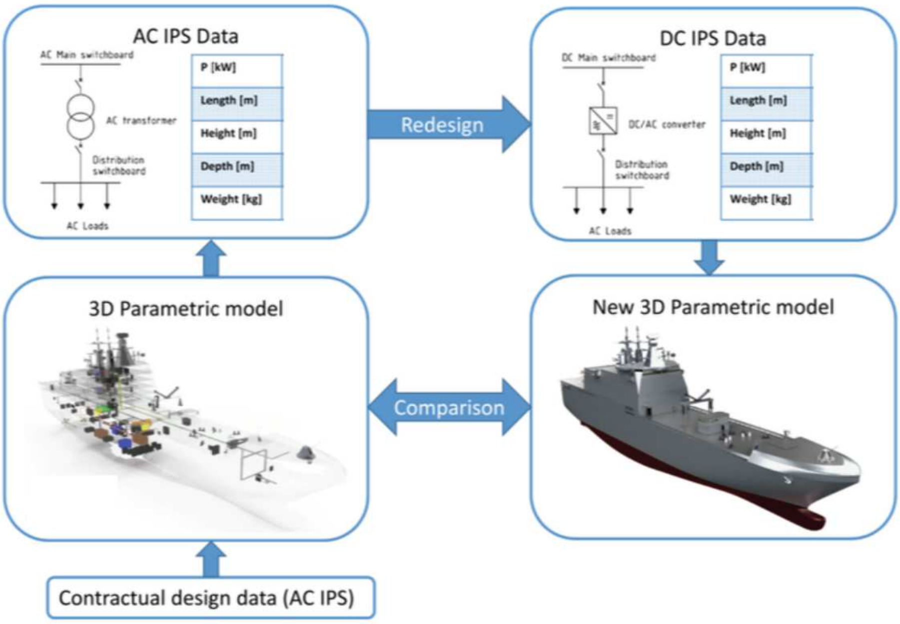

Figure 64 – Explicative block diagram of the redesign process [109]

5.3 Radial ac power system analysis

Given the reference combatant ship with ac radial power system depicted in Figure 63, the first step in the redesign process is the volumes and weights assessment of the actual reference ship electrical equipment. As stated before, the ship power system has been analyzed from the main power plants to the low voltage secondary distribution panels. All the load connections below the secondary distribution panels, with the exception of the LV/LV transformers, have not been taken into account as they remain unchanged among different power system configurations. Such analysis has been carried out in order to obtain values to be compared with the results of the analysis of the further proposed dc distribution systems.

The ship owner provided all the useful data to evaluate the weight and overall dimensions of the main components of the actual onboard distribution system. Nevertheless, some data were derived from educated guesses when they were not directly available. The electrical circuit booklet is one of the main documents in the shipboard power system definition as described in the chapter 3. Indeed, all the power system connections are listed arriving and departing form the onboard switchboards. Moreover, other important information are also specified such as the assumed cable length, the cable type and layout, the required circuit breaker, and the power and current absorbed by the connected load. The electrical circuit booklet has been disclosed by the ship owner, for instance.

In detail, the volumes and weights assessment has been carried out for the following components:

- Power cables.
- Switchboards (main, primary, and secondary).
- Main generators.
- Transformers and power converters upstream of secondary distribution switchboards.
- Transformers downstream of secondary distribution switchboards.

The LVdc zonal distribution system involves a radical change in the arrangement of the secondary distribution panels and, consequently, the cumbersome and heavy low frequency transformers are replaced by lighter power electronic devices. Thus, the volumes and weights assessment is needed also for the SWB and the LV/LV transformers connected to them with the aim to suitably compare the LVdc zonal distribution system with the actual reference ship one. On the other hand, the LVdc radial solution does not require such additional analysis since the SWBs are the same as in the ac radial distribution system.

Although weights and volumes relating to the generators, distribution boards, power converters and most of the transformers installed were given by the owner, some hypotheses are necessary to complete the analysis. These hypotheses regard the premagnetization transformers, the LV/LV transformers, the power cables, and the SWBs.

Firstly, the premagnetization transformers present in the system have been neglected since the relative data is missing and, thus, they are not even depicted in the single line diagram of Figure 63. This hypothesis is justified by their size in terms of rated power being it marginal with respect to the other electrical equipment (e.g., power transformers, generators). The power cables supplying the premagnetizaion transformers have been still considered. However, this first assumption is pejorative since it leads to a lighter ac power system.

Secondly, three LV/LV transformers lacked their respective volume and/or weight data. Since the supplier is the same for all the LV/LV transformers, some reasonable assumptions have been done exploiting the homothetic principle. Indeed, the missing data have been inferred relying on the size, the transformation ratio, and the type of connection of the transformer being analyzed. Therefore, the missing data have been derived as follows:

- 440/115 V - Dd - 10 kVA LV/LV distribution transformer: the weight was obtained by interpolation from the 15 kVA and 20 kVA 440/115 V - Dd transformers data.
- 440/240 V - Dd - 20 kVA LV/LV distribution transformer: the dimensions has been assumed equal to those of the transformer 440/240 V - Dy - 20kVA. Then, the weight of Dd and Dy configurations of the 440/240 V - 10 kVA transformer has been compared and a proportional weight coefficient has been applied to the 440/240 V - Dy - 20kVA transformer to assess the Dd configuration weight.
- 440/240 V - Dd - 25 kVA LV/LV distribution transformer: the dimensions has been derived from transformers of similar size. The weight has been inferred by the interpolation of the 10 kVA and 20 kVA the 440/240 V - Dd transformers weight.

The next assumption regards the power cables. The cable type provided in the electric circuit booklet is the Panzerflex ELX HF 6/10 kV for the MV section and the Panzerflex HF 0.6/1 kV for the LV on, both built by Prysmian. Since the data regarding the MV and LV power cables were unknown, the Prysmian MV-FHFX 6/10 kV and Prysmian HFX-U-FR 0.6/1 kV have been used. Of course, the formers have been employed in the MV section, while the latter in the LV one. The Panzerflex cable type complies with the RINAMIL standard (RINA standard for military vessels), nevertheless the chosen cable types comply with the required standards. Indeed, the requirements are tighter for cables to be installed onboard than the ones for land power systems. Not only the cables for shipboard installation should not be particularly bulky and rigid, but also that they must be halogen-free and have reduced emissions of black smoke and toxic gases. In case of fire, the escape routes must have a sufficient visibility favoring the ship evacuation. On the other hand, the complete absence of toxic substances in the cable insulation layers makes them safe for people and environmental-friendly too. The chosen cables are thus in accordance with the following standard:

- IEC 60092-350: general construction and test requirements.
- IEC 60092-351: insulating materials for shipboard and offshore units, power, control, instrumentation, telecommunication, and data cables.
- IEC 60092-353: power cables for rated voltages 1 kV and 3 kV.
- IEC 60092-359: sheathing materials for shipboard power and telecommunication cables.

- IEC 60332-3: test of the fire behavior on bunched cables (reduced flame propagation).
- IEC 60754-1: determination of the amount of halogen acid gas.
- IEC 61034-1/2: measurement of smoke density of cables burning under defined conditions (smoke density).
- IEC 60331: tests for electric cables under fire conditions - circuit integrity.
- IEC 60228: conductors of insulated cables.

Therefore, volume and weight have been assessed for both medium and low voltage power cables. The data of each cable have been obtained from their technical datasheets as per unit value (i.e., kg/m and m^3/m) and thus multiplied by the number of parallel cables for each bundle and the cable length as reported in the electrical circuit booklet.

The last assumption concerns the secondary distribution switchboards. Since the analysis of the onboard power system should stop at the SWB at first, their volume and weight data has not been provided. However, the zonal LVdc solution requires these values and therefore their assessment has been carried out. Regarding the volume, the 2D SWB dimensions have been inferred from the ship general arrangement plan. Then, the third dimension (the height) has been chosen among reasonable standard dimensions of commercially available components. The weight assessment is too complex instead to be carried out and thus this value is not given.

Finally, the resulting volumes and weights data for each equipment category will be used as a reference value in order to compare the below depicted innovative solutions.

5.4 Radial dc power system

5.4.1 The redesign methodology

This section depicts the innovative radial LVdc distribution. The new power system one line diagram has been maintained as similar as possible to the reference radial ac power system. Indeed, the ship power system have been redesigned from the main power plants to the low voltage secondary distribution panels. In this case the SWBs remain unchanged from the reference radial ac power system. Given this scenario, the radial LVdc power system one line diagram is illustrated in Figure 66. Such an innovative solution is comparable to the ac radial distribution depicted in Figure 63, unless the presence of ac/dc and dc/ac converters. In fact, the same number of distribution switchboards has been kept as well as the same number of connections. The only difference between the two diagrams is obviously the presence of the required power converters. Indeed, the latter aim to provide dc power supply to distribution grid rectifying the voltage generated by the onboard DGs and then supplying the SWBs with the required LVac. Moreover, power converters are also needed to supply the EPMs, the azimuth thruster, and the two shore panels. What have been described above allows to compare the reference shipboard ac power system with the new LVdc one, keeping constant as many design parameters as possible. Nonetheless, there is another difference the radial ac solution, carefully analyzing the one line diagram of the radial LVdc power system. Indeed, the connection between the two primary distribution switchboards is missing in the diagram. However, the power system reliability is not decreased by this specific design choice, which will be addressed below at the end of this section.

Therefore, the flowchart of the proposed redesign approach is depicted in Figure 65. Such approach consists of nine different steps. In detail, three colors are used in order to better understand the flowchart: the design process input data are presented in green, the assessed data are depicted in blue, and finally the design process output data are illustrated in red. The steps as briefly reported below:

- The choice of the dc voltage level is the first design step. Indeed, all the subsequent cascade steps depend on this choice, apart from the second and the third step that can be done in parallel to the first.
- Given the different QP voltage level and the needed power converter interface, the main MVac generators can be replaced with LVac ones.
- The analysis of the power required by each SWB is thus carried out. Therefore, the required current is assessed and can be exploited as input parameter for the fourth step along with the defined voltage level and the SWB required power.
- The power converters size is then evaluated. The power converters shall provide power greater than or at least equal to the required SWB power. Nevertheless, the n-1 criterion has been taken into account given the power converters modular structure resulting in a greater power availability.
- The dc circuit breakers have been chosen in the fifth step among Commercial Off-The-Shelf (COTS) components relying on the power converters capability to limit the fault currents [62].
- Thus, the switchboard sizing relies on COTS components too depending on the dc circuit braker chosen.

- The power cables have been sized considering the maximum power required by each converter and not the SWB one, of course. In the radial LVdc solution the cables length is provided avoiding its assessments through the CSI 3D model.
- The CSI 3D model gives the proof of concept of the proposed innovative distribution power system in the eighth step.
- Finally, the overall power system volume and weight is then evaluated.

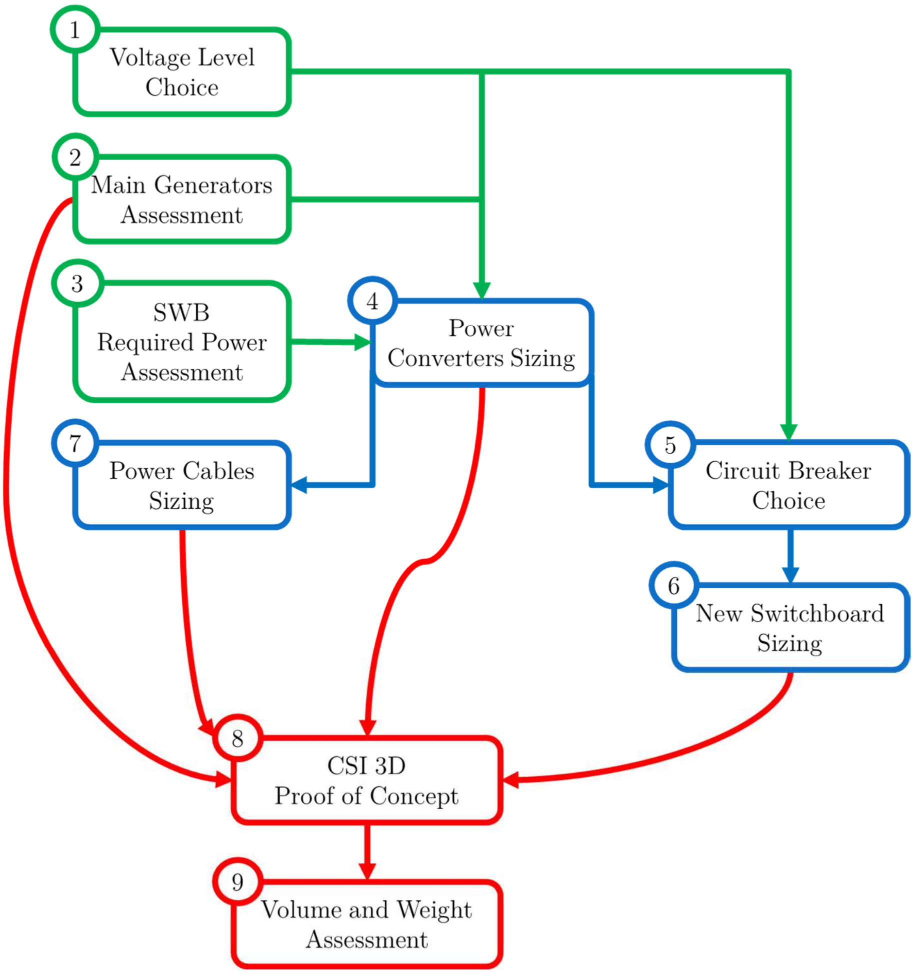

Figure 65 – Flowchart of the proposed radial dc redesign approach

5.4.2 The redesign process

Given this approach, a distribution voltage level equal to 1 kV dc was envisaged for the proposed power system, being a standard de facto in the shipboard LVdc power system as state in the section 2.3.3. This choice allows to exploit the same voltage level for both the QP and the QD switchboards. Thus, not only the propulsion transformers have been removed, but also the large step-down transformers have been stripped as can be noticed comparing Figure 63 with Figure 66.

Although the EPM propulsion engines and the azimuth thruster are the same as the reference ship, the choice of a new distribution voltage level has made it possible to replace the generators coupled to the diesel motors. Thus, the new electrical machines are the 2310 kVA synchronous AEM SE 500 S4 generators. Consequently, the ABB 2515 kW ACS880-304 12-pulse diode converters have been coupled to the new generators. This rectifier has been chosen since a power electronics device with bidirectional power flow was not required. Moreover, a bidirectional converter would have entailed an increase in complexity and greater overall dimensions. Besides, the choice of a 12-pulse scheme instead of 6-pulse converter results in a rectifier output waveform improvement that leads to a significant reduction in the output voltage ripple. This new configuration for the power plant has resulted in significant savings in terms of weight and dimensions, as explained below.

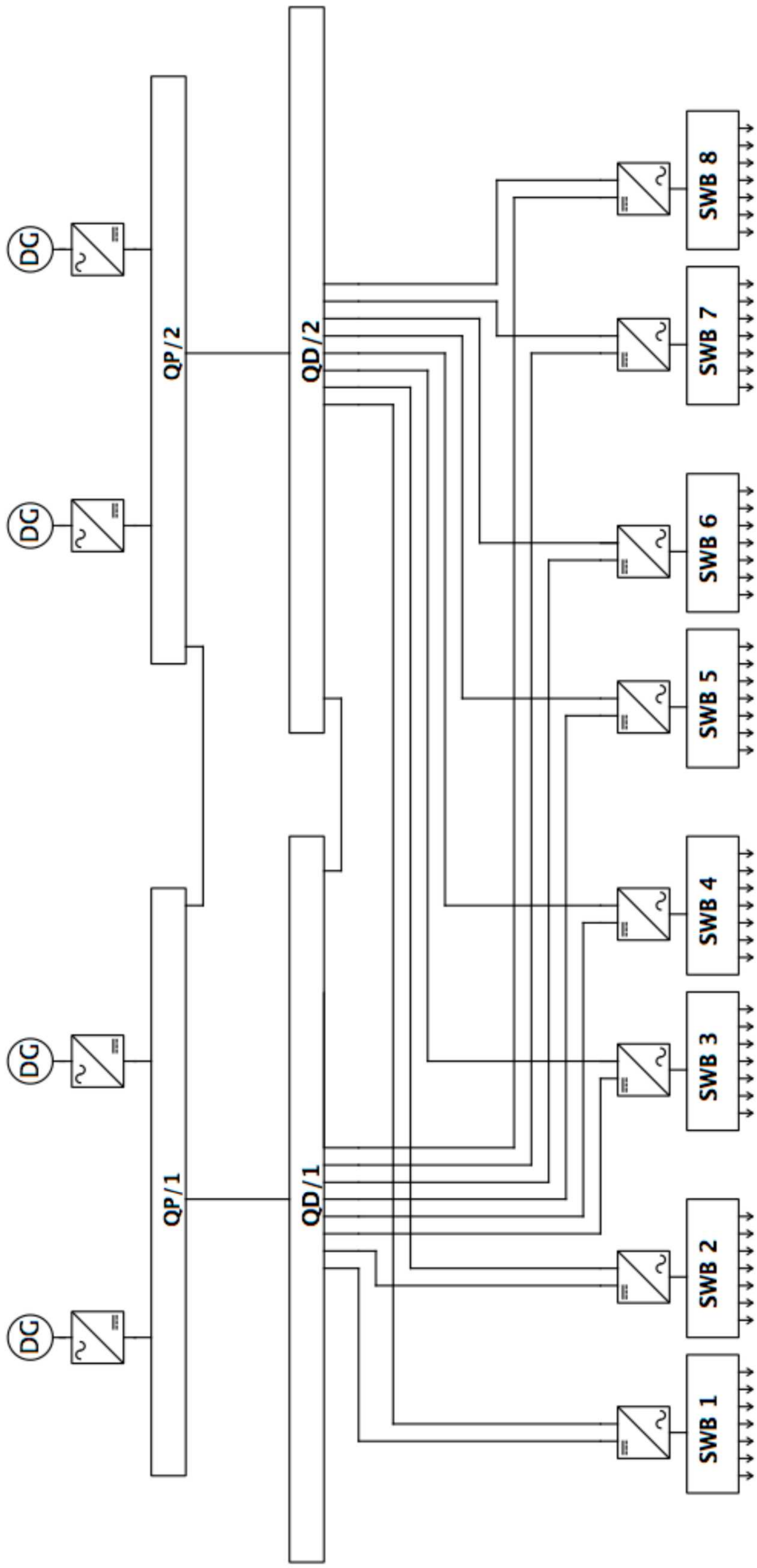

Figure 66 - Reference combatant ship with dc radial power system

Thus, the power required by the SWBs has been assessed. Such data can be found directly in the electrical circuit booklet already grouped by each panel. Nevertheless, the electrical circuit booklet analysis showed some incomplete data. Indeed, the load power factor data has been properly assumed when it was otherwise not available. Therefore, power factor values have been considered equal to 0.98, 0.85 and 1.00 for the transformers, the motors, and the remaining loads respectively, in accordance with typical data found in literature. This step was necessary to calculate the required SWB active and reactive power to be supplied by the converters. Thus, Table 9 shows an example of the generic SWB load assessment.

Table 9 – Generic SWB load assessment

Description	**Power** [W]	**Power Factor**	**Current** [A]
Load 1	P_1	PF_1	$I_1 = P_1/(V_{ac} \cdot PF_1 \cdot \sqrt{3})$
...	...	...	...
Load n	P_n	PF_n	$I_n = P_n/(V_{ac} \cdot PF_n \cdot \sqrt{3})$
Generic SWB	$\sum P_k$		$\sum I_k$

Table 10 – Power converters requirements

	Function	**Converter Type**	**P** [MW]	**A** [MVA]	**Vin** [V]	**Vout** [V]
1	dc power supply	ac/dc isolation not required	2100	2625	690 Vac - 60 Hz	1000 Vdc
2	EPM drive	dc/ac isolation not required	2416	3020	1000 Vdc	690 Vac - variable frequency
3	Thruster drive	dc/ac isolation not required	1000	1250	1000 Vdc	6600 Vac - variable frequency
4	Shore connection converter	dc/ac isolation required	1300	1625	1000 Vdc	690 Vac - 60 Hz
5	SWB supply	dc/ac isolation required	-	-	1000 Vdc	440 Vac - 60 Hz

Once the SWBs load assessment has been carried out, the power converters can thus be defined. Of course, the power converters sizing strictly depends on both the specific electrical requirements and the required isolation level. Indeed, the power system converters have been chosen according to the power required as well as to the input and output voltage values. Thus, the volume and weight assessment is needed for all the converters numbered in Table 10. Nevertheless, the first converter has already been evaluated and the ABB 2515 kW ACS880-304 12-pulse diode converters have been chosen. On the other hand, the remain converters sizing has been relied on both research studies and industrial knowledge.

The second converter is the EPM drive as depicted in Table 10. The EPM drive is composed by a chopper, a second order filter, and an inverter, as can be seen from the block diagram in Figure 67. The step-up chopper is needed along with the dedicated filter due to the high EPM voltage level. In fact, the chopper takes to boost the dc voltage before the inverter stage since its value is not enough to meet the EPM ac voltage level.

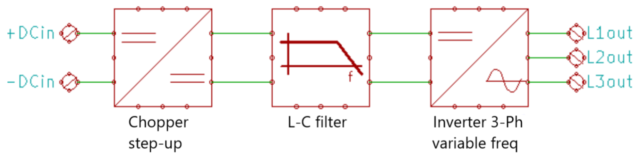

Figure 67 – EPM propulsion drive block diagram

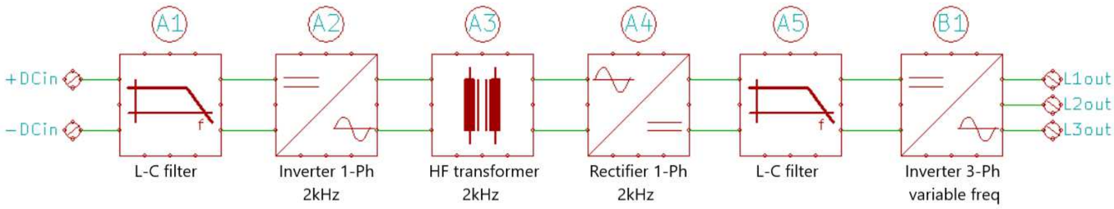

Figure 68 – Azimuth thruster drive block diagram

The same issue also occurs for the azimuth thruster, with the difference that in this case the required ac voltage is considerably high (see Table 10). Given this scenario, a step-up transformer is needed to overcome such an issue. Nonetheless, the transformer cannot be installed on the ac side due to the variable frequency output, hence the structure presented in Figure 68. Such a solution requires an SST that leads to significantly lower weight and volume compared to a machine of the same power, but at 50/60 Hz.

The fourth converter to be sized is the one supplying the shore panels. The step-up stage is again required at the inverter input since a 690 ac voltage has been assumed for the new shore panel. Indeed, a 690 phase-to-phase voltage corresponds to a star voltage of about 400 V. This voltage has a peak value of 566 V, which requires a dc bus with a minimum value equal to twice the peak value and so to 1122 V. Given this scenario, the same solution as in Figure 67 has been adopted. Therefore, such device has been oversized leading to a higher reliability in case of an inverter module failure.

Once the above converters have been defined, the devices connected to the secondary distribution panels are now to be designed. To increase the system safety, the converters have been endowed with galvanic isolation resulting in a block diagram as in Figure 68. Nevertheless, the SWB power converters have not been modeled as a single device but as a set of 100 kW sub-modules. Moreover, the n-1 criterion has been taken into account given the power converters modular structure. Thus, the converter is able to fully satisfy the power demand of the load even in the case of a single sub-module failure. Following this assumption, the power converters have been sized analyzing the power absorbed by each SWB. Finally, the devices volume and weight has been assessed depending on the required number of sub-modules whose values are known.

Once the converters have been assessed, the system has to be endowed with the proper circuit breakers. As depicted in the section 2.2.1, the absence of voltage or current zero crossing makes it difficult to extinguish the dc arcs and thus the build of suitable dc breakers is a complex task [54]. Nevertheless, in [51] is stated that "all the power electronics converters should be designed to limit fault currents to minimize the need for load side circuit breakers". Thereby, a fault current limitation capability has been assumed for the power electronics devices equals to 150% of the rated current.

Given this scenario, the dc circuit breakers have been chosen among COTS components. In particular, the ABB Sace Emax dc 4-pole withdrawable circuit-breakers comply with requirements of the proposed innovative power system. Nonetheless, the tie-breaker short circuit current overcomes the 5 kA ABB circuit breaker current limit. Thus, the UR60-82 circuit-breakers by Sécheron has been exploited for this purpose since its current limit is 6 kA complying with the tie-breaker requirement.

The next step depicted in Figure 65 is the switchboard sizing. Therefore, the ABB Artu-K switchboards have been selected to accommodate the Sace Emax dc circuit-breakers. On the other hand, the Sécheron MBS 500 switchboard has been instead considered to install the aforementioned UR60-82 circuit-breaker. Since the switchboards currently installed on the reference ship are IP[7] 32 certified, the same or higher protection code should be considered for the new switchboards. Indeed, the ABB switchboards are in accordance with the IP 65 code, while the Sécheron switchboard is IP 42 certified. Of course, the switchboard volume and weight assessment is a difficult task in an early stage design phase. Nevertheless, all the hypotheses aims to better evaluate the power system parameters for a first consistent comparison. In the design of the Artu-K switchboard, the weight of the horizontal distribution bars has been estimated considering the overall length of the switchboard (the weight is given in kg/m in the datasheet). Moreover, other switchboard components have been evaluated, as follows:

- Uprights.
- Base.
- Header.
- Plinth.
- Side flanges.
- Back cover.
- Side panels.
- Blind door.

Due to the lack of the cumbersome HV/LV transformer, the respective aft and bow QPs and QDs have been placed together in the same room. However, the switchboards are connected through a power cable and circuit breaker for a consistent comparison with the reference shipboard power system. Thus, this design choice made it possible to obtain more compact volume (the switch in the QD incoming feeder is no more required) and to place the switchboards in a single dedicated room. Given this scenario, QD-QD connection can be avoided being it already present between the main switchboards, as stated previously in this section. Nevertheless, an issue has been faced during the last step depicted in Figure 65: there was not space available to install the bow QP and DP in a "back-to-back" configuration as for the stern ones. Therefore, the ABB disconnector E4H/E MS has been interposed between the bow QP and QD despite the bow switchboard can be considered as unique block.

[7] The IP Code, or Ingress Protection Code, sometimes referred to as International Protection Code, IEC standard 60529 classifies and rates the degree of protection provided by mechanical casings and electrical enclosures against intrusion, dust, accidental contact, and water.

The dc cables sizing (the seventh step) has been performed by calculating the active power absorbed upstream of the dc/ac converters, assuming an overall device efficiency of 98%, in accordance with literature [110]. Thus, the dc cable capability has been calculated from the obtained power value. In addition, the power cables cross section has been chosen in order to maintain a safe 15% load margin, also paying attention to the optimization of cable weight and dimension. As an example, a distribution of 6//2x(1x240) instead of 5//2x(1x300) for each generator results in a weight saving of 440 kg/km. Regarding the power cables supplying the SWBs, a correction factor has been envisaged taking into account the ratio between the ac power cables ampacity (1169 A) and the required current of each SWBs. Although this choice has led to an increase in the cables cross section, a more faithful comparison has been carried out with the ac power distribution. Nevertheless, the cable oversizing maintenance leaves the way open to a possible future optimization.

As regards the power cables connecting the two main switchboards, the reference ship apparent power has been considered for this connection as an active power in the dc redesign. Indeed, the 5250 kVA connection between the two QPs has been dimensioned in such a way as to have a 5250 kW capability. While leading to an oversizing with respect to the ac power system, this hypothesis has maintained the same bottlenecks, thus making consistent the comparison between the two designs. In addition, the cables have been chosen considering the same operating temperatures reported in the circuit booklet.

Finally, the last two steps will be shown below to better compare both the redesign solutions. More precisely, the proof of concept of the proposed innovative distribution power system is depicted in the section 5.6 exploiting a CSI 3D model, while the volume and weight comparison with the reference ac power system is presented in the section 5.7.

5.5 Zonal dc power system

5.5.1 The redesign methodology

This section presents an innovative zonal LVdc distribution system with a zonal structure. The main advantages of such a power system architecture have previously been depicted in the section 2.2.2. Given the reference ship illustrated in the section 5.3, the only design constrain is the loads and power plants location and thus enhancing the designers' freedom in the definition of new innovative proposals. In addition, the integration of a new pulsed load has been evaluated in the zonal LVdc distribution system aiming to replace the one previously installed.

As can be seen from the single-line diagram shown in Figure 69, the shipboard power system has been modified up to the secondary distribution panels. In fact, four zone panels (Z) have been envisaged corresponding to the ship's four Main Vertical Zones (MVZ). In this context, it is recalled that the MVZs subdivide the ship into watertight sectors by means of bulkhead doors enhancing the ship survivability in case of flood or fire (see section 1.3). Therefore, electrical MVZs coincide with the ship watertight MVZs.

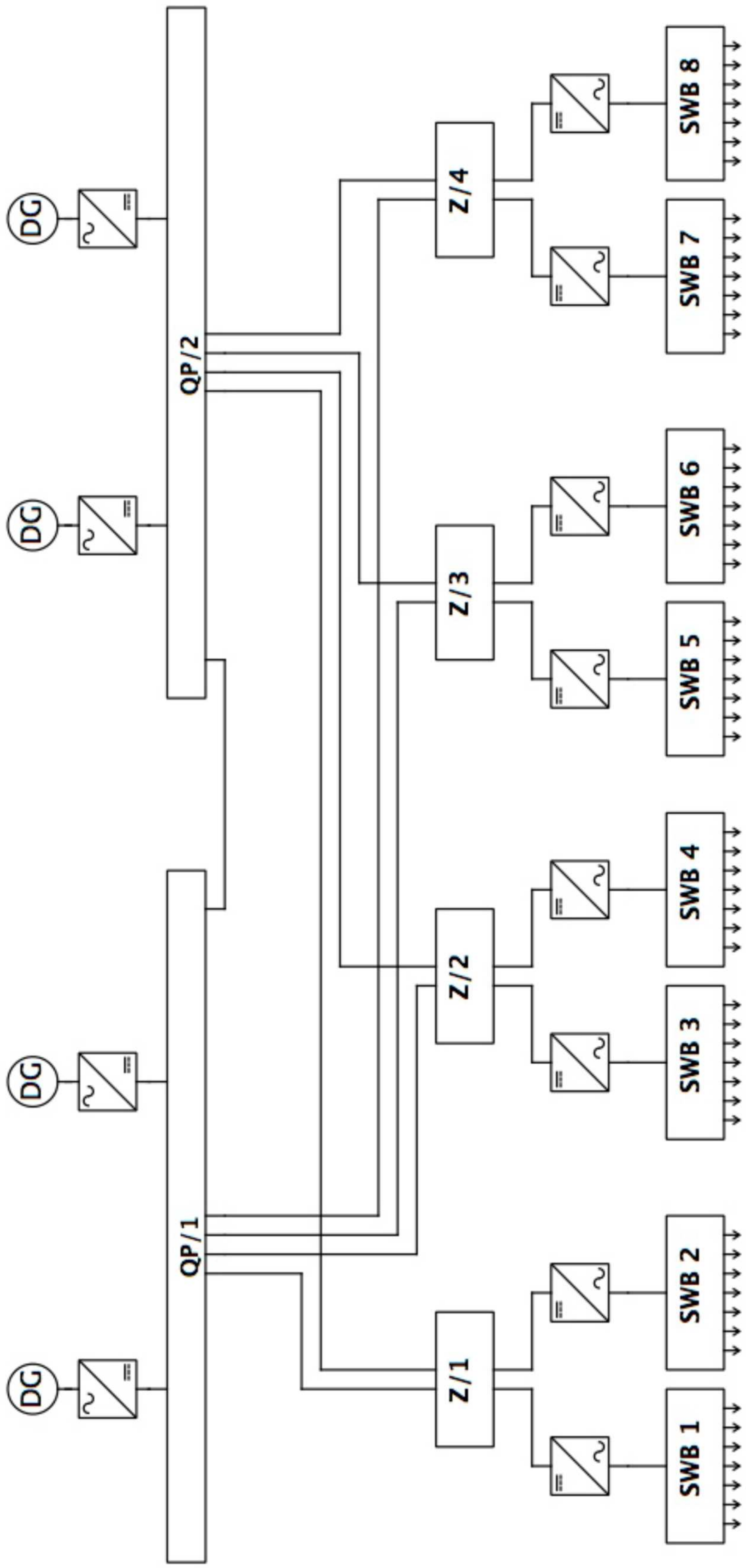

Figure 69 - Reference combatant ship with dc zonal power system

The four Zs are endowed with a dedicated panel section for each LVac required voltage level avoiding the connection of the previous SWBs. The required 440 V, 400 V, 240 V or 115 V power supply are ensured by dedicated converters for each panel section, despite being below the same SWB. Thus, such a solution made it possible to remove all the LV/LV transformers originally connected to the secondary distribution boards SWB. Moreover, the primary distribution panels (QDs) have been conceptually replaced by the zone Zs. Therefore, the shore connection panel is directly supplied by the main panel QP/2 despite being originally fed by the QD/2. The required redundancy has been maintained since there is a shore connection for both the bow and aft power plants.

As illustrated in the single-line diagram in Figure 69, the dashed rectangles indicate components located in the same electrical rooms. Moreover, the same is valid for the main distribution switchboards. In fact, the dc/dc converters feeding the Zs have been placed in the same room of the respective QP. The power converters enhance the power system reliability thanks to their improved control capabilities. Indeed, the dc/dc converter is a fully controllable device regulating the power flows in case of faults, load disconnections, or other anomalous scenarios in an acceptable time [62].

Therefore, the flowchart of the proposed redesign approach is similar to the one depicted in Figure 65. Nevertheless, some extra and different assumptions have been made in order to comply with the new design constraints resulting in the new flowchart presented in Figure 70. Indeed, the shipboard power system must be able to supply the power demand of the new pulsed load. Therefore, the ship's electrical balance has been analyzed considering the power demand of the new subsystem and the onboard generators capability curve. Such analysis has been carried out in the worst scenario, namely the one with the highest power demand. The ship electrical load balance presents large power gradients between different conditions (e.g., docked at the port, in low speed navigation, in high speed navigation, and so on). For the reference ship power system, the main electric load is the propulsion system whose power demand varies within wide limits depending on the speed of the ship.

Since the new load power demand can be supplied by the existing shipboard generators, there is no need to change the main power plants size. Thus, the design can proceed following a workflow similar to the one used for the radial dc redesign. Such approach consists of ten different steps, since the so-called zero step has been added. In detail, three colors are used in order to better understand the flowchart: the design process input data are presented in green, the assessed data are depicted in blue, and finally the design process output data are illustrated in red. The steps number two and three are no more in green as in the Figure 65 since they can strictly depend on the new load to be installed onboard. The steps as briefly reported below:

- Definition of the new load to be installed onboard together with the panel that feeds it.
- The choice of the dc voltage level is now the second design step despite it can be done in parallel to the step zero.
- The analysis of the power required by each SWB is thus carried out. Therefore, the required current is assessed and can be exploited as input parameter for the main generators' assessment depending on the new electrical load analysis.
- The main MVac generators can be replaced with LVac ones given the new load installation, the different QP voltage level, and the needed power converter interface.
- The power converters size is then evaluated. The power converters shall provide power greater than or at least equal to the required SWB power. Nevertheless, the n-1 criterion has been taken into account given the power converters modular structure resulting in a greater power availability.
- The dc circuit breakers have been chosen in the fifth step among COTS components relying on the power converters capability to limit the fault currents [62].
- Thus, the switchboard sizing relies on COTS components too depending on the dc circuit braker chosen.
- The power cables have been sized considering the maximum power required by each converter and not the SWB one, of course. In the zonal LVdc solution the cables length is assessed through the CSI 3D model.
- The overall power system volume and weight is then evaluated.
- Finally, the CSI 3D model gives the proof of concept of the proposed innovative distribution power system.

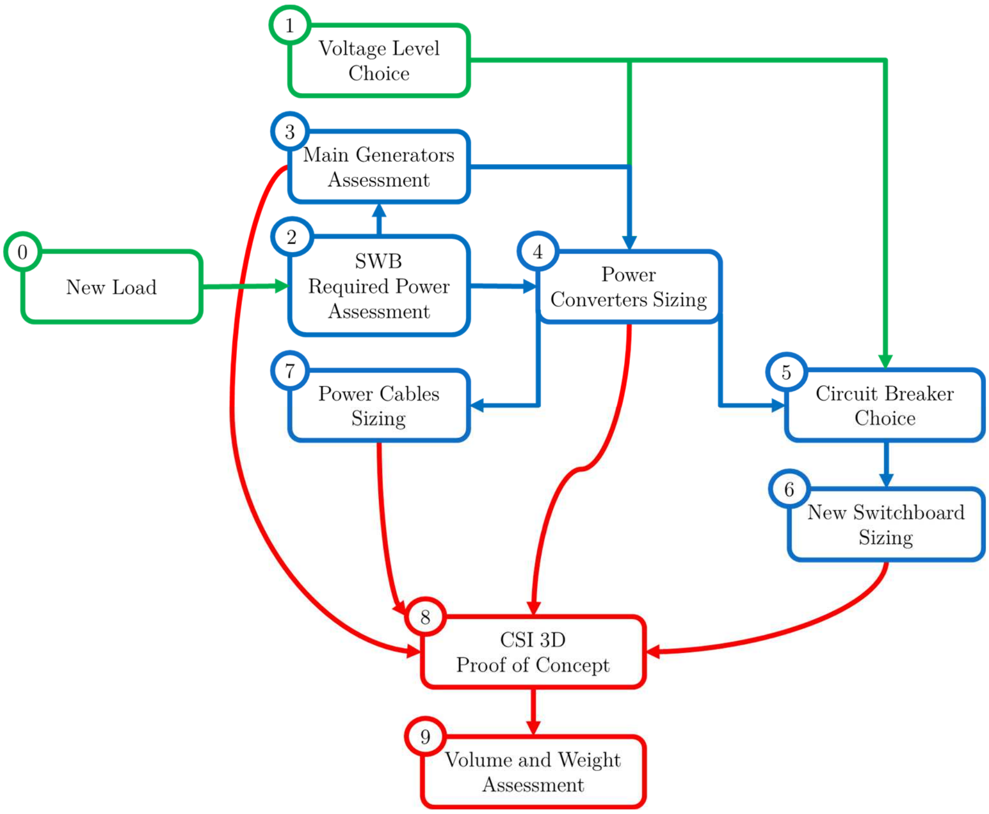

Figure 70 - Flowchart of the proposed zonal dc redesign approach

5.5.2 The redesign process

Given this approach, the ship's electrical balance has been analyzed considering the power demand of the new subsystem and the onboard generators capability curve. Such analysis has been carried out in the worst scenario as previously stated in the above section. Since the new load power demand can be supplied by the existing shipboard generators, there is no need to change the main power plants size. Thus, the design can proceed following a workflow similar to the one used for the radial dc redesign.

The substantial difference from the radial LVdc design can be identified in the choice not to consider the contemporary factor. Therefore, the zonal LVdc power system components result oversized giving space to the future new loads installation with minor modifications to the designed power system. By analyzing the electrical circuit booklet, all the previous SWBs loads have been grouped by the different required voltage level. Then a distribution voltage level equal to 1 kV dc was envisaged for the proposed power system while the main power plant assessment does not need to higher rated generators, as already said.

Once the SWBs load assessment has been carried out, the power converters can thus be defined as in the previous design. Indeed, the converters have the same design arrangement described in the previous section regarding the radial LVdc power system. However, some clarifications must be made. In fact, the contemporary factor has not been considered in the SWB redesign process and thus the dc/ac converters downstream the Z are capable of simultaneously supplying all the connected loads. Furthermore, the safety criterion n-1 has always been considered. These hypotheses result in an increased system reliability at the expense of higher weight and dimension of the power converters. Therefore, the obtained results can be further improved if it is deemed appropriate to proceed with a less precautionary sizing.

As regards the dc/ac converter feeding the 440 V loads in the MVZ 2, it has been designed to correctly supply the new load. Given this scenario, the average power absorbed by the pulsed load have been considered (275 kW). However, the inverter should be able to supply the peak power (equal to 492 kW) for an indicative time of 100 ms, average duration of the absorption peak at pulsed load start-up.

In the zonal distribution, an additional dimensioning is required, namely the dc/dc converters sizing. Such converters have been designed in a way similar to the one depicted in Figure 68 but with a dc output instead as presented in Figure 71. The converters are sized to fed half of the total power required by each Zs, since in normal operation they both feed the downstream switchboards. Moreover, an efficiency of the power electronics devices downstream of the Zs has been considered equal to 0.98 in the calculation of the overall system absorbed power, as in the previous section 5.4.2. Such converters have been sized without the safety criterion n-1, but always neglecting the contemporary factor. The system reliability is ensured by the contemporary connection of both the dc/dc converters. These design choices have again led to an oversizing of the converters on which further advantages in terms of weight and dimension could be obtained.

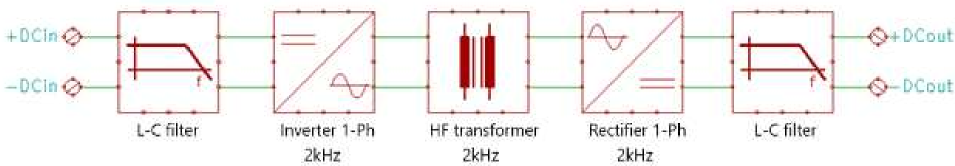

Figure 71 – Block diagram of the dc/dc converter

Once the converters have been assessed, the system has to be endowed with the proper circuit breakers. The protection switches have been chosen according to their rated current and voltage as for the radial LVdc power system. In fact, the presence of controlled converters allows to limit short-circuit currents also in the zonal power system as mentioned in the 1826 IEEE standard [62]. In addition to the circuit breakers previously exploited in 5.4.2, the ABB Sace Tmax dc circuit-breakers have used. Despite being designed for lower rated voltage and current the Sace Emax series, the Tmax circuit breakers can be exploited due to the limited power absorbed by some specific loads such as the 240 V loads in the MVZ1, for instance. Moreover, the 4-pole withdrawable configuration has been chosen for the Tmax devices. Nevertheless, these circuit-breakers are much more sensitive to the ambient temperature compared to the Emax series. Thus, a higher rated Tmax circuit breaker has often to be selected in order to meet the ambient temperature requirement.

The switchboard sizing has been carried out as in the section 5.4.2. Therefore, the ABB Artu-K switchboards have been selected to accommodate both the Emax and the Tmax dc circuit-breakers. In addition, the Sécheron MBS 500 switchboard has been instead considered to install the aforementioned UR60-82 circuit-breaker.

Once the switchboards have been assessed, the power cables have been sized choosing the Prysmian HFX-U-FR 0.6/1 kV cables to connect the entire LVdc distribution. Only the connection between the QPs and the Zs is missing since the other feeders are the same as in the radial dc design. Indeed, the cables have remained unchanged in both type and number for DGs, EPMs, shore panels, azimuth thruster, and the connection between the QPs.

In such a scenario, an ambient temperature of 55 $^\circ$C has been chosen as the reference ambient temperature to calculate the power cables capability. As illustrated in the section 4.6, the power electronics components can lead to higher room temperature especially in confined spaces and therefore a precautionary choice has been made in the presented redesign. Moreover, the power cables can deliver the maximum output power from the dc/dc converters and thus they have not been sized on the power required by the Z switchboard. This has led to an oversizing of these connections, but also to an enhanced safety condition. The effect of this design choice results in simpler integration of new power loads onboard since the cables are sized for rated current greater than the required ones. Moreover, the Z2 cables bundle has been designed in a way to be capable to supply the desired current to the pulsed load panel during the most demanding scenario (i.e., the peak power absorption phase).

Then the cables weight and volume have been optimized for all the cable bundles, always maintaining a maximum load capability of 85% of the rated current. In addition, the cable cross-sections and number of parallels have been selected to provide an installation ease downstream and upstream the dc/dc converters. Furthermore, the cables with cross-section less than 50 mm^2 have not been considered as a design choice, although smaller cross-sections can lead to further weight advantages. Indeed, the thinner the power cables the more parallel connections are needed to supply the same amount of power and thus resulting additional installation complexity.

Finally, the last two steps will be shown below to better compare both the redesign solutions. More precisely, the proof of concept of the proposed innovative distribution power system is depicted in the section 5.6 exploiting a CSI 3D model, while the volume and weight comparison with the reference ac power system is presented in the section 5.7.

5.6 LVdc redesign proof of concept

In order to verify the feasibility of the proposed systems, an integration phase of the aforementioned distribution systems has been envisaged during the design of the hull model created with the Paramarine software (QinetiQ). Such integration also allowed to estimate, already in the early stage design, weight and volume of the power cables used thanks to the assessment of the cable length in the parametric CSI software. The Paramarine® graphic environment allows to create and manage complex solids and surfaces. In order to intertwine this study with the one carried out in the previous section, an analysis of the spaces and dimensions of the electrical equipment have been carried out.

First of all, the reference ship has been modeled dividing the ship into zones according to the position of the watertight bulkheads. Moreover, the premises of interest for electrical equipment have been modeled as precisely as possible, according to the available general arrangement plans. Therefore, solids have been created to represent the installed equipment specifying their dimension, weight, and position referred to the center of gravity. Such data permits also to evaluate the vessel dynamic stability in different sea state scenarios. Nevertheless, naval architecture related considerations are out of the scope of this treatment.

The EPMs with their respective converters, sub-panels, diesel generators, transformers, distribution switchboards, and shore panels are basic elements and therefore they have been placed according to the general arrangement plans. The reference ship CSI 3D model highlighting the ac power system is given in Figure 72. In detail, green blocks are representative of the two main power plants, the EPMs, the azimuth thruster, and the shore panels, while the blue blocks depict all the other components.

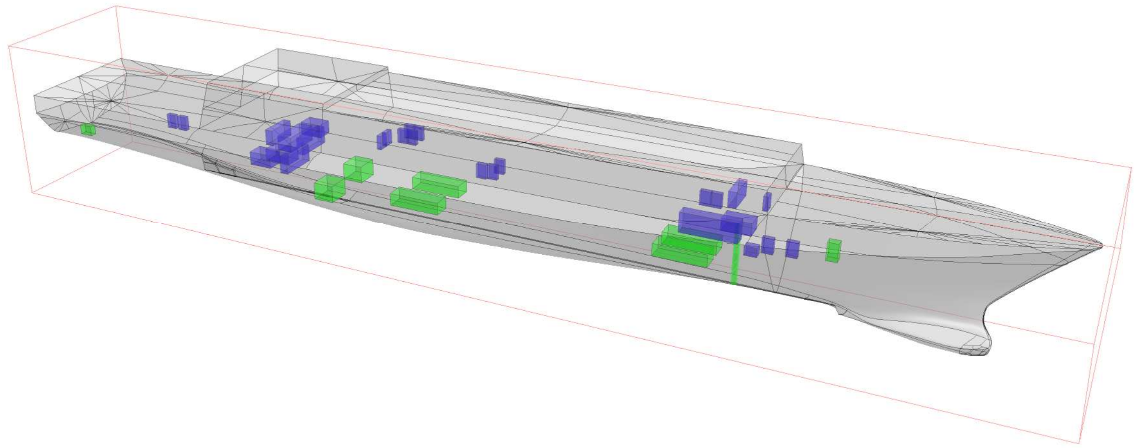

Figure 72 - Reference ship CSI 3D model highlighting the ac power system: in green the two main power plants, the EPMs, the azimuth thruster, and the shore panels; in blue the other components

Starting from these reference case study, the current reference ac power system has been replaced with the radial LVdc solution presented in the section 5.4. The propulsion converters have been replaced with more efficient and less bulky ones and most of the transformers have been eliminated. The power transformers occupy a substantial part of the engine room, especially the ones connected to the EPMs. Despite the numerous advantages of this solution (see section 2.2), there are some limiting factors that have created issues in the implementation of this configuration. It emerged that the spaces onboard are already restricted and are further compromised by the increase in volumes due to the need to insert converters for the shore panels and for each SWBs. Although the overall dimensions are reduced, the compliance with the redundancy and safety requirements limits the choice of positioning such new components. This happens especially in the forward and stern areas where the premises are almost completely dedicated to the performance of fundamental functions of the ship, such as mooring or combat. To solve these issues, some solutions have been found and thus leading to substantial changes in the layout of the rooms, as listed below:

- The respective zone QPs and the QDs switchboards have been unified in a single equipment. Their disposition can be seen in Figure 73 where the orange blocks represents the equipment sized for the LVdc radial solution. On the other hand, the green blocks indicates the unchanged SWBs which are the same as in the ac reference ship. In addition, the MVZ3 main switchboard room is given in Figure 74.
- Reversal of two offices with one electrical equipment room. In terms of total square footage there are no significant variations, but this new arrangement allows to assign the new SWBs converters to the MVZ2 that is the same as the panels they supply.

The remaining SWB converters have been placed in the spaces made free by the removal of the switchboards or transformers, especially in the engine and transformer rooms, trying to distance them as little as possible from the reference sub-panels. Such analysis leads to the assessment of the onboard power cable paths and thus allowing to proper calculate their size and weight. Finally, the reference ship CSI 3D model highlighting the LVdc radial power system is given in Figure 75. In detail, green blocks are representative of the two main power plants, the EPMs, the azimuth thruster, and the shore panels, while the orange blocks depict all the other components related to the proposed LVdc radial distribution.

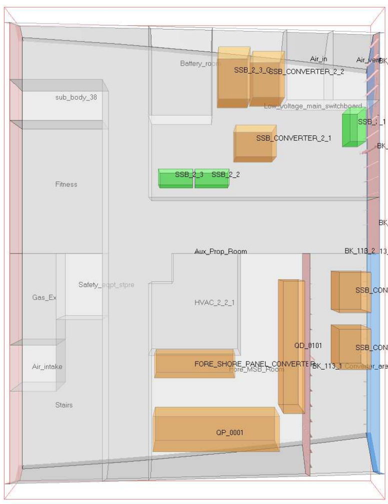

Figure 73 - 3D model of the MVZ2 main switchboard room with LVdc radial distribution

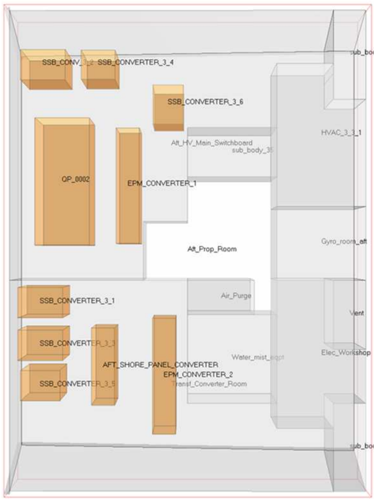

Figure 74 - 3D model of the MVZ3 main switchboard room with LVdc radial distribution

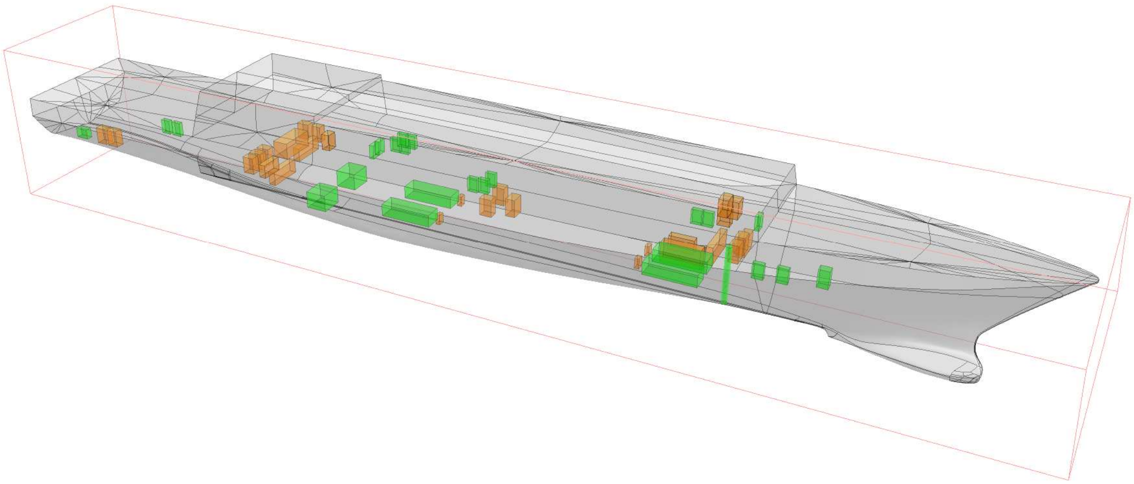

Figure 75 - Reference ship CSI 3D model highlighting the LVdc radial power system: in green the two main power plants, the EPMs, and the azimuth thruster; in blue the other components

A LVdc zonal configuration has been developed to propose an alternative that maintains the benefits outlined above (such as reducing the quantity of cables) but increasing power system reliability and the degree of safety. Moreover, such architecture is endowed with a new pulsed power load. The system reliability is enhanced by the definition of ad hoc zonal distribution panel for each of the four zones, unlike the system previously analyzed in which the QDs are only two. The change in the ship general equipment arrangement is quite radical. Indeed, new ac/dc and dc/dc power converters are needed in order to replace the SWBs and their downstream transformers. Although the total volumes have no significant variations, the constraints in the equipment arrangement are even more stringent than in the LVdc radial distribution. In fact, the Zs have to be positioned in the same room along with the respective dc/ac converters. In this scenario, a substantial review of some onboard spaces have been carried out. In particular, the following solutions have been implemented:

- In the MVZ1, the lack of space results in a room relocation in order to accommodate the Z1. The relocated room has been moved in a space free from the elimination of the SWBs in the MVZ2.
- The spaces dedicated to the most cumbersome electrical equipment remained the same in the MVZ2. The transformer, HV, and LV switchboard rooms have been exploited to accommodate all the elements. The LV switchboard room has been revised in order to include the dc/ac 440V converter, constituting a considerable footprint with its 8.4 m length as depicted in Figure 76.
- In the MVZ 3, the transformer/converter area of the aft engine room has been exploited as much as possible in order to easily place the bulky dc/ac 440V zone converter. The switchboard rooms present in the reference ship configuration have been merged in order to contain the main QP2 and the respective dc/dc zonal converters (Figure 77). Moreover, the LV main switchboard room has been kept free for any additional component accommodation.
- Finally, for the MVZ4 it has been decided to expand the aft switchboard room and to relocate the removed room in the previously depicted free space available in the MVZ3. This exchange results in no functionality reduction, but it allows to correctly arrange all the necessary components in the room, minimizing the cables length.

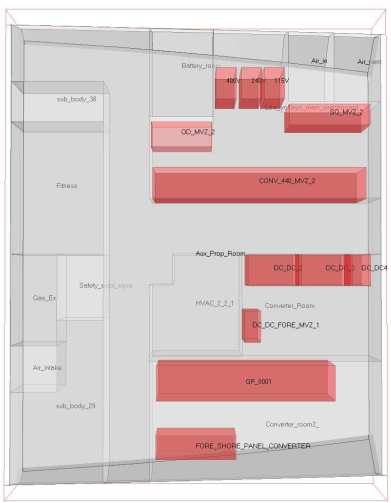

Figure 76 - New arrangement of the dc components for the MVZ 2

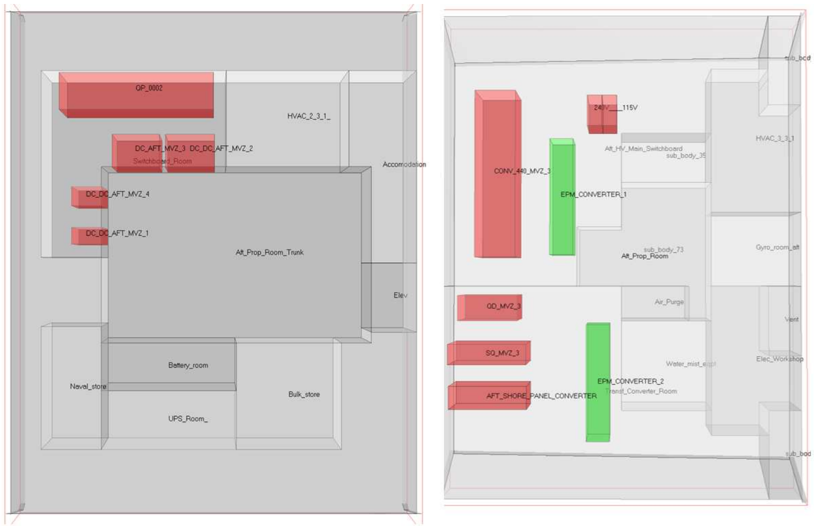

Figure 77 - For the MVZ 3, the new configuration of the switchboard room is shown in the left figure, while the right one shows the arrangement of the electrical equipments in the AM room aft

5.7 LVdc power systems comparative analysis

Starting from the conventional radial MVac power system layout, two new one line diagrams are provided in this chapter: the former redesign is endowed with a radial LVdc power system (Figure 66), the latter comes with a zonal LVdc distribution system (Figure 69). Moreover, a structure as similar as possible to the reference radial ac power system has been maintained for the former case. Conversely, the only constrain is the loads and power plants location for the latter case and thus enhancing the designers' freedom in the definition of new innovative proposals. In addition, the integration of a new pulsed load has been evaluated in the zonal LVdc distribution system aiming to replace the one previously installed.

The goal is, therefore, to evaluate the impact of the proposed solutions in terms of the overall power system weight and volume. In fact, the study of these values is of paramount importance in a ship, where the available space is always very limited, and the weight affects both the ship consumption (and therefore the vessel operating expenditure) and the dynamic performance of the ship itself.

Before the data could be compared, both the proposed innovative distribution systems have been integrated into the parametric model of the ship along with all the considered equipments. Through such model, all the components in the ship have been placed avoiding interferences with any other element already present onboard thanks to the careful evaluation of the ship's general arrangement plans.

However, the integration issues illustrated in the previous section arise from the choice to implement these innovative solutions as a refitting of an existing ship. Obviously, these difficulties would not have occurred if LVdc radial or zonal architecture had been adopted from the early stage design phase. Once all the components have been correctly placed inside the ship, the onboard power cable paths have been assessed and thus allowing to proper calculate their size and weight.

In this context, Table 11 shows the output data of the analysis carried out grouped by component category. The data are presented as a percentage of the reference ac shipboard power system comparing both the weight and the volume of the innovative distribution systems. Moreover, a bar chart representation of the same results is shown in Figure 78 and Figure 79 for the weight and the volume of the proposed LVdc distribution systems, respectively. The y-axis is given in the logarithmic scale.

Table 11 - Comparative analysis of different LVdc redesign proposed

Equipment	**Weight [%]**		**Volume [%]**	
	Radial dc	**Zonal dc**	**Radial dc**	**Zonal dc**
Cables	60.41	29.31	50.79	25.86
Switchboards	41.31	41.27	49.09	52.17
Transformers/Converters upstream SWB	92.61	72.75	114.69	74.11
Transformers/Converters downstream SWB	100.00	458.93	100.00	889.57
Main generators	57.14	57.14	40.17	40.17
SWB/new SWB			100.00	59.61
Total	66.47	63.95	78.82	86.78

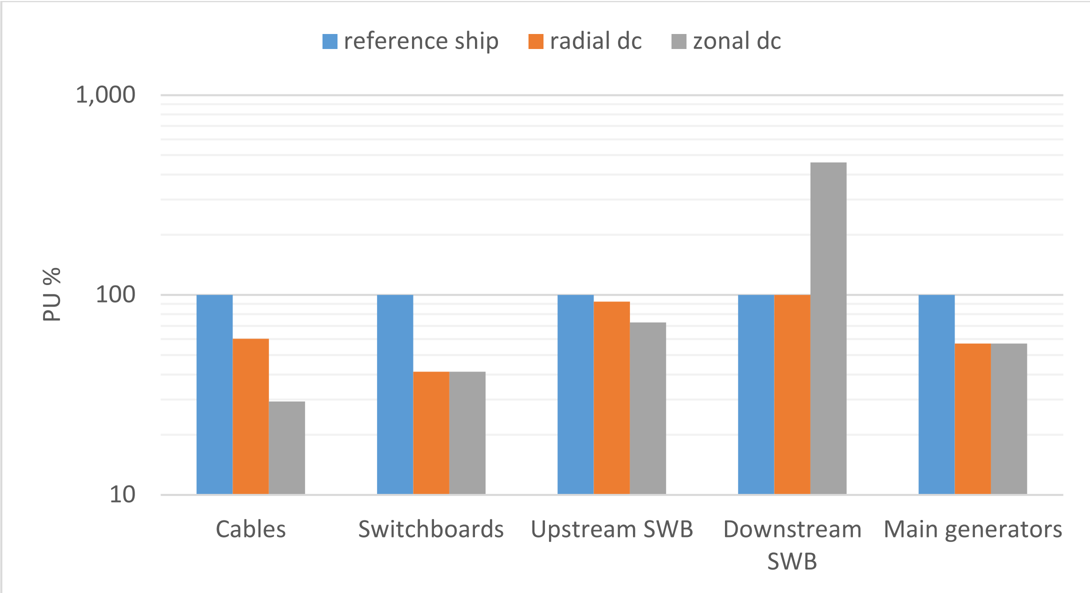

Figure 78 – LVdc power system weight comparison referred to the reference ship values grouped by sub-system (logarithmic scale)

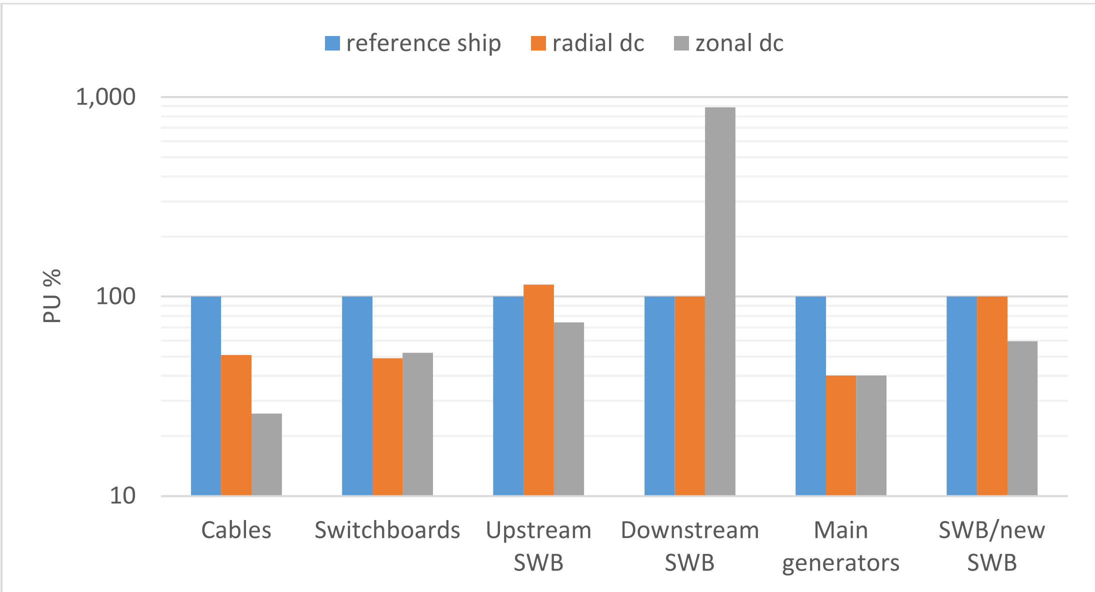

Figure 79 - LVdc power system volume comparison referred to the reference ship values grouped by sub-system (logarithmic scale)

Analyzing the above table, the replacement of MVac generators with new LVac ones results in considerable savings in terms of both weight and volume (see the redesign choice made in 5.4.1). Indeed, the exploitation of the distribution voltage level of 1 kV dc leads to new generators that are 43% lighter and 60% less bulky than the MVac ones.

Regarding the power cables, the solution that gives the greatest advantages is the LVdc zonal solution, although the radial dc one also leads to considerable improvements compared to the ac reference ship. These results derive from the considerations about the losses in a dc power system, as well as the exploitation of only two dc cables, unlike the three utilized in a three-phase ac power system. The large discard of the zonal LVdc network is in any case attributable to the considerable reduction in the number of connections between switchboards, since the SWBs have been removed and replaced with zone switchboards (see Figure 69).

Considering the zonal LVdc power system, in Table 11 it was necessary to modify the terms of comparison with respect to what has been done between the radial ac and the radial dc system. Removing the SWBs, in fact, a direct comparison between their weight and volume is impossible when the zonal case is considered. Consequently, the SWBs volume of the radial ac and dc cases has been compared with the new switchboards connected downstream of the dc/ac converters replacing them. These are called new SWBs for the sake of simplicity. The weight of such components cannot be compared with the reference ship SWBs since no data are available for them. Therefore, it was assumed that this value does not vary. This hypothesis is justified since the SWB loads have not been modified, and therefore neither the relative protection switches. As regards the Zs, on the other hand, these have been considered in the item "switchboards", and then compared with the QPs and QDs of the other solutions.

Analyzing the data shown in Table 11, the downstream converters of the zonal switchboards show a significant weight and volume increase compared to the radial solutions either ac or dc. Despite the removal of the LV/LV transformers present in the radial ac power system, this considerable weight increase is partly due to the choices made during the converters' sizing phase. Indeed, such converters have been sized to fully supply all the ac loads connected downstream, not knowing the quantity and location of any redundant loads on the SWBs. In the ac power system, the combination of loads that can be powered simultaneously has been evaluated directly by the designer of the onboard power system. Nevertheless, this information was not available, leading to a more conservative redesign for the zonal LVdc solution. In addition, more converters are needed with respect to a native dc power system. Indeed, to keep the downstream ac power system unchanged it not possible to optime the voltage level connection. With a view to a native dc power system project (zonal or not), greater advantages could therefore be obtained by arranging a direct connection to all the ship's loads. For instance, some loads already are endowed with a dc power (e.g., all the electronics equipment) and thus some conversion stages can be removed.

Finally, Table 11 also shows the overall data regarding the innovative distribution systems proposed in this chapter. Despite the significant weight increase due to the converters that replace the SWBS transformers, the LVdc zonal distribution is the lightest solution with a saving of 36.1% over the ac reference ship power system. This result derives above all from the weight reduction obtained from the decrease in the number of cable bundles, as well as from the different length of these deriving from a better arrangement of the new components onboard.

On the other hand, the less bulky solution is the radial LVdc distribution paying attention to the power system volume with a saving of 21.2% compared to the radial ac power system. The advantage that the zonal LVdc had in terms of weight is therefore lost due to the size of the large power converters installed downstream the Zs. The results obtained are also presented graphically in Figure 80 (Figure 81) depicting respectively the overall LVdc power system volume (weight) comparison referred to the reference ship values.

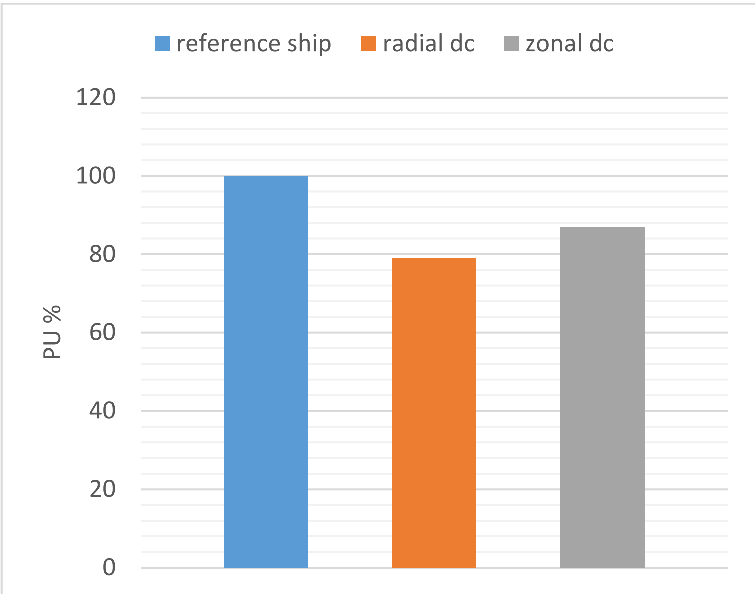

Figure 80 – Overall LVdc power system volume comparison referred to the reference ship values

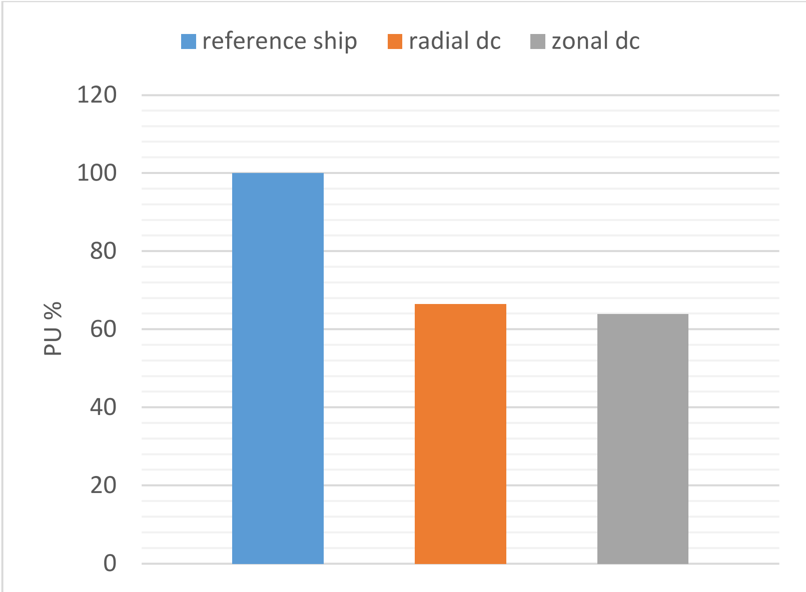

Figure 81 - Overall LVdc power system weight comparison referred to the reference ship values

5.7.1 Efficiency assessment

At the end of the volume/weight assessment, a brief consideration has been carried out regarding the performance of the electrical systems analyzed. Indeed, the introduction of new components but also the removal of others leads to the question of how the overall system efficiency varies in terms of power losses. Thus, the efficiency chain has been therefore considered for each solution presented in this redesign, starting from the main source of power (i.e., the DGs) up to the secondary switchboard loads, to calculate the overall efficiency. In the analysis, an efficiency of 0.99 and 0.98 has been chosen respectively for the power transformers and the power converters.

Therefore, an overall efficiency of 0.94 has been calculated for the zonal dc distribution system, following the path presented in Figure 82. Regarding the path from the DGs to the EPMs and the thruster, the efficiency is 0.96 since only two power converters stages are needed. The radial dc solution efficiency is just like the zonal dc distribution one regarding the path from the DGs to the EPMs and the thruster. Nevertheless, the radial dc power system efficiency is 0.95 considering the path depicted in Figure 82. The reference ship has thereby an efficiency higher than the two dc distribution system proposed in this thesis work concerning the power losses. Indeed, the efficiency of the path depicted in Figure 82 is 0.98 for the reference ship since there are only two conversion stages endowed with power transformers. On the other hand, the efficiency from DGs to EPMs is 0.97 referring to one-line diagram in Figure 63 while it is 0.99 from DGs to the azimuth thruster due to his DOL connection.

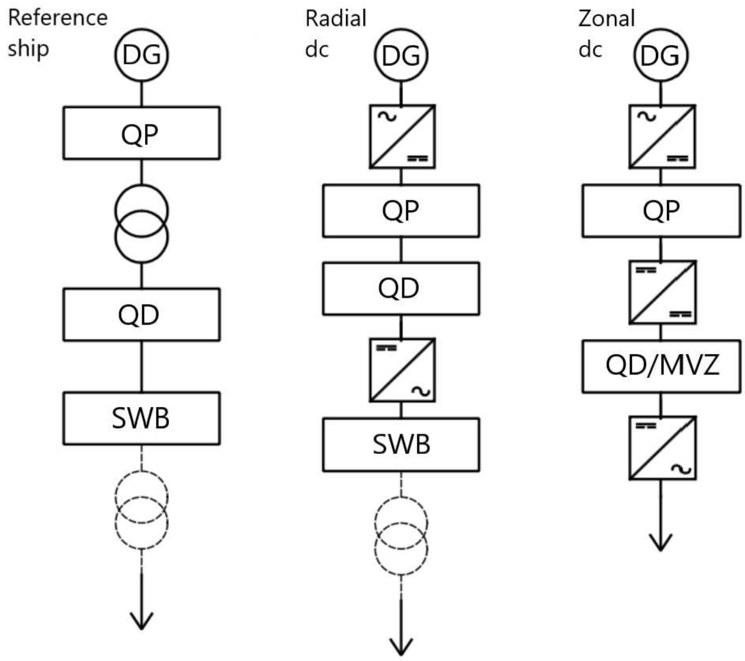

Figure 82 – Comparison between different distribution power system efficiency from the main source of power to the secondary switchboard loads

5.8 Conclusions

Finally, some considerations can be drawn from this chapter. The power system volumes and weights can be lowered adopting an innovative LVdc solution slightly worsening the power system efficiency. Moreover, the dc circuit breaker even small power losses have not been considered in such analysis and should be taken into account in further studies. However, the power cables weight and volume can be significantly reduced with proper design choices. Indeed, a higher voltage level permits to lower the power cable ampacity for the same power to be supplied and thus decreasing the power cable cross section. Moreover, a higher number of parallel cables is preferable to further reduce the cable bundle weight and volume, and for a better thermal management as demonstrated by the IPEC concept (see section 4.6). A higher number in parallel cables leads to the idea to carefully model the cable bundles in the cable trays as later described in the section 6.5.

It is clear that shipboard power distribution systems deal with a huge increase in power electronics devices. Their exploitation can enhance the ship power system capabilities and its reliability, but also adding disturbances caused by the power converters' switching frequency. Thus, the study of the high frequency disturbances propagation into a shipboard power system is not trivial, eventually leading to the need of a frequency-dependent models. Such issues will be addressed in the next chapter. However, the cable length assessment achieved through the CSI 3D modeling is paramount to correctly evaluate the high frequency disturbances propagation emphasizing the significance of work carried out in this chapter. Indeed, the combined exploitation of both CSI capabilities and software simulation can enhance the power system proof of concept definition.

6 High frequency disturbances propagation in the power system

6.1 Abstract

The innovative solutions proposed in the previous chapter can have a negative impact on the performance of the power system. For this reason, in this chapter, their impact on the onboard power system will be analyzed in order to prevent integration issues. Moreover, such analysis can have an impact in the definition of cable layout.

Specifically, the high frequency disturbances propagation will be assessed both in power cables and transformers though the development of suitable frequency dependent models. As later depicted, the cable length assessment will have a significant impact in the design of innovative shipboard power systems stressing the significance of work carried out in this thesis work. In addition, the model for foil-type transformers will be validated through experimental results emphasizing the need of a new approach to correct integrate shipboard power system equipment.

Finally, the cable bundles equivalent parameters will be assessed in the last sub-section of this chapter providing both a reliable inductance matrix reduction method and a Python code capable of obtaining the same results of finite element software. Referring to the proposed innovative approach in Figure 52, such step exploits the reliable information from the CSI software, depicted in the chapter 5, and thus allow to provide further benefits in the correct integration of the new devices.

6.2 Switching devices and harmonic content

Today's power electronic technologies improvements are leading to new design possibilities for electrical power systems as depicted through all this thesis work. As stated in the section 2.2, the power electronics converters are key enablers for the MVdc distribution systems [60]. In fact, power electronics converters are widely use in the notional shipboard power system with MVdc radial distribution shown in Figure 16.

Thus, the integration of full-controllable power converters in the ship power system enhances the 50/60 Hz system capabilities [111] or leads to harness dc power system sections [29], [64]. Given this scenario, the performance of the power system can be improved by leveraging power electronics, resulting in significant advantages already presented in the section 1.4:

- More functionalities can be implemented in the same component, resulting in a more compact power system design. Moreover, using static converters in place of electromechanical components can lead to a reduction in the equipment size as shown in the previous chapter.
- The widespread presence of power electronics devices can enable power flow management and current limiting in short circuit scenarios [62], [111].
- In Navy application, the integration of new sensors and weapon systems is easier, given the availability of a dc power supply [44], [45].

On the other hand, the switching frequency of the converters has an important impact on the system's power quality. Not only conventional issues like electromagnetic compatibility (EMC) issues, but also accelerated ageing of insulating systems can occur. In addition, an example of the harmonic induced heating in the machines is given in the IPEC analysis which has been carried out in the section 4.6.

To avoid this, passive or active harmonic filters can be used to enhance the shipboard power quality [112], but their design implies evaluating how the harmonic pollution affects the power system [93]. The study of the disturbance's propagation is complex, requiring both a deep understanding of the harmonic pollution sources behavior and an evaluation on their mutual interaction. Actually, the IEEE Std 519-2014 [113] sets an upper limit to the harmonics produced by a converter up to the 50^{th} one (i.e. 3 kHz in a 60 Hz system), which is only a subset of the possible harmonics injected into the system. Such a limit provides that the harmonics with a significant energy level are contained, thus avoiding both the excessive heating in the system components and the deformation of voltage waveform.

Conversely, for EMC studies the addressed frequencies are higher (more than 20 kHz), but the considered energy is lower. In this latter case, the aim is to assure the limitation in the interferences induced in other components. While a separated approach (low frequency analysis for a set of issues, and high frequency analysis for another) was feasible in the past, it is rapidly becoming untrustworthy due to the advancements in modern power electronics components. As an example, Pulse Width Modulation (PWM) converters not only inject disturbances due to their carrier wave (up to 10 kHz), but higher frequency disturbances (up to some MHz) due to the switching process of each single static component. Thereby, in an integrated power and energy system it is now possible to have high frequency disturbances injection with a significant energy level, thus leading to possibly harmful consequences for the system.

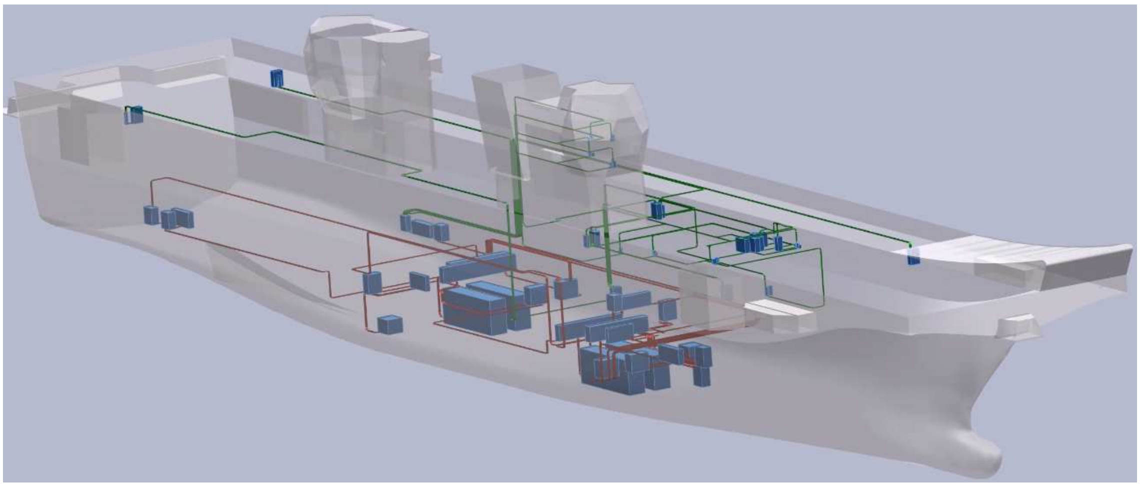

Figure 83 - 3D parametric model of IT Navy vessel highlighting the distribution system cableways [114]

An example of the possible issues related to such disturbances propagation is the significant increase in the failure rate of interface transformers, related to the introduction of modern high efficiency propulsion converters (with power electronics switches presenting lower turn on times in respect to the past ones) in shipboard power systems [115]. Such an issue will be addressed in detail later in the section 6.4. This highlights the presence of a damaging phenomenon related to high frequency disturbances propagation in power systems, currently not sufficiently addressed by actual power system design. Thus, a deeper analysis of the topic is needed, to assess the relationship among the high frequency disturbances and its effects on the power system.

The variation in system's parameters (resistances, conductances, capacitances, and inductances) at different frequencies is one of the first problems in a system affected by harmonic disturbances. In fact, when analyzing the system behavior over a wide frequency bandwidth, the conventional fixed parameters modeling becomes inapplicable. In literature many models can be found, each presenting a different approach to study the frequency-dependent phenomena [116]–[124]. However, most of them are focused on the analysis of a single component (mostly cables) or an end-to-end system. Conversely, there are some papers trying to approach the study of disturbances propagation in a complex shipboard system [57], [58], [125]–[128].

Another relevant issue to be considered is the dependence of the cable parameters on its surroundings. Indeed, it is well known that the parameters of a power cable depend on the ambient temperature, the presence of other cables nearby, the laying conditions, and so on. Moreover, each single cable can present several different boundary conditions along its entire length, due to its passage into several ship spaces. Therefore, this effect also needs to be correctly evaluated.

Given all these premises, the switching performance of the power electronic components must be considered in order to evaluate the amount of high frequency disturbances injection into complex electrical power systems. It is well known that the Laplace transformation of a step function in time results in a frequency function that spreads over all the frequencies. However, the market available components have are not ideal ones, thus presenting turn on and turn off times that affect the frequency spectrum, depending on the component technology.

A simplified model of the component turn on/off switching process can be made by means of a saturated ramp function. Such a function can then be analyzed by means of Laplace transform, allowing to evaluate the disturbances injected by a device's switch process. To better appreciate the effect, some existing power electronic switches have been analyzed. Their data are reported in Table 12, along with their features in terms of maximum voltage and maximum current allowable, turn on time, and turn off time. As depicted in Table 12, the turn on time (t_{on}) is lower compared to the turn off one (t_{off}) and therefore the former results in a higher harmonic content produced by the switch. Moreover, an exhaustive literature review regarding the power converters application in shipboard power system can be found in [129].

Table 12 - Market available power electronics switches

Device	**Max voltage (V)**	**Max current (A)**	**ton (ns)**	**toff (ns)**
SCR	8500	4240	500	530000
GTO	4500	2800	5000	3000
IEGT	4500	2600	700	2300
IGBT	6500	1000	160	500
MOSFET 1	100	209	110	120
MOSFET 2	900	23	20	25

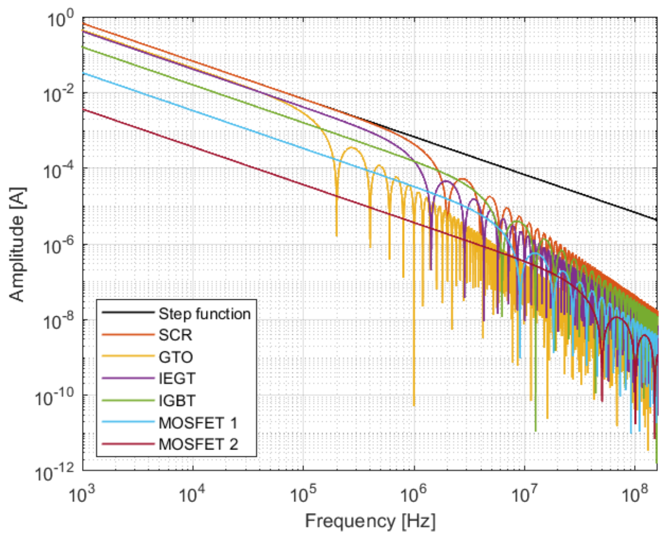

Figure 84 - Frequency spectrum of the switch on process [33]

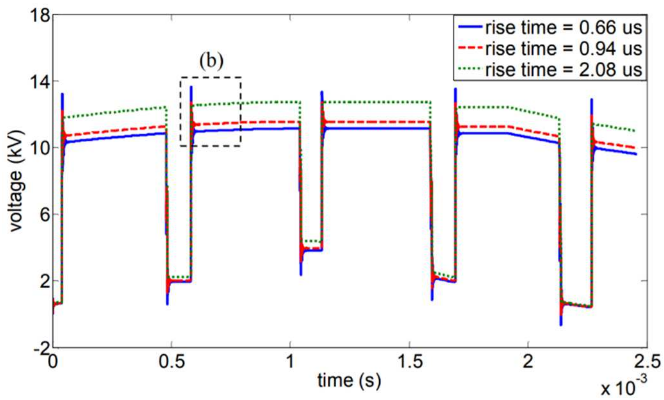

Figure 85 - Effect of the commutations of a PWM converter on the voltage at the transformer terminals [115]

Thus, the t_{on} value defines the worst case regarding the harmonic content spectrum. Given all these premises, equation (1) depicts the time-dependent turn on behavior of a single switch, while the relative Laplace transform is reported in (2).

$$R(X_f, t_{on}, t) = \frac{X_f}{t_{on}}[ramp(t) - ramp(t - t_{on})] \quad (1)$$

$$\mathcal{L}[\,R(X_f, t_{on}, t)\,] = \frac{X_f}{t_{on}} \frac{1 - e^{-s \cdot t_{on}}}{s^2} \quad (2)$$

where R is a function representing either a current or a voltage signal, X_f is the final value of the considered signal, t_{on} is the time needed to reach the final value, t is the time, $\mathcal{L}$ indicates the Laplace transform and s is the complex frequency operator.

By means of Eq. (2), the frequency spectrum of the switch on current transient can be obtained for each device reported in Table 12 (depicted in Figure 84). In particular, the saturated ramp slope has been determined through the rise time t_{on} and the maximum current value. The ideal step function spectrum is depicted in black in Figure 84, as a reference value. As can be seen, it contains all the spectrum components, from zero to hundreds MHz, with a decreasing amplitude. It can be also noticed that no differences in the frequency spectrum slopes are appreciable before 100 kHz, apart from their different gain (which is related to their maximum current capability). However, significant differences occur above that value. Among all the market available components, the "SCR" (in red in Figure 84) has the greatest amplitude in the high frequency spectrum, even if it presents a higher t_{on} in comparison to the "MOSFET 2" (in magenta in Figure 84). Thus, it can be concluded that the devices turn on process will surely excite an oscillation mode of the system, due to the wide frequency spread of the produced disturbances. An example can be made by considering Figure 85, where the effect of the commutations of a PWM converter on the voltage at the terminals of a transformer is given [115]. The voltage spikes resulting from the excitation of oscillating modes in the system are evident. Finally, also the device switching frequency is a parameter that must be considered. In fact, higher the switching frequency is, higher are the disturbances that are injected into the system each second. Obviously, such a simple analysis is useful for stating the possible presence of an issue, but it is not enough for providing an evaluation method.

6.2.1 Harmful consequences on the electrical insulation system

Given the rising number of power converters installed onboard, new approaches in the definition of the electrical equipment have been developed by the standards. The old approach is depicted in the block diagram in Figure 86, while the new one is given in Figure 87. The former approach does not require any additional information about the output voltage ripple of the inverter to be installed. In such scenario, the system integrator (the installer) have not to consider the stress levels associated with the converter-fed operation. However, the IEC 60034-18-41 [130] defines the stress categories as reported in Table 13. Four different stress categories levels have been identified for Type I machine insulation system.

A new approach is required due to the high number of power electronics converters: the installer informs the machine manufacturer about the voltages that will appear at the terminals to select the correct stress category, as illustrated in Figure 87.

Table 13 - Stress Categories Type I (only) [131]

Stress category	Overshoot factor (OF) U_p/U_{dc}	Impulse risetime t_r (µs)
A – Benign	OF $\leq$ 1,1	0,2 ± 0,1
B – Moderate	1,1 < OF $\leq$ 1,5	
C - Severe	1,5 < OF $\leq$ 2,0	
D - Extreme	2,0 < OF $\leq$ 2,5	

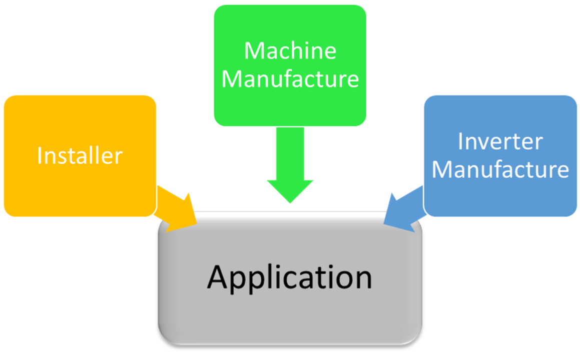

Figure 86 – Old approach in the power system integration

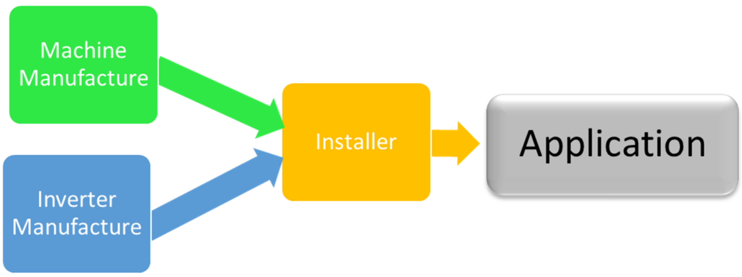

Figure 87 – New approach required due to the high number of power electronics converters

Thus, in the future the system integrator have to specify the voltage stress type as it appears at the terminals of the machine, for instance, taking into account the system configuration. Then, the machine manufacture will specify that the selected machine is classified according to the assessed stress category. In this context, the ship power system configuration can be affected by undesired issue that can arise from the cable layout and paths, electromagnetic interferences, and high frequency disturbances propagation. Therefore, the latter phenomenon will be carefully evaluated in order to give a comprehensive approach to the correct power system definition since the early stage design phase.

Manufacturers typically assign a rated voltage to a machine based on power system rated frequency. This assumes that voltage from the power supply is 50 or 60 Hz sinusoidal. In the case of electrical machines fed by converters, the conventional definition of voltage rating is no longer applicable, although the manufacturer may still assign a rated voltage for 50/60 Hz operation, putting it on the rating plate of the machine. In case of machines fed by power converters, a change in the nameplate is required in order to correctly take into account the values depicted in Table 13. The procedure is to apply the words "IRV X", where IRV means Impulse Rated Voltage and X defines the stress category level that the machine can withstand. For example, if the machine has been rated for 500 V sine-wave duty and moderate impulse duty, the rating plate will show 500 volts and IRV 2. Appearing IRV 2 on the nameplate, the use of this machine in stress category 3 or 4 is not allowed.

6.3 High frequency disturbances propagation in power cables

6.3.1 Frequency dependent parameters models

The disturbances propagation in a complex power system is affected by the physical elements that are encountered in its path (i.e., the cables, the converters, the transformers). Since the goal of this chapter is to better understand the high frequency disturbances propagation in complex distribution systems, the literature review analysis is focused on the frequency-dependent models and studies.

Many papers highlight the problem of harmonic pollution. They mainly refer to end-to-end case studies, such the transmission line systems [116]–[124]. They apply a well- known approach, based on the transmission line equations that are derived from the study of two closely spaced cables in unitary length distributed model (i.e., the RLCG cell depicted in Figure 88). The basic model requires as input parameters the series impedance Z, and the shunt admittance Y. These two parameters allows to model the behavior of the cable conductive materials and insulating materials, respectively. The two parameters have the following form:

$$Z(f) = R(f) + j2\pi f L(f) \tag{3}$$

$$Y(f) = G(f) + j2\pi f C(f) \tag{4}$$

where R (Ω/m) is the series resistance, L (H/m) is the series inductance, G (S/m) is the shunt conductance, and C (F/m) is the shunt capacitance of the cable system. All the elements of equations (3) and (4) are functions of frequency f (Hz) and can be evaluated as shown in Table 14.

Table 14 - Basic parameters of transmission lines

	Lecher wire	**Coaxial cable**
Arrangement	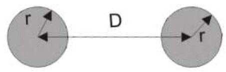	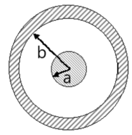
Capacitance	$C \approx \frac{\pi\varepsilon}{\ln\left(\frac{D}{r}\right)}$	$C \approx \frac{2\pi\varepsilon}{\ln\left(\frac{b}{a}\right)}$
Self-inductance	$L \approx \frac{\mu}{\pi}\, ln\left(\frac{D}{r}\right)$	$L \approx \frac{\mu}{2\pi}\, ln\left(\frac{b}{a}\right)$

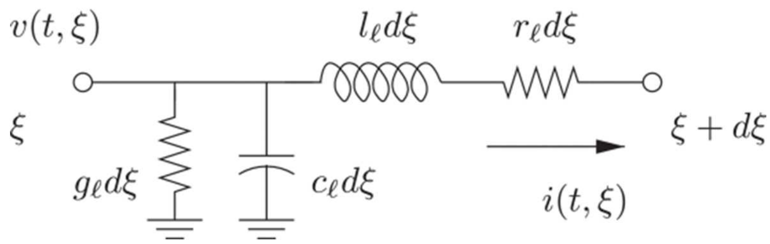

Figure 88 – Transmission RLCG line section of length dξ

The formulae are given for two different geometries: two unshielded infinite parallel cables, and two coaxial conductors with an insulating material between them. In the equations of Table 14, $\boldsymbol{\pi}$ is the conductor permeability; $\boldsymbol{\varepsilon}$ is the mean permittivity of the insulating material between the two conductors; D is the distance between the two cables of radius r in the first arrangement; a is the inner conductor radius; and b is the dielectric external radius in the second arrangement.

For studying a real power system, the simple formulae of Table 14 need to be evaluated considering two aspects: the cable layout and its insulating material properties. This can be done with several approaches, like EMTP-type programs [119], [120], finite element simulations (FEM) [132], [133], genetic algorithms [134], and by using experimental measurements [116], [134], [135]. In particular, in [117] the Universal Line Model (ULM) is proposed. Such a model is currently implemented in many EMTP-type programs, thus being used in most of the studies about these topics. In [134] the effects of frequency in cable modeling are stated and a comparison between different models behavior is carried out.

6.3.1.1 Frequency-dependent phenomena in RLCG parameters

The first frequency dependent phenomena is the well-known and well-studied skin effect. The most affected parameter is the series resistance, whose value increases with frequency [122], [136]. Such phenomenon has been addressed also in the section 4.6.2 to evaluate the effect over the power cable Joule losses [105]. Additionally, the skin effect influences the series inductance, as stated by [137]. The proximity effect is another phenomenon that influences both the R and L parameters [138]. Regarding the G and C, their dependency on frequency can be assessed through the complex permittivity concept [135]. The real part of the complex permittivity is related to the shunt capacitance value, while its complex part is referred to the shunt conductance. Therefore, different insulating materials and technologies lead to different values of the complex permittivity. Nowadays, the XLPE insulating technologies is taking over in ship applications, motivating the several studies carried out on its detailed modeling [121], [133]. In [132] a Vector Fitting (VF) method is provided to approximate the frequency behavior of a three-phase armored cable. Then, a sixth-order electrical network is derived from the resulting rational function. While being able to provide accurate results, such a method is not applicable for analyzing all the cables in a complex shipboard power system since it is fitted for a single specific cable geometry and layout.

6.3.1.2 Cable layout and shielding

Both the cable geometries and the distance between different cables are another paramount importance aspects to be considered. Several studies analyzing different geometries can be found in literature, and a detailed mathematical analysis is reported in [139]. In [133] the frequency-dependent RLCG parameters have been studied in presence of small geometric variations, in order to improve diagnostic evaluations. In [140] a configuration up to twelve underground cables is studied in detail, providing a representation of the modal propagation function contribution in the phase domain.

The study of the cable shield bonding is also not trivial according to [124], but it is not a real problem in an onboard power system. Indeed, in shipboard power system the maximum length of a cable can reach at most a hundred of meters, thereby making the cable shield bonding not required. Nevertheless, the presence of the shield should not be underestimated, affecting the cable frequency-dependent model, as highlighted in [117], [118], [120].

6.3.1.3 Disturbances propagation in ship power system

Regarding shipboard power system modeling, [127] presents a detailed model of electric ship propulsion system, built to evaluate the transient overvoltage during system's energization. Furthermore, [125] investigates the common-mode currents in the hull of an electric ship through scattering parameters, while [58] proposes a scalable method to model common-mode voltage and current in a complex IPES. In [57] a common-mode equivalent model for a two-zone MVdc ship power system is given. Finally, [128] evaluates the impact of switching frequency in MVdc microgrids through common-mode model too. Nonetheless, fixed parameters (not variable with frequency) are used in all these shipboard power system models, and most of them address common-mode system behavior. Conversely, this chapter focuses on a differential-mode model, given the disturbances in study.

6.3.1.4 Signals propagation in communication systems

Considering communication systems, the issue of high frequency signals propagation in complex systems is well known. Indeed, [136] deals with the performance of modems over a power line network, by using the two-port network representation. Hence, the transmission line equations should be introduced in order to deeper understand the signal propagation over a RLCG cell (Figure 88). Given (3) and (4), it is easy to determine the characteristic impedance Z_C and the propagation constant γ of a cable as:

$$Z_C(f) = \sqrt{\frac{Z(f)}{Y(f)}} \tag{5}$$

$$\gamma(f) = \sqrt{Z(f)\,Y(f)} \tag{6}$$

Therefore, (5) and (6) are useful to calculate the ABCD matrix to obtain the transfer function of two cables transmission line. The ABCD matrix can be used to put into relation the input voltage and current (V_1, I_1) and the output ones (V_2, I_2) in a general two-port network:

$$\begin{bmatrix} V_1 \\ I_1 \end{bmatrix} = \begin{bmatrix} A & B \\ C & D \end{bmatrix} \begin{bmatrix} V_2 \\ I_2 \end{bmatrix} \tag{7}$$

The A, B, C and D constants are determined by the solution of the RLGC model differential equations. The final result (8) depends on the cable propagation constant γ, the cable length l, and the cable characteristic impedance Z_C:

$$\begin{bmatrix} A & B \\ C & D \end{bmatrix} = \begin{bmatrix} \cosh(\gamma l) & Z_C \sinh(\gamma l) \\ \frac{1}{Z_C} \sinh(\gamma l) & \cosh(\gamma l) \end{bmatrix} \tag{8}$$

In [136] the chain matrix theory is used to model an entire power line system. In fact, the ABCD representation of the two-port circuits in cascade is the product of the single two-port circuit matrices. Such an approach is used to measure the performance of complex power line system analyzing the cables frequency response in the 1-30 MHz band. While [136] still uses fixed-frequency parameters, the chain matrix approach seems to be a useful mean to approach the issue of cable different boundary conditions along its entire length.

6.3.1.5 Final Comments

In this brief review, several frequency-dependent cable models have been depicted. Each model tries to assess how cable frequency-dependent parameters are affected by different phenomena: skin effect, proximity effect, cable shield bonding, complex permittivity variations, geometry, and layout. Moreover, a possible approach to the study of the propagation of high frequency disturbances in power systems is given in [136], constituting a possible base on which proceeding with the studies. Regarding complex power systems, in literature the analysis of shipboard power system has always been done by using fixed parameters' models. In addition, several papers focus on the power system common-mode harmonic disturbances propagation, while the issue in study is related to differential-mode models. Finally, methodological approaches to the complex system modeling are not provided.

6.3.2 Proposed approach for the shipboard power system modeling

As aforementioned, the dependence of the parameters over the frequency can significantly affect the results. Most of the above modeling approaches are based on parameters that are calculated at a single frequency, thereby making impossible to correctly evaluate the disturbance propagation when a high frequency spectrum disturbance is present (see Figure 84).

To this aim, an investigation about the differences among fixed-parameters models and variable frequency parameters ones is needed. The approach here applied is to define an eased frequency-dependent model, and then compare its outcomes with some commonly used models. The goal is to find if it is possible to use a simplified model without introducing excessive approximations in the results. The simplified model will then be useful in order to ease the overall system evaluation of the high frequency disturbances propagation in complex integrated power systems.

In order to study the frequency disturbances propagation, the knowledge of the real system is needed (cable RLCG parameters). In particular, it is paramount to determine the cableways paths through the entire ship. For this purpose, three-dimensional parametric modeling (e.g., Figure 62 and Figure 83) is important in order to correctly identify and subsequently model the interferences that can occur in the onboard power system.

The model reported in Figure 88 is analyzed through the already presented ABCD matrix approach in order to evaluate the difference between fixed parameters model compared to frequency-dependent one. In [114] such analysis has been carried out exploiting a Laplace domain function, but with poor results. To make it possible to compare the modeling results, a 20 meters copper cable insulated in cross-linked polyethylene (XLPE) is used as a case study. Such a cable has been chosen among the reference ship power system cables and, in particular, the MV cable has been utilized in the ABCD matrix approach evaluation. The geometry and the electrical specification of all the reference ship power system cables are reported in Table 15. Moreover, these data have been utilized both in the section 6.5 and in the chapter 7.

Table 15 - Reference ship power system cable dimensions

Cable type	A	B	C	D
Voltage [kV]	6/10	0.6/1	0.6/1	0.6/1
Conductor Diameter [mm]	11.5	14.3	18.1	20.4
Insulation Thickness [mm]	3.4	1.2	1.6	1.7
Outer Diameter [mm]	26.9	22.5	27.5	31.0
Net Cross Section [$\mathbf{mm^2}$]	70	120	185	240
Datasheet Admittance (60 Hz) [Ω/km]	0.142	0.109	0.105	0.106
Datasheet Resistance (20°C) [Ω/km]	0.270	0.153	0.0991	0.0754
Calculated Resistivity (20°C) [$\mathbf{\Omega \cdot mm^2/km}$]	0.0189	0.01836	0.01833	0.01809
Relative permeability	1			
Relative permittivity	2.3			
Dissipation factor	0.002			

The Table 14 formulae for the coaxial cable geometry have been used to evaluate the RLCG parameters, due to the case study cable physical structure. Thus, three different cases have been assessed:

- Case A: cable parameters are calculated at their dc value.
- Case B: cable parameters are frequency-dependent. Resistance R(f) and self-inductance L(f) are calculated considering the skin effect, while capacitance C(f) and conductance G(f) are dependent on the relative permittivity variation with frequency ε(f).
- Case C: cable parameters are calculated at their resonance frequency value (detected in the Case B).

Equation (8) is therefore been used to assess the frequency-dependent trend of the *A*, *B*, and *C* values of the presented 20 meters MV cable. The *D* value trend is not shown here because it is equal to A, given the ABCD matrix symmetry. The trend of the A, B, and C is depicted in Figure 89, Figure 90, and Figure 91 respectively, in the three considered cases.

By comparing the figures, it is clear that the Case C cannot be used in place of Case B when modeling a cable with frequency-dependent parameters. Moreover, the ABCD approach present the same trend up to tens of kHz frequency range, in both the Case A and the Case B. Instead, Case C is completely wrong in all the three cases. Thus, Figure 89, Figure 90, and Figure 91 demonstrate that a fixed-frequency parameter model is not suitable for the evaluation of the high frequency disturbances propagation in a complex shipboard power system.

Moreover, the proposed approach leads to similar results for Case A and Case B up to 10^5 Hz and thus when considering low frequency behavior. Therefore, the conventional modeling approach can be useful for conventional studies, but it is unsuitable for the high frequency disturbances propagation assessment. In addition, it allows using the chain matrix theory, making it possible to build the model of a complex onboard power system by means of single ABCD matrices combinations or embedded in a power system simulator as the one later presented in the chapter 7.

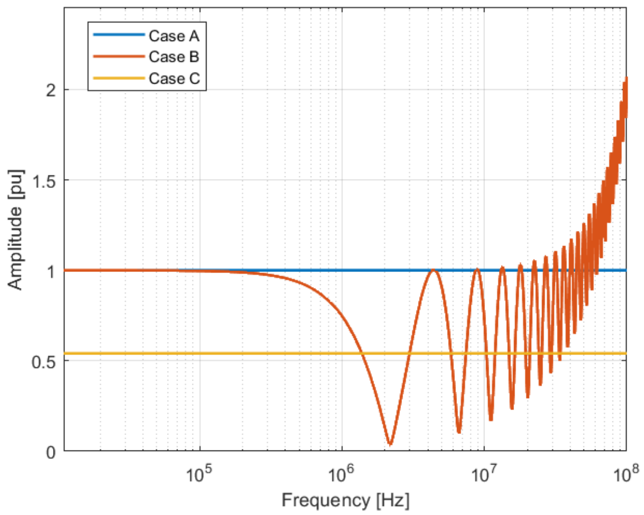

Figure 89 – A (or D) value frequency-dependent magnitude trend

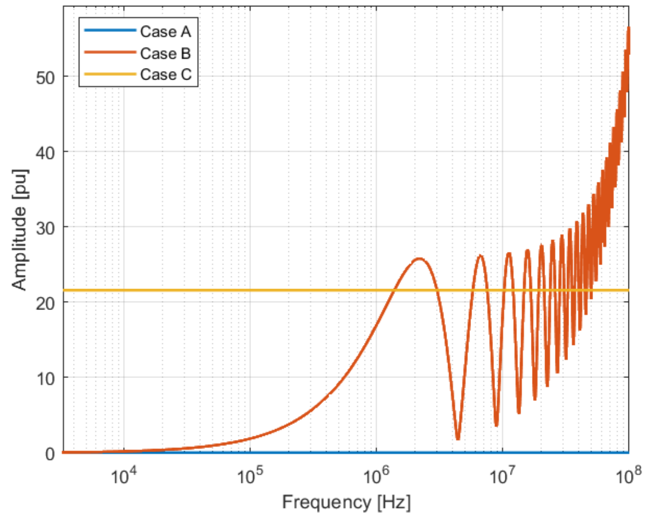

Figure 90 - B value frequency-dependent magnitude trend

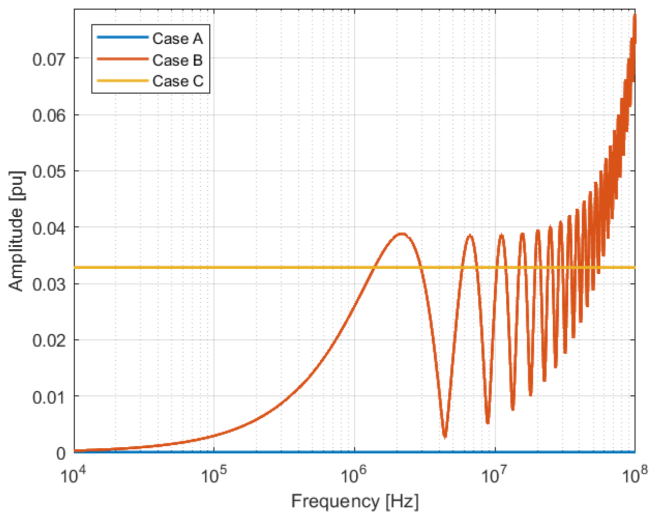

Figure 91 - C value frequency-dependent magnitude trend

6.3.3 The cable length impact

The cable length assessment (point O in Figure 38) is one of the most important information in order to perform harmonic pollution analyses [33], [98]. Indeed, higher the signal's frequency higher the impact of the cable length on the possible arise of undesired resonances in the power cables according to the travelling waves model as shown above. Thus, there is a need to anticipate all the possible information regarding the power system design in previous stages in order to better evaluate the innovative power system performance. Therefore, these new devices cannot be integrated as a mere refitting in the existing ship power systems but shall be integrated in a better and rational manner.

Luckily, the parametric 3D ship model contains detailed data about the ship power system equipment including cables layout and their onboard paths. Thus, the power cable length can be assessed relying on real scale software models. The cable length assessment is paramount in dc power systems since it affect the power system short circuit behavior as stated by [141], [142]. For instance, the current derivative value depends on the cable length, line loading, and fault impedance.

Nevertheless, the ABCD matrix values dependency on cable length has been assessed assuming the actual cable path is unknown. The A-value magnitude trend has been evaluated for different cable lengths range from 10 to 100 meters in the Case B scenario, as illustrated in Figure 92. Furthermore, the cable electrical properties and geometry are the same previous reported in Table 15 for cable type A. This simulation has been carried out in order to prove the great impact of the cable length on the cable parameters variation. In fact, when the cable length increase the amplitude of the A-value frequency-dependent magnitude rapidly rise for lower frequencies. However, the A-value is the V_1/V_2 ratio in a no load scenario (I_2=0) and it means that A-values close to zero lead to overvoltage for the same input voltage V_1. In particular, dangerous A-values magnitude can be reached by the 50 to 100 meters cables in the range from 10^5 to 10^6 Hz. These frequencies can be produced by power electronics devices as stated in the section 6.2.

Moreover, the A-value magnitude trend has been assessed not only for the cable type A, but also for the others three cable type illustrated in Table 15. Thus, the output values of such analysis have been depicted in Table 16 where the minimum A-value magnitude value is shown for each cable type along with the respective frequency occurrence. Mainly two considerations can be highlighted in the above mentioned table. The former is that the frequency, where the minimum A-value magnitude occurs, does not depend on the cable type considered. Regarding equation (8), this means that the cable propagation constant $\boldsymbol{\gamma}$ is not affected by the cable geometry changes and thus A-value magnitude varies with cable length only. The latter, instead, is that the cable length is inversely proportional to the frequency at which the minimum point is located. Indeed, higher the cable length magnitude lower such frequency value.

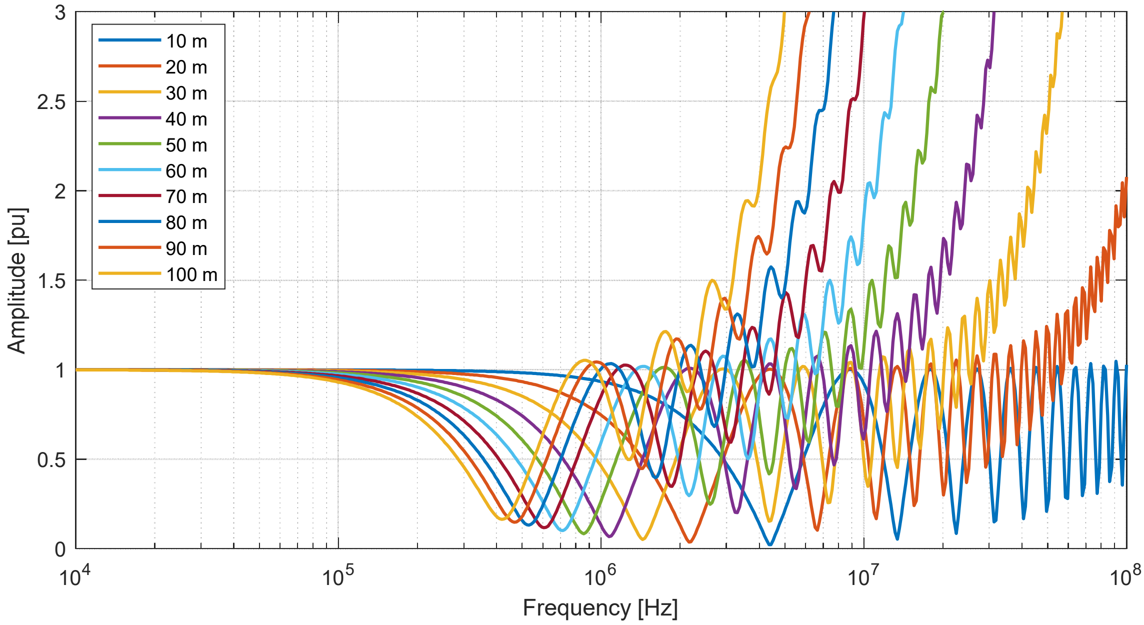

Figure 92 - A-value frequency-dependent magnitude trend for different cable length

Table 16 - ABCD matrix A-value magnitude trend for different cable types

Length [m]	**Frequency [Hz]**	**Cable type**			
		A	**B**	**C**	**D**
10	4.35E+06	0.023073668	0.022667999	0.022627	0.022661
20	2.16E+06	0.036871294	0.037686071	0.037159	0.036842
30	1.44E+06	0.051750205	0.053954579	0.052928	0.052231
40	1.07E+06	0.068381757	0.070627987	0.069541	0.068813
50	8.59E+05	0.084362478	0.087610341	0.086167	0.085167
60	7.14E+05	0.100614354	0.104303817	0.102683	0.101555
70	6.05E+05	0.116687103	0.11987238	0.118375	0.117356
80	5.32E+05	0.132577449	0.136759416	0.134913	0.133629
90	4.67E+05	0.148341236	0.152127032	0.150375	0.149174
100	4.18E+05	0.164111304	0.168035336	0.166209	0.16496

Resuming, the study of the propagation of high frequency disturbances in shipboard power systems is becoming an issue, given the rising number of onboard static converters. The wide frequency spread of the disturbances injected into the system by modern power electronics is making it necessary to rely on frequency dependent models, in place of conventional models with parameters evaluated at a fixed frequency. The development of a trustworthy modeling approach (refer to section 4.4) is useful for identifying specific system weaknesses, related to the disturbances propagation. Particular attention must be paid to the correct system definition, and subsequently to the frequency-dependent parameters calculations, as highlighted in this subsection. Cable length and path must be also known with a good accuracy, in order to properly calculate the system parameters. Thus, the use of 3D parametric software is paramount to study the shipboard power system frequency-dependent model and thus highlighting the need of new methods and tools to correctly deal with innovative solutions. In this subsection, it has been shown that the fixed parameters approach fails at frequencies higher than 10^5 Hz.

6.4 High frequency disturbances propagation in power transformers

6.4.1 Transformer technologies onboard

Nowadays, shipboard power distribution systems deal with an increase in number and power of static converters [143]. On one hand power electronics bring several important advantages in the integrated power system, ranging from reduced sizes of power management and frequency conversion devices through solid state transformers [144], to increased power system controllability [99]. Furthermore, power electronic devices allow to embed dc power system sections in the onboard power system, better exploiting new power sources (e.g. batteries and fuel cells) or ensuring better performance to a specific section of the power system [145].

On the other hand, static converters are known to introduce disturbances in the system in a vast range of frequencies, not only because of the switching frequency but also because the fast raise/fall time, as previously depicted in 6.2. Moreover, the use of passive filters is preferably avoided onboard due to their overall dimensions and weight. Therefore, with a view to define a methodology to handle the whole IPES of the ship, beside power management, the effects of frequency disturbances propagation are proving to be not negligible in such a complex system. In order to cope with the frequency disturbances, a systematic study on the system components and their connections is necessary. Indeed, high frequency disturbances can have undesirable effect on the power system performance: they accelerate components thermal and electrical ageing [32], they deteriorate the system power quality [146], and they may cause resonances and dissymmetry [114]. The common models, based on low frequency (or even dc) parameters can be unsuitable for the task, leading to the need of frequency dependent modeling approaches.

In the case of high power applications, the transformers and electronic power converters are frequently coupled, separated by the short distances induced by shipboard environment. Fast transitions due to the switching of solid state devices are injected within the transformer windings and unexpected resonances can thereby arise also in the transformer, thus leading to undesired overvoltage and faults caused by travelling waves reflections.

In shipboard applications, oil cooled transformers are replaced by dry-type transformers since the former are meant to work in vertical position, which cannot be granted onboard, and the presence of oil itself is avoided for environmental risks, fire risk and maintenance issues. dry-type transformers on the other hand do not present these disadvantages but they require a more effective cooling system. Two main technologies are used in dry transformers: VPI and Cast-Resin. The latter is more compact, but the heat transmission is reduced due to the presence of the encapsulation resin. The selection among the two technologies is related to the rated power and the efficiency of the cooling system.

Primary and secondary windings of dry transformers can be realized using foils or rectangular conductors or both. The manufacturing of a foil coil results much faster and easier than any other type of winding, therefore significantly cheaper. Typically, a thin foil of copper or aluminum, covered with a foil of Nomex or Nomex+Mylar, is wrapped around a support in a number of turns according to the design specifications (Figure 93 shows an example of a winding manufacturing).

Depending on the applications, transformers can be realized with one or two secondary sides with a specified phase shift (e.g., the propulsion system of large cruisers requires to produce multiple three-phase systems with different phase shift to supply 6 or 12 pulse rectifiers to reduce the harmonic distortion). The study of high frequency disturbance effects should not neglect to consider the presence of multiple windings on the same column and the transmission of signals between different windings, even if a shield is interposed. In order to reduce the complexity of the investigation, a two foil-winding transformer is considered here. This type of winding is characterized by high capacities between subsequent turns since the turn surface can be of the order of the square meter and the dielectric thickness of the order of a tenth of a millimeter.

6.4.2 Model for foil-type transformers

The models usually used for power transformers are generally conceived to study their input-output characteristics at the working frequency of 50 or 60 Hz. Originally, studies of higher frequencies behavior inside the power transformers were limited to lightning-induced overvoltage. Nowadays fast voltage transients are known to occur both in the operation of circuit breakers and the switching of electronic converters, which involve frequencies in higher ranges than lightning.

The study of internal voltage distributions can be done by building a model with a high number of concentrated parameter elements or by applying a continuous model, using distributed parameter models. Distributed parameter models rely on the solution of differential equations, which remain consistent as the frequency gets higher. Among distributed parameter models, the Multiconductor Transmission Line (MTL) model can be easily exploited to study the signal propagation in a transformer. MTL models have been developed in the field of telecommunications to study the so called "cross-talk" phenomenon, which is caused by the capacitive-inductive coupling among conductors. The effect is that a signal injected in one conductor propagates to nearby conductors too.

While a complete explanation of the system construction is out of the scope of this thesis, a general description of the complete MTL model and of how it is used to describe a transformer is useful to understand its potential and limits. The general MTL consists of n parallel conductors, each having a certain amount of resistive, inductive, and capacitive coupling with all others. In our case each line of the MTL represents a single turn of the transformer. Because there are n conductors, the resistive, inductive and capacitive parameters are represented by $n \times n$ matrices (built as described in [139]). These matrices will be referred as R, L, C and G.

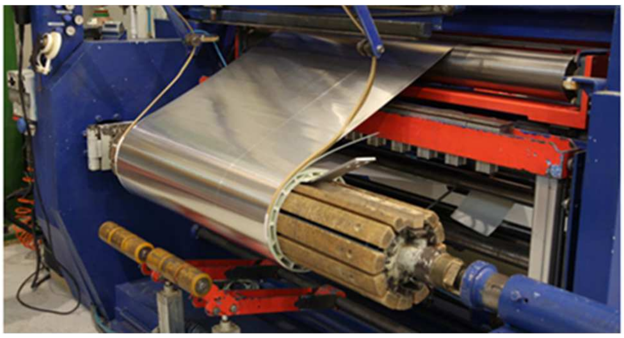

Figure 93 - Foil transformer manufacturing. The conductor foil is wound together with the insulator

Each line (or turn) of a foil-type transformer is modeled by distributed parameters contained in the elements of matrices R, L, C and G. All elements are defined as a linear density ([Ω/m]), R and L are longitudinal parameters while C and G define transversal parameters. For a single line, the scheme would be as in Figure 88 and all the parameters would be defined by degenerate matrices of a single element.

In this multiconductor line case, R matrix is populated only on the diagonal. The diagonal elements $R_{(i,i)}$ contain the linear resistivity of line *i*. Similarly, L matrix contains the linear auto-inductance in the diagonal, in the off-diagonal positions (*i,j*) the mutual inductance between line *i* and line *j*. In the off-diagonal, matrix C contains the linear capacity between line *i* and line *j*, these elements are negative as they are calculated as ratio between the voltage of one line and the charge accumulated on the other line when all other lines are grounded, this charge must be of the opposite sign of the voltage. On the diagonal each element is calculated as sum of all the other on the same line (or column), but with positive sign. If losses in the capacity are relevant, these can be easily included by using complex valued capacities. Finally, the transversal conductivity G can be generally ignored.

6.4.2.1 From the MTL model to the transformer model

The MTL has *n* physical inputs, including both the windings and the screen, defined by $2n$ variables (voltages and currents). Other $2n$ variables are necessary to define the *n* outputs, this implies that in general the linear relation between inputs and outputs is defined by a $2n \times 2n$ system, which can be derived by the R, L, C matrices [139]. In Figure 94 is therefore depicted how the MTL model can correctly represents the foil-type transformer model.

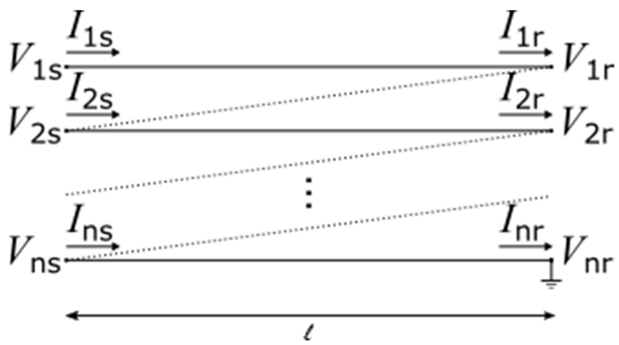

Figure 94 – Multiconductor lines connected in parallel

The problem can be formulated so that a vector containing both input and output voltages equals a linear combination of the currents, so the matrix corresponding to the linear system can be seen as an impedance matrix (Z) as in equation (9), where V_i, V_o, I_i and I_o are n-dimensional concatenated column vectors representing respectively input and output voltages and input and output currents. Z is a $2n \times 2n$ matrix.

$$\begin{bmatrix} \mathrm{V_i} \\ \mathrm{V_o} \end{bmatrix} = \mathrm{Z} \begin{bmatrix} \mathrm{I_i} \\ \mathrm{I_o} \end{bmatrix} \tag{9}$$

In this case the model represents a two winding transformer with a screen (Scr) between high voltage and low voltage windings (respectively LV and HV), this introduces in the model some constraints that reduce the complexity of the system. As each line describes one turn, the connection of a turn to the next one implies that voltage and current at the end of a line is equal to the ones at the beginning of the next line, which is defined by (10).

$$\begin{cases} \mathrm{V}_{\mathrm{i}(i)} = \mathrm{V}_{\mathrm{o}(i-1)} \\ \mathrm{I}_{\mathrm{i}(i)} = \mathrm{I}_{\mathrm{o}(i-1)} \end{cases} i \in W \tag{10}$$

where W is a subset of {1, … ,n} excluding the indexes relative to the first turn of each winding and the one of the screens. The outputs of the last turn of the LV winding, of the screen and of the last turn of the HV winding are not connected to subsequent turns and therefore excluded from (10). These terminals are connected to an impedance toward ground respectively equivalent to 0, open circuit and load, which define (11).

$$\begin{cases} V_{oLV}(end) = 0 \\ V_{oScr} = Z_{oScr} \cdot I_{oScr} \\ V_{oHV}(end) = Z_{load} \cdot I_{oHV}(end) \end{cases} \tag{11}$$

Equations (10) and (11) can be exploited to reduce the order of the system. Some linear operations [147] can be done to get rid of redundant variables. The final result is that the voltage vector has $(n+3)$ elements, the first of which is the voltage input and the others are 0. The current variables vector is reduced to $(n+3)$ dimension and the matrix is consistently reduced to $(n+3) \times (n+3)$ dimension ($\mathrm{Z_{red}}$) taking into account the output impedances connected to the 3 terminals. Finally, the system appears as in (12).

$$\begin{bmatrix} V_i(1) \\ 0 \\ \vdots \\ 0 \end{bmatrix} = [\mathrm{Z_{red}}] \begin{bmatrix} I_{\mathrm{i}} \\ I_{\mathrm{oLV}} \\ I_{\mathrm{oScr}} \\ I_{\mathrm{oHV}} \end{bmatrix} \tag{12}$$

The system can be solved by the matrix inverse inserting the desired input in (13). After all currents have been calculated, the voltages can be obtained by (9).

$$\begin{bmatrix} I_{\mathrm{i}} \\ I_{\mathrm{oLV}} \\ I_{\mathrm{oScr}} \\ I_{\mathrm{oHV}} \end{bmatrix} = [\mathrm{Z_{red}}]^{-1} \begin{bmatrix} V_i(1) \\ 0 \\ \vdots \\ 0 \end{bmatrix} \tag{13}$$

6.4.2.2 <u>Model construction for a foil-type transformer</u>

The first problem that has to be solved for an MTL model is the evaluation of the parameters to insert in the matrices. For any type of winding R is diagonal, and the non-zero elements contain the linear resistivity of the corresponding turns. Generally, evaluating the L and C parameters becomes cumbersome when the geometry of the windings is complex and mutual capacity and inductance between elements depend on many factors, especially if two windings are considered. In literature there are several papers dealing with this problem [148], [149], [150], [151] and others.

Foil-type transformer parameter evaluations can be significantly easier than other types of winding because of its geometry. A substantial simplification is introduced for an accurate calculation of the capacitance matrix C elements. The thickness of the foil is negligible compared to the width. The capacitance between two nearby turns is mainly due to the width of the foil while the thickness of the foil, involved in boundary effects and in the capacity towards non-nearby turns, is normally inferior by at least two orders of magnitude. In C, the capacitance between two nearby turns occupies the positions just over and just beneath the diagonal (i, $i\pm1$), the other off-diagonal elements refer to non-nearby turns for which the related capacity is negligible. the diagonal elements of the matrix are calculated as sum of the off-diagonal elements of the same line (with positive sign), so finally C can be considered a tridiagonal matrix.

The evaluation of the inductance matrix L is strongly dependent on frequency. In the order of industrial frequency, the induction flux flows mainly inside the core, and therefore it concatenates all turns almost equally. The matrix elements can be easily calculated from (14)

$$\mathrm{L_c} = \mu \cdot \frac{S}{\ell} \tag{14}$$

where S is the magnetic circuit section and ℓ the equivalent length. The difference caused by leakage fluxes can be neglected because they are relatively minor compared to the main flux, as they follow consistent parts of their path in air. Conversely, at very high frequencies, the core can be regarded as a conductor that rejects completely the flux [148], in this case the majority of the flux follow paths that are completely in air. In this case the L matrix can be easily calculated (15) from the vacuum capacitance matrix C_0,

$$\mathrm{L}_0 = \mu_0 \varepsilon_0 \, \mathrm{C}_0^{-1} \tag{15}$$

where μ_0 and ε_0 are respectively the vacuum magnetic permeability and the vacuum dielectric constant, C_0 is calculated as the C matrix but substituting with vacuum the space occupied by dielectric material.

The frequency range that represents the transition from industrial to very high frequency domain is not clearly defined. The amount of flux that is able to flow in the core is increasingly reduced by eddy currents therefore apparently reducing the core magnetic permeability [152], [153] or, equivalently, its apparent section. The apparent core section depends on the core lamination thickness and on the penetration depth δ of the flux, which depends on electrical resistivity ρ and local magnetic permeability μ, which is affected by magnetic nonlinearities as saturation and hysteresis. In this model nonlinearities have been neglected so the penetration depth can be calculated as in(16), where f represents the frequency.

$$\delta = \sqrt{\frac{2\rho}{2\pi f \mu}} \tag{16}$$

The core section used to calculate the inductance parameters is reduced from the real section S_0 to the apparent section S_a when the δ is lower than half the lamination thickness t_l (17), this value is summed to the flux obtained by (15).

$$S_\mathrm{a} = S_0 \cdot \frac{\min(2\delta, t)}{t_\mathrm{l}} \tag{17}$$

Table 17 - Transformer main construction parameters

Column equivalent radius [mm]	60.76	
Window dimensions H x W [mm]	540 x 313.5	
Windings height [mm]	500	
Average air gaps (column-LV-Scr-HV-Tank) [mm]	7.74 – 2.5 – 2.5 - 90	
Inter-turn insulation: Mylar [mm]	0.091	$\varepsilon_r = 3.3$
Dielectric barrier: Fiberglass – resin [mm]	2	$\varepsilon_r = 4.8$
Number of turns, LV - HV.	45 - 113	
Conductor LV: Aluminum W x thick [mm]	0.2	
Screen: Aluminum [mm]	2	
HV internal insulation [mm]	2	
Conductor HV Aluminum Wxthick [mm].	0.5	

6.4.3 Model result

The model has been developed based on the project for the prototype of a 50kVA transformer with a 1000/400V transformation ratio with two windings of respectively 45 and 113 turns. The main transformer construction parameters are reported in Table 17. A simulation has been performed over 39 frequency values spanning from 50 Hz to 10 MHz. In Figure 95 the amplitude of the voltage is represented with respect to the turn number and the frequency. In particular, the turn number is growing upward, and the frequency, growing from left (at 50 Hz) to right (at 10 MHz), is represented in logarithmic scale. The surface appears divided in three parts, the lowest (representing turns from 1 to 45) represents the low voltage winding, the voltage is injected through the first turn, which is the lowest. The second part, that looks like a thin ribbon in the middle, represents the grounded screen, indexed 46. The third part, the highest, represents the high voltage winding, with turns indexed from 47 to 159.

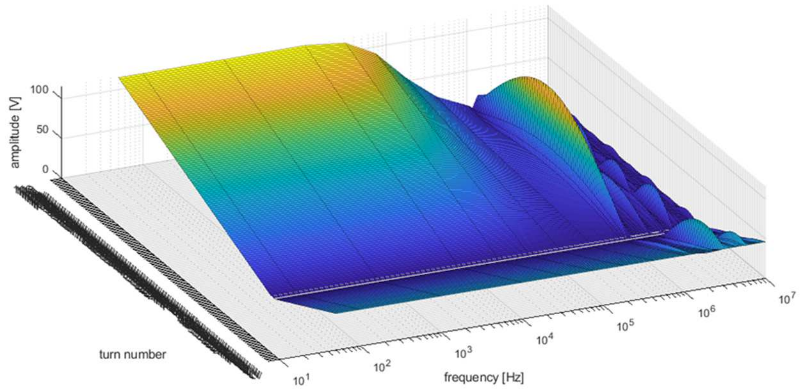

Figure 95 - Voltage output, of the MTL model referred to ground. The amplitude (vertical axis) is represented with respect to the turn number (left horizontal axis) and the frequency (right horizontal axis in logarithmic scale) [98]

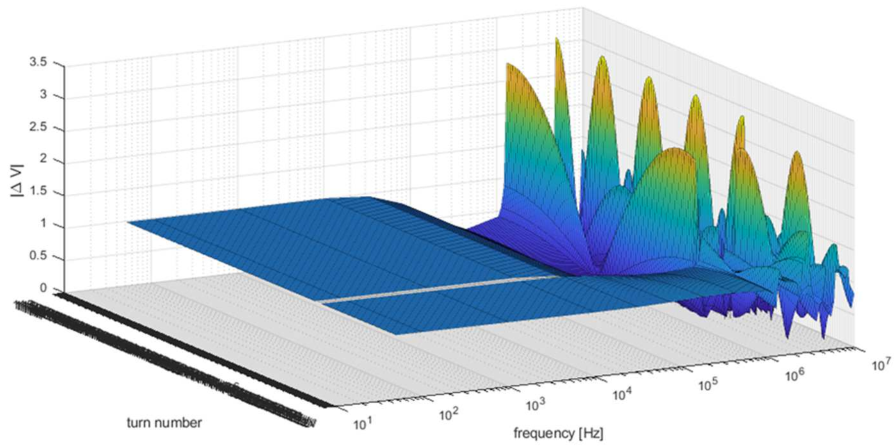

Figure 96 - Turn¬to-turn voltage. The amplitude (ΔV on the vertical axis) is represented with respect to the turn number (left horizontal axis) and the frequency (right horizontal axis in logarithmic scale) [98]

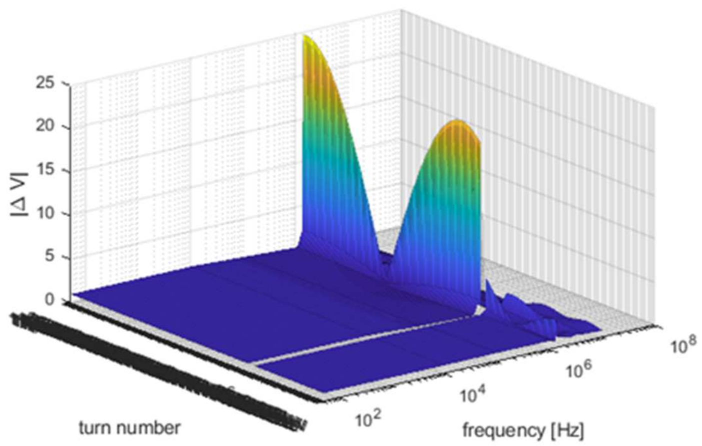

Figure 97 - The surface aspect if a frequency near the resonance is included [98]

Looking at two surfaces representing the windings, it can be seen that from 50 Hz to about 10 kHz, the transformer behaves normally, with a linear voltage decrease to 0 on the LV winding and increases linearly from the first turn to the output of the HV winding. Between 10 kHz and 1 MHz, while the LV winding continues to act normally, in the HV winding the voltage still increases linearly, but with lower rate if compared with lower frequencies. Slightly above 1 MHz a strongly nonlinear behavior occurs, causing a localized overvoltage in the HV winding. It should be noted that this occurs when the voltage in injected on the LV winding and the output HV voltage is by far under the nominal value. This underlines the difficulty to diagnose the problem from the external connections. Finally, it should be noted that even though the HV winding output drops at high frequencies, this does not mean that the winding has become insensitive to the other winding input. The information of Figure 95 can be better detailed to highlight the electrical stress acting on the turn-to-turn insulant. Figure 96 represents the turn-to-turn voltage calculated as $\Delta V_i = V_{(i+1)} - V_i$, with respect to the frequency and turn number as in Figure 95. In Figure 96 it can be seen that the turn-to-turn voltage is constant between 50 Hz and 10 kHz, confirming a normal behavior. From 10 kHz to 1 MHz the turn-to-turn voltage is still almost constant through both windings, but in the high voltage winding its value decreases with frequency. At 1MHz, the turn-to-turn voltage is no longer linear and slightly above 1 MHz, localized overvoltage occur at both ends of the high voltage winding.

Other overvoltage frequencies are found before the 10 MHz limit reached from the simulation which demonstrate that the low voltage winding is vulnerable too. The voltages seen in this simulation reach three times the normal values which may be under the dielectric rigidity of the material but still it might affect the ageing of the dielectric material. Moreover, the resonance frequency is inside the examined range. Including in the analysis a frequency near enough to the resonance, the overvoltage would be such that the dielectric rigidity of the insulation would be easily exceeded, as shown in Figure 97.

6.4.4 Experimental model validation

In order to proper validate the results depicted in the previous sub-section, a foil-type transformer prototype has been built. More precisely, the prototype of a 50kVA transformer with a 1000/400V transformation ratio with two windings of respectively 113 and 45 turns.

Thus, Figure 98 shows the 3D drawing of the transformer where the windings are highlighted in red. Then, the prototype has been built with coils that can be accessible for measurement, as illustrated in Figure 99. Above the central column the internal sockets of the secondary winding are visible, on the opposite side, not visible, those of the primary winding. In detail, the aim of the black cables is to carry the measured signal from the specific coil to a terminal block installed on the transformer chassis. Indeed, both the primary HV and secondary LV terminal block are depicted in Figure 100, respectively on the left and on the right. Regarding Figure 99, the red cables represent the earth connection among the shields of the secondary winding for all the three columns, while the blue cables allow to connect the three secondary LV windings in a star or delta configuration.

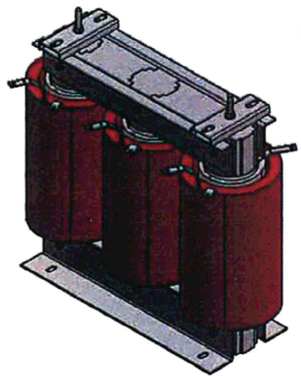

Figure 98 – Rendering model of the studied 1000/400V transformer

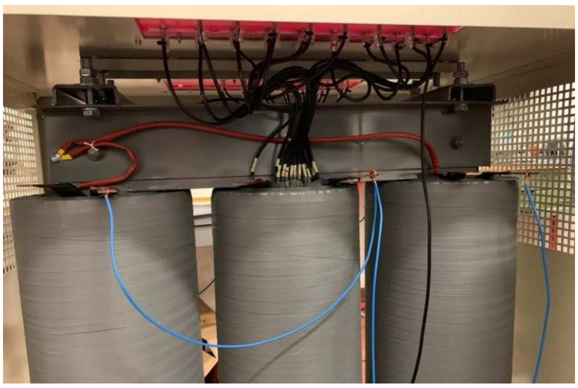

Figure 99 - The built prototype of the 50kVA transformer

Figure 100 – Detail of the primary HV (left) and secondary LV (right) terminal block

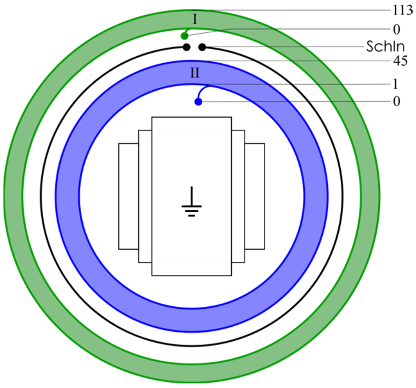

Figure 101 – Schematic central column top view highlighting the coils numeration paradigm

A schematic central column top view is also given in Figure 101 highlighting the coils numeration paradigm as a reference to better comprehend the experimental analysis. The main transformer construction parameters are reported in Table 17. The experimental model validation simulation has been performed over 100 frequency values ranging from 50 Hz to 10 MHz. In addition, the signal has been injected into the secondary LV terminals assuming a power converter supplied by the LV winding, as in the case of a shipboard propulsion transformer. Thereby, the voltage has been assessed within the two windings and in a turn-to-turn scenario in order to validate the model developed in the previous sections.

The model provides the maximum voltage value for each turn and on an arbitrary number of frequencies: Nevertheless, it was not possible to systematically check all the values for practical reasons. Moreover, only a subset of coils are available for measurement, and then each measurement requires the equipment manual adjustment limiting the number of measurements. In this context, the performed measurements have been accurately chosen aiming at the best compromise between performance and time.

In order to properly describe the research activity, the equipment used is reported here below:

- Oscilloscope PeakTech mod. 1265 (data acquisition)

- Bandwith: 30 Mhz
- sample rate 250 Msa/s

- Function generator GW Instek SFG-1013 (signal injection)
  - Frequency range: 0.1 Hz – 3 MHz
  - Sine wave maximum distortion: -40dBc (0.1 Hz – 2 MHz)

Thus, in Figure 102 is illustrated the experimental model validation setup where both the oscilloscope (bottom right) and the function generator (bottom left) are presented. Moreover, the test setup scheme is briefly given in Figure 103. In such a scheme, all the connection of the experimental model validation are reported. The blue devices in Figure 103 are the oscilloscope (top) and the function generator (bottom). Moreover, the black wires represent the probes shield connection, while the red and green wires indicate the probe signal connection for the channel one and channel two, respectively.

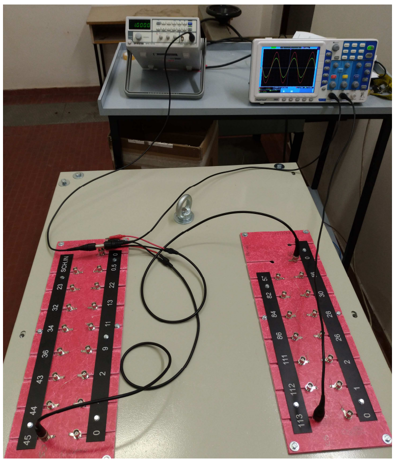

Figure 102 – Test setup

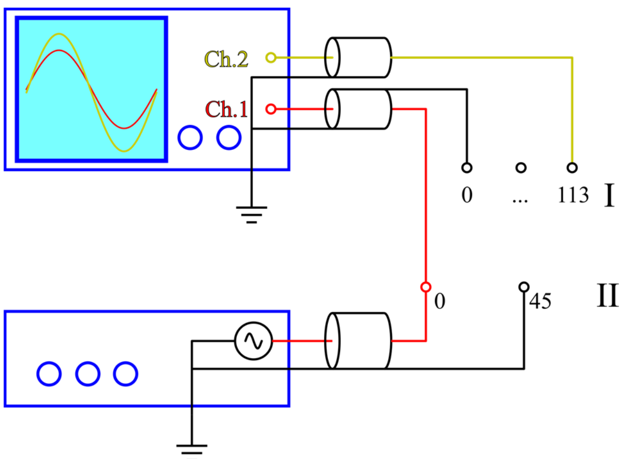

Figure 103 - Test setup scheme

The model shows non-linearities above 100 kHz. Thus, the measurement starts from a frequency of 10 kHz and it proceeds at regular frequency intervals by measuring the voltage at the end and in the middle of the primary winding. These two points have been chosen according with the simulation result since they turned out to be the most critical points. When non-linearity has been detected, the frequency intervals have been reduced to identify the resonance point with higher precision.

Figure 104 shows an example of the resonance phenomenon measurement. A sinusoidal signal with an amplitude of 880mV and a frequency of 213 kHz was injected into the terminals of the secondary winding. A voltage of 2.2V is expected at the output terminal at nominal frequency in response to a 1000/400 transformation ratio. Nevertheless, the value of 13.2V has been measured at 213 kHz, highlighting the presence of the resonance predicted with the mathematical model. The oscilloscope output data are briefly reported in Table 18. In other cases, values up to twenty times higher than those expected at the rated frequency have occurred.

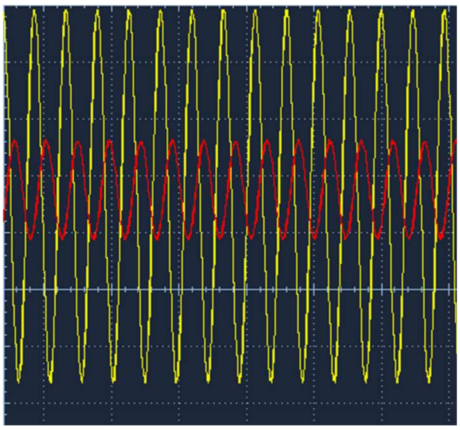

Figure 104 – Oscilloscope display output

Table 18 – Oscilloscope output data

	CH1	CH1
Frequency [kHz]	213.900	213.900
Period [µs]	4.675	
Sampling [µs]	0.050	
Peak-Peak [V]	0.880	13.2

The semi-transparent surface in Figure 105 represents the results of the analytical model. Moreover, the red samples represent the results of the measurements carried out on the coils 57 and 113 of the primary winding (respectively 106 and 162 in the figure) for various frequencies. At the frequency of 228 kHz, determined as the resonant frequency in the second test session, voltage measurements have been carried out along the primary winding for all available sockets (green line). Where the measurements have been made, the points are highlighted by a vertical line and a circular marker. For technical reasons, the secondary winding has been powered at a reduced voltage and the output voltage have been scaled accordingly for consistency comparison with the mathematical model.

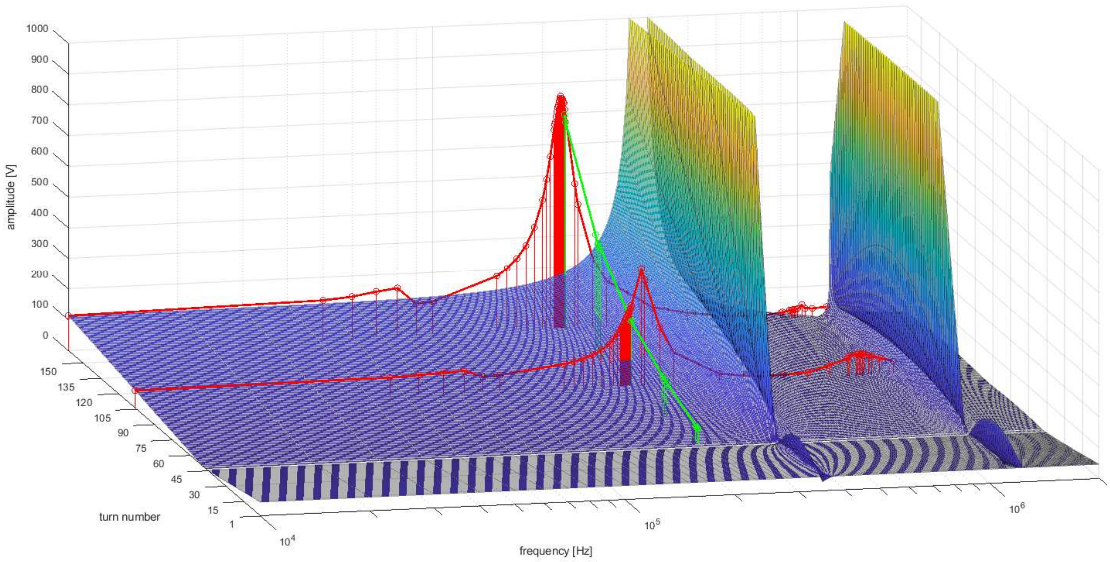

Figure 105 – Comparison between the analytical model and the experimental results.

Regarding Figure 105, it is clear that the model has correctly predicted the presence of resonance peaks and, approximately, their position. Although the mathematical model can be considered validated by the results of the measurements, the need to improve the calibration of the parameters has been highlighted. The evident reduction in amplitude and frequency of the peaks present in the measurement, compared to what is predicted by the model, can be attributed to the approximation in the evaluation of the coil-coil capacity or to the air capacity change due to environmental variations. Considering a change in model resistance due to the skin effect, a reduction in the resonance peak has been obtained, but not an appreciable shift in frequency.

A substantial frequency shift has been instead obtained considering that the flux can also pass within the penetration thickness calculated for the iron, in addition to the dielectric one, as the test frequency varies. Further improvement can be obtained in the precision of the resonant frequency prediction by inserting the iron saturation in the model for the penetration thickness.

During the measurements, which took place in 3 sessions over 24 hours, a significant shift in frequency of the resonance peak occurred (from 215 to 228 kHz). The cause should be found in environmental variations. Furthermore, significant differences have been found on the resonance frequencies as the internal connections of the transformer vary. For example, the connection of the star point affects the resonance frequency if it is made on the internal or external side of the columns. Such phenomenon justifies a systematic investigation of the effect of the connections (star point side, star-delta connection, earth connection of the star point) and on the screen effect that should be carried out in future assessments.

6.5 Equivalent parameters evaluation for cable bundles

6.5.1 Standards for electrical installation in ship

Power cables are not a negligible part of the of the shipboard power system, thus making their modelling still a point of interest, as stated throughout this chapter. In addition to that, the cable parameters (resistance, conductance, capacitance, and inductance) have a significant effect on several of the issues related to power conversion exploitation (such as harmonic distortion propagation). Since cable parameters can be affected by many factors (like frequency, ambient temperature, and electromagnetic interference, cable and shielding materials and structure, laying condition in the cable tray, and so on), the correct integration of power electronics converters onboard requires their careful assessment.

In such a scenario, cable layout can be assessed before the ship building phase, thus allowing to evaluate their parameters when correction actions can still be applied with limited (or even null) costs due to what have been said in Figure 46. Given these premises, the goal of the section is to evaluate the power lines equivalent parameters, by taking into account the cables disposition in the cable tray. Such data will be later utilized to perform the analysis in the chapter 7. Therefore, three different approaches have been used to calculate the n-dimension inductance matrix in several cable arrangements (selected among the ones approved by regulations in force). In addition, the same approach has been used to evaluate the power lines equivalent conductance. Nevertheless, the cable disposition in the cable tray has a negligible effect over the cable equivalent conductance since all the considered cables are shielded.

During the basic design stage several different preliminary calculations are made. As an example, data from cable manufacturers datasheets are used to perform the short-circuit calculation (point P in Figure 38). The cable arrangement in the cable tray is not taken into account in such studies, thus possibly leading to less accurate results. While such an effect can be considered negligible for short circuit calculations (due to the presence of other elements with significant impedance in the system, like transformers, and the conventional oversizing coefficients promoted by the standards procedures), it may be significant for other classes of studies, like in harmonic distortion estimation. Therefore, the accuracy of the inductance calculation may become critical in the future (e.g., dc power system [141]), when most of the onboard loads will become power electronics converters, supporting the study of the effect on the cable parameters of the cable arrangement in the cable trays.

The international standard governing the design of electrical installation in ship is the IEC 60092 part 352 [17]. Such standard states that it is necessary to use single core cables for circuits rated in excess of 20 A, and thus it means that most of the cables in both MVac and LVac sections must be single core ones. The standard also requires that the distance measured between the external covering of two adjacent cables is not greater than one cable diameter. Moreover, the IEC standard provides the correct disposition for a three-phase two cables per phase system (Figure 106), with the aim of assuring an equal division of the current among the paralleled cables.

To allow a more effective comparison among the methods that are proposed in the next section, the ac reference ship, illustrated in the section 5.2, has been chosen as a case study for this analysis. The main power cables data are again reported in Table 15 Moreover, the cable admittance is given (in Ω/km) and thus the cable inductance can be easily obtained knowing the system rated frequency (60 Hz). Nevertheless, the insulation technology is the same for all the four cable. The shipboard power lines have different cable per phase configurations, due to the feeders required ampacity. Since the manufacturer specifies special precaution for single core cables installation in cable trays (as illustrated in Figure 107), these arrangements have been added to the IEC standard dispositions. Therefore, the resulting case study configurations are the following:

- *Cable type A* is the only MVAC cable in the IPES and it can be found in two different configurations called *A1* and *A2*. These two configurations are depicted in Figure 106, case *A1* on the left and case *A2* on the right.
- *Cable type B* has six cable per phase. Thus, it can be arranged in two different configurations of three separated six cables groups, called *B1* and *B2*. The former configuration has two columns and three rows for each group (Figure 107a), while the latter presents three columns and two rows (Figure 107b).

- *Cable type C* has ten cables per phase, arranged like Figure 107c.
- *Cable type D* has eighteen cables per phase, thus they are arranged in nine groups of six bundles, each formed by two rows and three columns (similarly to Figure 107c).

Given different configuration arrangements for *Cable A* and *Cable B*, six different cases are present: *A1*, *A2*, *B1*, *B2*, *C*, and *D*. Thus, simulations of each case have been performed in order to assess their inductance matrix.

Figure 106 - Cable disposition in the cable tray in case of two cables per phase, defined by IEC 60092 part 352 (cases A1 and A2)

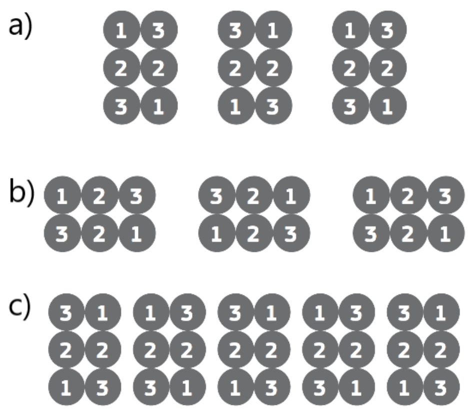

Figure 107 - a) Six cables per phase arrangement with two columns and three rows for each group (case B1); b) Six cables per phase arrangement with three columns and two rows for each group (case B2); c) Ten cables per phase arrangement with two columns and three rows for each group (case C)

6.5.2 Inductance matrix calculation exploiting different software tools

To study how different cables layout in the cable tray affect the power line inductance matrix, three different approaches have been used. The first two methods exploit FEM software to assess the *n*-dimension inductance matrix for a multicables line in a 2D simulation scenario. The third approach uses an analytical model implemented in Python to evaluate the inductance matrix for the six studied cases. The same cables geometry and distances are used for each case, in order to compare the inductance matrices consistently. The inner conductor of all the cables is actually composed by thin strands of copper.

However, in the simulations such conductor has been modeled as a solid core one, for reducing the computational load.

6.5.2.1 FEMM calculation

Finite Element Method Magnetics (FEMM) 4.2 is an open source finite element solver for 2D and axisymmetric magnetic, electrostatic, heat flow, and current flow problems with graphical pre- and post-processors. FEMM has also a Matlab plugin, by means of which the inductance matrix calculation has been fully automated. Indeed, all the setup data has been coded within a Matlab script depicted in Appendix A. In a *n*-cable system the inductance matrix size is *n*x*n*. Therefore, FEMM energizes one by one all the *n*-cables in the system and the L_{ij} is calculated as:

$$L_{ij} = \frac{\psi_i}{I_j} \tag{18}$$

where I_j is the *j*-th energized cable and ψ_i is the magnetic flux linked with the *i*-th cable.

6.5.2.2 COMSOL calculation

COMSOL Multiphysics 5.5 is a cross-platform Finite Element Analysis (FEA), solver and Multiphysics simulation software. COMSOL uses the same approach depicted in (18), but all the electric and geometric data have to be implemented through the software. The *j*-th cable is energized and the flux penetrating the *i*-th cable is calculated as shown in Figure 108.

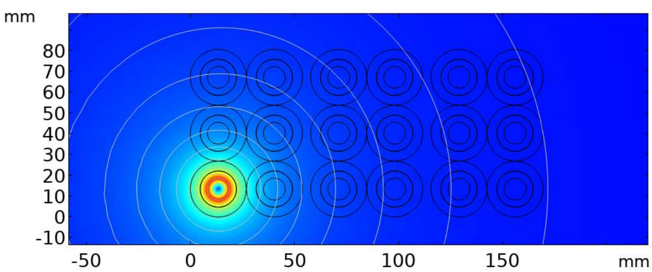

Figure 108 - Performed COMSOL simulation example in the case B1 [154]

6.5.2.3 Python code implementation

Finally, a Python code has been implemented in order to calculate the inductance matrix for all the six cases considered, by means of an analytical approach. The full Python code is given in Appendix B.

Firstly, the distance between conductors has been evaluated, to build a distance matrix. In such matrix the cable radiuses constitute the diagonal elements, while the *i*-th to *j*-th conductors' distances (assessed among cable centers) are on the non-diagonal elements. Secondly, the conductors distance matrix is used to calculate the inductance matrix, using the formulas:

$$L_{ii} = \frac{\mu_0}{2\pi}\left(0.25 + log\frac{1}{r}\right) \tag{19}$$

$$L_{ij} = \frac{\mu_0}{2\pi} log\frac{1}{d_{ij}} \tag{20}$$

where μ_0 is the air magnetic permeability, L_{ii} is the *i*-th cable auto inductance, and L_{ij} is the mutual inductance between the *i*-th and the *j*-th cable.

6.5.2.4 Inductance matrix reduction methods

All the inductance matrices calculated in the previous section have the following structure:

$$[L] = \begin{bmatrix} L_{11} & \cdots & L_{1n} \\ \vdots & \ddots & \vdots \\ L_{n1} & \cdots & L_{nn} \end{bmatrix} \tag{21}$$

where the following is valid:

$$\begin{bmatrix} \psi_1 \\ \vdots \\ \psi_n \end{bmatrix} = [L] \begin{bmatrix} I_1 \\ \vdots \\ I_n \end{bmatrix} \tag{22}$$

The (21) *n*x*n* matrices can be used as they are to perform several different studies, like the ones for electrical transients, or for assessing cross-talking phenomena. Nonetheless, these matrices are still too complex to be used for preliminary studies during system design, requiring too much computational power to solve an entire ship power system composed by them. Consequently, the inductance matrices have to be reduced to a single equivalent inductance value, to allow the designers performing fast analyses of different solutions in basic design stage. Once a reduced subset of suitable system designs is found by means of the simplified approach, it is possible to use the full *n*x*n* matrices to accurately analyze the significant phenomena. To this aim, two different methods are here used. To further simplify the evaluation, two hypotheses have been applied to both methods: the first assumption is an equal subdivision of the phase current between all the paralleled conductors (I), the second is that the sum of all the phase currents equals to zero (II). The results will allow to compute the power lines equivalent inductance for the three approaches presented in the previous section, and to compare the results with the manufacturer inductance, taking into account the cables real disposition in the cable tray.

The first method to calculate the power line equivalent inductance considering the cable layout in the cable tray is divided in two steps. The first step is the reduction of the *n*-dimensional system (22) to an equivalent three-dimensional one (24). This is made possible by means of the following assumptions. It is assumed that the overall flux for each phase is equal to the sum of all the magnetic fluxes linked with the cables of the same phase. Also, given the hypothesis (I), the sum of all the paralleled cables currents is the phase current. Therefore, a single inductance can be calculated for each phase of the cable. An example is given for the L_{AA} value:

$$L_{AA} = \sum_{i=1}^{\frac{n}{3}} \sum_{j=1}^{\frac{n}{3}} L_{ij} \tag{23}$$

By applying (23) for each phase and phase-to-phase inductance, nine inductances are calculated:

$$\begin{bmatrix} \psi_A \\ \psi_B \\ \psi_C \end{bmatrix} = \begin{bmatrix} L_{AA} & L_{AB} & L_{AC} \\ L_{BA} & L_{BB} & L_{BC} \\ L_{CA} & L_{CB} & L_{CC} \end{bmatrix} \begin{bmatrix} I_A \\ I_B \\ I_C \end{bmatrix} \tag{24}$$

By assuming that the non-diagonal values in the new three-dimensional inductance matrix are equal ($L_{AB} = L_{AC} = L_{BA} = L_{CA} = L_{CB} = M$), thanks to the cable disposition in the cable tray, it is then possible to apply the hypothesis (II). The final result is the following equivalent inductance:

$$\psi_i = (L_i - M)I_i \tag{25}$$

The second method uses the magnetic decoupling to calculate the power line equivalent inductance. Indeed, a *n*-cable system can be considered as a *n*-single-phase magnetic decoupled system, where the sum of all the currents equals to zero. The calculation of the equivalent inductance of the conductor *s* can be carried out considering a fictitious system of (*n*-1) single-phase lines, where each system is composed by the conductor *s* and one of the others (*n*-1) conductors. Thus, the fictitious system just defined is completely equivalent to the real n-cable system if the currents $I_1, \dots, I_n$ circulate in the (*n*-1) single-phase lines and the currents $-I_1, \dots, -I_n$ circulate in the conductor *s*, respectively. In fact, all the conductors of the fictitious system will be crossed by the currents that would interest them in the real system in this way (the conductor *s* too). The total magnetic flux linked with the conductor *s* can thereby be calculated as the sum of half of the fluxes linked with the (*n*-1) coils that are equivalent to the single-phase lines just descripted:

$$\psi_s = \psi_{s1} + \cdots + \psi_{s(s-1)} + \psi_{s(s+1)} + \cdots + \psi_{sn} \tag{26}$$

Thus, the generic magnetic flux ψ_{sj} is:

$$\psi_{sj} = \left[0.46log\frac{D_{sj}}{r} + 0.05\right](-I_j) \tag{27}$$

and finally, the formula of the total magnetic flux linked with the conductor *s* is:

$$\psi_s = \left[0.05 + 0.46log\frac{1}{r}\right](I_s) + 0.46\sum_{j=1, j\neq s}^{n} \log D_{sj}(-I_j) \tag{28}$$

To apply (28), appropriate hypotheses should be introduced in order to define the total magnetic flux linked with the conductor *s* as a function of the current that flows through. It is otherwise not possible to derive the conductor *s* equivalent inductance in the case of the single-phase line and then, decouple magnetically the conductor *s* from the other (*n*-1) cables. Nevertheless, the conductor *s* equivalent inductance can be determined if a particular three-phase system is chosen. In fact, all the system currents are known if the three-phase system works under direct sequence symmetrical sinusoidal conditions. Thus, the currents that run through three conductors are a triad of direct sequence of vectors I_A, $I_B = \alpha^2 I_A$, $I_C = \alpha^2 I_A$, $\alpha = e^{j2/3\pi}$. Given the hypothesis (I), the current is split equally between the cables of the same phase in the case of multiple cable per phase. Therefore, the magnetically decoupled equivalent inductance is assessed for each conductor. Finally, the power line equivalent inductance is determined as the average of the equivalent inductances of each conductor.

6.5.3 Equivalent inductance evaluation results

As aforementioned, the cables arrangement in the cable tray can remarkably affect the power line equivalent inductance. Moreover, the power line layout in the cable tray is unknown until the shipyard starts building the ship. Thus, a comparison has been carried out between the inductance value given by the manufacturer in its datasheets and the inductance calculated through the methods proposed in the previous section. Thereby, all the results are presented in terms of relative variation in respect to the corresponding manufacturer given inductance.

The result of the First Method application to all the six cases is reported in Figure 109. The First Method leads to a maximum equivalent inductance value which is always higher than the manufacturer one in the case of the FEMM calculated inductance matrix (blue bars in Figure 109). The value peaks to more than eight time higher (8.15) for the case *A2*. The cases *C* and *D* are the only two where the resulting equivalent inductance is lower than manufacturer one. Specifically, this happens for the First Method used on Python and COMSOL calculated inductance matrix (orange and gray bars respectively in Figure 109).

A detailed comparison is depicted in Figure 110 to highlight the differences between the two methods in calculating the power line equivalent inductance. In fact, the two layouts for the *Cable A* are analyzed and thus some considerations can be made. Firstly, the First Method results are roughly double the one attained by means of Second Method, considering Python and COMSOL input. Secondly, case *A2* has equivalent inductance values 25% lower than case *A1* applying the Second Method. Moreover, also the case *B2* has equivalent inductance values lower than case *B1* as illustrated in Figure 111. Furthermore, the equivalent inductance values range from -6.52% (blue bar) to -2.39% (gray bar) for the case *B2* in Figure 111 while they change from -1.18 (blue bar) to +7.60 (gray bar) for the case *D* in Figure 111. Thirdly, it is evident that the Second Method leads to values that are close to the manufacturer ones.

Despite a general reduction for cases *A2*, *B1*, and *B2*, higher the number of cables per phase, higher the power line equivalent inductance (with reference to the corresponding manufacturer given inductance) as can be seen for case *C* (ten parallel cables per phase) and case *D* (eighteen parallel cables per phase) in Figure 111. Nevertheless, it should be noticed that the comparison is not only among different cable layouts but also between different cable geometries. Thus, a more detailed analysis is needed to evaluate the equivalent inductance increase with the number of parallel cables per phase.

The overall conclusion is that the First Method is not suitable to evaluate the effect of cables arrangement in the cable tray on the power line equivalent inductance. Such effect is demonstrated by huge range of variation of the resulting inductances values in Figure 109 (from 33% to 815% of the constructor reported inductance). Instead, the Second Method leads to equivalent inductance values ranging from -6.52% (blue bar for the case *B2* in Figure 111) to +20.75% (case *A1* gray bar in Figure 111) of the manufacturer data, which is closer to the expected result of the proximity effect of the cables. Thus, the effect of cables arrangement in the cable tray on the power line equivalent inductance is not negligible and it should be taken into account in the early stage design phase. Finally, the proposed Python code provides results similar to the two considered FEM software, thus validating the use of such an analytical simplified approach. Such a result is relevant, because the Python approach is faster than performing finite elements calculations, thus making it suitable for the integration in a CSI software architecture for automatically evaluate the cables parameters during the ship power system design phase.

Thus, such approach be considered an effective mean to pursue the assessment of the equivalent inductance dependence over the cable layout. In this regard, further should be carried out in the future, by proving the effectiveness of both the Python code and the presented Second Method over a higher number of cases. Thereby, more information about the integrated power system will be available to enhance its capability and reliability since the early stage design phase.

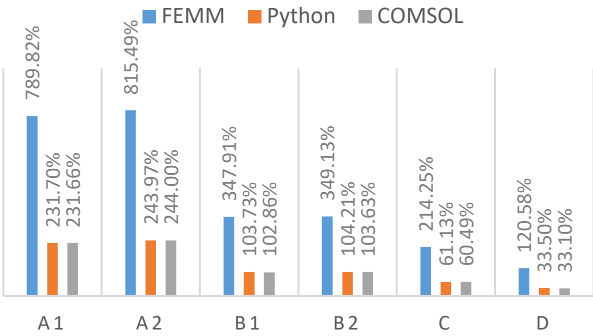

Figure 109 - First Method applied to all the six cases studied, inductance variation in respect to cable manufacturer datasheet value [154]

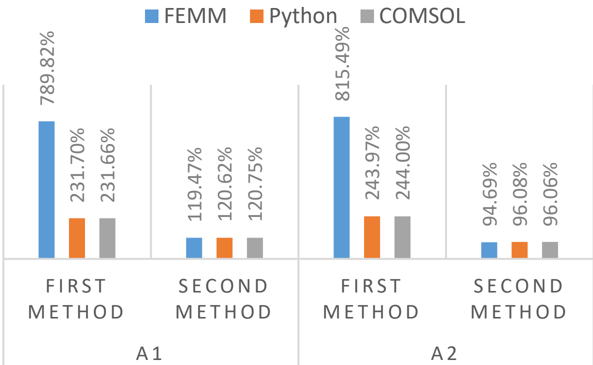

Figure 110 - Detailed comparison between the two different cable layouts for the Cable A, inductance variation in respect to cable manufacturer datasheet value [154]

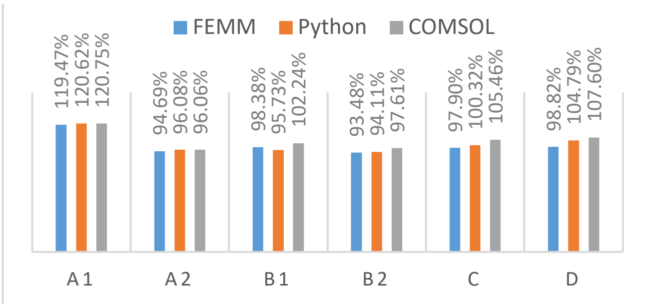

Figure 111 - Second Method applied to all the six cases studied, inductance variation in respect to cable manufacturer datasheet value [154]

6.6 Conclusions

The innovative solutions proposed in the previous chapter can have a negative impact on the performance of the power system. For this reason, in this chapter, their impact on the onboard power system has been analyzed in order to prevent integration issues. Moreover, such analysis can have an impact in the definition of cable layout.

Specifically, the high frequency disturbances propagation has been assessed both in power cables and transformers though the development of suitable frequency dependent models. As previous depicted, the cable length assessment has a significant impact in the design of innovative shipboard power systems stressing the significance of work carried out in this thesis work. In addition, the model for foil-type transformers has been validated through experimental results emphasizing the need of a new approach to correct integrate shipboard power system equipment.

Then, the cable bundles equivalent parameters have been assessed in the last sub-section of this chapter providing both a reliable inductance matrix reduction method and a Python code capable of obtaining the same results of finite element software. Referring to the proposed innovative approach in Figure 52, such step exploits the reliable information from the CSI software, depicted in the chapter 5, and thus allow to provide further benefits in the correct integration of the new devices.

Finally, the cable bundles equivalent parameters assessed through this process will then be utilized as an input value for the software simulation carried out in the next chapter. More precisely, the equivalent inductance calculated with the Second Method exploiting the Python-based calculation will be used.

7 Power system simulator

7.1 Abstract

Dome is a power system analysis tool developed by Professor Milano and his research group at University College Dublin. It is a Python-based software tool founded on two main principles: modularity and reusability of the code. The code is based on a reduced number of milestones that have to be available, but how such milestones solve their duty is not relevant for the main kernel. Each milestone is composed by several independent Python modules. Moreover, the user can also provide his own custom modules and the required modules are loaded at run-time. These are generally less than 1% of available modules. Hence, the project can grow indefinitely without affecting performance. Thus, different models accuracy have been evaluated against their computational load to find out the best compromise in a similar way as in [155].

Referring to the proposed innovative approach in Figure 52, this model provides a dynamic representation of the reference ac shipboard power system and its endowed with the data assessed in the previous chapter (i.e., the cable length and the cable bundles equivalent parameters). Such analysis allow to correct evaluate shipboard power system behavior exploiting both the reliable information from the CSI software, depicted in the chapter 5, and the equivalent parameters evaluation for the defined cable bundles.

7.2 A Python-based software tool for power system analysis

The basic requirements that a programming language has to satisfy to be eligible for scientific studies and, in particular, for power system analysis, are the availability of efficient and easy-to-use libraries for [156]:

- Basic mathematical functions (e.g., trigonometric functions and complex numbers).
- Multi-dimensional arrays (e.g., element by element operations and slicing).
- Sparse matrices and linear algebra (e.g., sparse complete LU factorization).
- Eigenvalue analysis of non-symmetrical matrices.
- Advanced and publishing-quality plots.

The requirements above reduce the choice to an only a handful of programming languages. This is clearly captured by the software tools for power system analysis that are currently actively developed. Neglecting proprietary software tools, open-source packages are mainly developed in scientific languages, e.g., Matlab, and in well-structured system languages, e.g., Java. An in-depth discussion about advantages and drawbacks of scientific and system programming languages is given in [157].

Among Matlab-based packages there are PST [158], PSAT [159], and MatPower [160]. Among packages based on system programming languages there are InterPSS [161], developed in Java, and OpenDSS [162], developed in Delphi. In recent years, the Python language have been chosen by some small project such as PYPOWER, which is a port of MatPower to Python, and minpower. Python language is mature enough for power system analysis. Moreover, the Python-based software tool can be extended by means of open-source scientific libraries to provide a performance comparable to proprietary solutions.

Given this scenario, Dome is a modular Python package that takes full advantage of the features of this modern scripting language, such as inheritance, introspection, laziness, and polymorphism, for power system analysis. Dome can solve power flow, continuation power flow, optimal power flow, small signal analysis, short-circuit analysis, network equivalencing and time domain analysis. The Dome project pillars are below depicted:

- Stating a new paradigm for power system analysis. This involves, but is not limited to, the implementation of novel models, algorithms, and routines.
- Developing efficient state-of-art serial and parallel software tools (e.g., multicore, cluster, GPUs, etc.) for power system analysis. The focus is always on large sets of data.
- Providing a common platform to compare existing models and algorithms used in power system analysis.
- Providing a canonical model, i.e., a universal data format converter, for power system models.

Further detail about the Python as a scripting language for power system analysis can be found in [156]. However, Figure 112 briefly summarizes the structure of Dome for the sake of clarity.

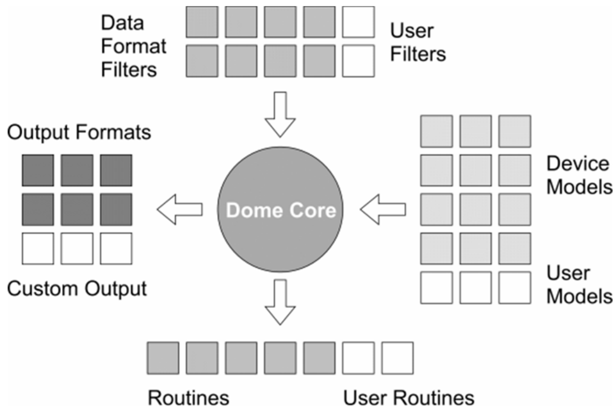

Figure 112 - Qualitative representation of the structure of Dome [156]

7.3 Shipboard power system analysis through different model approaches

The conventional Transient Stability Model (TSM) assumes that the frequency is constant and equal to the nominal one for the definition of network parameters such as transmission line series reactances and shunt susceptances [155]. This approximation is widely adopted in simulation software tools for transient stability analysis. However, during a transient triggered by a large disturbance, e.g., the outage of a large infeed, synchronous machine rotor speeds can deviate significantly from their nominal value. This variation can be properly captured by Electromagnetic Transients (EMT) models, which include detailed three-phase ac dynamic models of all elements of the grid. But EMT models are computationally too heavy to be used for the stability analysis of large power systems.

Some proprietary software tools allow utilizing a modified version of the TSM with inclusion of a variable frequency for the reactances of transmission lines and loads. For instance, the center of inertia (COI) can be used as a reference frequency, i.e., the weighted average of synchronous machine rotor speeds connected to the network. However, the frequency of the COI is unique for the whole system and cannot account for local variations of the frequency.

Given this scenario, the Professor Milano and his research team at University College Dublin (UCD) developed a Frequency Dependent Model (FDM) for transient stability analysis based on the frequency divider formula (FDF) presented in [163] that overcomes the issue above. The FDF shows that the value of the frequency varies as a continuum along the branches of the grid and synchronous machine rotor speeds constitute the boundary conditions. Hence, during a transient, the frequency not only varies from bus to bus, but also along the length of series reactances of transmission lines and transformers.

The FDM has been proven to be suitable for the transient stability analysis of large power system, as demonstrated in [155]. Therefore, the FDM behavior has been also evaluated in the transient stability analysis of the reference shipboard power system presented in the chapter 5. Such work has been carried out during the PhD period abroad at the UCD.

7.3.1 Simulation set-up

The model of the proposed reference ship (see Figure 63) consists of 35 buses, 51 distribution lines and transformers, and 19 loads. Based on this topology, a dynamic model has been developed including 4 conventional synchronous generators modeled with sixth order synchronous machine models with automatic voltage regulators and turbine governors, 10 constant power loads, and 8 frequency dependent loads. This model provides a dynamic representation of the reference ac shipboard power system and its endowed with the data assessed in the previous chapters (i.e., the cable length and the cable bundles equivalent parameters).

Thus, such software simulation is performed with enhanced data thanks to the combined approach exploited in thesis work (see Figure 52). Indeed, the cable length has been assessed through the CSI software exploitation in the chapter 5, while the cables parameters have been evaluated through the approach presented in the chapter 6, section 6.5.

Moreover, constant power loads and frequency dependent ones have been assessed considering the preliminary electric load balance. Indeed, the ship propulsion can be considered a constant power load, as a first approximation since it is supplied by power converters. Regarding the remaining loads, the 60% of them can be treated as frequency dependent loads (e.g., HVAC system, pumps, service loads, and so on). This assumption has been made referring to both the preliminary electric load balance and analysis carried out during the Naval Smart Grid research program [32], [64]. On the other hand, the remaining 40% is considered a constant pq load.

Given this context, the frequency dependent loads have been modeled in the two ways below depicted:

- AM, the fifth order asynchronous machine model has been used in this case along with reference data taken from [102]
- FDL, general frequency dependent loads has been assumed in this case, given the following reference data from [102]: $\alpha p=0.1$, $\alpha q=0.6$, $\beta p=2.8$ and $\beta q=1.8$.

This choice has been done in order to better evaluate the behavior of different frequency dependent load models in the shipboard transient stability analysis. In addition, the three different models have been compared, resulting in a total of six cases simulated. In particular:

- The TSM considers constant reactances and susceptances everywhere in the power system.
- The FDM is based on the frequency divider formula [163] and it applies to loads, branches and synchronous machines.
- The DPM includes machine flux and line dynamics.

Note that the DPM is the dqo transformation of the fully-fledged EMT model with the following approximations: (i) load is assumed perfectly balanced; (ii) no harmonics are considered; and (iii) the fundamental frequency is shifted by means of the dqo transformation [155].

To analyze the impact of different frequency dependent models a ship operative condition has been chosen. In detail, all the four onboard generators are active providing the 61% of their active power capability. Moreover, the most relevant load in the system's electric loads balance has been chosen as the perturbing load, that is the power propulsion system. In the considered operative scenario the propulsion system requires the 60% of the total ship power balance. Thus, only a single electric propulsion motor disconnection and reconnection has been evaluated during the 20 second simulations. The load disconnection first happens at 5 seconds, then the load reconnection is at 15 seconds letting the power system reach a steady state value. Given this power system set-up, the resulting frequency transients have been evaluated with the three different proposed models and the two different load models, for a total of six cases.

7.3.2 Simulation result

The Python code needed to run the Dome simulation and plot the respective results is given in Appendix C. The different models have been tested to prove their effectiveness in the simulation of different power systems load transient scenarios. Thus, different models accuracy have been evaluated against their computational load to find out the best compromise in a similar way as in [155].

The first simulation result is depicted in Figure 113 and it has been performed with a time step of 0.01 s. Such simulation carries out a comparison between the two different frequency-dependent load models in the TSM. In detail, the blue line represents the TSM model frequency transient endowed with AM load, while the red line depicts the TSM model with FDL load. The transient is referred to the frequency measured at the DG1 terminals. Thus, a different transient behavior both in the perturbating load disconnection and reconnection can be appreciated in Figure 113. The FDL load scenario (red line) leads to a higher transient peak value up to 5% of the nominal frequency and a slightly lower time response than the AM load scenario. Such difference is caused by the different parameters used for the frequency dependent loads modeled (i.e., AM and FDL).

What has been observed for the TSM, can also be found in the same simulation performed with the FDM as illustrated in Figure 114. In this case, however, the transient peak due to the perturbating load disconnection is slightly higher than in the TSM for the AM case, reaching a value around 6%.

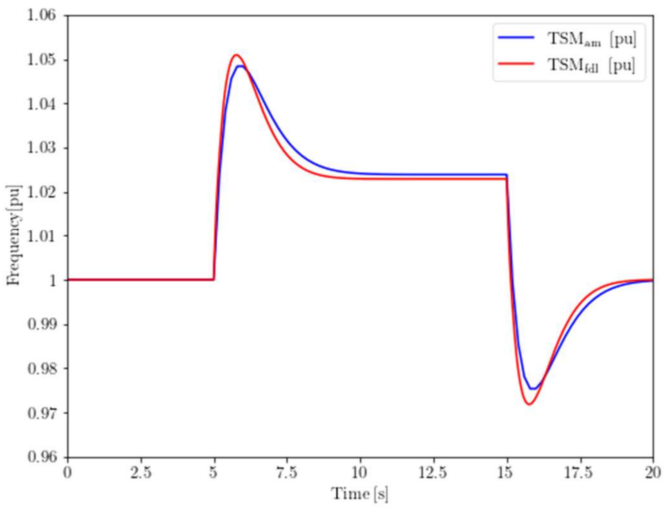

Figure 113 – Comparison between the two different frequency-dependent load models in the TSM. The DG1 frequency is displayed in per unit of the nominal one for all cases

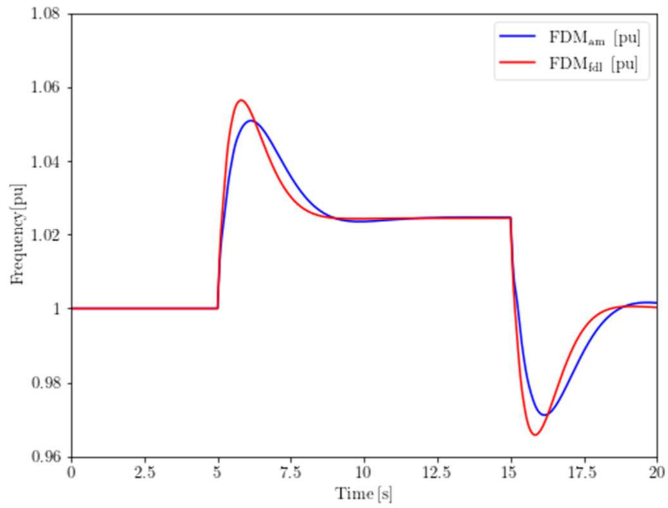

Figure 114 – Comparison between the two different frequency-dependent load models in the FDM. The DG1 frequency is displayed in per unit of the nominal one for all cases

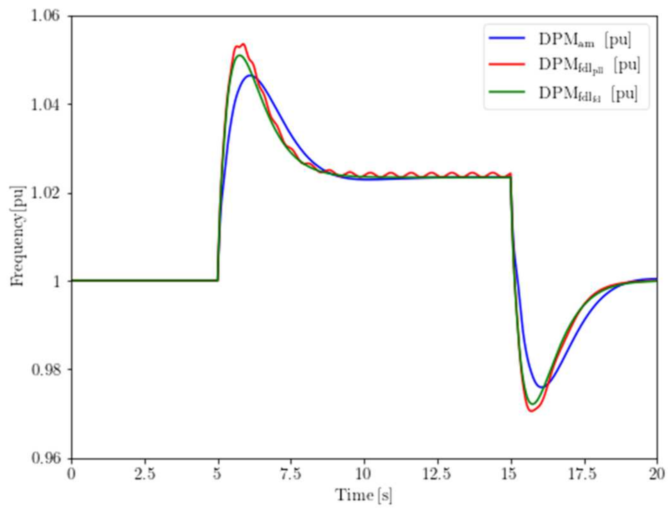

Figure 115 – Comparison between the two different frequency-dependent load models in the DPM. The DG1 frequency is displayed in per unit of the nominal one for all cases

Moreover, the same applies to the DPM, as shown in Figure 115. Nevertheless, a third case is here presented since the reference frequency for the FDL has been determined through two different ways. The former (red line transient in Figure 115) uses a synchronous reference frame Phase-Lock Loop (PLL), while the latter (green line transient in Figure 115) exploits the frequency divider formula. It can be concluded that the PLL leads to misleading measurements if not proper values are assessed for its PI regulator. The time step changed to 0.001 s for both FDM and DPM simulations.

Therefore, a comparison have been carried out to compare the different power system models in the case of the same frequency dependent load models: FDL in Figure 116 and AM in Figure 117. In both figures the DG4 frequency is displayed in per unit of the nominal one for all cases. The TSM transient response is represented by the blue line, while the DPM and the FDM is depicted with the red and green line, respectively. In Figure 116, the TSM and the DPM transient due to the perturbating load disconnection are stackable while the FDM differs both in the transient peak value and in slightly the steady state value. Instead, all the three transient behaviors are different in the Figure 117.

Finally, a comparison of the computational load required by the different proposed simulations has been carried out and the results are presented in Table 19. Nevertheless, the different models analyzed have not shown significant differences in the shipboard power system scenario as in the [155]. Further evaluation in the Dome software should be carried out in order to solve minor model issues and later to simulate both the LVdc power system proposed in this thesis work. However, a comprehensive approach has been utilized and can be exploited since the early stage design phase.

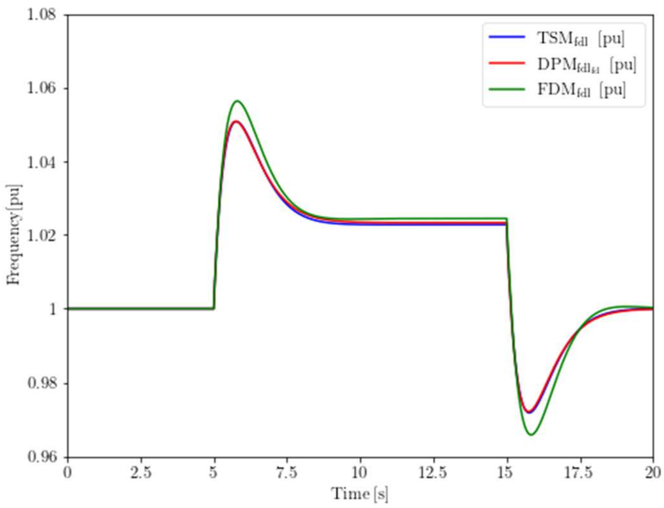

Figure 116 – Comparison between the three different models with FDL load model. The DG4 frequency is displayed in per unit of the nominal one for all cases

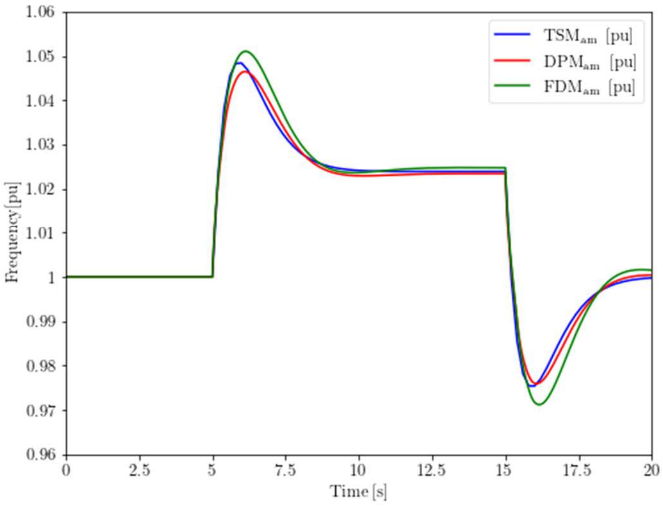

Figure 117 – Comparison between the three different models with AM load model. The DG4 frequency is displayed in per unit of the nominal one for all cases

Table 19 – Comparison of the computational load between the different proposed simulations

		Frequency dependent load representation	
		AM	**FDL**
Power system model	**TSM**	0.213 [s]	1.5495 [s]
	FDM	31.8489 [s]	28.292 [s]
	DPM	30.3984 [s]	24.2834 [s]

Conclusion

Nowadays, the marine power systems' sector is undergoing significant changes, due to both the ever-increasing ship-owners' efficiency requirements and pollution regulations. Moreover, the recent improvements in power electronics technologies are key enablers for the design of innovative power systems, by taking advantage of the new devices capabilities. The power electronics exploitation allows building power systems in which the power flow, the faults response, and the loads can be controlled by the converters through suitable algorithms. Such capabilities are even more critical for naval applications, where the introduction of electrically powered innovative sensors and weapons require an improvement in ship's power and energy system capabilities.

Designing such complex systems is difficult, due to two main issues: the classic ship design process has been conceived when ships were simpler, thus it is becoming inadequate to address the design of modern complex ships; and the proposal of new distribution systems and components imply designing the onboard power system having no previous knowledge on which to base. Moreover, it should be noticed that the existing shipboard power system solutions may evolve in the future resulting in the need of a completely different devices or components. Consequently, the system integrator must be aware to evaluate new and different design choices regardless of the technology or component utilized.

Due to that, the aim of this thesis was to present innovative methods and tools, applicable to the shipboard integrated power system, able to address the issues given by both the conventional design process and the desire to install on board new subsystems, whatever the components are. In this context, Computer System Integration (CSI) software allow to produce three-dimensional parametric models. The parametric 3D ship model contains mainly detailed data about the ship power system equipment including cables layout and their onboard paths. Therefore, such data can be used as input for power system simulation software increasing the knowledge of the system already in the early stage design phase.

Feasible design choices have been defined exploiting these software capabilities together combined. In addition, such combined capabilities are a mean to provide consistent data on which base innovative design decisions exploring different design choices and thus lowering the design times and costs. By reducing the effort required to obtain the same information, or with the same amount of time and resources invested before signing the contract, feasible solutions can be proposed, and their price can also be estimated more accurately. Furthermore, innovative subsystems can be integrated avoiding an uncontrolled cost increase.

To reach such a goal a wide review of the state of the art have been done, with the aim of allowing to understand the context, why innovative methods and tools are needed, and how they can be used as an aid in design. Each point have been discussed focusing on the aim of this thesis, thus presenting topics, bibliography, and considerations tailored to direct the reader to comprehend the impact of the proposed methods and tools.

The proposed methods and tools are able to aid the designers in decision-making activities related to the ship design process. Indeed, combined CSI and simulation software approach permits to accurately evaluate the shipboard power system parameters in early stage design where any changes to the power system layout do not lead to a considerable cost increase. In this scenario, the new concept of space reserved on board is proposed as a mean to accommodate the future power system in a modular manner. Moreover, the space reservation impact on the overall ship design can be evaluated from the early stage design phase.

Then, a reference surface combatant ship has been chosen as case study in order to apply the redesign method presented. Thanks to the CSI software exploitation, the feasibility and the validity of the proposed redesign method has been proven comparing the actual ship power system and other two innovative dc power system architectures. Indeed, the two proposed LVdc power systems result in both volume and weight reduction.

Nevertheless, the innovative solutions proposed can have a negative impact on the performance of the power system. For this reason, their impact on the onboard power system has been analyzed in order to prevent integration issues. Specifically, the high frequency disturbances propagation has been assessed in power cables through the development of suitable frequency dependent model, highlighting the cable length impact over such phenomena. Therefore, the need of the CSI software has been proven in evaluate the onboard cable paths in the early stage design. Moreover, a foil-type transformer model is proposed and then validated through experimental results emphasizing the need of a new approach to correct integrate shipboard power system equipment. The cable bundles equivalent parameters are also assessed, providing both a reliable inductance matrix reduction method and a Python code capable of obtaining the same results of finite element software.

Finally, a modular software endowed with the previously calculated parameters has been used to simulate the reference ship power system. Detailed data about the cables length and their equivalent parameters have been assessed thanks to the combined approach proposed in this thesis work. In addition, the power system simulations have been evaluated in terms of their accuracy and the computational load required by the different models proposed. Nevertheless, the different models analyzed have not shown significant differences. However, a comprehensive approach has been utilized and can be exploited since the early stage design phase.

Concluding, the entire ship 3D model have been endowed with parametric (and shared among the designers) data in order to enhance the early stage design capabilities. Thus, specific system weaknesses can be tackled through the development of the reliable modelling approach proposed exploiting both frequency-dependent mathematical models and CSI software capabilities. In fact, the cable path and lengths definition allows to correctly assess the impact of high frequency disturbances propagation in the shipboard power system.

Appendix A

Here is presented the Matlab code to perform the FEMM simulation depicted in the section 6.5.2.

```
function [Cmat Lmat]=multiCL(Cxyf,RR,eps_r,CDom,RDom,scr,Ppoli,closed)
if nargin==0
    Cxyf=[ -0.7,0,1; 0.7,0,2; 0,  0,3];
    RR=[0.1 0.2];
    eps_r=4;
    CDom=[0 0];
    RDom=1.5;
    Ppoli=[-1.2 0.2; -1.2 -0.21; 1.2 -0.21; 1.2  0.2];
        scr=1;
end
nc=size(Cxyf,1);
if ~exist('scr','var')
    scr=false;
end
if ~exist('Ppoli','var')
    Ppoli=0;
end
    extra_nLayers=8;
    extra_Rratio=2;
    Airmesh=RDom/60;
openfemm()

newdocument(1)

defineESProperties(eps_r,nc)
drawESCables(Cxyf,RR,scr)
makeESDom(CDom,RDom)
airESDom(CDom(1),CDom(2)-RDom*49/50,Airmesh)
makeESExtraDom(CDom,RDom,Airmesh,extra_nLayers,extra_Rratio);
if Ppoli~=0
    drawESPline(Ppoli);
end
ei_zoomnatural

Cmat=calcC(Cxyf,scr);

newdocument(0)
defineEMProperties(eps_r,nc)
drawEMCables(Cxyf,RR)
makeEMDom(CDom,RDom)
airEMDom(CDom(1),CDom(2)-RDom*49/50,Airmesh)
makeEMExtraDom(CDom,RDom,Airmesh,extra_nLayers,extra_Rratio);

if Ppoli~=0
%    drawEMPline(Ppoli);
end
mi_zoomnatural

Lmat=calcL(Cxyf);


if ~nargin
```

```
    Cmat
    Lmat
end

end

function drawEMCables(C,R)
    for i=1:size(C,1)
        Cx=C(i,1); Cy=C(i,2);Gr=C(i,3);
        mi_addnode(Cx-R(1),Cy);
        mi_addnode(Cx+R(1),Cy);
        mi_addarc(Cx-R(1),Cy,Cx+R(1),Cy,180,1);
        mi_addarc(Cx+R(1),Cy,Cx-R(1),Cy,180,1);
        mi_addblocklabel(Cx,Cy);
        mi_selectlabel(Cx,Cy);
        mi_setblockprop('Cu',1,0,['I_c',num2str(i)],0,i,1);
        mi_clearselected;
        if R(2)>R(1)
            mi_addnode(Cx-R(2),Cy);
            mi_addnode(Cx+R(2),Cy);
            mi_addarc(Cx-R(2),Cy,Cx+R(2),Cy,180,1);
            mi_addarc(Cx+R(2),Cy,Cx-R(2),Cy,180,1);
            mi_addblocklabel(Cx,Cy-(R(1)+R(2))/2);
            mi_selectlabel(Cx,Cy-(R(1)+R(2))/2);
            mi_setblockprop('Diel',0,R(1)/10,'<None>',0,0,0);
            mi_clearselected;
        end
        if R(3)>R(2)
            mi_addnode(Cx-R(3),Cy);
            mi_addnode(Cx+R(3),Cy);
            mi_addarc(Cx-R(3),Cy,Cx+R(3),Cy,180,1);
            mi_addarc(Cx+R(3),Cy,Cx-R(3),Cy,180,1);
            mi_addblocklabel(Cx,Cy-(R(2)+R(3))/2);
            mi_selectlabel(Cx,Cy-(R(2)+R(3))/2);
            mi_setblockprop('Diel',0,R(2)/10,'<None>',0,0,0);
            mi_clearselected;
        end
    end
end

function defineEMProperties(mur_Fe,nc)

mi_probdef(0,'meters','planar',1e-8,1,30)
mi_snapgridoff()
    mi_addmaterial()
    mi_addmaterial('Fe',mur_Fe,mur_Fe)
    mi_addmaterial('Cu',1,1,0,0,58)
    mi_addmaterial('Diel',1,1)
    mi_addboundprop('Per1',0,0,0,0,0,0,0,0,4,0,0)
    mi_addboundprop('Per2',0,0,0,0,0,0,0,0,4,0,0)
    mi_addpointprop('zeroA',0,0)
    for i=1:nc
        mi_addcircprop(['I_c',num2str(i)], 0, 1)% zero current
    end
    mi_addcircprop('I1', 1, 1)% current injection
end

function defineESProperties(e,nc)

ei_probdef('meters','planar',1e-12,1,30)
ei_snapgridoff()
```

```
    ei_addmaterial('Air',1,1,0)
    ei_addmaterial('Diel',e,e,0)
    ei_addboundprop('Per1',0,0,0,0,3)
    ei_addboundprop('Per2',0,0,0,0,3)
    ei_addpointprop('zeroV',0,0)
    for i=1:nc
        ei_addconductorprop(['V_c',num2str(i)], 0, 0, 1)% prescribed voltage
    end
    ei_addconductorprop('VV', 1, 0, 1)%prescribed voltage
    ei_addconductorprop('V0', 0, 0, 1)%prescribed voltage
end

function L=calcL(Conds)
nc=size(Conds,1);
L=zeros(nc);
    for i=1:nc
        mi_selectgroup(i);
        mi_setblockprop(['C' num2str(i)],1,0,'I1',0,i,1);
        mi_setblockprop('Cu',1,0,'I1',0,i,1);
        mi_clearselected;
        mi_saveas('ML.fem');
        mi_analyze();
        mi_loadsolution;
        for j=1:nc %leggo i flussi concatenati ai conduttori
            if j==i
                phi_c=mo_getcircuitproperties('I1');
            else
                phi_c=mo_getcircuitproperties(['I_c' num2str(j)]);
            end
            L(i,j)=phi_c(3);
        end
        mi_selectgroup(i);
            mi_setblockprop('Cu',1,0,['I_c' num2str(i)],0,i,1);
            mi_clearselected();
        mi_saveas('ML.fem');
    end
end
function C=calcC(Conds,scr)
if scr
    nc=1;
else
    nc=size(Conds,1);
end

C=zeros(nc);
    for i=1:nc
        ei_selectgroup(i);
            ei_setarcsegmentprop(1,0,0,i,'VV');
            ei_clearselected();
        ei_saveas('MC.fee');
        ei_analyze();
        ei_loadsolution;
        for j=1:nc
            if j==i
                vc=eo_getconductorproperties('VV');
            else
                vc=eo_getconductorproperties(['V_c' num2str(j)]);
            end
            C(i,j)=vc(2);
        end
        ei_selectgroup(i);
```

```
            ei_setarcsegmentprop(1,0,0,i,['V_c' num2str(i)]);
            ei_clearselected();
        ei_saveas('MC.fee');
    end
end

function makeEMDom(CDom,RDom)
mi_addnode(CDom(1)-RDom,CDom(2));
mi_addnode(CDom(1)+RDom,CDom(2));
mi_addarc(CDom(1)-RDom,CDom(2),CDom(1)+RDom,CDom(2),180,180);
mi_selectarcsegment(CDom(1),CDom(2)-RDom);
mi_setarcsegmentprop(1,'Per1',0,0);
mi_clearselected()
mi_addarc(CDom(1)+RDom,CDom(2),CDom(1)-RDom,CDom(2),180,180);
mi_selectarcsegment(CDom(1),CDom(2)+RDom);
mi_setarcsegmentprop(1,'Per2',0,0);
mi_clearselected()
end

function makeESDom(CDom,RDom)
ei_addnode(CDom(1)-RDom,CDom(2));
ei_addnode(CDom(1)+RDom,CDom(2));
ei_addarc(CDom(1)-RDom,CDom(2),CDom(1)+RDom,CDom(2),180,180);
ei_selectarcsegment(CDom(1),CDom(2)-RDom);
ei_setarcsegmentprop(1,'Per1',0,0,'<None>');
ei_clearselected()

ei_addarc(CDom(1)+RDom,CDom(2),CDom(1)-RDom,CDom(2),180,180);
ei_selectarcsegment(CDom(1),CDom(2)+RDom);
ei_setarcsegmentprop(1,'Per2',0,0,'<None>');
ei_clearselected()
end

function makeEMExtraDom(Cmod,Rmod,Airmesh,nLayers,Rratio)
    Cextra=Cmod+[2.5*Rmod 0];
    Cx=Cextra(1);
    Cy=Cextra(2);
    mi_addnode(Cx-Rmod,Cy);
    mi_addnode(Cx+Rmod,Cy);
    mi_addarc(Cx-Rmod,Cy,Cextra(1)+Rmod,Cy,180,1);
    mi_selectarcsegment(Cx,Cy-Rmod);
        mi_setarcsegmentprop(1,'Per1',0,0);
        mi_clearselected;

    mi_addarc(Cx+Rmod,Cy,Cx-Rmod,Cy,180,1);
    mi_selectarcsegment(Cx,Cy+Rmod);
        mi_setarcsegmentprop(1,'Per2',0,0);
        mi_clearselected;
    mi_addnode(Cx,Cy)
    mi_selectnode(Cx,Cy);
        mi_setnodeprop('zeroA',0)
        mi_clearselected;
    for i=1:nLayers
        mi_addnode(Cx-Rmod/Rratio^i,Cy);
        mi_addnode(Cx+Rmod/Rratio^i,Cy);
        mi_addarc(Cx-Rmod/Rratio^i,Cy,Cx+Rmod/Rratio^i,Cy,180,2);
        mi_addarc(Cx+Rmod/Rratio^i,Cy,Cx-Rmod/Rratio^i,Cy,180,2);

        mi_addblocklabel(Cx,Cy-Rmod*(1/Rratio^(i+1)+1/Rratio^i)/2)
        mi_selectlabel(Cx,Cy-Rmod*(1/Rratio^(i+1)+1/Rratio^i)/2);
        mi_setblockprop('Air',0,Airmesh/Rratio^i,0,0,0,0);
```

```
        mi_clearselected;
    end

    mi_addblocklabel(Cx,Cy-Rmod*(1/Rratio+1)/2)
    mi_selectlabel(Cx,Cy-Rmod*(1/Rratio+1)/2);
        mi_setblockprop('Air',0,Airmesh,0,0,0,0);
        mi_clearselected;
end
function makeESExtraDom(Cmod,Rmod,Airmesh,nLayers,Rratio)
    Cextra=Cmod+[2.5*Rmod 0];
    Cx=Cextra(1);
    Cy=Cextra(2);
    ei_addnode(Cx-Rmod,Cy);
    ei_addnode(Cx+Rmod,Cy);
    ei_addarc(Cx-Rmod,Cy,Cextra(1)+Rmod,Cy,180,1);
    ei_selectarcsegment(Cx,Cy-Rmod);
        ei_setarcsegmentprop(1,'Per1',0,0,'<None>');
        ei_clearselected;

    ei_addarc(Cx+Rmod,Cy,Cx-Rmod,Cy,180,1);
    ei_selectarcsegment(Cx,Cy+Rmod);
        ei_setarcsegmentprop(1,'Per2',0,0,'<None>');
        ei_clearselected;
    ei_addnode(Cx,Cy)
    ei_selectnode(Cx,Cy);
        ei_setnodeprop('zeroV',0,0)
        ei_clearselected;
    for i=1:nLayers
        ei_addnode(Cx-Rmod/Rratio^i,Cy);
        ei_addnode(Cx+Rmod/Rratio^i,Cy);
        ei_addarc(Cx-Rmod/Rratio^i,Cy,Cx+Rmod/Rratio^i,Cy,180,2);
        ei_addarc(Cx+Rmod/Rratio^i,Cy,Cx-Rmod/Rratio^i,Cy,180,2);

        ei_addblocklabel(Cx,Cy-Rmod*(1/Rratio^(i+1)+1/Rratio^i)/2)
        ei_selectlabel(Cx,Cy-Rmod*(1/Rratio^(i+1)+1/Rratio^i)/2);
        ei_setblockprop('Air',0,Airmesh/Rratio^i,0);
        ei_clearselected;
    end

    ei_addblocklabel(Cx,Cy-Rmod*(1/Rratio+1)/2)
    ei_selectlabel(Cx,Cy-Rmod*(1/Rratio+1)/2);
        ei_setblockprop('Air',0,Airmesh,0);
        ei_clearselected;
end

function drawESCables(C,R,scr)
    for i=1:size(C,1)
        Cx=C(i,1); Cy=C(i,2);Gr=C(i,3);
        ei_addnode(Cx-R(1),Cy);
        ei_addnode(Cx+R(1),Cy);
        ei_addarc(Cx-R(1),Cy,Cx+R(1),Cy,180,1);
        ei_addarc(Cx+R(1),Cy,Cx-R(1),Cy,180,1);
        ei_selectarcsegment(Cx,Cy-R(1));
        ei_selectarcsegment(Cx,Cy+R(1));
        ei_setarcsegmentprop(1,0,0,i,['V_c',num2str(i)]);
        ei_clearselected;
    ei_addblocklabel(Cx,Cy);
    ei_selectlabel(Cx,Cy);
        ei_setblockprop('<No Mesh>',0,1,0);
        ei_clearselected;
        if R(2)>R(1)
```

```
            ei_addnode(Cx-R(2),Cy);
            ei_addnode(Cx+R(2),Cy);
            ei_addarc(Cx-R(2),Cy,Cx+R(2),Cy,180,1);
            ei_addarc(Cx+R(2),Cy,Cx-R(2),Cy,180,1);
            ei_addblocklabel(Cx,Cy-(R(1)+R(2))/2);
            ei_selectlabel(Cx,Cy-(R(1)+R(2))/2);
            ei_setblockprop('Diel',0,R(1)/10,Gr);
            ei_clearselected;
            if scr
                ei_selectarcsegment(Cx,Cy+R(2));
                ei_selectarcsegment(Cx,Cy-R(2));
                ei_setarcsegmentprop(1,0,0,0,'V0');
                ei_clearselected();
            end
        end
        if R(3)>R(2)
            ei_addnode(Cx-R(3),Cy);
            ei_addnode(Cx+R(3),Cy);
            ei_addarc(Cx-R(3),Cy,Cx+R(3),Cy,180,1);
            ei_addarc(Cx+R(3),Cy,Cx-R(3),Cy,180,1);
            ei_addblocklabel(Cx,Cy-(R(2)+R(3))/2);
            ei_selectlabel(Cx,Cy-(R(2)+R(3))/2);
            ei_setblockprop('Diel',0,R(2)/10,Gr);
            ei_clearselected;
        end
    end
end

function airEMDom(airX,airY,meshSize)
    mi_addblocklabel(airX,airY);
    mi_selectlabel(airX,airY);
    mi_setblockprop('Air',0,meshSize,0,0,0,0);
    mi_clearselected;

end
function airESDom(airX,airY,meshSize)
    ei_addblocklabel(airX,airY);
    ei_selectlabel(airX,airY);
    ei_setblockprop('Air',0,meshSize,0);
    ei_clearselected;

end

function drawESPline(P)
    n=size(P,1);
    ei_addnode(P(1,:));
    for i = 2:n
        ei_addnode(P(i,:))
        ei_addsegment(P(i-1,:),P(i,:));
        ei_selectsegment((P(i-1,:)+P(i,:))/2);
        ei_setsegmentprop('<None>',0,1,0,99,'V0')
        ei_clearselected();
    end
end
```

Appendix B

Here is presented the Python code to perform the simulation depicted in the section 6.5.2.

```
import os
import math
import numpy as np

def nTo3(matrix, numPar):
    try:
        a = matrix[:int(numPar), :int(numPar)]
        b = matrix[:int(numPar), int(numPar):int(numPar*2)]
        c = matrix[:int(numPar), int(numPar*2):]
        d = matrix[int(numPar):int(numPar*2), :int(numPar)]
        e = matrix[int(numPar):int(numPar*2), int(numPar):int(numPar*2)]
        f = matrix[int(numPar):int(numPar*2), int(numPar*2):]
        g = matrix[int(numPar*2):, :int(numPar)]
        h = matrix[int(numPar*2):, int(numPar):int(numPar*2)]
        i = matrix[int(numPar*2):, int(numPar*2):]

        A = a.sum()
        B = b.sum()
        C = c.sum()
        D = d.sum()
        E = e.sum()
        F = f.sum()
        G = g.sum()
        H = h.sum()
        I = i.sum()

        matrix3 = np.array([[A,B,C],[D,E,F],[G,H,I]])
        return matrix3
    except Exception as e:
        print("Error reading file ''. Son sciopà! Error: "+str(e))
        return None

def threeToPU(matrix3):
    try:
        sum = 0.0
        for i in range(0,3):
            for j in range(0,3):
                if i == j:
                    sum = sum + matrix3[i][j]
                else:
                    sum = sum - matrix3[i][j]/2

        return sum
```

```
    except Exception as e:
        print("Error reading file ''. Son sciopà! Error: "+str(e))
        return None

#****
#main
#****

# electrical parameters
aB =                        # power base [MVA]
vB =                        # Voltage base [kV]
zB = vB*vB/aB                   # Impedance base [ohm]
f0 =                          # System frequency [Hz]
# Fundamental constant
mu0 = np.pi*4e-7                # [H/m]
eps0 = 1/(mu0*pow(299792458,2)) # [F/m]
alpha = complex(-0.5,np.sqrt(3)/2)
# cable data
rCond = 0.0105/2                # [m]
rCab = 0.0269/2                 # [m]
pCond = 1.85e-8                 # conductor resistivity [ohm*m]
tIns = 0.0034                   # thickness of the first insulation layer [m]
epsR = 2.3                      # relative dielectric constant
tShi = 0.0001                   # thickness of the shield [m]
length = 1                      # cable length [m]

# Cable position and phase
pos = np.array([[0,0,1],[0.027,0,2],[0.054,0,3]]) # [m]
posPar = pos[np.argsort(pos[:, 2])]

numCond = int(np.shape(pos)[0])
numPar = int(numCond/3)
distCond = np.zeros((numCond,numCond))
lMatrix = np.zeros((numCond,numCond))
lApp = np.empty(numCond, dtype=complex)
lMatrix3 = np.zeros((3,3))

print("number of conductors =", posPar)
print(" ")

# Calculate distance matrix
for i in range(numCond):
    for j in range(numCond):
        if i == j:
            distCond[i][j] = rCond
        else:
```

```
            distCond[i][j] = float(np.sqrt(pow(posPar[i][0]-
posPar[j][0],2)+pow(posPar[i][1]-posPar[j][1],2)))

# Calculate L matrix classic formula
for i in range(numCond):
    for j in range(numCond):
        if i == j:
            lMatrix[i][j] = mu0/(2*np.pi) *(0.25+np.log(1/distCond[i][j])) [(H/m)
]
        else:
            lMatrix[i][j] = mu0/(2*np.pi) *(np.log(1/(distCond[i][j]))) # [(H/m)]

lMatrix3 = nTo3(lMatrix, numPar)
lpu = threeToPU(lMatrix3)
xpu = lpu*2*np.pi*f0*length/zB     pu inductance [ohm]

# subsceptance calcultaion
cap = 2*np.pi*eps0*epsR/np.log((rCond+tIns)/rCond)*length              # [F]
b = 2*np.pi*f0*cap                                                 # [S]
bpu = b*zB
```

Appendix C

Here is presented the Python code to run Dome and perform the simulation depicted in the section 7.3.2

```
#!/usr/bin/env python
# -*- coding: utf-8 -*-

import os

def readFile(path):
    try:
        f = open(path,'r')
        rawData = f.read()
        f.close()

        data = rawData.decode('utf-8')

        return data
    except Exception as e:
        print("Error reading file '"+path+"'. Son sciopà! Error: "+str(e))
        return None

def writeFile(path,rawData):
    try:
        f = open(path,'w')

        data = rawData.encode('utf-8')

        t = f.write(data)
        f.close()
        return True
    except Exception as e:
        print("Error writing file '"+path+"'.  Son sciopà anca mi! Error: "+str(e
))
        return False

def executeFile(oryPath,newCommand,dmPath,typeSim):
    try:
        dmData = readFile(oryPath)
        modifiedDmData = dmData+newCommand
        #write dm file
        dmData = writeFile(str(dmPath),modifiedDmData)
        #run line command
        os.system("dome "+dmPath+" -r "+typeSim)
        return True
```

```
    except Exception as e:
        print("Error writing file '"+path+"'.  Son sciopà anca mi! Error di execu
teFile: "+str(e))
        return False

#****
#main
#****
print("Cosa simuliamo oggi? Initialized...")
PATH = list(range(10))
PATH[0] = "./1tsm_pq"
PATH[1] = "./2tsm_fdl"
PATH[2] = "./3dpm_pqdyn"
PATH[3] = "./4dpm_fdl_pll"
PATH[4] = "./5dpm_fdl_fd"
PATH[5] = "./6fdm_pq"
PATH[6] = "./7fdm_fdl"

# for i in range (0,7):
    os.system("dome core -r TDS "+PATH[i]+".dm")

# plot system frequency


# plot TSM DPM FDM dg 1
os.system("dome plot "+PATH[0]+".dat 0 15 "+PATH[1]+".dat 0 5 "+PATH[2]+".dat 0 9
7 "+PATH[3]+".dat 0 79 "+PATH[4]+".dat 0 79 "+PATH[5]+".dat 0 15 "+PATH[6]+".dat
0 5 -l --position=1 --ylabel=\Frequency[pu] --output=TSM_DPM_FDM_frequency_dg1 --
export=png")

# plot TSM DPM FDM dg 4
os.system("dome plot "+PATH[0]+".dat 0 18 "+PATH[1]+".dat 0 8 "+PATH[2]+".dat 0 1
00 "+PATH[3]+".dat 0 82 "+PATH[4]+".dat 0 82 "+PATH[5]+".dat 0 18 "+PATH[6]+".dat
 0 8 -l --position=1 --ylabel=\Frequency[pu] --output=TSM_DPM_FDM_frequency_dg4 -
-export=png")
# plot am dg 4
os.system("dome plot "+PATH[0]+".dat 0 18 "+PATH[2]+".dat 0 100 "+PATH[5]+".dat 0
 18 -l --position=1 --ylabel=\Frequency[pu] --output=am_frequency_dg4 --
export=png")
# plot fdl dg 4
os.system("dome plot "+PATH[1]+".dat 0 8 "+PATH[4]+".dat 0 82 "+PATH[6]+".dat 0 8
 -l --position=1 --ylabel=\Frequency[pu] --output=fdl_frequency_dg4 --
export=png")

# plot TSM dg 1
os.system("dome plot "+PATH[0]+".dat 0 15 "+PATH[1]+".dat 0 5 -l --position=1 --
ylabel=\Frequency[pu] --output=TSM_frequency_dg1 --export=png")
```

```
# plot DPM dg 1
os.system("dome plot "+PATH[2]+".dat 0 97 "+PATH[3]+".dat 0 79 "+PATH[4]+".dat 0
79 -l --position=1 --ylabel=\Frequency[pu] --output=DPM_frequency_dg1 --
export=png")

# plot DPM flux dg 2
os.system("dome plot "+PATH[2]+".dat 0 118 "+PATH[3]+".dat 0 100 "+PATH[4]+".dat
0 100 -l --position=1 --ylabel=$\psi_d[pu]$ --xmin=4.9 --xmax=5.2 --
output=DPM_flux_dg2 --export=png")

# plot FDM dg 1
os.system("dome plot "+PATH[5]+".dat 0 15 "+PATH[6]+".dat 0 5 -l --position=1 --
ylabel=\Frequency[pu] --output=FDM_frequency_dg1 --export=png")

# plot FDM flux dg 2
os.system("dome plot "+PATH[5]+".dat 0 36 "+PATH[6]+".dat 0 26 -l --position=1 --
ylabel=$\psi_d[pu]$ --xmin=4.9 --xmax=5.2 --output=FDM_flux_dg2 --export=png")

# plot DPM pll fd
os.system("dome plot "+PATH[3]+".dat 0 79 "+PATH[4]+".dat 0 79 -l --position=1 --
ylabel=\Frequency[pu] --output=DPM_fd_pll_dg1 --export=png")

print("Mission accomplished.")
```

References

[1] E. Skjong, E. Rødskar, M. Molinas, T. A. Johansen, and J. Cunningham, "The Marine Vessel's Electrical Power System: From its Birth to Present Day," *Proc. IEEE*, vol. 103, no. 12, pp. 2410–2424, Dec. 2015, doi: 10.1109/JPROC.2015.2496722.

[2] G. Sulligoi and A. K. Rathore, "Guest Editorial Marine Systems Electrification," *IEEE Trans. Transp. Electrification*, vol. 2, no. 4, pp. 504–506, Dec. 2016, doi: 10.1109/TTE.2016.2626838.

[3] C. Sulzberger, "First Edison Lights at Sea: The SS Columbia Story, 1880-1907 [History]," *IEEE Power Energy Mag.*, vol. 13, no. 1, pp. 92–101, Jan. 2015, doi: 10.1109/MPE.2014.2362477.

[4] J. J. Cunningham, "An AC Pioneer: United Electric Light Power Company [History]," *IEEE Power Energy Mag.*, vol. 11, no. 3, pp. 84–98, May 2013, doi: 10.1109/MPE.2013.2245589.

[5] H. C. Coleman, "Electric propulsion for ships," *Electr. Eng.*, vol. 64, no. 7, pp. 246–249, Jul. 1945, doi: 10.1109/EE.1945.6441147.

[6] R. Tolf, *The Russian Rockefellers: The Saga of the Nobel Family and the Russian Oil Industry.* Stanford, CA,USA: Hoover Institution Press, Stanford University, 1976.

[7] E. Skjong, R. Volden, E. Rodskar, M. Molinas, T. A. Johansen, and J. Cunningham, "Past, Present, and Future Challenges of the Marine Vessel's Electrical Power System," *IEEE Trans. Transp. Electrification*, vol. 2, no. 4, pp. 522–537, Dec. 2016, doi: 10.1109/TTE.2016.2552720.

[8] J. F. Hansen and F. Wendt, "History and State of the Art in Commercial Electric Ship Propulsion, Integrated Power Systems, and Future Trends," *Proc. IEEE*, vol. 103, no. 12, pp. 2229–2242, Dec. 2015, doi: 10.1109/JPROC.2015.2458990.

[9] A. Vicenzutti, D. Bosich, G. Giadrossi, and G. Sulligoi, "The Role of Voltage Controls in Modern All-Electric Ships: Toward the all electric ship.," *IEEE Electrification Mag.*, vol. 3, no. 2, pp. 49–65, Jun. 2015, doi: 10.1109/MELE.2015.2413437.

[10] S. Fang, Y. Wang, B. Gou, and Y. Xu, "Toward Future Green Maritime Transportation: An Overview of Seaport Microgrids and All-Electric Ships," *IEEE Trans. Veh. Technol.*, vol. 69, no. 1, pp. 207–219, Jan. 2020, doi: 10.1109/TVT.2019.2950538.

[11] D. Alexander, "Hybrid Electric Drive for Naval Combatants," *Proc. IEEE*, vol. 103, no. 12, pp. 2267–2275, Dec. 2015, doi: 10.1109/JPROC.2015.2453395.

[12] R. Hepburn, "'Why a naval architect likes an electric ship' for SPEEDAM 2008 Ischia, Italy June 11th – 13th, 2008," in *Automation and Motion 2008 International Symposium on Power Electronics, Electrical Drives*, Jun. 2008, pp. 591–593, doi: 10.1109/SPEEDHAM.2008.4581220.

[13] T. J. McCoy, "Integrated Power Systems—An Outline of Requirements and Functionalities for Ships," *Proc. IEEE*, vol. 103, no. 12, pp. 2276–2284, Dec. 2015, doi: 10.1109/JPROC.2015.2480597.

[14] "International Maritime Organization, SOLAS Consolidated Edition, IMO, 2014." .

[15] A. Vicenzutti, V. Bucci, G. Sulligoi, and R. Pelaschiar, “Impact of Safe Return to Port rules on passenger ships power systems design,” in *2016 AEIT International Annual Conference (AEIT)*, Oct. 2016, pp. 1–7, doi: 10.23919/AEIT.2016.7892787.
[16] “IEEE Recommended Practice for Electrical Installations on Shipboard–Marine Sectors and Mission Systems,” *IEEE Std 454-2018*, pp. 1–16, Feb. 2019, doi: 10.1109/IEEESTD.2019.8643869.
[17] “‘Electrical installations in ships,’ IEC 60092.” .
[18] C. Craig and M. Islam, “Integrated Power System Design for Offshore Energy Vessels and Deepwater Drilling Rigs,” *IEEE Trans. Ind. Appl.*, vol. 48, no. 4, pp. 1251–1257, Jul. 2012, doi: 10.1109/TIA.2012.2200091.
[19] G. Lipardi *et al.*, “Electric loads characterization in an aircraft carrier with ring-bus distribution system,” in *2015 International Conference on Electrical Systems for Aircraft, Railway, Ship Propulsion and Road Vehicles (ESARS)*, Mar. 2015, pp. 1–6, doi: 10.1109/ESARS.2015.7101467.
[20] M. Cupelli *et al.*, “Power Flow Control and Network Stability in an All-Electric Ship,” *Proc. IEEE*, vol. 103, no. 12, pp. 2355–2380, Dec. 2015, doi: 10.1109/JPROC.2015.2496789.
[21] G. Sulligoi, “All electric ships: present and future after 20 years of research and technical achievements,” *undefined*, 2011. .
[22] A. G. Exposito, J. L. M. Ramos, and J. R. Santos, “Slack bus selection to minimize the system power imbalance in load-flow studies,” *IEEE Trans. Power Syst.*, vol. 19, no. 2, pp. 987–995, May 2004, doi: 10.1109/TPWRS.2004.825871.
[23] “Part 6: Control, Electrical, Refrigeration and Fire.” Lloyd’s Register, Rules and Regulations for the Classification of Ships, Jul. 2020.
[24] K. E. Nicholson, R. L. Doughty, L. Mane, G. Miranda, and F. D. Pulaski, “Cost effective power management systems,” *IEEE Ind. Appl. Mag.*, vol. 6, no. 2, pp. 23–33, Mar. 2000, doi: 10.1109/2943.823196.
[25] F. D. Kanellos, G. J. Tsekouras, and N. D. Hatziargyriou, “Optimal Demand-Side Management and Power Generation Scheduling in an All-Electric Ship,” *IEEE Trans. Sustain. Energy*, vol. 5, no. 4, pp. 1166–1175, Oct. 2014, doi: 10.1109/TSTE.2014.2336973.
[26] T. Ericsen, “The Second Electronic Revolution (It’s All About Control),” *IEEE Trans. Ind. Appl.*, vol. 46, no. 5, pp. 1778–1786, Sep. 2010, doi: 10.1109/TIA.2010.2057400.
[27] D. Bosich, A. Vicenzutti, R. Pelaschiar, R. Menis, and G. Sulligoi, “Toward the future: The MVDC large ship research program,” in *2015 AEIT International Annual Conference (AEIT)*, Oct. 2015, pp. 1–6, doi: 10.1109/AEIT.2015.7415251.
[28] J. E. Huber and J. W. Kolar, “Volume/weight/cost comparison of a 1MVA 10 kV/400 V solid-state against a conventional low-frequency distribution transformer,” in *2014 IEEE Energy Conversion Congress and Exposition (ECCE)*, Sep. 2014, pp. 4545–4552, doi: 10.1109/ECCE.2014.6954023.

[29] D. Bosich, R. A. Mastromauro, and G. Sulligoi, “AC-DC interface converters for MW-scale MVDC distribution systems: A survey,” in *2017 IEEE Electric Ship Technologies Symposium (ESTS)*, Aug. 2017, pp. 44–49, doi: 10.1109/ESTS.2017.8069258.

[30] R. Soman, M. M. Steurer, T. A. Toshon, M. O. Faruque, and R. M. Cuzner, “Size and Weight Computation of MVDC Power Equipment in Architectures Developed Using the Smart Ship Systems Design Environment,” *IEEE J. Emerg. Sel. Top. Power Electron.*, vol. 5, no. 1, pp. 40–50, Mar. 2017, doi: 10.1109/JESTPE.2016.2625030.

[31] M. C. D. Piazza, M. Luna, G. L. Tona, M. Pucci, A. Accetta, and A. Pietra, “A New Method for Selecting the Voltage Level for an Advantageous Transition to DC Distribution in Ships,” in *2018 IEEE International Conference on Electrical Systems for Aircraft, Railway, Ship Propulsion and Road Vehicles International Transportation Electrification Conference (ESARS-ITEC)*, Nov. 2018, pp. 1–5, doi: 10.1109/ESARS-ITEC.2018.8607438.

[32] A. Colavitto *et al.*, “Naval Smart Grid Research Program: Phase 2,” in *2018 IEEE International Conference on Electrical Systems for Aircraft, Railway, Ship Propulsion and Road Vehicles International Transportation Electrification Conference (ESARS-ITEC)*, Nov. 2018, pp. 1–6, doi: 10.1109/ESARS-ITEC.2018.8607638.

[33] A. Colavitto, A. Vicenzutti, D. Bosich, and G. Sulligoi, “Open Challenges in Future Electric Ship Design: High-Frequency Disturbance Propagation in Integrated Power and Energy Systems on Ships,” *IEEE Electrification Mag.*, vol. 7, no. 4, pp. 98–110, Dec. 2019, doi: 10.1109/MELE.2019.2943983.

[34] J. E. Rucker, J. L. Kirtley, and T. J. McCoy, “Design and analysis of a permanent magnet generator for naval applications,” in *IEEE Electric Ship Technologies Symposium, 2005.*, Jul. 2005, pp. 451–458, doi: 10.1109/ESTS.2005.1524714.

[35] A. Vicenzutti, G. Trincas, V. Bucci, G. Sulligoi, and G. Lipardi, “Early-Stage design methodology for a multirole electric propelled surface combatant ship,” in *2019 IEEE Electric Ship Technologies Symposium (ESTS)*, Aug. 2019, pp. 97–105, doi: 10.1109/ESTS.2019.8847793.

[36] N. Doerry and J. Amy, “Electric ship power and energy system architectures,” in *2017 IEEE Electric Ship Technologies Symposium (ESTS)*, Aug. 2017, pp. 1–10, doi: 10.1109/ESTS.2017.8069356.

[37] D. Kumar and F. Zare, “A Comprehensive Review of Maritime Microgrids: System Architectures, Energy Efficiency, Power Quality, and Regulations,” *IEEE Access*, vol. 7, pp. 67249–67277, 2019, doi: 10.1109/ACCESS.2019.2917082.

[38] K. Kim, K. Park, G. Roh, and K. Chun, “DC-grid system for ships: a study of benefits and technical considerations,” *J. Int. Marit. Saf. Environ. Aff. Shipp.*, vol. 2, no. 1, pp. 1–12, Nov. 2018, doi: 10.1080/25725084.2018.1490239.

[39] N. Doerry and J. V. Amy, “Design Considerations for a Reference MVDC Power System,” Nov. 2016.

[40] N. Doerry and J. Amy, “MVDC Distribution Systems,” Mar. 2018.

[41] N. Zohrabi, J. Shi, and S. Abdelwahed, “An overview of design specifications and requirements for the MVDC shipboard power system,” *Int. J. Electr. Power Energy Syst.*, vol. 104, pp. 680–693, Jan. 2019, doi: 10.1016/j.ijepes.2018.07.050.
[42] G. Sulligoi, D. Bosich, A. Vicenzutti, and Y. Khersonsky, “Design of Zonal Electrical Distribution Systems for Ships and Oil Platforms: Control Systems and Protections,” *IEEE Trans. Ind. Appl.*, vol. 56, no. 5, pp. 5656–5669, Sep. 2020, doi: 10.1109/TIA.2020.2999035.
[43] H. Li, W. Li, M. Luo, A. Monti, and F. Ponci, “Design of Smart MVDC Power Grid Protection,” *IEEE Trans. Instrum. Meas.*, vol. 60, no. 9, pp. 3035–3046, Sep. 2011, doi: 10.1109/TIM.2011.2158152.
[44] S. Hundertmark and O. Liebfried, “Power Supply Options for a Naval Railgun,” *ArXiv170905901 Phys.*, Sep. 2017, Accessed: May 31, 2018. [Online]. Available: http://arxiv.org/abs/1709.05901.
[45] A. L. Gattozzi *et al.*, “Power system and energy storage models for laser integration on naval platforms,” in *2015 IEEE Electric Ship Technologies Symposium (ESTS)*, Jun. 2015, pp. 173–180, doi: 10.1109/ESTS.2015.7157884.
[46] N. Doerry, J. Amy, and C. Krolick, “History and the Status of Electric Ship Propulsion, Integrated Power Systems, and Future Trends in the U.S. Navy,” *Proc. IEEE*, vol. 103, no. 12, pp. 2243–2251, Dec. 2015, doi: 10.1109/JPROC.2015.2494159.
[47] L. Farrier, C. Savage, and R. Bucknall, “Simulating Pulsed Power Load Compensation using Lithium-ion Battery Systems,” in *2019 IEEE Electric Ship Technologies Symposium (ESTS)*, Aug. 2019, pp. 45–51, doi: 10.1109/ESTS.2019.8847802.
[48] M. R. Doyle, D. J. Samuel, T. Conway, and R. R. Klimowski, “Electromagnetic aircraft launch system-EMALS,” *IEEE Trans. Magn.*, vol. 31, no. 1, pp. 528–533, Jan. 1995, doi: 10.1109/20.364638.
[49] R. Smart *et al.*, “Using S3D to analyze ship system alternatives for a 100 MW 10,000 ton surface combatant,” in *2017 IEEE Electric Ship Technologies Symposium (ESTS)*, Aug. 2017, pp. 96–103, doi: 10.1109/ESTS.2017.8069266.
[50] NavSEA, “Naval Power and Energy Systems Technology Development Roadmap.” 2019.
[51] “IEEE Recommended Practice for 1 kV to 35 kV Medium-Voltage DC Power Systems on Ships,” *IEEE Std 1709-2018 Revis. IEEE Std 1709-2010*, pp. 1–54, Dec. 2018, doi: 10.1109/IEEESTD.2018.8569023.
[52] D. Perkins, T. Vu, H. Vahedi, and C. S. Edrington, “Distributed Power Management Implementation for Zonal MVDC Ship Power Systems,” in *IECON 2018 - 44th Annual Conference of the IEEE Industrial Electronics Society*, Oct. 2018, pp. 3401–3406, doi: 10.1109/IECON.2018.8592830.
[53] S. R. Rudraraju, A. K. Srivastava, S. C. Srivastava, and N. N. Schulz, “Small signal stability analysis of a shipboard MVDC power system,” in *2009 IEEE Electric Ship Technologies Symposium*, Apr. 2009, pp. 135–141, doi: 10.1109/ESTS.2009.4906506.

[54] X. Pei, O. Cwikowski, D. S. Vilchis-Rodriguez, M. Barnes, A. C. Smith, and R. Shuttleworth, “A review of technologies for MVDC circuit breakers,” in *IECON 2016 - 42nd Annual Conference of the IEEE Industrial Electronics Society*, Oct. 2016, pp. 3799–3805, doi: 10.1109/IECON.2016.7793492.

[55] J. V. Amy and N. H. Doerry, “MVDC grounding and common mode current control,” in *2017 IEEE Electric Ship Technologies Symposium (ESTS)*, Aug. 2017, pp. 64–70, doi: 10.1109/ESTS.2017.8069261.

[56] J. Dentler and K. Pettersen, “Distribution and grounding issues involved in naval ship integration of an electric gun system,” *IEEE Trans. Magn.*, vol. 29, no. 1, pp. 929–933, Jan. 1993, doi: 10.1109/20.195702.

[57] M. Bosworth, H. Ravindra, M. Steurer, and S. Pekarek, “Common-mode equivalent modeling of a notional two-zone MVDC ship power system,” in *2017 IEEE Electric Ship Technologies Symposium (ESTS)*, Aug. 2017, pp. 79–83, doi: 10.1109/ESTS.2017.8069263.

[58] A. D. Brovont and S. D. Pekarek, “Equivalent circuits for common-mode analysis of naval power systems,” in *2015 IEEE Electric Ship Technologies Symposium (ESTS)*, Jun. 2015, pp. 245–250, doi: 10.1109/ESTS.2015.7157897.

[59] S. D. Sudhoff *et al.*, “A reduced scale naval DC microgrid to support electric ship research and development,” in *2015 IEEE Electric Ship Technologies Symposium (ESTS)*, Jun. 2015, pp. 464–471, doi: 10.1109/ESTS.2015.7157911.

[60] T. Ericsen, “The ship power electronic revolution: Issues and answers,” in *2008 55th IEEE Petroleum and Chemical Industry Technical Conference*, Sep. 2008, pp. 1–11, doi: 10.1109/PCICON.2008.4663984.

[61] “IEEE Guide for Control Architecture for High Power Electronics (1 MW and Greater) Used in Electric Power Transmission and Distribution Systems,” *IEEE Std 1676-2010*, pp. 1–47, Feb. 2011, doi: 10.1109/IEEESTD.2011.5712778.

[62] “IEEE Standard for Power Electronics Open System Interfaces in Zonal Electrical Distribution Systems Rated Above 100 kW,” *IEEE Std 1826-2020 Revis. IEEE Std 1826-2012*, pp. 1–44, Nov. 2020, doi: 10.1109/IEEESTD.2020.9271958.

[63] D. Schneider, “Clad in controversy,” *IEEE Spectr.*, vol. 50, no. 8, pp. 32–37, Aug. 2013, doi: 10.1109/MSPEC.2013.6565558.

[64] G. Sulligoi *et al.*, “Naval smart grid: Integrated Power System for all electric naval vessels with control and reliability characteristics,” in *2014 AEIT Annual Conference - From Research to Industry: The Need for a More Effective Technology Transfer (AEIT)*, Sep. 2014, pp. 1–6, doi: 10.1109/AEIT.2014.7002060.

[65] *J. Momoh and L. Mili, Operation and Control of Electric Energy Processing Systems*, IEEE Press Series on Power Engineering. Wiley, 2010.

[66] ESRDC, “ESRDC Notional Ship Data.” May 2017.

[67] J. M. Prousalidis, P. Mouzakis, E. Sofras, D. Muthumuni, and O. Nayak, “On studying the power supply quality problems due to thruster start-ups,” in *2009 IEEE Electric*

Ship Technologies Symposium, Apr. 2009, pp. 440–448, doi: 10.1109/ESTS.2009.4906549.
[68] B. Fan, C. Wang, Q. Yang, W. Liu, and G. Wang, "Performance Guaranteed Control of Flywheel Energy Storage System for Pulsed Power Load Accommodation," *IEEE Trans. Power Syst.*, vol. 33, no. 4, pp. 3994–4004, Jul. 2018, doi: 10.1109/TPWRS.2017.2774273.
[69] B. J. McRee, D. A. Wetz, D. A. Dodson, and J. M. Heinzel, "Hardware-in-the-Loop Model Validation of Charging Capacitors With Multipulse Rectifiers for High Rep-Rate Shipboard-Pulsed DC Loads," *IEEE Trans. Plasma Sci.*, vol. 46, no. 10, pp. 3591–3598, Oct. 2018, doi: 10.1109/TPS.2018.2829264.
[70] A. Vlachokostas *et al.*, "Ship-to-grid integration: Environmental mitigation and critical infrastructure resilience," in *2019 IEEE Electric Ship Technologies Symposium (ESTS)*, Aug. 2019, pp. 542–547, doi: 10.1109/ESTS.2019.8847858.
[71] A. Vicenzutti, F. Tosato, G. Sulligoi, G. Lipardi, and L. Piva, "High voltage ship-to-shore connection for electric power supply support in landing operations: An analysis," in *2015 IEEE Electric Ship Technologies Symposium (ESTS)*, Jun. 2015, pp. 364–369, doi: 10.1109/ESTS.2015.7157920.
[72] M. Brenna *et al.*, "A Review on Energy Efficiency in Three Transportation Sectors: Railways, Electrical Vehicles and Marine," *Energies*, vol. 13, no. 9, Art. no. 9, Jan. 2020, doi: 10.3390/en13092378.
[73] K. L. Peterson, P. Chavdarian, M. Islam, and C. Cayanan, "Tackling ship pollution from the shore," *IEEE Ind. Appl. Mag.*, vol. 15, no. 1, pp. 56–60, Jan. 2009, doi: 10.1109/MIAS.2008.930901.
[74] "IEC/IEEE International Standard - Utility connections in port – Part 1: High voltage shore connection (HVSC) systems – General requirements," *IECIEEE 80005-12019*, pp. 1–78, Mar. 2019, doi: 10.1109/IEEESTD.2019.8666180.
[75] Y. Khersonsky, M. Islam, and K. Peterson, "Challenges of Connecting Shipboard Marine Systems to Medium Voltage Shoreside Electrical Power," *IEEE Trans. Ind. Appl.*, vol. 43, no. 3, pp. 838–844, May 2007, doi: 10.1109/TIA.2007.895810.
[76] G. Sulligoi, D. Bosich, R. Pelaschiar, G. Lipardi, and F. Tosato, "Shore-to-Ship Power," *Proc. IEEE*, vol. 103, no. 12, pp. 2381–2400, Dec. 2015, doi: 10.1109/JPROC.2015.2491647.
[77] American Bureau of Shipping, "Direct Current (DC) Power Distribution Systems for Marine and Offshore Applications." Jul. 2018.
[78] Lloyd's Register, "Rules for Direct Current Distribution Systems." Jul. 2019.
[79] RINA, "Rules for Fuel Cells Installation in Ships." Jan. 2018.
[80] International Group of Authorities (Editor: Thomas Lamb), *Ship Design and Construction*. The Society of Naval Architects and Marine Engineers, 2003.
[81] L. Braidotti, S. Bertagna, A. Marinò, D. Bosich, V. Bucci, and G. Sulligoi, "An Application of Modular Design in the Refitting of a Hybrid-electric Propelled Training

Ship," in *2020 AEIT International Annual Conference (AEIT)*, Sep. 2020, pp. 1–6, doi: 10.23919/AEIT50178.2020.9241114.

[82] M. Baret *et al.*, "Amerigo Vespucci: Retrofitting of propulsion and generation systems on the italian training's tall ship," in *Automation and Motion 2014 International Symposium on Power Electronics, Electrical Drives*, Jun. 2014, pp. 319–326, doi: 10.1109/SPEEDAM.2014.6872133.

[83] J. Chalfant, "Early-Stage Design for Electric Ship," *Proc. IEEE*, vol. 103, no. 12, pp. 2252–2266, Dec. 2015, doi: 10.1109/JPROC.2015.2459672.

[84] R. M. Wideman, "Project Management Examined." Unpublished lecture material for the University of Victoria, British Columbia, 1980.

[85] R. Menis, A. da Rin, G. Sulligoi, and A. Vicenzutti, "All electric ships dependable design: Implications on project management," in *2014 AEIT Annual Conference - From Research to Industry: The Need for a More Effective Technology Transfer (AEIT)*, Sep. 2014, pp. 1–6, doi: 10.1109/AEIT.2014.7002061.

[86] P. Mandel and C. Chryssostomidis, "A Design Methodology for Ships and other Complex Systems," *Philos. Trans. R. Soc. Lond. Ser. Math. Phys. Sci.*, vol. 273, no. 1231, pp. 85–98, 1972.

[87] G. Buja, A. da Rin, R. Menis, and G. Sulligoi, "Dependable design assessment of Integrated Power Systems for All Electric Ships," in *Railway and Ship Propulsion Electrical Systems for Aircraft*, Oct. 2010, pp. 1–8, doi: 10.1109/ESARS.2010.5665218.

[88] J. K. Liker, D. K. Sobek, A. C. Ward, and J. J. Cristiano, "Involving suppliers in product development in the United States and Japan: evidence for set-based concurrent engineering," *IEEE Trans. Eng. Manag.*, vol. 43, no. 2, pp. 165–178, May 1996, doi: 10.1109/17.509982.

[89] X. She, A. Q. Huang, and R. Burgos, "Review of Solid-State Transformer Technologies and Their Application in Power Distribution Systems," *IEEE J. Emerg. Sel. Top. Power Electron.*, vol. 1, no. 3, pp. 186–198, Sep. 2013, doi: 10.1109/JESTPE.2013.2277917.

[90] H. Chen and D. Divan, "Design of a 10-kV · A Soft-Switching Solid-State Transformer (S4T)," *IEEE Trans. Power Electron.*, vol. 33, no. 7, pp. 5724–5738, Jul. 2018, doi: 10.1109/TPEL.2017.2749430.

[91] J. Huber and J. Kolar, "Solid-State Transformers: On the Origins and Evolution of Key Concepts," *IEEE Ind. Electron. Mag.*, vol. 10, pp. 19–28, Sep. 2016, doi: 10.1109/MIE.2016.2588878.

[92] V. Bucci, U. La Monaca, D. Bosich, G. Sulligoi, and P. Andrea, "Integrated Ship Design and CSI Modeling: A New Methodology for Comparing Onboard Electrical Distributions in the Early-Stage Design," 2018, pp. 124–132, doi: 10.3233/978-1-61499-870-9-124.

[93] A. Colavitto, A. Contin, A. Vicenzutti, G. Sulligoi, and M. McCandless, "Impact of harmonic pollution in junctions between DC cables with different insulating technologies: electrical and thermal analyses," presented at the 2019 IEEE Milan PowerTech.

[94] D. J. Jurkiewicz, J. Chalfant, and C. Chryssostomidis, "Modular IPS machinery arrangement in early-stage naval ship design," in *2013 IEEE Electric Ship Technologies Symposium (ESTS)*, Apr. 2013, pp. 121–127, doi: 10.1109/ESTS.2013.6523722.

[95] NavSEA, "Naval Power and Energy Systems Technology Development Roadmap." 2017.

[96] G. Trincas, *A rational approach, ship design*, 2016th ed. .

[97] A. Vicenzutti *et al.*, "Early-stage design of shipboard integrated power systems: CSI-based multiple solutions comparison," in *2017 IEEE Electric Ship Technologies Symposium (ESTS)*, Aug. 2017, pp. 478–485, doi: 10.1109/ESTS.2017.8069325.

[98] N. Barbini, A. Colavitto, A. Vicenzutti, A. Contin, and G. Sulligoi, "High Frequency Modeling of Foil Type Transformers for Shipboard Power Electronic Power Distribution Systems," in *2019 AEIT International Annual Conference (AEIT)*, Sep. 2019, pp. 1–6, doi: 10.23919/AEIT.2019.8893420.

[99] A. Colavitto, A. Vicenzutti, G. Sulligoi, and G. Lipardi, "Voltage and frequency regulation in high power AC islanded microgrid with static converter interfaced generators," in *2018 18th International Conference on Harmonics and Quality of Power (ICHQP)*, May 2018, pp. 1–6, doi: 10.1109/ICHQP.2018.8378927.

[100] K. Satpathi, A. Ukil, and J. Pou, "Short-Circuit Fault Management in DC Electric Ship Propulsion System: Protection Requirements, Review of Existing Technologies and Future Research Trends," *IEEE Trans. Transp. Electrification*, vol. 4, no. 1, pp. 272–291, Mar. 2018, doi: 10.1109/TTE.2017.2788199.

[101] G. Sulligoi, A. Vicenzutti, M. Chiandone, D. Bosich, and V. Arcidiacono, "Generators electromechanical stability in shipboard grids with symmetrical layout: Dynamic interactions between voltage and frequency controls," in *AEIT Annual Conference 2013*, Oct. 2013, pp. 1–5, doi: 10.1109/AEIT.2013.6666812.

[102] R. Marconato, *Electric Power Systems*, CEI-Italian Electrotechnical Committee. Milan, 2002.

[103] C. M. Cooke, C. Chryssostomidis, and J. Chalfant, "Modular integrated power corridor," in *2017 IEEE Electric Ship Technologies Symposium (ESTS)*, Aug. 2017, pp. 91–95, doi: 10.1109/ESTS.2017.8069265.

[104] C. Chryssostomidis and C. M. Cooke, "Space reservation for shipboard electric power distribution systems," in *2015 IEEE Electric Ship Technologies Symposium (ESTS)*, Jun. 2015, pp. 187–192, doi: 10.1109/ESTS.2015.7157886.

[105] M. McCandless *et al.*, "Thermal Analysis of MVDC Power Corridor," in *2019 IEEE Electric Ship Technologies Symposium (ESTS)*, Aug. 2019, pp. 106–112, doi: 10.1109/ESTS.2019.8847881.

[106] J. Chalfant, M. Ferrante, and C. Chryssostomidis, "Design of a notional ship for use in the development of early-stage design tools," in *2015 IEEE Electric Ship Technologies Symposium (ESTS)*, Jun. 2015, pp. 239–244, doi: 10.1109/ESTS.2015.7157896.

[107] J. d Á. Ferrandis, J. Chalfant, C. M. Cooke, and C. Chryssostomidis, "Design of a Power Corridor Distribution Network," in *2019 IEEE Electric Ship Technologies Symposium (ESTS)*, Aug. 2019, pp. 284–292, doi: 10.1109/ESTS.2019.8847939.

[108] A. Vicenzutti, A. Colavitto, M. Chiandone, and G. Sulligoi, "Dependability analysis of cyber security in All-Electric Ships," in *2018 AEIT International Annual Conference*, Oct. 2018, pp. 1–5, doi: 10.23919/AEIT.2018.8577280.

[109] D. Bosich *et al.*, "Early-stage design of integrated power and energy systems for naval vessels electrification: Advanced modeling using CSI," in *2017 IEEE Transportation Electrification Conference and Expo (ITEC)*, Jun. 2017, pp. 387–392, doi: 10.1109/ITEC.2017.7993302.

[110] M. Braun, "Reactive power supplied by PV inverters - cost-benefit-analysis," in *The compiled state-of-the-art of PV solar technology and deployment. 22nd European Photovoltaic Solar Energy Conference, EU PVSEC 2007. Proceedings of the international conference. CD-ROM*, 2007, pp. 2940–2946.

[111] G. Sulligoi, A. Vicenzutti, V. Arcidiacono, and Y. Khersonsky, "Voltage Stability in Large Marine-Integrated Electrical and Electronic Power Systems," *IEEE Trans. Ind. Appl.*, vol. 52, no. 4, pp. 3584–3594, Jul. 2016, doi: 10.1109/TIA.2016.2544833.

[112] S. V. Giannoutsos and S. N. Manias, "A Systematic Power-Quality Assessment and Harmonic Filter Design Methodology for Variable-Frequency Drive Application in Marine Vessels," *IEEE Trans. Ind. Appl.*, vol. 51, no. 2, pp. 1909–1919, Mar. 2015, doi: 10.1109/TIA.2014.2347453.

[113] "IEEE Recommended Practice and Requirements for Harmonic Control in Electric Power Systems," *IEEE Std 519-2014 Revis. IEEE Std 519-1992*, pp. 1–29, Jun. 2014, doi: 10.1109/IEEESTD.2014.6826459.

[114] A. Colavitto, A. Vicenzutti, D. Bosich, and G. Sulligoi, "Modeling of Power Cables in Shipboard IPES for assessing High Frequency Disturbances Propagation," in *2019 IEEE Electric Ship Technologies Symposium (ESTS)*, Aug. 2019, pp. 337–344, doi: 10.1109/ESTS.2019.8847926.

[115] P. Gómez, F. P. Espino-Cortés, and F. de León, "Computation of the dielectric stresses produced by PWM type waveforms on medium voltage transformer windings," in *2011 Annual Report Conference on Electrical Insulation and Dielectric Phenomena*, Oct. 2011, pp. 199–202, doi: 10.1109/CEIDP.2011.6232631.

[116] O. Breien and I. Johansen, "Attenuation of travelling waves in single-phase high-voltage cables," *Proc. Inst. Electr. Eng.*, vol. 118, no. 6, pp. 787–793, Jun. 1971, doi: 10.1049/piee.1971.0150.

[117] A. Morched, B. Gustavsen, and M. Tartibi, "A universal model for accurate calculation of electromagnetic transients on overhead lines and underground cables," *IEEE Trans. Power Deliv.*, vol. 14, no. 3, pp. 1032–1038, Jul. 1999, doi: 10.1109/61.772350.

[118] B. Gustavsen, “Validation of frequency-dependent transmission line models,” *IEEE Trans. Power Deliv.*, vol. 20, no. 2, pp. 925–933, Apr. 2005, doi: 10.1109/TPWRD.2004.837676.

[119] B. Gustavsen, J. A. Martinez, and D. Durbak, “Parameter determination for modeling system transients-Part II: Insulated cables,” *IEEE Trans. Power Deliv.*, vol. 20, no. 3, pp. 2045–2050, Jul. 2005, doi: 10.1109/TPWRD.2005.848774.

[120] A. Ramirez, J. L. Naredo, and P. Moreno, “Full frequency-dependent line model for electromagnetic transient simulation including lumped and distributed sources,” *IEEE Trans. Power Deliv.*, vol. 20, no. 1, pp. 292–299, Jan. 2005, doi: 10.1109/TPWRD.2004.835037.

[121] P. Wagenaars, P. A. A. F. Wouters, P. C. J. M. van der Wielen, and E. F. Steennis, “Approximation of Transmission Line Parameters of Single-Core XLPE Cables,” in *Conference Record of the 2008 IEEE International Symposium on Electrical Insulation*, Jun. 2008, pp. 20–23, doi: 10.1109/ELINSL.2008.4570267.

[122] N. Idir, Y. Weens, and J. Franchaud, “Skin effect and dielectric loss models of power cables,” *IEEE Trans. Dielectr. Electr. Insul.*, vol. 16, no. 1, pp. 147–154, Feb. 2009, doi: 10.1109/TDEI.2009.4784562.

[123] Y. Huangfu, L. D. Rienzo, and S. Wang, “Frequency-Dependent Multi-Conductor Transmission Line Model for Shielded Power Cables Considering Geometrical Dissymmetry,” *IEEE Trans. Magn.*, vol. 54, no. 3, pp. 1–4, Mar. 2018, doi: 10.1109/TMAG.2017.2751958.

[124] I. Lafaia, J. Mahseredjian, A. Ametani, M. T. C. de Barros, I. Koçar, and Y. Fillion, “Frequency and Time Domain Responses of Cross-Bonded Cables,” *IEEE Trans. Power Deliv.*, vol. 33, no. 2, pp. 640–648, Apr. 2018, doi: 10.1109/TPWRD.2017.2734891.

[125] M. Rahmani and M. Mazzola, “Modeling of common mode currents on electric ship hull using scattering parameters,” in *2015 IEEE Electric Ship Technologies Symposium (ESTS)*, Jun. 2015, pp. 156–160, doi: 10.1109/ESTS.2015.7157879.

[126] S. Kulkarni and S. Santoso, “Estimating transient response of simple AC and DC shipboard power systems to pulse load operations,” in *2009 IEEE Electric Ship Technologies Symposium*, Apr. 2009, pp. 73–78, doi: 10.1109/ESTS.2009.4906496.

[127] M. Brenna, F. Foiadelli, and D. Zaninelli, “An Analysis of Transient Overvoltages during the Energization of Electric Ship Propulsion Systems,” *Sci. World J.*, 2015, doi: 10.1155/2015/458068.

[128] A. D. Brovont and S. D. Pekarek, “Impact of switching frequency and edge rates on common-mode current in MVDC microgrids,” in *2017 IEEE Electric Ship Technologies Symposium (ESTS)*, Aug. 2017, pp. 16–24, doi: 10.1109/ESTS.2017.8069254.

[129] S. Castellan, R. Menis, A. Tessarolo, F. Luise, and T. Mazzuca, “A review of power electronics equipment for all-electric ship MVDC power systems,” *Int. J. Electr. Power Energy Syst.*, vol. 96, pp. 306–323, Mar. 2018, doi: 10.1016/j.ijepes.2017.09.040.

[130] "IEC 60034-18-41:2014/AMD1:2019 Qualification and type tests for Type I electrical insulation systems used in rotating electrical machines when fed from voltage converters," 2019. .

[131] A. Cavallini, G. C. Montanari, and L. Fornasari, "The evolution of IEC 60034-18-41 from technical specification to standard: Perspectives for manufacturers and end users," in *2012 IEEE International Power Modulator and High Voltage Conference (IPMHVC)*, Jun. 2012, pp. 160–164, doi: 10.1109/IPMHVC.2012.6518704.

[132] N. Y. Abed and O. A. Mohammed, "Frequency-Dependent Coupled Field-Circuit Modeling of Armored Power Cables Using Finite Elements," *IEEE Trans. Magn.*, vol. 47, no. 5, pp. 930–933, May 2011, doi: 10.1109/TMAG.2010.2085036.

[133] T. Maier, T. Leibfried, A. Wagner, and C. Freitag, "Frequency-Dependent Line Parameters of an XLPE Power Cable Relating to Geometric Variations," in *2018 Condition Monitoring and Diagnosis (CMD)*, Sep. 2018, pp. 1–6, doi: 10.1109/CMD.2018.8535868.

[134] C. R. Valdez, R. M. Tallam, and R. J. Kerkman, "A new frequency-dependent-model for cables," in *2008 IEEE International Conference on Electro/Information Technology*, May 2008, pp. 151–158, doi: 10.1109/EIT.2008.4554285.

[135] G. Mugala, R. Eriksson, and P. Pettersson, "Comparing two measurement techniques for high frequency characterization of power cable semiconducting and insulating materials," *IEEE Trans. Dielectr. Electr. Insul.*, vol. 13, no. 4, pp. 712–716, Aug. 2006, doi: 10.1109/TDEI.2006.1667728.

[136] T. Esmailian, F. R. Kschischang, and P. G. Gulak, "In-building power lines as high-speed communication channels: channel characterization and a test channel ensemble," *Int. J. Commun. Syst.*, vol. 16, no. 5, pp. 381–400, 2003, doi: 10.1002/dac.596.

[137] O. M. O. Gatous and J. Pissolato, "Frequency-dependent skin-effect formulation for resistance and internal inductance of a solid cylindrical conductor," *Antennas Propag. IEE Proc. - Microw.*, vol. 151, no. 3, pp. 212–216, Jun. 2004, doi: 10.1049/ip-map:20040469.

[138] Y. Weens, N. Idir, R. Bausiere, and J. J. Franchaud, "Modeling and simulation of unshielded and shielded energy cables in frequency and time domains," *IEEE Trans. Magn.*, vol. 42, no. 7, pp. 1876–1882, Jul. 2006, doi: 10.1109/TMAG.2006.874306.

[139] C. R. Paul, *Analysis of Multiconductor Transmission Lines*, 2nd ed. John Wiley & Sons, Inc., 2007.

[140] I. Kocar and J. Mahseredjian, "Accurate Frequency Dependent Cable Model for Electromagnetic Transients," *IEEE Trans. Power Deliv.*, vol. 31, no. 3, pp. 1281–1288, Jun. 2016, doi: 10.1109/TPWRD.2015.2453335.

[141] S. Kim, S. Kim, and D. Dujic, "Extending Protection Selectivity in DC Shipboard Power Systems by Means of Additional Bus Capacitance," *IEEE Trans. Ind. Electron.*, vol. 67, no. 5, pp. 3673–3683, May 2020, doi: 10.1109/TIE.2019.2916371.

[142] S. Beheshtaein, R. M. Cuzner, M. Forouzesh, M. Savaghebi, and J. M. Guerrero, “DC Microgrid Protection: A Comprehensive Review,” *IEEE J. Emerg. Sel. Top. Power Electron.*, pp. 1–1, 2019, doi: 10.1109/JESTPE.2019.2904588.

[143] J. F. Hansen and F. Wendt, “History and State of the Art in Commercial Electric Ship Propulsion, Integrated Power Systems, and Future Trends,” *Proc. IEEE*, vol. 103, no. 12, pp. 2229–2242, 2015, doi: 10.1109/JPROC.2015.2458990.

[144] Xu She, A. Q. Huang, and R. Burgos, “Review of Solid-State Transformer Technologies and Their Application in Power Distribution Systems,” *IEEE J. Emerg. Sel. Top. Power Electron.*, vol. 1, no. 3, pp. 186–198, Sep. 2013, doi: 10.1109/JESTPE.2013.2277917.

[145] B. Florkowska, P. Zydron, J. Roehrich, and M. Florkowski, “Performance of cables and machines insulation at various parameters of impulse stimulus,” in *2010 International Conference on High Voltage Engineering and Application*, Oct. 2010, pp. 144–147, doi: 10.1109/ICHVE.2010.5640843.

[146] M. M. Islam, M. R. Hossain, R. A. Dougal, and C. W. Brice, “Analysis of real-world power quality disturbances employing time-frequency distribution,” *Clemson Univ. Power Syst. Conf. PSC 2016*, pp. 1–5, 2016, doi: 10.1109/PSC.2016.7462816.

[147] Z. Luna Lopez, P. Gomez, F. P. Espino-Cortes, and R. Pena-Rivero, “Modeling of Transformer Windings for Fast Transient Studies: Experimental Validation and Performance Comparison,” *IEEE Trans. Power Deliv.*, vol. 32, no. 4, pp. 1852–1860, Aug. 2017, doi: 10.1109/TPWRD.2016.2583379.

[148] P. Gómez and F. De León, “Accurate and efficient computation of the inductance matrix of transformer windings for the simulation of very fast transients,” *IEEE Trans. Power Deliv.*, vol. 26, no. 3, pp. 1423–1431, 2011, doi: 10.1109/TPWRD.2011.2104370.

[149] D. J. Wilcox, W. G. Hurley, and M. Conlon, “Calculation of self and mutual impedances between sections of transformer windings,” *IEE Proc. C Gener. Transm. Distrib.*, vol. 136, no. 5, p. 308, 1989, doi: 10.1049/ip-c.1989.0041.

[150] A. Theocharis and M. Popov, “Modelling of foil-type transformer windings for computation of terminal impedance and internal voltage propagation,” *IET Electr. Power Appl.*, vol. 9, no. 2, pp. 128–137, Feb. 2015, doi: 10.1049/iet-epa.2014.0135.

[151] A. Soloot, H. Høidalen, and B. Gustavsen, “Influence of the winding design of wind turbine transformers for resonant overvoltage vulnerability,” *IEEE Trans. Dielectr. Electr. Insul.*, vol. 22, no. 2, pp. 1250–1257, Apr. 2015, doi: 10.1109/TDEI.2015.7076828.

[152] C. Dannatt, “The variation of the magnetic properties of ferromagnetic laminae with frequency,” *J. Inst. Electr. Eng.*, vol. 79, no. 480, pp. 667–680, Dec. 1936, doi: 10.1049/jiee-1.1936.0209.

[153] C. Dannatt, “Discussion on ‘The variation of the magnetic properties of ferromagnetic laminae with frequency,’” *J. Inst. Electr. Eng.*, vol. 80, no. 482, pp. 231–231, Feb. 1937, doi: 10.1049/jiee-1.1937.0039.

[154] A. Colavitto, A. Vicenzutti, and G. Sulligoi, “Equivalent Inductance Evaluation for Cable Bundles in Shipboard Integrated Power and Energy Systems,” in *2020 AEIT International Annual Conference (AEIT)*, Sep. 2020, pp. 1–5, doi: 10.23919/AEIT50178.2020.9241192.

[155] F. Milano and Á. O. Manjavacas, “Frequency-Dependent Model for Transient Stability Analysis,” *IEEE Trans. Power Syst.*, vol. 34, no. 1, pp. 806–809, Jan. 2019, doi: 10.1109/TPWRS.2018.2871639.

[156] F. Milano, “A python-based software tool for power system analysis,” in *2013 IEEE Power Energy Society General Meeting*, Jul. 2013, pp. 1–5, doi: 10.1109/PESMG.2013.6672387.

[157] H. P. Langtangen, “Python Scripting for Computational Science,” vol. 3, 2008.

[158] J. H. Chow and K. W. Cheung, “A toolbox for power system dynamics and control engineering education and research,” *IEEE Trans. Power Syst.*, vol. 7, no. 4, pp. 1559–1564, Nov. 1992, doi: 10.1109/59.207380.

[159] F. Milano, “An open source power system analysis toolbox,” in *2006 IEEE Power Engineering Society General Meeting*, Jun. 2006, p. 1 pp.-, doi: 10.1109/PES.2006.1708946.

[160] R. D. Zimmerman, C. E. Murillo-Sánchez, and R. J. Thomas, “MATPOWER: Steady-State Operations, Planning, and Analysis Tools for Power Systems Research and Education,” *IEEE Trans. Power Syst.*, vol. 26, no. 1, pp. 12–19, Feb. 2011, doi: 10.1109/TPWRS.2010.2051168.

[161] M. Zhou and S. Zhou, “Internet, Open-source and Power System Simulation,” in *2007 IEEE Power Engineering Society General Meeting*, Jun. 2007, pp. 1–5, doi: 10.1109/PES.2007.385492.

[162] R. C. Dugan and T. E. McDermott, “An open source platform for collaborating on smart grid research,” in *2011 IEEE Power and Energy Society General Meeting*, Jul. 2011, pp. 1–7, doi: 10.1109/PES.2011.6039829.

[163] F. Milano and Á. Ortega, “Frequency Divider,” *IEEE Trans. Power Syst.*, vol. 32, no. 2, pp. 1493–1501, Mar. 2017, doi: 10.1109/TPWRS.2016.2569563.

Papers

[32] A. Colavitto *et al.*, “Naval Smart Grid Research Program: Phase 2,” in *2018 IEEE International Conference on Electrical Systems for Aircraft, Railway, Ship Propulsion and Road Vehicles International Transportation Electrification Conference (ESARS-ITEC)*, Nov. 2018, pp. 1–6, doi: 10.1109/ESARS-ITEC.2018.8607638.

[33] A. Colavitto, A. Vicenzutti, D. Bosich, and G. Sulligoi, “Open Challenges in Future Electric Ship Design: High-Frequency Disturbance Propagation in Integrated Power and Energy Systems on Ships,” *IEEE Electrification Mag.*, vol. 7, no. 4, pp. 98–110, Dec. 2019, doi: 10.1109/MELE.2019.2943983.

[93] A. Colavitto, A. Contin, A. Vicenzutti, G. Sulligoi, and M. McCandless, “Impact of harmonic pollution in junctions between DC cables with different insulating technologies: electrical and thermal analyses,” presented at the 2019 IEEE Milan PowerTech.

[98] N. Barbini, A. Colavitto, A. Vicenzutti, A. Contin, and G. Sulligoi, “High Frequency Modeling of Foil Type Transformers for Shipboard Power Electronic Power Distribution Systems,” in 2019 AEIT International Annual Conference (AEIT), Sep. 2019, pp. 1–6, doi: 10.23919/AEIT.2019.8893420.

[99] A. Colavitto, A. Vicenzutti, G. Sulligoi, and G. Lipardi, “Voltage and frequency regulation in high power AC islanded microgrid with static converter interfaced generators,” in 2018 18th International Conference on Harmonics and Quality of Power (ICHQP), May 2018, pp. 1–6, doi: 10.1109/ICHQP.2018.8378927.

[105] M. McCandless et al., “Thermal Analysis of MVDC Power Corridor,” in 2019 IEEE Electric Ship Technologies Symposium (ESTS), Aug. 2019, pp. 106–112, doi: 10.1109/ESTS.2019.8847881.

[108] A. Vicenzutti, A. Colavitto, M. Chiandone, and G. Sulligoi, “Dependability analysis of cyber security in All-Electric Ships,” in 2018 AEIT International Annual Conference, Oct. 2018, pp. 1–5, doi: 10.23919/AEIT.2018.8577280.

[114] A. Colavitto, A. Vicenzutti, D. Bosich, and G. Sulligoi, “Modeling of Power Cables in Shipboard IPES for assessing High Frequency Disturbances Propagation,” in 2019 IEEE Electric Ship Technologies Symposium (ESTS), Aug. 2019, pp. 337–344, doi: 10.1109/ESTS.2019.8847926.

[154] A. Colavitto, A. Vicenzutti, and G. Sulligoi, “Equivalent Inductance Evaluation for Cable Bundles in Shipboard Integrated Power and Energy Systems,” in 2020 AEIT International Annual Conference (AEIT), Sep. 2020, pp. 1–5, doi: 10.23919/AEIT50178.2020.9241192.